



DIPLOMARBEIT

„The mechanism of plasma-membrane as well as
endoplasmic reticulum resident ion channels in Ca^{2+}
Signalling“

verfasst von

Maria Christine Riedl

angestrebter akademischer Grad

Magistra der Pharmazie (Mag.pharm.)

Linz, Februar 2014

Studienkennzahl lt. Studienblatt:

A 449

Studienrichtung lt. Studienblatt:

Diplomstudium Pharmazie

Betreut von:

Univ.- Prof. Dr. Christoph Romanin

Inhaltsverzeichnis

Danksagungen

Widmung

Eidesstattliche Erklärung

1 Inhaltsverzeichnis

2	Zusammenfassung.....	11
3	Abstract.....	13
4	Introduction	15
4.1	Calcium, Calcium homeostasis – physiological functions	15
4.2	Calcium signaling and transduction pathways	15
4.2.1	Intracellular Ca^{2+} Signaling	15
4.3	Structure and stoichiometry of STIM1 and Orai proteins	19
4.3.1	Stromal Interaction Molecule 1 (STIM 1) – a sensitive ER-located Ca^{2+} sensor	19
4.3.2	Orai – the pore-forming promoter.....	21
4.4	Calcium release-activated Calcium (CRAC) channel, structure and function – The CRAC coupling machinery.....	23
4.5	An introduction in Transient receptor potential (TRP) channels.....	25
4.5.1	The TRPC family – The “canonical” TRPCs.....	26
4.5.2	The TRPV (vanilloid receptor) subfamily.....	28
4.6	Physiology of the myocardial muscle cell	33
4.6.1	Cardiomyocytes and calcium	33
4.7	Cellular calcium channels	33
4.8	An introduction in Ryanodine receptors (RyRs) and the Reticulon/Nogo family of proteins.....	37
4.8.1	The 3 subtypes, especially ryanodine receptor 2 (RyR2) cardiac/ calcium release channel.....	37

4.9	The Reticulon/Nogo family of proteins	38
4.10	Cardiac excitation-contraction coupling (physiology of the heart, functions, action potential and calcium-induced calcium release, CICR)	40
4.10.1	The action potential of the heart.....	40
4.10.2	The action potential of the nerve cell	41
4.10.3	Difference between the action potential of the heart and other excitable cells.....	43
4.10.4	Calcium-induced calcium release, CICR.....	45
4.11	The disease-linked RyR2 mutations	47
5	Task	49
6	Material and Methods.....	51
6.1	Cell culture.....	51
6.1.1	Cell lines – Human embryonic kidney (HEK293) cells	51
6.1.2	Media and chemicals for HEK293.....	51
6.1.3	Cell cultivation.....	52
6.1.4	Transfection	53
6.1.5	Bio-Rad Reagent (following manufacturers protocol).....	53
6.2	Ca ²⁺ Imaging with FURA-2	54
6.2.1	The Ca ²⁺ indicator Fura-2: Structure and chemical characteristics	54
6.2.2	Fluorescent measurements with Fura-2.....	55
6.2.3	The Ca ²⁺ imaging setup	57
6.3	Solutions and chemicals	58
6.3.1	Extracellular solution with 0, 1, 2 mM Ca ²⁺	58
6.3.2	Fura-2AM.....	58
6.3.3	Hank's Balanced Salt Solution (HBSS).....	58
7	Results	59
7.1	Calcium-release activated Calcium (CRAC) channel blockers, GSK-7975A ..	59
7.2	Canonical transient receptor potential (TRPC) 1 acts as a negative regulator for vanilloid TRPV6-mediated Ca ²⁺ influx.....	65
7.3	The reticulon protein RTN1A interacts with and modulates the ryanodine receptor 2 via its aminoterminal domain	71
8	Discussion.....	76

8.1	Calcium-release activated Calcium (CRAC) channel blockers, GSK-7975A ..	76
8.2	Canonical transient receptor potential (TRPC) 1 acts as a negative regulator for vanilloid TRPV6-mediated Ca^{2+} influx.....	78
8.3	The reticulon protein RTN1A interacts with and modulates the ryanodine receptor 2 via its aminoterminal domain	81
9	List of Abbreviations.....	83
10	References.....	85
11	Peer reviewed publications	91
12	Curriculum vitae	92

Danksagungen

Für alle, die mich in dieser stressigen Zeit ertragen haben und meinen Launen ausgeliefert waren!

Ich danke meinen Freundinnen Conny, Cornelia, Carina und Andrea, die stets ein offenes Ohr für mich haben, mich zum Lachen bringen und immer für mich da sind.

Eine Abschlussarbeit schreibt sich nicht allein, weshalb ich mich bei all jenen bedanken möchte, die durch ihre fachliche und persönliche Unterstützung zum Gelingen dieser Diplomarbeit beigetragen haben.

Mein Dank gilt Herrn Prof. Dr. Christoph Romanin für das Bereitstellen dieses Themas der Diplomarbeit und die freundliche Hilfsbereitschaft, die er mir entgegenbrachte.

Ebenso geht ein besonderer Dank an meine Betreuer Dr. Isabella Derler, Dr. Rainer Schindl und Dr. Martin Muik. Sie standen mir jederzeit bei Fragen hilfreich zur Seite, bei Problemen mit der Formulierung und haben mich beim Gegenlesen erheblich unterstützt.

Schließlich danke ich all meinen Kollegen der Gruppe für dieses abwechslungsreiche Zeit an der Biophysik in Linz.

Widmung

Für meine Eltern,
die mich unterstützt haben, immer für mich da sind
und mir mein Studium ermöglicht haben.

Ich möchte meinen Eltern, Regina und Ludwig, auf diesem Wege meinen ganz besonderen Dank aussprechen, dass sie mich auf meinem bisherigen Lebensweg immer begleitet haben und mich in all meinen Entscheidungen unterstützt haben.

Mein Vater hat mich gelehrt, in noch so schwierigen Lebenslagen nach vorne zu blicken und in meine eigenen Stärken zu vertrauen.

„Danke liebe Mama und lieber Papa, dass ihr so wunderbare Eltern seid und mir immer mit Rat und Tat zur Seite steht.“

Danke für alles.

Eidesstattliche Erklärung

Ich erkläre an Eides statt, dass ich die vorliegende Diplomarbeit selbstständig und ohne fremde Hilfe verfasst, andere als die angegebenen Quellen und Hilfsmittel nicht benutzt bzw. die wörtlich oder sinngemäß entnommenen Stellen als solche kenntlich gemacht habe.

Die vorliegende Diplomarbeit ist mit dem elektronisch übermittelten Textdokument identisch.

Maria Christine Riedl

2 Zusammenfassung

Meine Diplomarbeit beschäftigt sich mit der Regulation zellulärer Prozesse durch Kalzium über 3 verschiedene Signalisierungswege. Kalzium stellt einen der wichtigsten Mineralstoffe des menschlichen Körpers dar. Unter anderem dient er als Baustein von Knochen und Zähnen und übt dort wichtige Stützfunktionen aus. Dieser lebenswichtige sekundäre Botenstoff ist an verschiedensten Signalwegen beteiligt, in fast allen Zelltypen vertreten und steuert ein breites Spektrum von zellulären Prozessen. Beispielsweise ist Kalzium im Nervensystem, bei der Übermittlung von Impulsen, im Herzen, an der Regulation des regelmäßigen Herzschlags wie auch an der Gentranskription beteiligt.

Kalzium gelangt über Poren, den sogenannten Ionenkanälen in die Zellmembran in die Zelle. Diese Transmembranproteine ermöglichen, elektrisch geladenen Teilchen, das Durchqueren der Zellmembran. In dieser Diplomarbeit habe ich Ionenkanäle, welche vorwiegend für Kalzium selektiv sind mittels der Kalzium-Imaging Technik analysiert. Hiermit kann die Kalziumkonzentration in der Zelle direkt anhand seiner Fluoreszenzfärbung festgestellt werden.

Der erste Teil meiner Arbeit befasst sich mit der Charakterisierung von Kalzium-Kanal-Blockern bezüglich ihrer Wirkung auf den sehr wichtigen speicherregulierten Kalzium-Einstrom-Weg, dem sogenannten „Calcium release-activated Calcium“-Weg (CRAC). Dieser wird durch die beiden Schlüsselkomponenten STIM1 und Orai1 vollständig rekonstituiert. Das Protein STIM1 (Stromal Interaction Molecule 1) dient als Kalzium Sensor im ER. Sinkt die Kalziumkonzentration im ER, koppelt es an ORAI1 dem CRAC-Ionenkanal und gelangt durch diesen in die Zelle.

Die Kalzium-Kanal-Blocker der Firma Glaxo Smith Kline (GSK) wurden auf die beiden Proteine STIM1/Orai1 ausgetestet. Um einen indirekten Einfluss auf STIM1 und Orai1 auszuschließen, wurde zuerst die Wirkung der Blocker auf die Speicherentleerung in Zellen ohne künstlich eingebrachten Proteinen ausgetestet. Nachdem dies jedoch unbeeinflusst blieb, kann ein indirekter Einfluss auf STIM1/Orai1 ausgeschlossen werden. Ich konnte weiter feststellen, dass der zellspezifische CRAC-Strom gehemmt wurde, in Korrelation zu den Resultaten meiner Kollegen an künstlich eingebrachten STIM1/Orai1-Proteinen.

Im zweiten Thema beschäftigte ich mich mit der Regulation eine Gruppe von ligandengesteuerten Ionenkanälen, den sogenannten transient receptor potential channels auseinander insbesondere (TRPC1, canonical) und (TRPV6, vanilloid).

Ich zeigte einerseits, dass TRPC1 allein nach der Speicherentleerung keinen Kalzium-Einstrom in die Zellen zeigte. Andererseits wies ich nach, dass TRPC1 den durch TRPV6 induzierten Kalzium Einstrom in die Zelle reduziert. Dies deutet auf eine mögliche Koregulation von TRPV6 und TRPC1 hin, welche durch Patch-Clamp- und FRET-Experimente meiner Kollegen bestätigt wurden.

Im letzten Thema setzte ich mich damit auseinander, dass Mutationen im kardialen Ryanodin-Rezeptor (RyR2) zu einer erhöhten Öffnungswahrscheinlichkeit des RyR2 beitragen, die zu einer spontanen Kalzium-Freisetzung aus dem sarkoplasmatischen Retikulum (SR) führen. In Folge kann es zu ventrikulären Tachykardien bis hin zum plötzlichen Herztod kommen.

Die Zellen versuchen die Konzentration an intrazellulärem Kalzium möglichst gering zu halten, jedoch Mutationen können zu einem abnormen intrazellulären Kalzium Anstieg führen. Ich untersuchte HEK293 Zellen mit RyR2 mit und ohne seinen Bindungspartner RTN1A. In Gegenwart dieses Bindungspartners verminderte sich die Freisetzung von Kalzium. Dies deutet auf einen möglichen inhibitorischen Effekt von RTN1A auf die RyR2 Aktivität hin.

Zusammenfassend liefern meine Resultate zur Funktion verschiedener Kalzium-Ionenkanäle einen wichtigen Beitrag zum grundlegenden Verständnis von Kalzium Signalisierungswegen.

3 Abstract

In my diploma thesis I studied three different calcium signaling mechanisms in the human cell. Calcium is one of the most important mineral substances of the human body. It is found in bones and teeth in order to fulfil supporting functions. This essential second messenger functions as a main player in different signaling cascade pathways, in almost all cell types and regulates a wide spectrum of cellular processes. Calcium is for example involved in the nervous system, where it triggers impulses, in the heart for the regulation of the periodic heart beat, as well as in genetic transcription.

Calcium enters the cell via pores in the cell membrane, the so-called ion channels. These transmembrane proteins enable electrically charged particles to move across the cell membrane. In this diploma thesis I analyzed in particular ion channels, which are mainly calcium selective utilizing the Calcium-Imaging Technique. This technique enables to measure the intracellular calcium concentration directly via a fluorescence dye, which changes emission wave length and intensity in dependence of the calcium concentration.

In the first part of my work I characterized calcium-channel-blockers regarding their effects on the calcium release-activated calcium (CRAC) channel. This channel is fully reconstituted by the two key players STIM1 and Orai1. The protein STIM1 is the calcium sensor of the ER. If the calcium concentration in the ER decreases, STIM1 couples to Orai1, the CRAC-ion channel and lets calcium pass into the cell.

The calcium-channel blockers of the company Glaxo Smith Kline (GSK) were tested on the both proteins STIM1/Orai1. To exclude, that these substances inhibit CRAC/ STIM1-Orai1 currents indirectly, I tested their effects on cells containing no artificially introduced proteins for influence on intracellular calcium levels upon calcium store depletion in dependence of the blockers. No influence could be detected, suggesting that an indirect effect on CRAC/ STIM1-Orai1 can be excluded. In addition I detected that cell-specific CRAC entry was reduced by the blockers, in correlation with the diminished calcium currents of STIM1/Orai1 proteins.

In the second part I dealt with the regulation of ligand-gated ion channels, the transient receptor potential channels, in particular (TRPC1, canonical) and (TRPV6, vanilloid).

On the one side TRPC1 alone showed after the store-depletion no calcium entry into the cell. On the other side I demonstrated that TRPC1 co-expressed with TRPV6 induces a reduced calcium influx into the cell. This shows a possible co-regulation of TRPV6 with TRPC1, which confirms the results of my colleagues employing the patch-clamp- and FRET-experiments.

In the last part I investigated mutations in the cardiac ryanodine-receptor (RyR2), which can lead to a higher open probability of the RyR2 channel as well as a spontaneous calcium release from the sarcoplasmic reticulum (SR).

In consequence it can lead to ventricular tachycardia (VT) and finally also to sudden death. The cells try to keep a low intracellular concentration, but the mutations can trigger an abnormal sarcoplasmic reticulum calcium increase. I investigated HEK293 cells with RyR2 alone or co-expressed with RTN1A. In the presence of RTN1A a decreased calcium release via RyR2 was detected. The results indicate an inhibitory effect of RTN1A on the RyR2 activity.

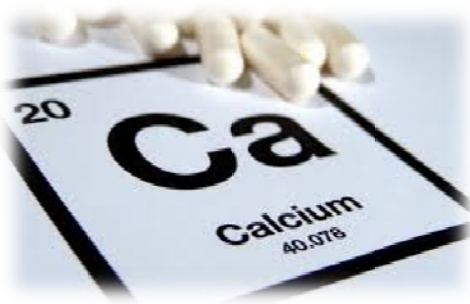
Summing up my results display a significant contribution to the function of different ion channels and to the basic knowledge of calcium signaling pathways.

4 Introduction

4.1 Calcium, Calcium homeostasis – physiological functions

4.2 Calcium signaling and transduction pathways

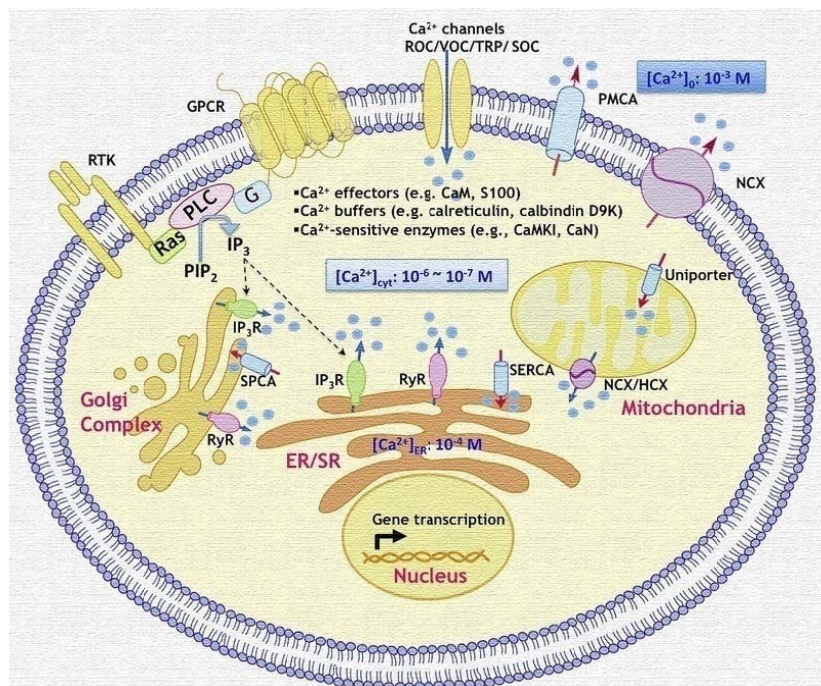
Calcium (Ca^{2+}) is a very important signal system and regulates a bright spectrum of different cellular processes. It triggers processes from gene transcription, cell proliferation over muscle contraction until exocytosis at synaptic endings. This signaling system is always remodeled to get for each cell type the best condition. An important factor is the calcium sensitive protein phosphatase CaN (calcineurin), which activates the transcription factor NFAT (nuclear factor of activated T-cells). An abnormal calcium signaling remodeling involves a number of major diseases such as heart disease, schizophrenia, BD (bipolar disorder) and AD (Alzheimer's disease) [1].



4.2.1 Intracellular Ca^{2+} Signaling

Figure 4-1:

Calcium signaling machinery at a glance[2]



A very important mechanism for intracellular calcium disposal into other compartments is the phosphoinositide (PI) pathway, whereby G protein-coupled receptors (GPCRs) initiate phospholipase C β (PLC β) and tyrosine kinase receptors (TKR) trigger PLC γ . The signaling cascade results into sharing phosphatidylinositol

4,5-bisphosphate, (PIP_2) to 1,4,5-inositol trisphosphate ($\text{Ins}(1,4,5)\text{P}_3$ or IP_3) and in the same reaction, produces diacylglycerol (DAG).

DAG, the second messenger signaling lipid is the famous stimulator of protein kinase C (PKC), but also a key player in calcium signaling.

After IP_3 binding to the IP_3 receptor (IP_3R), which is found in the ER membrane, intracellular calcium level increases [3]. Diacylglycerol (DAG) is phosphorylated by a calcium sensitive DAG kinase to produce phosphatidic acid, while DAG lipase converts DAG to arachidonic acid (AA) (Figure 4-1).

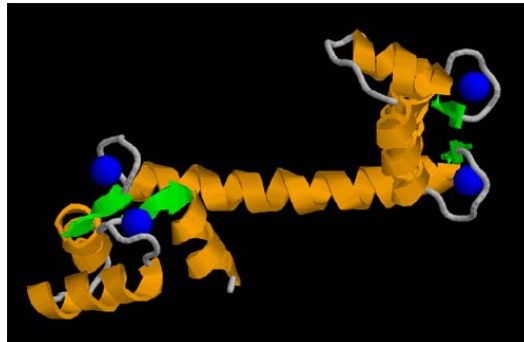


Figure 4-2:

Calmodulin – calcium: blue, alpha-helices: orange, beta-sheet: green [4]

When calcium binds the conformation of the Calmodulin domains convert. It is activated by phosphorylation pathways. Calmodulin has four EF-hand motifs, each with affinities for calcium and each plays an important role for binding of calcium (Figure 4-2).

Phosphatidylinositol 4,5-bisphosphate (PIP_2) and Calmodulin (either calcium bound or free) are both highly negatively charged, but Calmodulin is soluble and cytosolic and in addition PIP_2 is bound to inner leaflets of plasma membranes by its acyl chains.

Calcium Pumps and ion exchangers are essential for signaling

There are two kinds of ATPase pumps. The sarcoendoplasmic reticular calcium ATPases (SERCA pumps) push two calcium into the endoplasmic reticulum (ER) or in the other way, the plasma membrane calcium ATPases (PMCA pumps) push one calcium per adenosinetriphosphate (ATP) hydrolyzed in the extracellular space (Figure 2-3) [5].

Other mechanisms are the $\text{Na}^+/\text{Ca}^{2+}$ - and the $\text{Na}^+/\text{Ca}^{2+}$ - K^+ exchangers which replace one calcium ion for three sodium ions or cotransport one potassium ion with one calcium ion in exchange for four sodium ions.

The PMCAs, which have a high-affinity and low-capacity and are effective over a long duration and the $\text{Na}^+/\text{Ca}^{2+}\text{-K}^+$ exchangers with low-affinity and high-capacity complement one another.

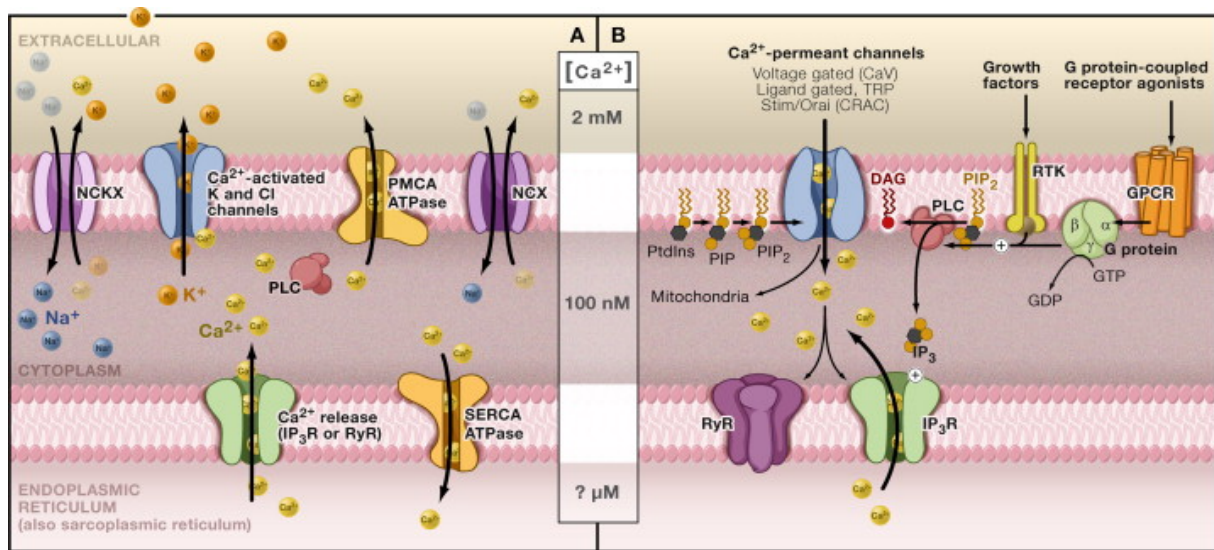


Figure 4-3:

Ca^{2+} pumps and ion exchangers are essential for signaling

(A) Resting cell: the cytoplasmic Ca^{2+} concentration level is maintained at 100 nM via plasma membrane Ca^{2+} ATPase and endoplasmic reticular Ca^{2+} ATPase transporters. The $\text{Na}^+/\text{Ca}^{2+}$ exchanger is exchanging three Na^+ ions for one Ca^{2+} . Intracellular Ca^{2+} hyperpolarizes many cells by activating K^+ channels and sometimes Cl^- channels. This decreases voltage-dependant Ca^{2+} channel activity but increases the driving force across Ca^{2+} -permeant channels. **(B)** Excitatory Ca^{2+} signaling: the plasma membrane ion channels are triggered to open by changes in voltage, extra- or intracellular ligand binding. Initial increases in Ca^{2+} concentration trigger more release, mainly from the endoplasmic reticulum via ryanodine receptors. G-protein coupled receptor or receptor tyrosine kinase-mediated activation of phospholipase C (PLC) cleaves phosphatidylinositol bisphosphate (PIP_2) into inositol trisphosphate (IP_3) and diacylglycerol (DAG). IP_3 is a ligand for the intracellular IP_3R channel located in the membrane of the endoplasmic reticulum [5].

Ligand-gated channels (TRP), Stim/Orai channels (CRAC), Ryanodin channels (RyR) and Voltage-gated calcium-selective channels (CaVs)

The mechanism of the channels works with a paddle-shaped helix-turn-helix loop with positively charged residues. When there is a run in charge, the paddle moves and the channel “gate” opens.

Transient receptor potential (TRP) ion channels are build by tetrameric assembly around a pore and are placed in intracellular membranes. Most of the TRP are ligand-gated, nonselective ion channels. The family of transient receptor potential (TRP) channels consists of 28 mammalian channels and can be classify in seven main subfamilies, where the TRPC (Canonical) family come to the fore. They are activated by PLC and can works, in some cases, as SOCs. It's important to mention, that they “can”, because it's differing to I_{CRAC} channel.

Store-Operated Calcium Entry; the Stim/Orai Channel (SOC) Mechanism

Store operated calcium channels, or SOCs, is the most receptor-activated calcium entry pathway in non-excitable cells and mediates pivotal functions in correct gene expression, cell growth, differentiation, secretion and calcium homeostasis[6].

Calcium passes across the cell membrane through the endoplasmic reticulum (ER) into the cytoplasm continuously and SERCAs pump it back into the ER. If the SERCA pumps are blocked, in the ER there is calcium depletion and a calcium entry mechanism is activated, it is the so called store-operated calcium entry (SOCE pathway). The SOC pathway is just activated by calcium store depletion. That sets this pathway apart from other signaling pathways and beyond all question that the ER has to be in contact with the plasma membrane during the calcium release. This question and others were all answered after the discovery of the presence of SOCs. In 1986, James Putney proposed in his fundamental review the mechanism of regulated calcium entry in non-excitable cells, a concept of capacitative (later termed store-operated) calcium influx [6, 7].

The most well-known, explored SOC, is the calcium release activated calcium (CRAC) channel, electrophysiologically considered to characterize the molecular basis, the calcium release-activated calcium current, or I_{CRAC} , which has been first found in mast cells, where CRAC channels play essential roles [8, 9]. Not only in mast cells for degranulation, but also in T lymphocytes are these channels necessary for activation [10-13]. Calcium current, or I_{CRAC} , is the biophysical fingerprint of the cell by patch clamp studies. It is a non-voltage-gated current and the main characteristics are, that this current has an exceedingly high sensitivity for calcium linked with a very low conductivity [6, 14]. In the switching on of the I_{CRAC} channel the two proteins, STIM1 and Orai1 play key roles.

In 2005, STIM1 (Stromal interaction molecule 1) has been discovered as the mammalian ER calcium sensor [15, 16] and regulator of the store-operated calcium influx and CRAC function and shortly after in 2006 the discovery of Orai1/CRACM1 as an essential member of the mammalian CRAC channel succeeded [17-19]. Since these breakthroughs, especially reached with RNAi-Screens, STIM1 and Orai1 are directly connected to the CRAC machinery but key questions stayed open, like, is Orai1 part of the CRAC channel itself? How does STIM1 activate Orai1 at the ER-plasma-membrane-junction?

STIM1 is a single transmembrane-spanning domain protein, aggregates in the ER below Orai1, a four-transmembrane domain protein, in the plasma membrane. Orai1 turns out to be I_{CRAC} channel itself and by this way the Stim/Orai complex is activated.

To answer the basal question: How does STIM1 initiate Orai1 at the ER-plasma-membrane-junction? 2008 a study has demonstrated that STIM1 oligomerization, hence rearrangement

of STIM1 and Orai1 and derived from a modification in the intracellular calcium level. This chain of events results in the activation of CRAC channel[20]. In 2009 a study highlighted two domains of the whole STIM1-structure, which are jointly responsible for building the STIM1-Orai1 complexes. That needs the C-terminal polybasic domain of STIM1 and the 107-aa CRAC activation domain (CAD) of STIM1.

First the C-terminal polybasic domain of STIM1 is necessary for STIM1 targeting to ER-PM junctions in lack of Orai1. Second, a highly conserved 107-aa CRAC activation domain (CAD) of STIM1 was identified, which binds directly to the N and C termini of Orai1 to open the CRAC channel. In addition to this study it has been detected that the coupling of STIM1 and Orai1 is crucial for the rearrangement, clustering and initiating of CRAC channels after calcium store depletion. The research results of this study with STIM1 mutants also specify clearly that clustering and activation of the CRAC-channel are two separate processes[21].

Yet another point to note, that the formation of punctae by STIM1 and Orai1 is contingent on coexpression of both proteins. In particular, STIM1 works independent of Orai1, but Orai1 needs to be associated with the binding regions of STIM1, that both proteins form colocalized punctae after store depletion, that activates I_{CRAC} in HEK293[22]. That controls CRAC channel activation.

Because of the particular importance of STIM1 and Orai1 the topics will be discussed in detail after (below).

4.3 Structure and stoichiometry of STIM1 and Orai proteins

4.3.1 Stromal Interaction Molecule 1 (STIM 1) – a sensitive ER-located Ca^{2+} sensor

STIM1 the protein, which is responsible for the Ca^{2+} store depletion-mediated Ca^{2+} influx, this protein is part of a family with two members (STIM1 and STIM2). It contains an **N-terminal ER luminal Ca^{2+} binding EF-hand**, a single transmembrane domain, and a long cytosolic C-terminal part. The **EF-hand**, a helix-loop-helix motif with negatively charged residues, binds Ca^{2+} and senses the luminal Ca^{2+} concentration.

A sterile-alpha motif (SAM), including two N-linked glycosylation sites, is situated after the EF-hand luminal and is next to the transmembrane domain (Figure 4-4).

The long **cytosolic C-terminal part** is responsible for interaction with and activation of Orai1 channels and endogenous CRAC channels. Necessary in special are the coiled-coil domain and lysine –rich regions.

STIM1 is affiliated in the ER membrane and sense calcium via an EF hand calcium-binding site located in the lumen of the ER. This sensor protein first aggregate, the aggregation comprises four STIM1 proteins. Following ER store depletion than the STIM1 oligomers distribute into punctuate clusters next to the plasma-membrane, where the clusters play a

decisive role for STIM1/Orai1 coupling, CRAC channel activation and refilling the calcium stores.

In detail the cytosolic STIM1 C terminus makes interaction with the crucial important putative coiled-coil domain structure in ORAI1 and both activate channel function, they generate calcium inward currents, now without ORAI1-STIM1 cluster building. The key component is the coiled-coil domain of ORAI1[23].

STIM2 the second protein of the STIM family, which is just expressed in mammals, not in worms and flies[15, 16], has about 61% equality in structure to STIM1 and differ substantially in their C-terminal region after the ERM/coiled-coil domain [24]. STIM2 is capable of initiating Orai1-3 [25]. STIM2 is also activated with the EF-hand, but has a lower calcium sensitivity and regulates the basal influx of calcium.

In addition to homomeric STIM1-STIM1 interactions, this protein can also build interactions with STIM2, so-called heteromers [26, 27]. STIM2 aggregates only like STIM1 when calcium is available[24] and this is based on the different binding rate between STIM1 and STIM2 to the EF-hand [28].

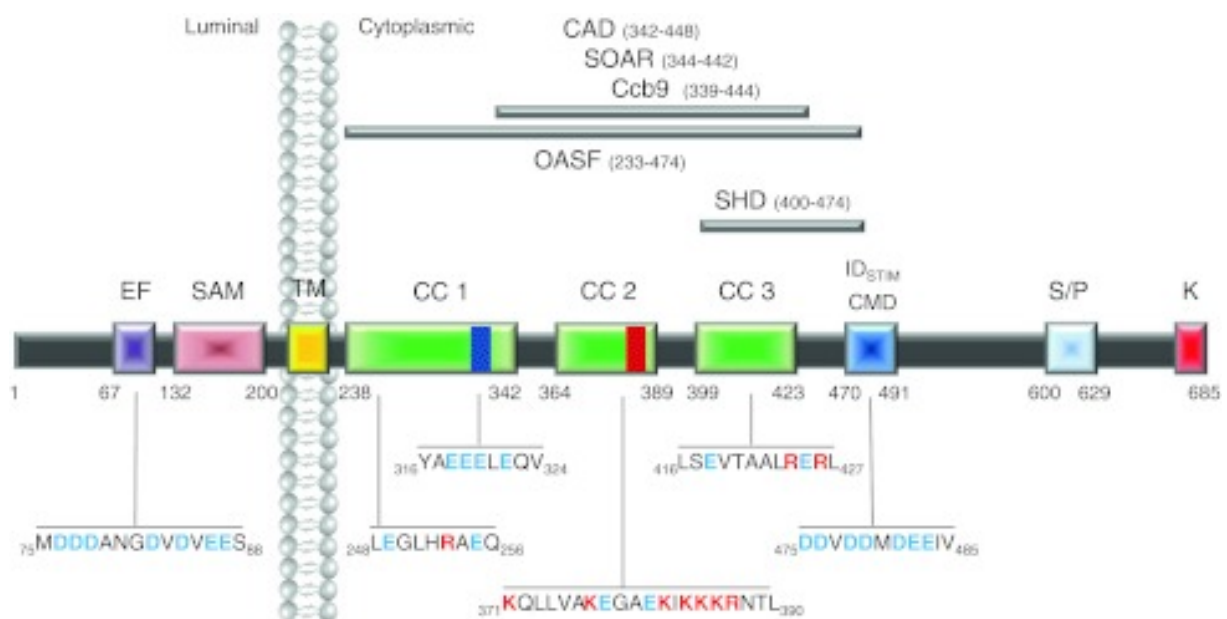


Figure 4-4:

Functional domains of human STIM1. From left to right: EF canonical/hidden EF-hand motif, SAM sterile alpha motif, TM transmembrane domain, CC1/CC2/CC3 coiled-coil domains 1–3, CMD CRAC modulatory domain, ID_{STIM} inactivation domain of STIM1, SHD STIM1 homomerization domain, S/P serine/proline-rich region, K polybasic cluster. The minimal functional regions within STIM1 are highlighted on the top: CAD CRAC activating domain, SOAR stim Orai-activating region, Ccb9 coiled-coil domain region containing region b9, OASF Orai-activating small fragment. The respective sequences include amino acids that have been reported to play a crucial role in STIM1 activation and function (charged amino acids are highlighted in blue (-) or red (+))[29]

4.3.2 Orai – the pore-forming promoter

Orai1 is part of a family including three homologs (Orai1, Orai2, and Orai3). Each contains a cytosolic N terminus, four transmembrane (TM) segments linked by two extracellular and one intracellular loop, and a cytosolic C terminus. A recent released paper in 2012 has shown the eagerly awaited crystal structure of Orai1, that the channel is formed from a hexamer of six Orai subunits arranged around a central axis[30].

All three Orai proteins form highly Ca^{2+} -selective channels within the plasma membrane. They have also in common that in their C terminus is a putative coiled-coil domain, a so-called protein interaction motif (Figure 2-5). In recent studies, it is occupied, that the cytosolic C-terminus of Orai1 is indispensable for STIM1 coupling and afterwards in initiating CRAC currents (I_{CRAC}). The N-terminus in conjunction with the key amino acid arginine in position 91 arranges first the (open-close mechanism) gating than the coupling with STIM1[23, 31].

The extracellular loop between the third and fourth transmembrane segment contain an N-glycosylation site [32, 33], but it is not necessary for the functionality of the Orai1 protein[34]. Another common characteristic is, that Orai proteins can form homo- as well as heteromers [31, 35]. A latest study[36] describes the necessity of oligomerization of Orai1 subunits, because assessments of four Orai1 subunits build the component for the functional CRAC channel.

For the high calcium selectivity of Orai pores, the negatively charged residues of transmembrane domain one and three, but also the first loop domain, are responsible[33, 37-39].

Orai 1, 2, and 3 have the same behavior concerning their inactivation profiles and 2-aminoethyldiphenyl borate (2-APB) sensitivity. 2-Aminoethoxydiphenyl borate (2-APB) is a reliable blocker of store-operated calcium entry but an inconsistent inhibitor of InsP_3 -induced Ca^{2+} release.

A natural single point mutation at position 91 (ORAI1R91W) involving in impaired T-cell signaling, which leads to severe combined immunodeficiency (**SCID**) syndrome[40-42]. This point mutation (R91W) has devastating effects on the SCID patients. It destroys I_{CRAC} in human T-cells[11, 17-19], but how it works isn't clear until yet. This Orai1 R91W mutant causes after passive store-depletion a fully loss of store operated calcium entry or rather current activation[17, 43, 44]. The complete lack of store operated function of Orai1 R91W is linked to a retained coupling to STIM1, hence interference in permeation/gating[43].

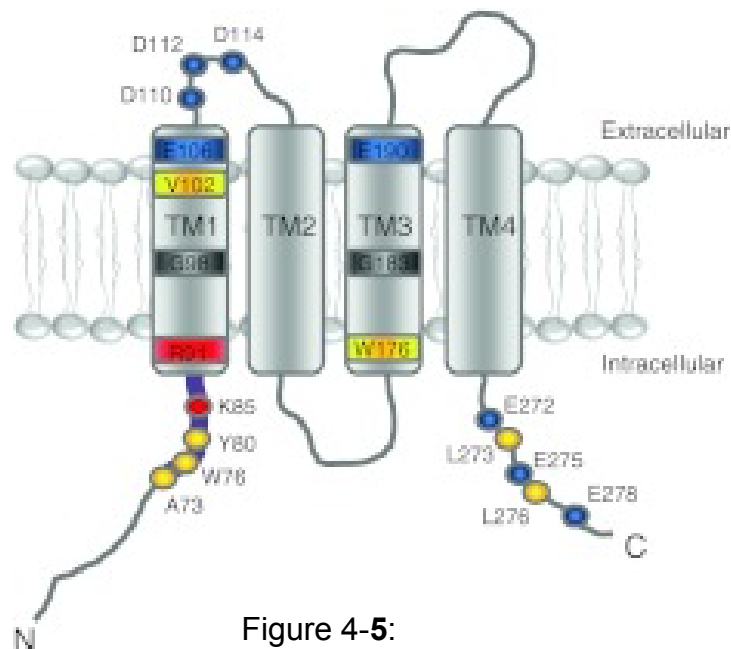


Figure 4-5:

Functional domains of Orai1.Representing of a single Orai1 subunit with selectively *highlighted* residues that are critical for channel function (*blue* (-), *red* (+), *yellow* (hydrophobic)). In detail, the conserved region (*thick purple line*) on the distal end of the amino terminus contains crucial amino acids for channel gating (K85, R91) as well as Ca^{2+} -dependent CaM binding (A73, W76, Y80). Transmembrane domain 1 (TM1) buries the pore-forming residues and the selectivity filter whereas transmembrane domain 3 (TM3) might allosterically affect channel gating. The carboxyl terminus comprises charged (E272, E275, E278) as well as hydrophobic (L273, L276) amino acids that possibly account for coiled-coil domain formation and STIM coupling[29].

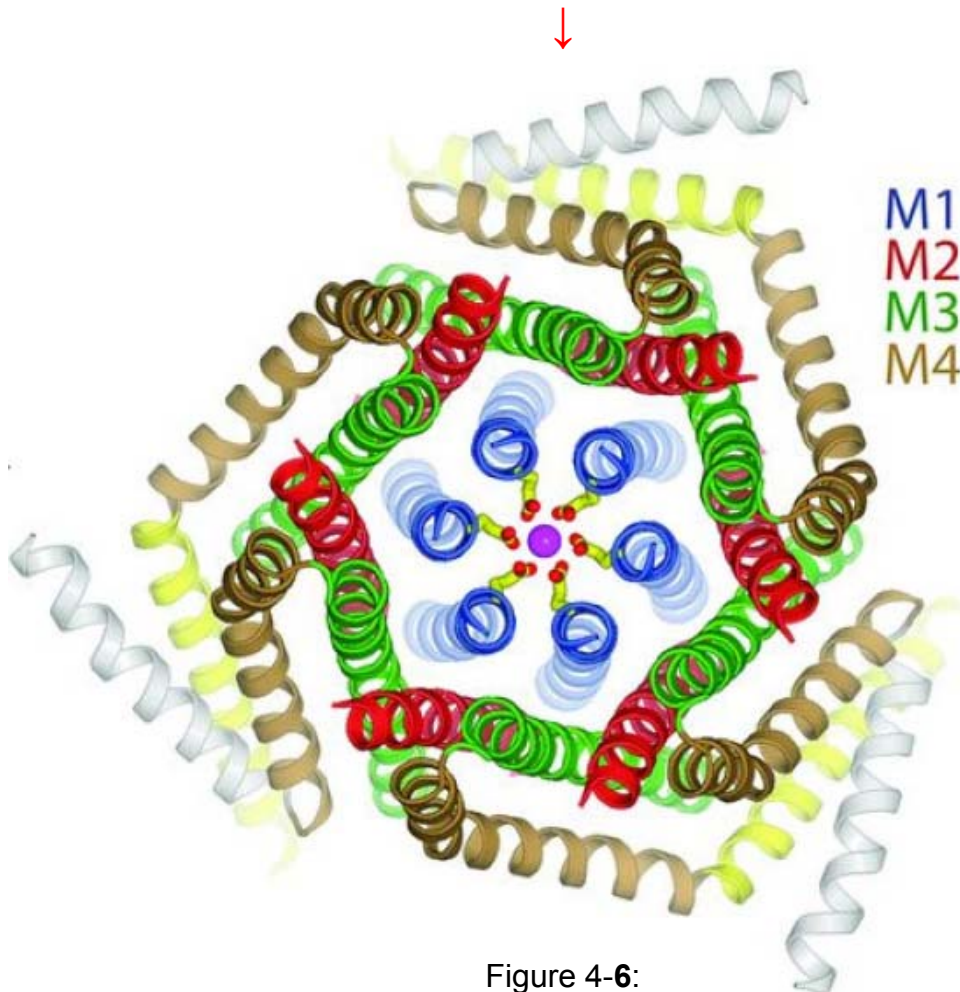


Figure 4-6:

Crystal structure of Orai. Orthogonal view of the Orai-channel from the extracellular side. The TM1 are highlighted in blue, calcium in magenta and the glutamate residues in yellow[30].

4.4 Calcium release-activated Calcium (CRAC) channel, structure and function – The CRAC coupling machinery

It took over 20 years to do intense research, to find out which molecular components are definitely part of the CRAC channel and how the signalling machinery works. In these studies the molecular choreography of the CRAC channel transpired provoking. The first channels which give consideration to be part of CRAC channels, were proteins of the canonical transient receptor potential (TRP) family[6], especially from the TRPV = Vanilloid family, the member TRPV6=CaT1. Different groups did research on this question: Is CaT1 the molecular basis of CRAC? To sum up it could be said, after intense work with siRNA, that you cannot equate CaT1 with CRAC, and the CaT1 protein is not a subunit of CRAC. None of the tested ion channels of the TRP family showed all of the electrophysiological and pharmacological characteristics like CRAC currents.

By the actual state of scientific knowledge, the big breakthrough was in 2005 and shortly after 2006, two components are necessary and are parts of the CRAC channel machinery. On this account the CRAC channel is also known under the designation STIM1/Orai1 complex. Consequently STIM1 and Orai1, the two proteins are the putative key components of CRAC. So far, the detailed mechanism of the direct delivery of information of STIM1 to the calcium release-activated calcium/ORAI1 channel is still featureless [23]. But to clarify the interaction between these two proteins, the Förster resonance energy transfer (FRET) technique was used. The Confocal FRET Fluorescence microscopy has the advantage that this technique detects interactions between proteins in a distance <10 nm. The results show that STIM1 and ORAI1 interact, which results in calcium influx[23].

These results, to identify the components and characterize the calcium (Ca^{2+}) release-activated calcium (CRAC) current, or I_{CRAC} , in mast cells[8] as well in Jurkat T-Cells[45, 46] have facilitated the practice of the patch-clamp technique. The biophysical characteristics of the CRAC channel declare a high sensitivity for calcium, an improving current/ voltage relationship into the cell and an exponentially low single channel conductivity[6].

Under resting conditions STIM1 is homogeneously distributed within the ER membrane [16, 47] and the N-terminal EF-hands of STIM1 sense the luminal calcium concentration [15, 16]. In response to store-depletion, hence a low luminal calcium level, STIM1 proteins oligomerize at junctional ER sites close to the plasma membrane[15, 20, 22, 47-50]. As a result of, STIM1 clusters in punctae and this leads to the activation of CRAC channels. The cytosolic C-terminal region, in special the second coiled-coil domain [51] of STIM1 interacts with Orai and induces the activation of CRAC/Orai. The second coiled-coil domain (CC2) and part of

the third coiled-coil domain (CC3) in particular the following STIM1 C-terminal portions, all including the similar sequences play a crucial role for activation and coupling to Orai proteins: CAD: CRAC activating domain (aa 342-448), SOAR: STIM Orai-activating region (aa 344-442), OASF: Orai-activating small fragment (aa 233-450), Ccb9: coiled-coil domain region containing region b9 (aa 339-444)[21, 52-54].

In Orai1 additionally to the C-terminus also the N-terminus is involved in CRAC channel initiation[21]. The C-terminal coiled-coil interaction domain of Orai1 includes acidic residues, whereas the second coiled-coil domain of STIM1 contains in the majority of basic residues. The combination of acidic and basic amino acids initiate STIM1/Orai coupling [55-57]. Highlighted in the Orai N-terminus for coupling activation is the single residue aa K85 [58]. If Orai1 includes K85E (O3 K60E), Orai channels have lost their activation and coupling mechanism [58].

STIM1/Orai complexes display co-clustered puncta in the plasma membrane (6, 68, 71, 80), which triggers calcium influx into the cell (to replenish the calcium store). Eight STIM1 and four Orai molecules together form the complex for the highest calcium influx[59].

4.5 An introduction in Transient receptor potential (TRP) channels

Transient receptor potential (TRP) channels have been first discovered in a *Drosophila* mutant in 1969[60]. In the photoreceptor cell of the TRP deficient fly, the channel emits transient instead of sustained response to bright light, as a result, *trp* (*transient* receptor potential)[61]. The first *trp* gene has been cloned in 1989[62].

The family of transient receptor potential (TRP) channels consists of 28 mammalian channels and can be classified in seven main subfamilies: the TRPC (**C**anonical) family, the TRPV (**V**anilloid) family, the TRPM (**M**elastatin) family, the TRPP (**P**olycystin) family, the TRPML (**M**ucolipin) family, the TRPA (**A**nkyrin) family and the TRPN (**N**OMPC) family[63-68] (Fig. 2.7). The TRP channels have been arousing interest, because some members of the family could function as intracellular calcium release channels (e.g. TRPV1 und TRPM8) supplementary as plasmalemmal calcium channels [69, 70]. All TRPC proteins are built of six transmembrane domains (TM1-TM6) with a so-called re-entrant pore-lining loop located between the 5th and 6th transmembrane segments form homo- or hetero-tetramers and form cation selective channels [71].

TRP channels can be stimulated in different ways by intra- und extracellular messengers, chemical, mechanical, and osmotic stress, and by depleted intracellular calcium stores[66]. All TRPCs have a sequence homology of minimum 20% and have together consensus sequences which are contact points for serine/threonine and tyrosine kinases[71].

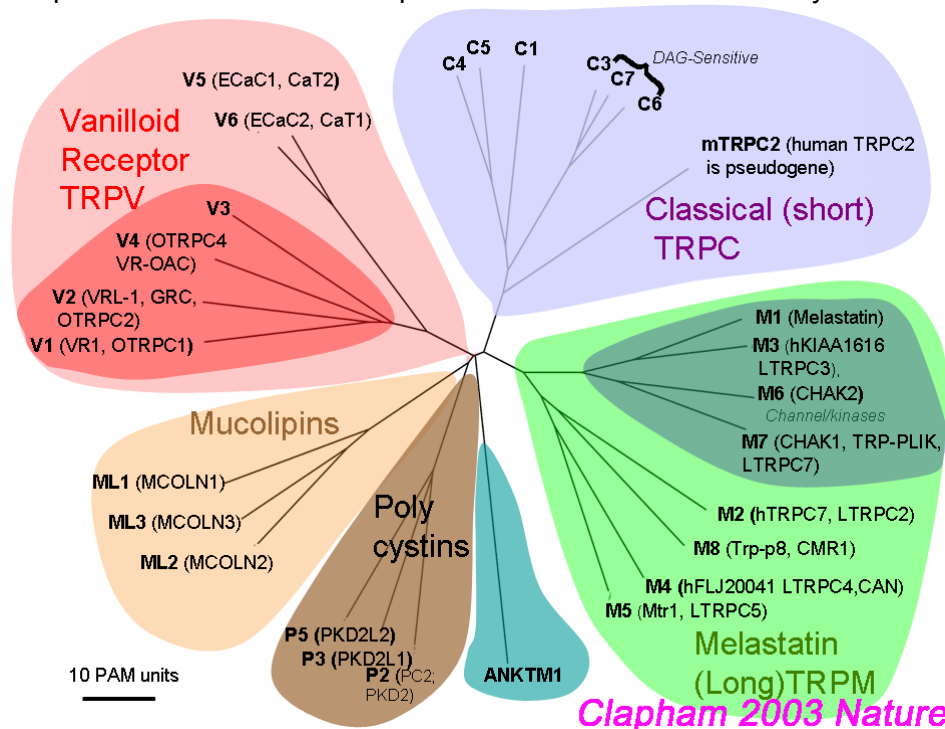


Figure 4-7: **Mammalian TRP family tree.** The evolutionary distance is shown by the total branch lengths in point accepted mutations (PAM) units, which is the mean number of substitutions per 100 residues[66].

4.5.1 The TRPC family – The “canonical” TRPCs

This mammalian TRPC family which includes seven channels is splitted in four subfamilies, based on sequence similarities: TRPC1, TRPC2, TRPC3/6/7 and TRPC4/5.

Function and tissue expression of members of the TRPC family

TRPC1 is an essential intracellular located channel [72], ubiquitously expressed [71] and this channel has become associated to be a molecular candidate for SOCs [73][74-81].

TRP channels are formed by tetramers of six transmembrane (TM) domain subunits which include a pore between TM5 and TM6 (Figure 4-8 A) [82].

TRPC1 build *heterotetramers* (Figure 4-8 B), possibly with TRPC4, TRPC5 [83] and TRPC3 and TRPP2 subunits in vascular tissues. These interactions are essential in trafficking or translocation of TRPC1 to the plasma membrane [84].

Caveolin 1 has a crucial role in localization of TRPC channels to the plasma membrane. Furthermore, the caveolin-scaffolding domain (CSD) (Figure 4-8 A, orange colour) facilitates in interactions between TRPC channels and caveolae and is involved in activation and/or inactivation of SOCE [85].

The TRP-box, a 23-25 amino-acid-long region, is also a very important domain of TRPC1. The TRP-domain is located just after S6 (Figure 4-8 A, lime-green colour) and participates in subunit assembling or allosteric modulation of channel gating [86].

TRPC2 is a pseudogene in humans [87][88] but in rodents it is highly expressed in the dendritic tip of the vomeronasal sensory neurons which is important for pheromone detection [89]. TRPC2 is found in spermatozoa, where it is important for calcium signaling upon stimulation by egg ZP3 [90].

TRPC3/6/7 structures form a receptor-operated, DAG-stimulated, constitutively active channels [87] and appear in the brain and in smooth and cardiac muscle cells [66, 72]. G-protein coupled receptors trigger phosphoinositide (PI) pathways to activate these channels. The channels are activated by the second messenger diacylglycerol (DAG) and protein kinase C (PKC) activation [3]. This subfamily is also called as *DAG-sensitive* TRPC-channels [87].

TRPC4 is well expressed in endothelium [91, 92], smooth muscle [93], supposedly in intestinal pacemaker cells (ICC, intestinal cells of Cajal) [94, 95], in many brain regions [72], in kidney [96] and in adrenal gland [97].

TRPC5 is broadly expressed in brain and multiple other tissues [72].

Figure 1

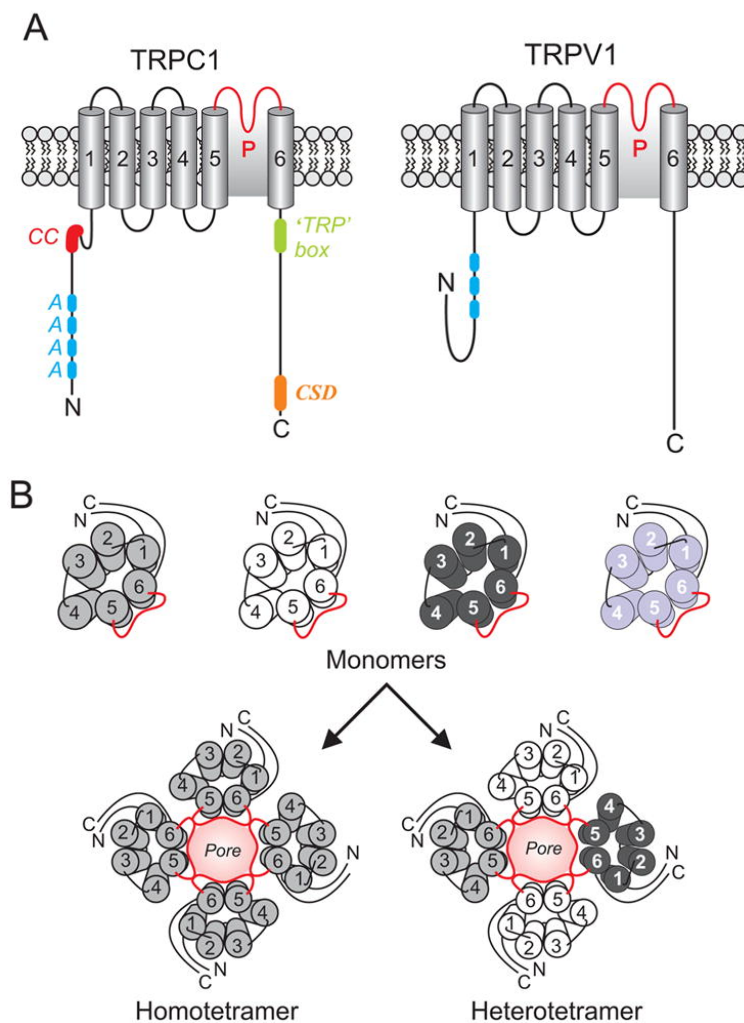


Figure 4-8:

Structure of TRP Channels. (A) Topological structure of TRPC1 and TRPV1. Six transmembrane domains (TM1–TM6), ankyrin repeats or ankyrin-like domains (A), pore region (P), TRP box, caveolin-scaffolding (CSD) and coiled-coil (CC) domains are shown. (B) Subunit arrangement of TRP monomers into functional homo- or hetero-tetrameric channels with a central ion-conducting pore[98].

4.5.2 The TRPV (vanilloid receptor) subfamily

The TRPV (“vanilloid”) family is structured in four groups of mammalian TRPVs: TRPV1/TRPV2, TRPV3, TRPV4 and TRPV5/6 based on sequence similarities[99, 100].

TRPV1-4 are nonselective cation channels functioning as sensors and TRPV5/6 are calcium-selective channels and contribute to the calcium controlled progresses[101].

A short overview of the members of this subfamily focuses on function and tissue expression[101].

	function	high expression- distribution
TRPV1	Heat sensor	Trigeminal and dorsal root ganglia
TRPV2	Heat sensor	Brain, spinal cord, lung, spleen, intestine, kidney
TRPV3	Heat sensor	Central nervous system, spinal cord, skin, testis
TRPV4	Osmoreceptor	Kidney, trachea, salivary gland, fat, testis
TRPV5	Apical Ca ²⁺ transporter	Kidney
TRPV6	Apical Ca ²⁺ transporter	Intestine , placenta, pancreas, prostate, salivary gland, testis, kidney

Table1:

Function and tissue expression of TRPV Channels[101]

Here, I will focus especially on TRPV1 and TRPV6, because TRPV1 is the founding member of a subfamily of thermosensitive TRP channels[86] which are heat-activated. TRPV1 is the best-characterized member of the vertebrate TRP family, because of the role in pain physiology. In this context TRPV1 and the TRPVs 1-4 subfamily, which are also be activated by temperature stimuli (table 1) are considered important targets for analgesic drugs[102, 103].

My thesis focuses also on the investigations in TRPV6, which is essential for calcium homeostasis.

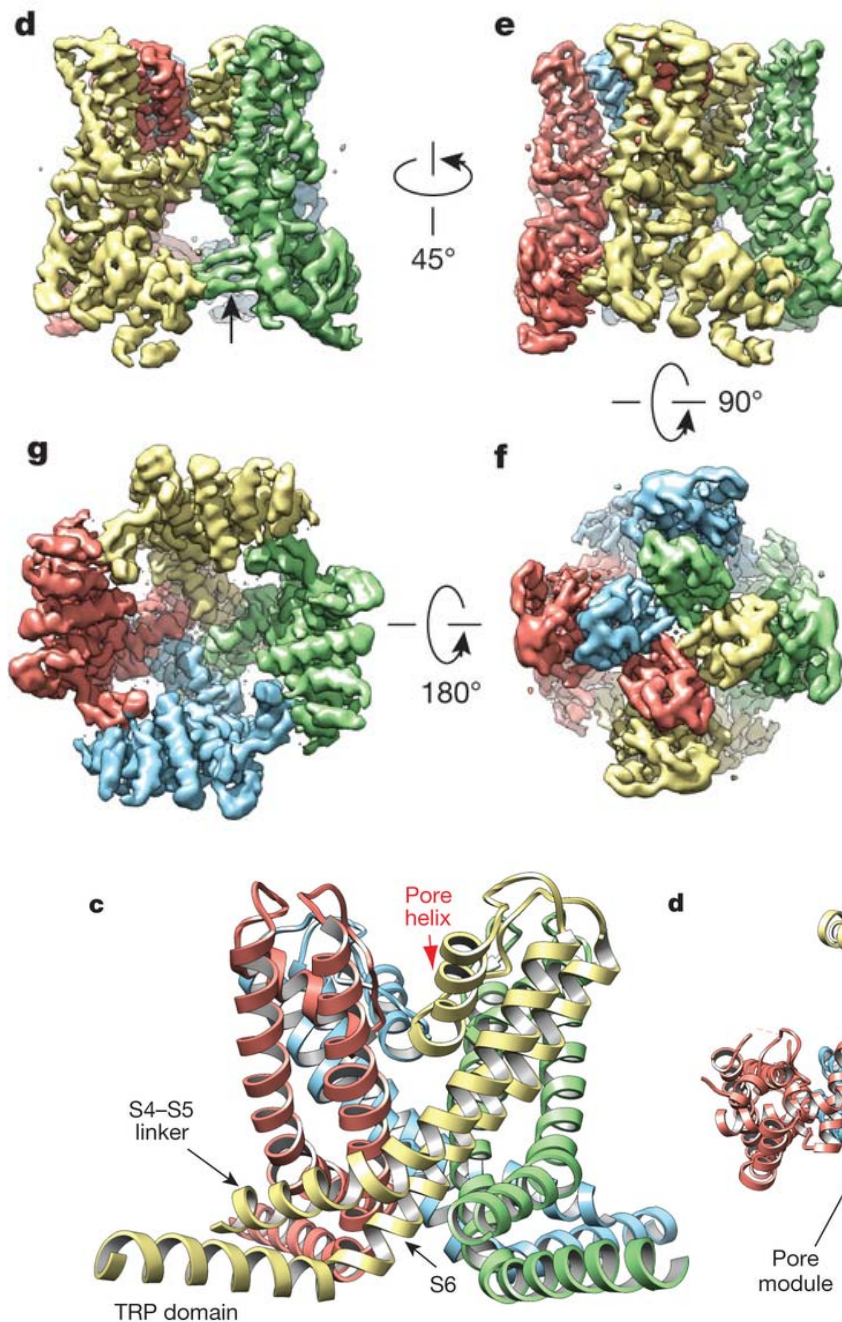


Figure 4-9:
3D reconstruction of TRPV1 determined by single-particle cryo-EM. d-g, Four different views of the TRPV1 channel are shown, from side (d, e), top (f) and bottom (g). The arrow in panel d indicates β -sheet structure in the cytosolic domain of TRPV1[86].

Figure 4-10:

c, Ribbon diagram focusing in on side view of S5-P-S6 pore with TRP domains. **d**, Bottom view focusing on transmembrane core, including S1-S4, S5-P-S6 and TRP domains [86].

The vanilloid receptor1, TRPV1, which permeates calcium and sodium through the channel[104, 105] was found in dorsal root ganglion and trigeminal ganglion neurons and is also highly expressed in spinal, peripheral nerve terminals, but also in the pancreas and non-neuronal nerve terminals[106]. This receptor provides sensation of scalding heat and pain (nociception).

Activation of TRPV1 is regulated by a wide variety of mechanical and physical stimuli and by different mechanism. On the one hand agonists such as capsaicin, resiniferatoxin, and olvanil activate the vanilloid (capsaicin) receptor. Furthermore the receptor is temperature-pH-dependent and opens the channel by heat above 43 °C and low pH ($\leq 5,9$ acidic conditions)[63, 106]. On the other hand also endogenous lipids, so called “endovanilloids”, activate TRPV1[107] like the nucleoside adenosine[108].

This channel was structurally solved using electron cryo-microscopy, at 3.4 Å resolution. The structure of the TRPV1 channel is shown in four different views (Figure 4-9). Around a central ion pathway TRPV1 features a four-fold symmetry by transmembrane segments 5-6 (S5-S6). Between these segments a loop segment forms the selectivity filter, which is bordered by S1-S4 voltage-sensor-like domains (Figure 4-10 a, b). The S1-S4 linker interacts with the TRP domain (Fig. 4-10a, yellow colour), a 23-25-amino acid-long region located just after S6. The TRP domain has been intended to exhibit crucial functions in subunit assembly or allosteric modulation of channel gating.

4.5.2.1 Vanilloid transient receptor potential 6 (TRPV6) channel

The epithelial calcium channel TRPV6, member of the vanilloid transient receptor potential subfamily, was in the old nomenclature named as CaT1/ECaC2[6, 99, 101].

TRPV6 is a constitutively active channel and is inactivated at a high intracellular calcium level above 100 nM. This calcium channel is highly expressed in the proximal intestine, pancreas, placenta, prostate and salivary gland [63, 101]. The hormonally active form of vitamin D, 1,25-dihydroxyvitamin D₃ (1,25(OH)₂D₃), a principal factor that maintains calcium homeostasis, regulates the gene expression of TRPV6 in intestine[101] and the mRNA is also expressed in Caco-2 cells, a human large intestine cancer cell line[109]. In terms of expression in prostata cells, TRPV6 is associated with cancer progression. As this gene is only upregulated in cancer cells, but not in benign prostate cells, it can be used as a prognostic marker and therefore the channel can be used as a target for therapeutic research[110].

In the TRPV family only the TRPV5 and 6 are highly calcium selective and calciumregulated channels[111-113]. Both channels are 100 times more permeable to calcium than sodium ($P_{Ca}/P_{Na} > 100$)[101]. Additional to the high inward rectifying calcium currents, TRPV6 is also permeable to other divalent ions in descending order: $Ca^{2+} \gg Ba^{2+} > Sr^{2+} > Mn^{2+}$.

In modeling based on the potassium KcsA structure suggests a pore helix with a central aspartate D541(orange coloured), for the selectivity filter. It is expected that the positive charged calcium ion binds the negatively charged side chain of the aspartate. The pore diameter of 5,4Å regulates the selectivity for calcium over other cations (Figure 4-9). In the absence of divalents TRPV5/6 become readily permeable for monovalent ions, while the trivalent lanthanide cation (La^{3+}) inhibit these channels[114].

At very low expression levels of TRPV6 it is activated by calcium store depletion. That gives reason for involvement of TRPV6 in the calcium release-activated calcium (CRAC) channel mechanism. The similarity of the TRPV6 and CRAC channel currents support the linkage to be all or a part of the CRAC pore[114]. However, it could be definitely distinguished between the TRPV6 currents and those of endogenous CRAC current by their current-voltage relationship in divalent free solution permeation[115]. Supplementary, TRPV6 and CRAC show different pharmacological effects[6].

Furthermore also TRPC1 might be a part of SOCE, but it is still in debate if TRPs, in particular TRPC1 form these calcium channels[6].

A functional TRPV6 channel is composed of four subunits that can form homo-tetramers- but also heterotetrameric complexes with TRPV5, which exhibits distinct channel properties[116]. TRPV6 consists of six transmembrane domains (TMs), cytosolic N and C

termini and a pore loop between transmembrane domains 5 and 6. The N-terminus of TRPV6 includes four ankyrin repeat domains and some PKA phosphorylation sites. The first extracellular loop includes glycosylation site. The N- as well as the C-terminus displays various predicted PKC phosphorylation sites.

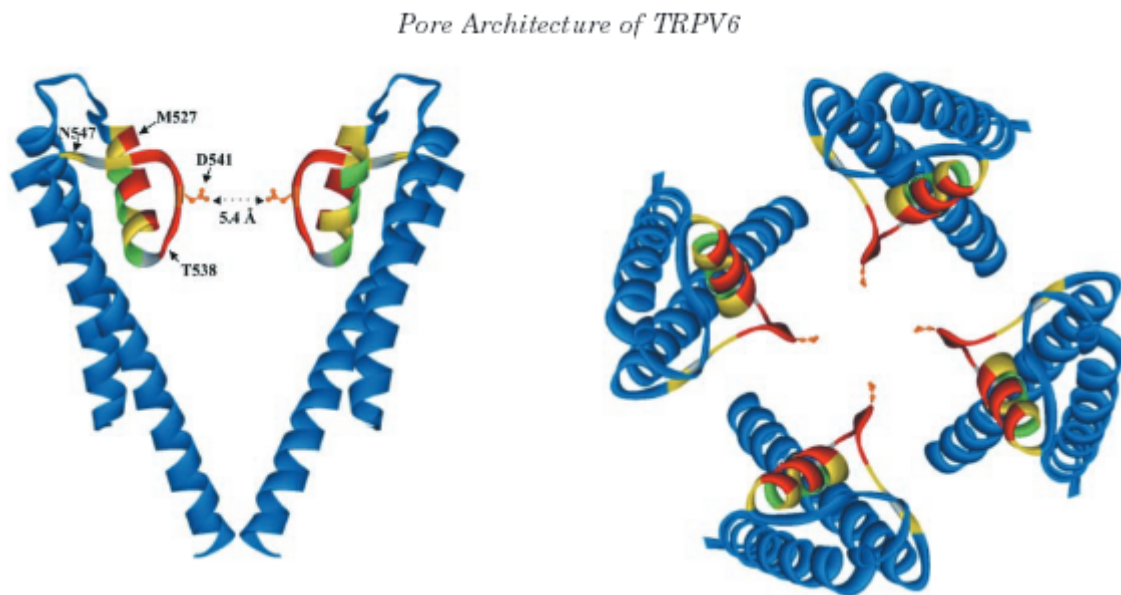


Figure 4-11:

Model of the TRPV6 pore region, based on the KcsA structure.

Two views of the structure are shown, looking sideways at two oppositesubunits (left) or looking down from the external solution to the complete homotetrameric channel[117].

4.6 Physiology of the myocardial muscle cell

In the following chapters I would like to give a summary of the importance of the calcium homeostasis of heart muscle cells and the consequence of mutations in Ryanodine receptors (RyR2). The mutations result in a calcium imbalance and trigger extraordinary oscillations. The oscillations are responsible for cardiac diseases like ventricular tachycardia and which could result in loss of life.

4.6.1 Cardiomyocytes and calcium

The cellular calcium concentration is very important for many physiological processes and plays a key role in the functionality of cells. In muscle cells the calcium concentration is significantly involved in contraction functions. Furthermore calcium is most important for the membrane depolarization at the action potential in cardiomyocytes. The consequence of which is, that the regulation of the calcium homeostasis is essential not only for the individual cells but also for the functionality of the whole organism (beating of the heart, the heart cycle).

The extracellular calcium concentration $[Ca^{2+}]_e$ is with $\sim 1,2$ mM 10.000 times higher than the cytoplasmic calcium concentration $[Ca^{2+}]_i$ (~ 100 nM) in the resting state. The luminal calcium concentration in the sarcoplasmic reticulum (SR) in muscle cells reaches high concentrations 0,5-1 mM as compared to the mitochondrion and the nuclear (it is equal to the cytoplasm concentration)[117]. In case of membrane depolarization the cytoplasmic calcium concentration $[Ca^{2+}]_i$ rises up to the 10 fold.

4.7 Cellular calcium channels

Calcium Channels are a group of transmembrane ion channels which let calcium pass through the membrane (have a permeability to the ion calcium). The channels are differentiating between voltage-dependent calcium channels (VDCCs) and ligand-gated ion channels (LGICs).

For the muscular contraction the VDCCs are most important and can be divided into: L-type calcium channels (LTCC, L for Long-lasting also named as dihydropyridine receptors; DHPRs) and T-type calcium channels (TTCC, T for Transient) [118].

A high membrane potential activates L-type calcium channels. They open more slowly and remain open longer compared to T-type channels. For this reason L-type channels are important in maintaining an action potential, while T-type channels are important in triggering them[119].

Voltage-gated calcium-selective channels (CaVs) are the fastest calcium signaling proteins and they are activated at depolarized membrane potentials. For activation there is a paddle-shaped helix-turn-helix loop containing positively charged residues (usually arginines) [120]. A change in voltage moves the paddle that the channel “gate” opens.

Via voltage-gated calcium channels calcium passes into the cytoplasm or rather in the transversal tubule and initiates the opening of the release channels for calcium in the sarcoplasmic reticulum. This process is called calcium-induced calcium release (CICR), which is further described later in this chapter. Thus calcium acts as the second messenger that goes from the voltage-gated channels to the release channels (Figure 2-10). The transversal tubules and the sarcoplasmic reticulum are not connected directly. As a consequence the excitation-contraction coupling proceeds slower in myocardial cells as compared to skeletal muscle[121].

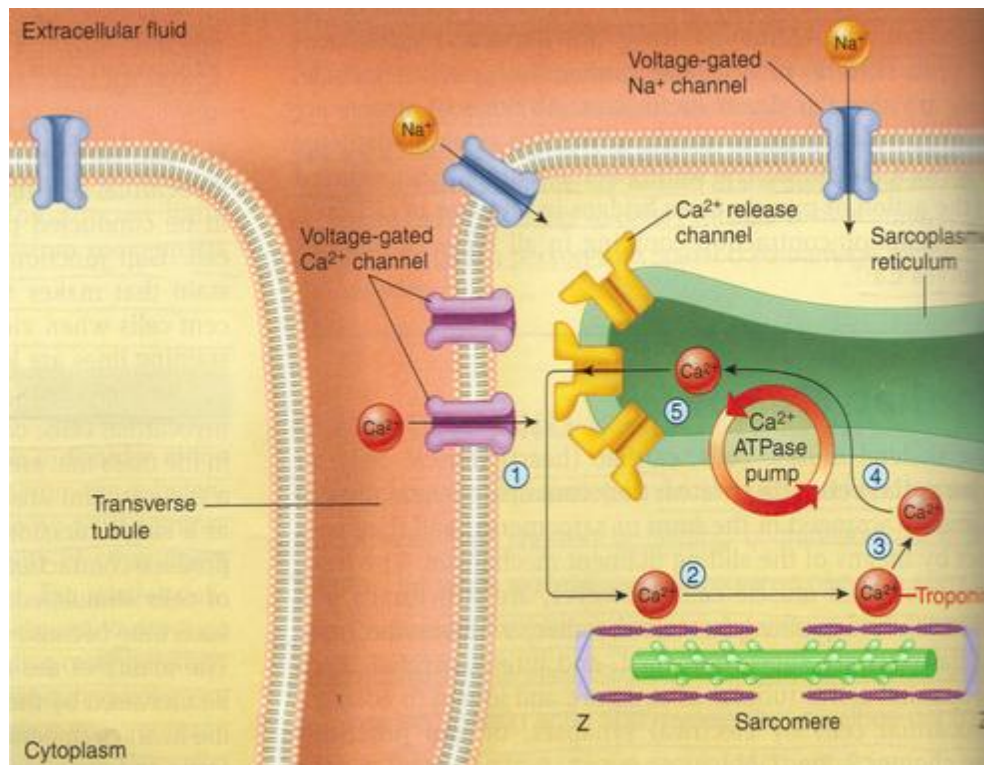


Figure 4-12:

Calcium channels play a pivotal role in muscle contraction. On each activation (depolarization) Na^+ and Ca^{2+} ions pass through Voltage-gated Na^+ - and L-Type- Ca^{2+} -channels out of the interstitium into the ventricular myocytes. Entering calcium binds to a calcium release channel in the heart muscle cells, the sarcoplasmic reticulum. This SR releases a huge amount of calcium through the second release channel, the ryanodine receptor 2 out into the cytosol and binds to the contractile proteins. In special it interacts with the regulator protein Troponin C and this leads to an interaction with myosin and actin, a shortening of the muscle and this results finally in contraction[122].

The sarcoplasmic reticulum calcium ATPase (SERCA) induces a calcium reuptake in the sarcoplasmic reticulum. By this way the process of contraction is terminated. The remaining amount of free calcium is transported through the in the plasma membrane situated sodium-calcium ($\text{Na}^+/\text{Ca}^{2+}$) exchanger (NCX) (3 Na^+ for one Ca^{2+}) or the plasma membrane calcium ATPase (PMCA) out of the cell. This progress, the calcium efflux causes relaxation[123].

The plasma membrane calcium ATPase (PMCA), the sarcoplasmic reticulum calcium ATPase (SERCA) and the plasmalemmal sodium-calcium ($\text{Na}^+/\text{Ca}^{2+}$) exchanger (NCX) are together the main regulatory processes in controlling the intracellular calcium concentration $[\text{Ca}^{2+}]_i$ and transport calcium in the extracellular space [124].

The ATPase pumps are intended for pushing on the one hand two calcium ions via the sarcoplasmic reticulum calcium ATPase (SERCA) pumps uphill into the endoplasmic reticulum (ER). On the other hand one calcium ion goes downhill out of the cell via plasma membrane calcium ATPases (PMCA) pumps.

The mechanism of action of the ATPases is to sustain low intracellular calcium concentration $[\text{Ca}^{2+}]_i$ and is controlled by ATP hydrolyses.

A second mechanism is the sodium-calcium ($\text{Na}^+/\text{Ca}^{2+}$) (NCX) exchanger. The main task of this exchanger is to transport one calcium ion out of the cell in exchange for three sodium ions during the cell's relaxation phase.

The two different mechanisms (pumps and exchanger) complement one another. The high-affinity and low capacity of the PMCAs and contrary the low-affinity and high capacity of the sodium-calcium exchanger let them work very actual sustaining low intracellular calcium concentration $[\text{Ca}^{2+}]_i$ [125].

Until now they have found two different channels which releases intracellular calcium, the inositol 1,4,5-triphosphat-receptors (IP_3R) and ryanodine receptor (RyR) [126].

The activation of the two release channels inositol 1,4,5-triphosphat-receptors (IP_3R) and ryanodine receptors (RyR) is followed by a calcium store-depletion of the SR and consequently to an increase of the cytoplasmic calcium $[\text{Ca}^{2+}]_i$.

In the heart muscle the IP_3 receptors can assume the functions of the RyR2 just in a minor degree.

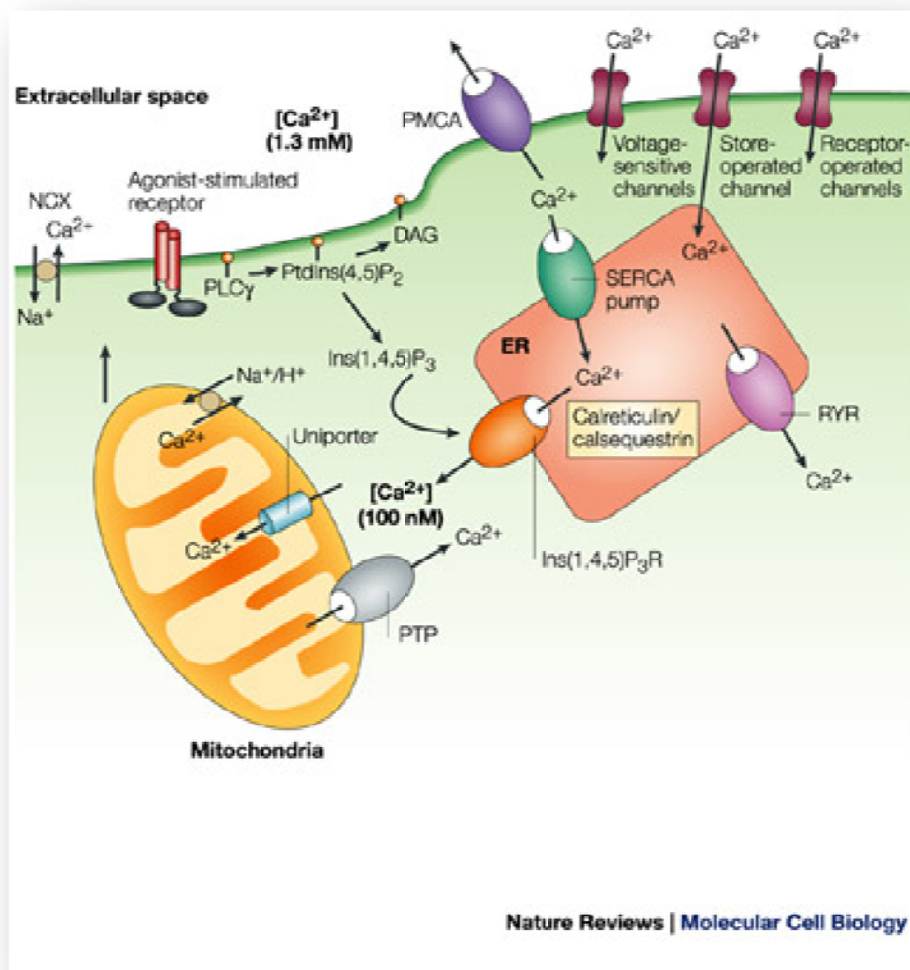


Figure 4-13:

Cellular Ca^{2+} import through the plasma membrane occurs largely by receptor-operated, voltage-sensitive and store-operated channels. The largest Ca^{2+} store in cells is found in the endoplasmic- (ER) or sarcoplasmic reticulum (SR), with local Ca^{2+} concentrations reaching millimolar levels. Ca^{2+} levels in the ER are affected by the relative distribution of sarco(endo)plasmic reticulum Ca^{2+} -ATPase (**SERCA**) pumps and of inositol-1,4,5-trisphosphate ($\text{Ins}(1,4,5)\text{P}_3$) receptors ($\text{Ins}(1,4,5)\text{P}_3\text{Rs}$) and ryanodine receptors (RYRs), as well as by the relative abundance of Ca^{2+} -binding proteins (calreticulin, calsequestrin) in the endoplasmic- or sarcoplasmic reticulum¹³⁶. The cytosolic Ca^{2+} concentration in unstimulated cells is kept at ≈ 100 nM by both uptake into the ER and Ca^{2+} extrusion into the extracellular space by the plasma-membrane Ca^{2+} -ATPase (PMCA). ER Ca^{2+} release is triggered by agonist stimulation through the generation of $\text{Ins}(1,4,5)\text{P}_3$ through hydrolysis of phosphatidylinositol-4,5-bisphosphate ($\text{PtdIns}(4,5)\text{P}_2$) operated by a phospholipase C ($\text{PLC}\gamma$). Ca^{2+} efflux from cells is regulated primarily by the PMCA, which binds calmodulin and has a high affinity for Ca^{2+} . Ca^{2+} efflux might also be mediated by the $\text{Na}^+/\text{Ca}^{2+}$ -exchanger (NCX)[127].

This chapter concentrates on the possible consequences of mutated cardiac ryanodine receptors (RyR2) channels. These mutations can lead to spontaneous action potentials, are considered as ventricular extrasystoles and this causal chain of events may trigger arrhythmias. These spontaneous calcium releases cause afterdepolarisations and an increase in the incidence of extrasystoles and sustained ventricular arrhythmias[128]. For this reason in the following pages the physiological meaning and functioning of these ryanodine receptors (RyR2) channels will be explained.

4.8 An introduction in Ryanodine receptors (RyRs) and the Reticulon/Nogo family of proteins

4.8.1 The 3 subtypes, especially ryanodine receptor 2 (RYR2) cardiac/ calcium release channel

The ryanodine-sensitive calcium channels, the biggest familiar ion channel group, also called ryanodine receptors, are intracellular calcium-release channels expressed in heart and brain and these channels have three isoforms (RyR 1-3) which have influence on the calcium signaling. They mediate the release of calcium ions from the sarcoplasmic reticulum (SR) of myocytes and trigger a cascade of events. The outcome of this is muscle contraction. But the RyRs are also necessary for neurotransmission.

The efforts to isolate RyRs from striated muscle using ^3H -ryanodin was a success and shows that RyRs form homotetramers with molecular weights of $\sim 2,2\text{MDa}$ and each monomer comprises of about 5 000 amino acids. The three Ryanodine receptor isoforms (Ryr1, 2 and 3) are present in mammals and have a common sequence identity of $\sim 66\%$. The receptor protein is a transmembrane protein, approximately about 80 percent of the protein reaches in the cytoplasm appears as foot structures. The remaining 20 percent represents the transmembrane domain and a small percentage reaches in the SR-luminal.

RyR1 has been the first studied and cloned isoform [129, 130] mostly expressed in skeletal muscle and in the cerebellar Purkinje neurons. RyR2 occurs in cardiac muscle [131, 132], but also in smooth muscle and the nervous system [133, 134]. RyR3 is found at low levels in different cell types including the nervous system and skeletal muscles of the diaphragm [134].

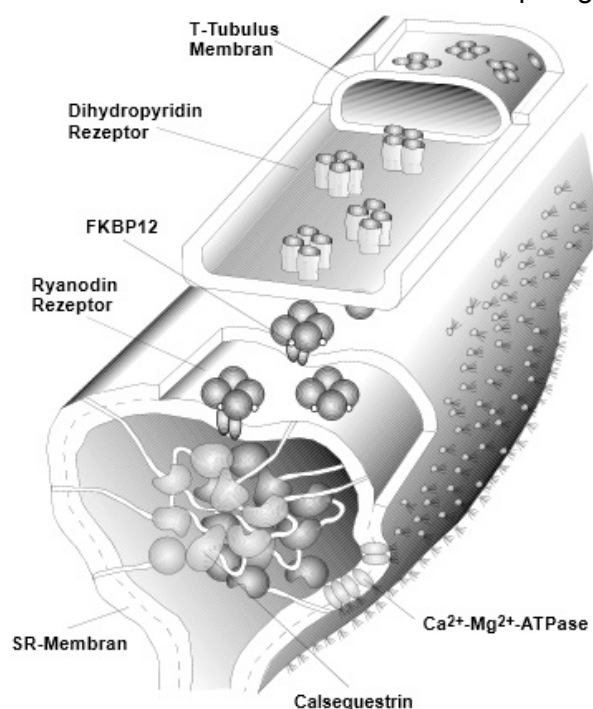


Figure 4-14

The ryanodine receptor in skeletal muscles

RyR2 channel complex (RyR2) is a homotetramer in the membrane of the sarcoplasmic reticulum (SR).

Opposite of this homotetramer are complexes of four dihydropyridine receptors situated in the membrane of the t-tubules. In the gap between the terminal cistern and the t-tubules reaches the foot structure of the ryanodine receptor [135].

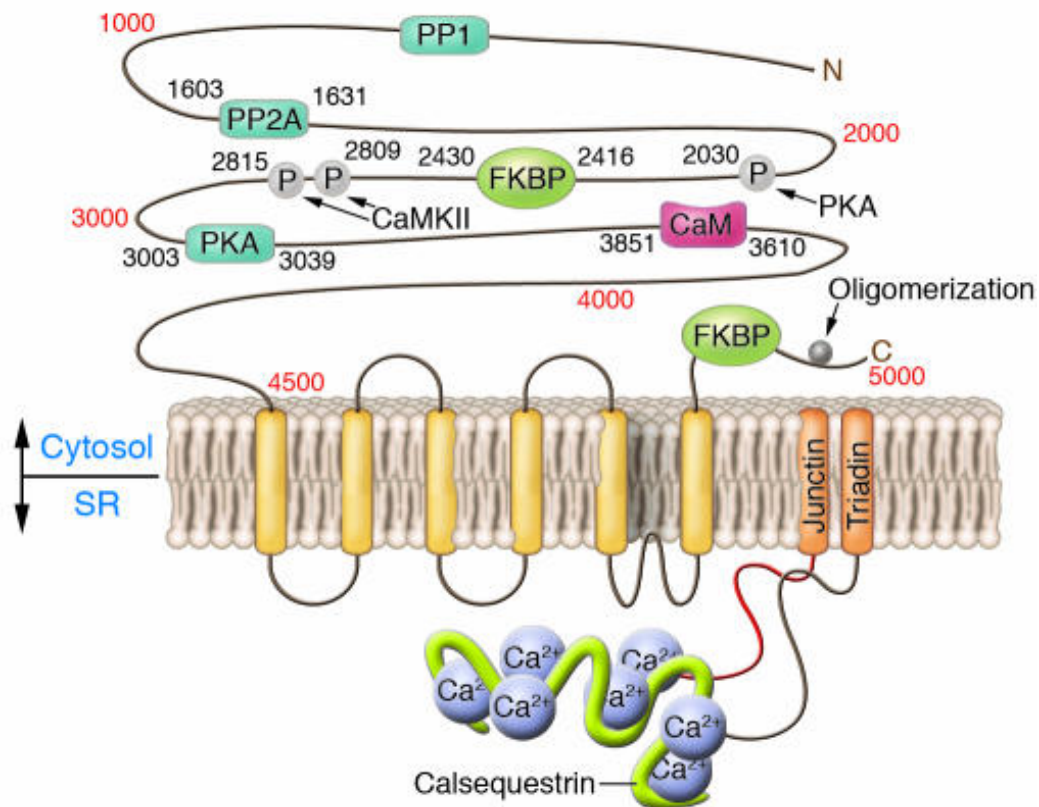


Figure 4-15

The RyR2-monomer structure including the sites of interaction with ancillary proteins and phosphorylation sites. P: phosphorylation sites, PKA: protein kinase A, PP1: protein phosphatase 1, PP2: protein phosphatase 2a, CaM: Calmodulin, CaMKII: calmodulin-dependent protein kinase II, FKBP: FK506-binding protein, SR: sarcoplasmic reticulum[136].

4.9 The Reticulon/Nogo family of proteins

The Reticulons (RTNs) are very old in history and appear in all eukaryotes, including plants and fungi[137]. They are an eukaryotic protein family and in mammals 4 reticulon genes are familiar (RTN1, -2, -3, and -4/NogoA), which encode various protein isoforms [138, 139]. In their structure, all reticulons have a reticulon homology domain (RHD) in common, a C-terminally located domain of ~200 amino acids composed of two short hairpin domains. Despite of this domain, the isoforms have only little sequence homology.

The molecular structures of all four proteins (RTN₁₋₄) look alike in the highly conserved carboxy-terminal reticulon homology domain (RHD) -range from 150 aa to 201 aa- also known as Nogo-66 receptor, a conserved region at the carboxy-terminal end of the molecule comprising two hydrophobic regions flanking a hydrophilic loop [138]. In contrast to the similarities, each RTN isoform has a different amino-terminal sequence.

It is not yet clear how the Reticulons work exactly in the human body. A well-known function is that the Reticulons link with their ER retention motif to the endoplasmic reticulum (ER) and

contribute in ER functions like the membrane transport (to other membrane compartments such as Golgi, endosomes ...) cell division and apoptosis. Another function is to stabilize the ER, for example connecting the ER with the cytoskeleton. Not as an individual RTN gene, but in complexes formed in homo- or heteromers the Reticulons (especially RTN1, RTN3 and RTN4) have importance for cellular functions[139].

RTN1A, the first discovered protein member in this family, is a reticulon protein, expressed in neurons of the mammalian central nervous system. This reticulon protein has predominant localization in the endoplasmic reticulum (ER). RTN1A gene is also found in neuroendocrine tumors and can assist as a neuroendocrine tumor marker.

The best characterized, member of the reticulon family is the RTN4, also known as **Neurite outgrowth inhibitor (Nogo)**, is a protein that blocks neurite outgrowth to the central nervous system, restricting the regenerative capabilities of the mammalian CNS after injury[137].

There are three different isoforms of the protein: Nogo-A, B and C. Only Nogo-A is expressed in the neurons, the other two isoforms Nogo-B and Nogo-C, are not located in the neurons.

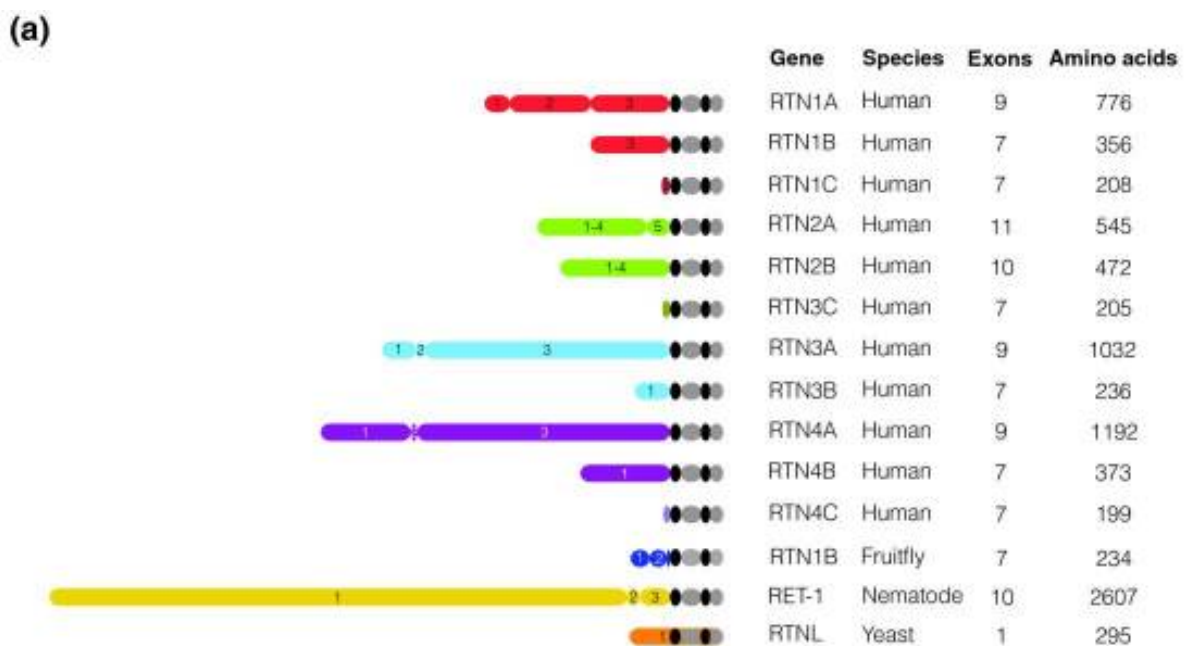


Fig. 4-16

The structure and membrane topology of reticulons. (a) Structure of reticulon proteins. Numbers refer to the exons that encode the protein regions. Black ovals represent hydrophobic regions [138].

4.10 Cardiac excitation-contraction coupling (physiology of the heart, functions, action potential and calcium-induced calcium release, CICR)

4.10.1 The action potential of the heart

During the diastole (relaxation of the heart muscle after a systole) the negative membrane potential of about ~ -80 mV is maintained in potassium conductivity. The depolarization of neighbor cells leads to an activation of sodium channels. The sodium influx results in a depolarized membrane potential of about $+30$ mV, hence a positive change of current.

Depolarized opened calcium channels enable the influx of calcium through the cell, which results in the plateau phase of the action potential. The influx starts the release from the sarcoplasmic reticulum (SR). The increase of the intracellular calcium concentration $[Ca^{2+}]_i$ lets calcium link to the myofilament protein troponin C and the systole (development of tension and contraction of the heart muscle) starts.

Due to the depolarization “delayed rectifier” potassium channels are opened and these channels initiate the repolarization to the resting state.

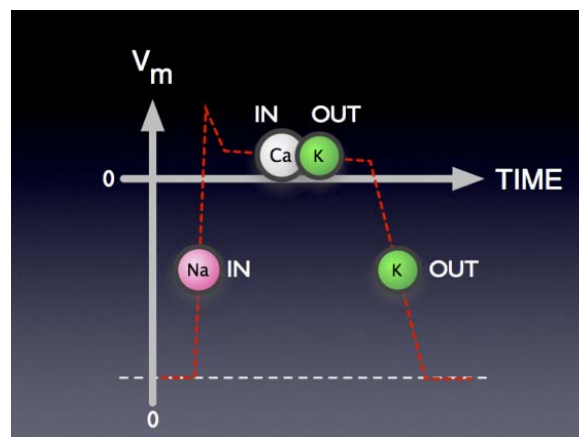
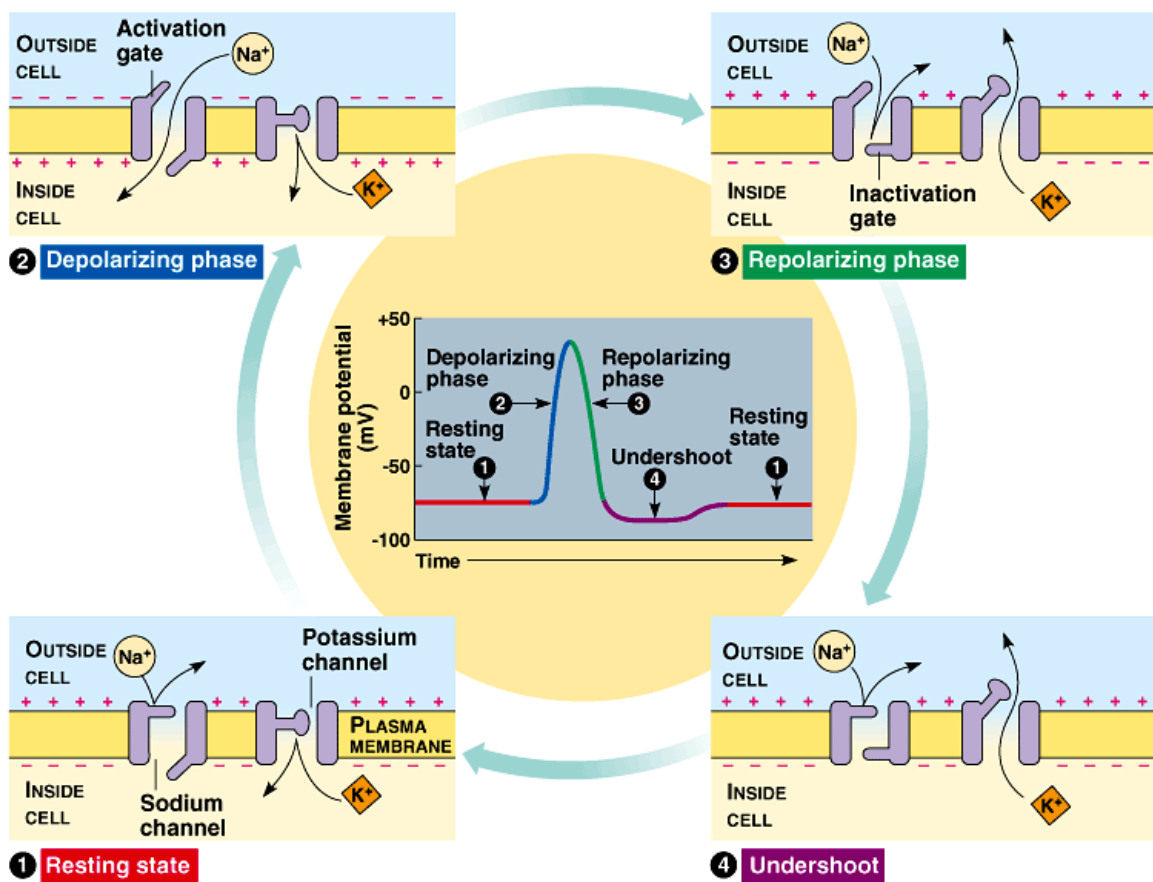


Figure 4-17

The action potential is divided into 4 phases:

- **Phase 1:** The process of the voltage change from -70 mV to $+30$ mV between inside and outside the cell is called **depolarization**. The depolarization generates a short voltage peak (**initial peak**) and is about $+30$ mV. **Na^+ moves in the cell.**
- **Phase 2:** After this initial peak, the value drops down a little (is about 0 mV) and stays for a while. **Na^+ channels are closed; Ca^{2+} and K^+ channels are opened (plateauphase).**
- **Phase 3:** Connecting to the plateauphase, there is a repolarization, in which the sodium-potassium-pump is very important. **K^+ ions moves outside the cell.**
- **Phase 4:** The resting potential follows after the repolarization.

4.10.2 The action potential of the nerve cell



Copyright © Pearson Education, Inc., publishing as Benjamin Cummings.

Figure 4-18

The action potential of the nerve cell[140]

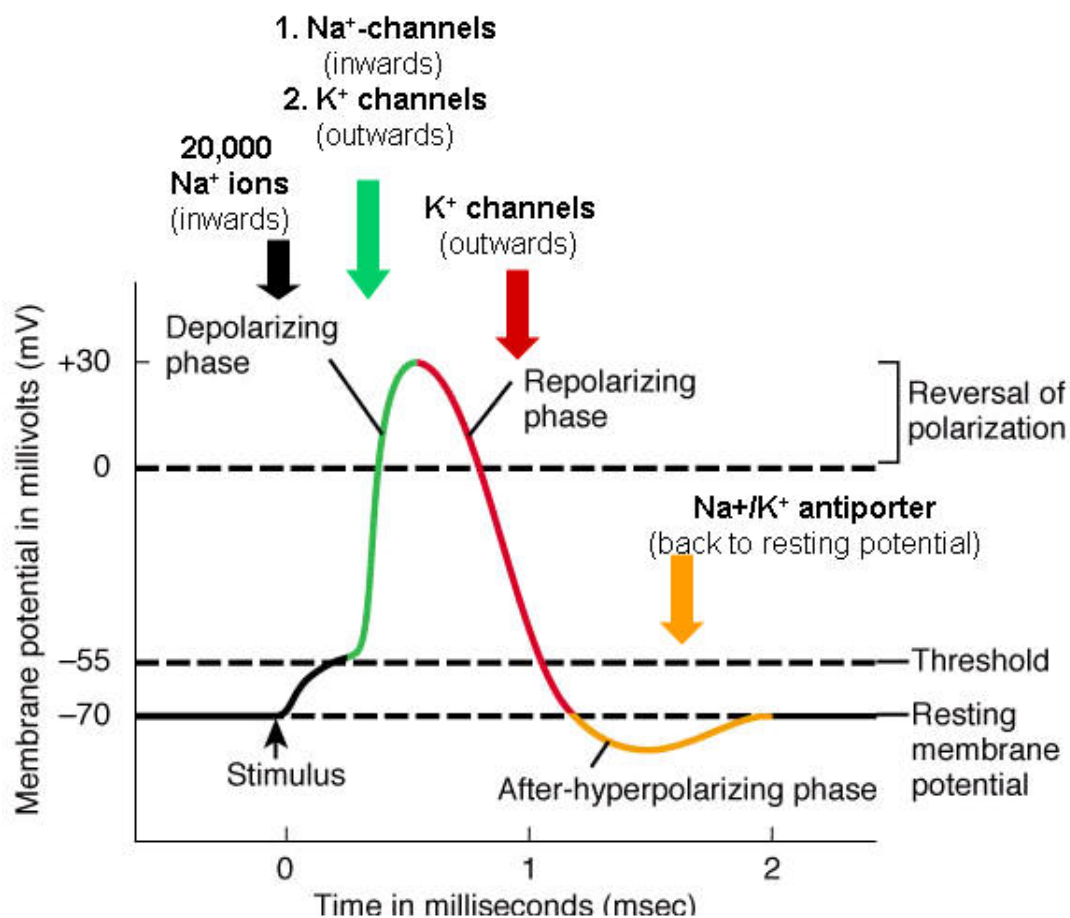


Figure 4-19

The different phases and events of a typical action potential in a nerve cell

- Anerve impulse or a **stimulus** in the dendrites of a nerve cell causes that the voltage in the dendrite of the neuron will become less negative. This change in the membrane potential, called **depolarization**, will cause the voltage-gated sodium channels to open and drive the interior potential from -70 mV up to -55 mV and the process continues.
- If the action reaches the threshold, more sodium channels are open. The rapid influx makes the inside of the cell membrane positively charged, up to about +30 mV.
- After the voltage gets positive, the sodium channels close or inactivate and the voltage-gated potassium channels open. Potassium ions move out of the cell, the membrane voltage gets negative again. This process is called **repolarization**. The potassium channels stay open until the membrane potential becomes in the basic situation, at least as negative as the resting potential of about -70 mV.
- The membrane potential gets often more negative (to about -90 mV) than the resting potential for a very short period, this is called **after-hyperpolarization**. Hyperpolarization prevents the neuron from receiving another stimulus during this time, or at least raises the threshold for any new stimulus.
- After hyperpolarization, the sodium/potassium pump is responsible for bringing the membrane back to the resting state of about -70 mV[141].

4.10.3 Difference between the action potential of the heart and other excitable cells

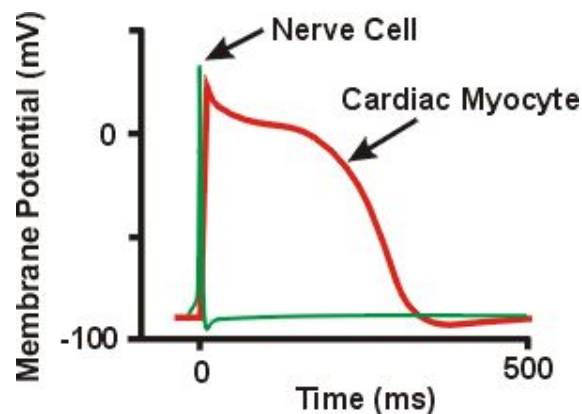


Figure 4-20

The main difference between the action potential in the nerve cell and the heart cell is the time period. In a nerve cell it takes about 1-2 ms and in the heart cell from 220 to 400 ms. This big difference is from the aspect that cardiac muscle cells have an long calcium influx, with slowly opened calcium channels, the so-called calcium plateau phase. In this phase no additionally action potential can be triggered and by this way the pumping ability of the heart is controlled[142].

There is a significantly difference between the action potential in the heart and the action potentials in neural and skeletal muscle cells.

The main difference lies in the time period of the action potentials. An action potential in a typical **nerve cell** appears and moves along the nerve fiber very short in a duration of about **1-2 ms**. Compared with the nerve cell, in skeletal muscle cells or heart cells the action potential lasted significantly longer. In skeletal muscle cells, the action potential duration is approximately 2-5 ms and in **heart cells** the duration range from **220 to 400 ms**(Figure 4-20). Hence, another clear difference refers to the role of calcium ion in depolarization. In nerve and muscle cells, the depolarization phase is triggered by an opening of sodium channels. The calcium plateau phase is the key characteristic of the cardiac action potential in comparison to the potential of other excitable cells. The slow calcium influx prolongs the duration of the action potential and is responsible for the characteristic plateau phase. In this process the reduction of potassium channels takes simultaneously place. The plateau phase of the heart cell is very important and takes over a very significant function. Therefore it plays a protective role. During the plateau phase of the heart cell no additional action potential can be started. It will be considered as the refractory period of the heart, where the pumping ability of the heart is controlled.

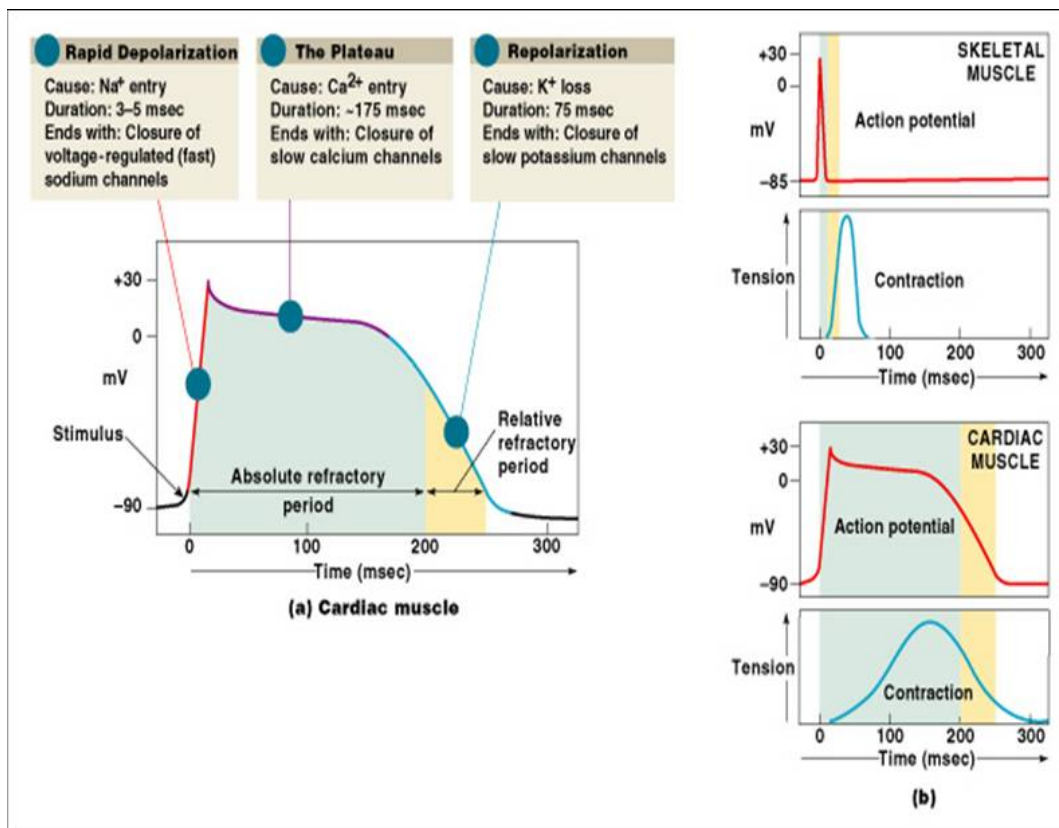


Figure 4-21

Comparison of the action potential of the nerve cell with the action potential of the heart cell.

Duration of the action potential of the nerve cell is 1-2 ms, of the heart cell 220-400 ms; The nerve needs only one Hundredth of the time in comparison to the heart cell[143].

4.10.4 Calcium-induced calcium release, CICR

Depolarized membrane potentials of sarcolemma results in conformational changes of the dihydropyridine receptor (DHPR) L-type calcium channels, a small inward calcium current and furthermore activation of the second release channels, the ryanodine receptors. This phenomenon is called calcium induced calcium release (CICR)[144]. However the RYRs are opened, either through mechanical-gating or CICR, calcium is released from the SR and is able to bind to Troponin C on the actin filaments, actin and myosin. Consequently the muscles contract through the sliding filament mechanism, causing shortening of sarcomeres and muscle contraction.

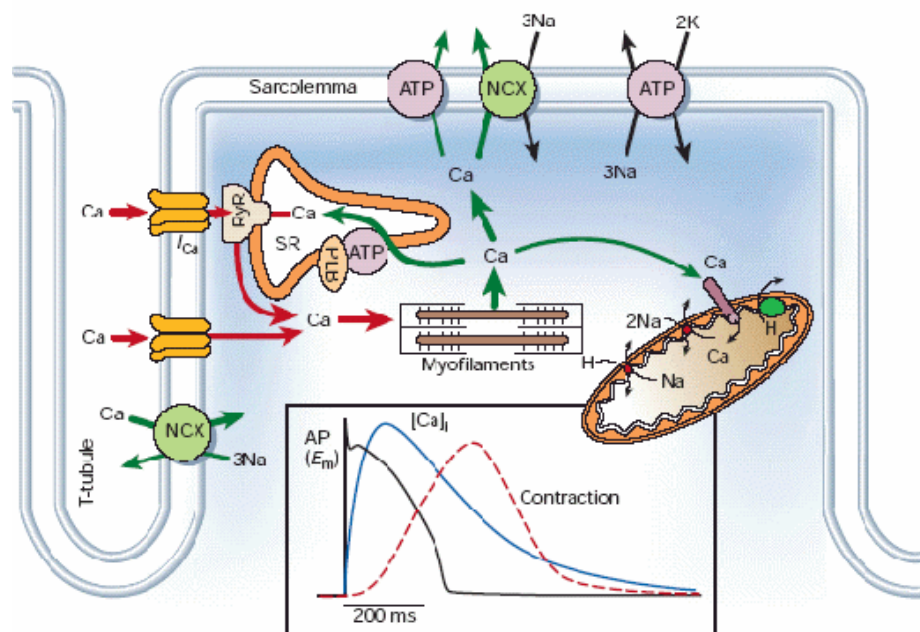


Figure 4-22:

Cardiac excitation–contraction coupling. Ca²⁺ entry through LTCC activates RyR2 to release sarcoplasmic reticulum (SR) Ca²⁺ stores into the cytosol where the Ca²⁺ binds to myofilaments leading to cell shortening and cardiac contraction. Ca²⁺ is subsequently pumped back into the SR through SERCA and out of the cell through the sodium–calcium exchanger and the plasmalemmal Ca²⁺ pump. RyR2 is a homotetramer regulated by many proteins (for simplicity these proteins are depicted here on only one RyR monomer)[145].

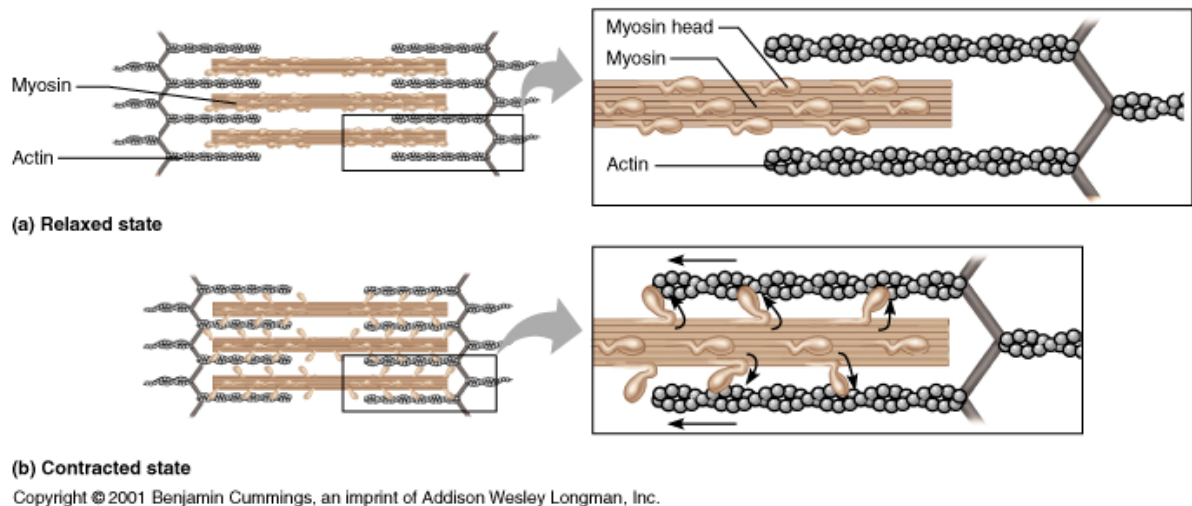


Figure 4-23:
Actin and myosin binding

Interaction of myosin with actin leads to a shortening of the muscle and this results finally in contraction[146].

In summary it can be said, therefore, that the coupling of calcium and contraction has four important control points:

- 1) The actual influx of calcium through the cell membrane, which starts the process, is subject to regulation. This is important, since a large influx will result in larger releases from the calcium reservoir.
- 2) The sensitivity of the RyR can be altered so that more calcium is required for a large release.
- 3) The quantity of calcium in the sarcoplasmic reticulum can be adjusted.
- 4) The ability of the contractile proteins to react to calcium can be adapted to the organism's need for an increased or reduced stroke volume.

4.11 The disease-linked RyR2 mutations

A calcium store overload in the sarcoplasmic reticulum (SR) makes the calcium release channel (RyR) very sensitive to open the gate and a so called “spontaneous SR calcium release” happens[147]. It is mentioned as store-overload-induced calcium release (SOICR)[148]. This large SR calcium spillover may cause spontaneous calcium release during repolarization. It activates the $3\text{Na}/\text{Ca}^{2+}$ -exchanger, which results in an increased sodium influx and this initiates a membrane depolarization resulting in an action potential (called “afterdepolarizations”). This delayed after depolarizations (DADs) can lead to ventricular arrhythmias, especially ventricular tachycardia (VT) and in the last resort to sudden death[144].

Catecholaminergic polymorphic ventricular tachycardia (CPVT) belongs to the family of inbred Ventricular Tachycardia and in the worst case linked with syncope and sudden death. CPVT is the consequence of emotional or physical stress or an infusion of catecholamines and the affected patients have functionally normal hearts[149, 150]. This disease, which can be triggered by the mutations in the two cardiac SR proteins, can lead in the cardiac calsequestrin (CASQ2) to an autosomal recessive form and in the cardiac ryanodine receptor (RyR2) to a dominant form. Furthermore there is an involvement of RyR2 mutations due to arrhythmogenic right ventricular cardiomyopathy type 2 (ARVD2) [151-155].

To this date about 40 disease-linked RyR2 mutations have been discovered and the mutations will be structured in the regions where they are expressed. Hence they are localized in the N-terminal, C-terminal or in the central region.

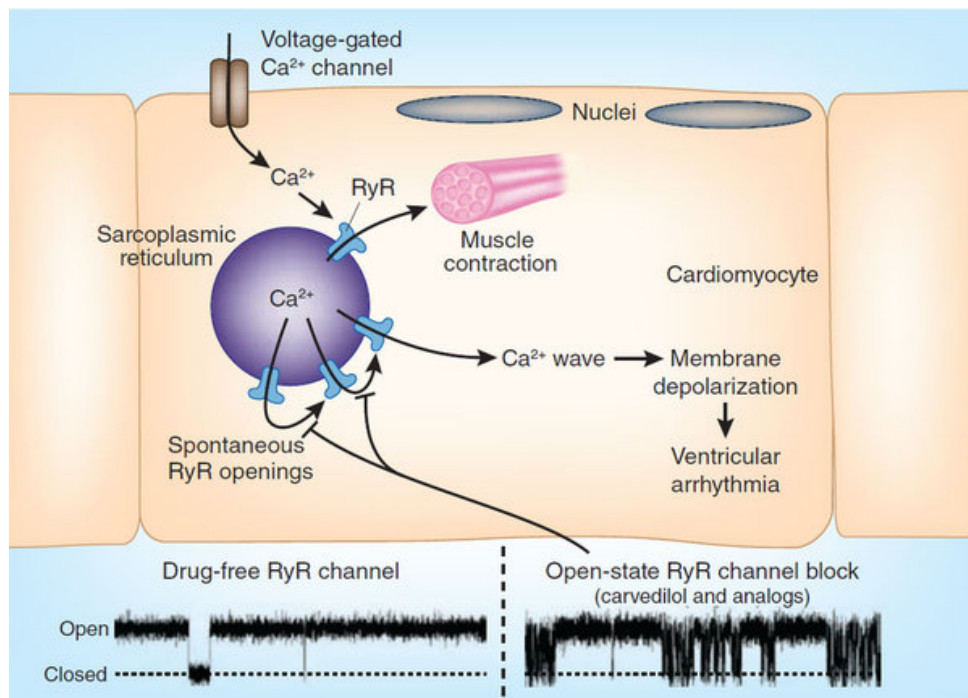


Figure 4-24:

Calcium moves through the voltage-gated L-type channels inside the cell. The reverse RyR2 releases calcium from the sarcoplasmic reticulum to the cytosol, which initiates an increasing $[Ca^{2+}]_i$ and consequential muscle contraction, which mediates calcium waves. Spontaneous RyR openings increases both Ca^{2+} influx and SR Ca^{2+} uptake, resulting in a large SR Ca^{2+} spillover and that can lead to delayed after depolarizations and triggered ventricular arrhythmia[156].

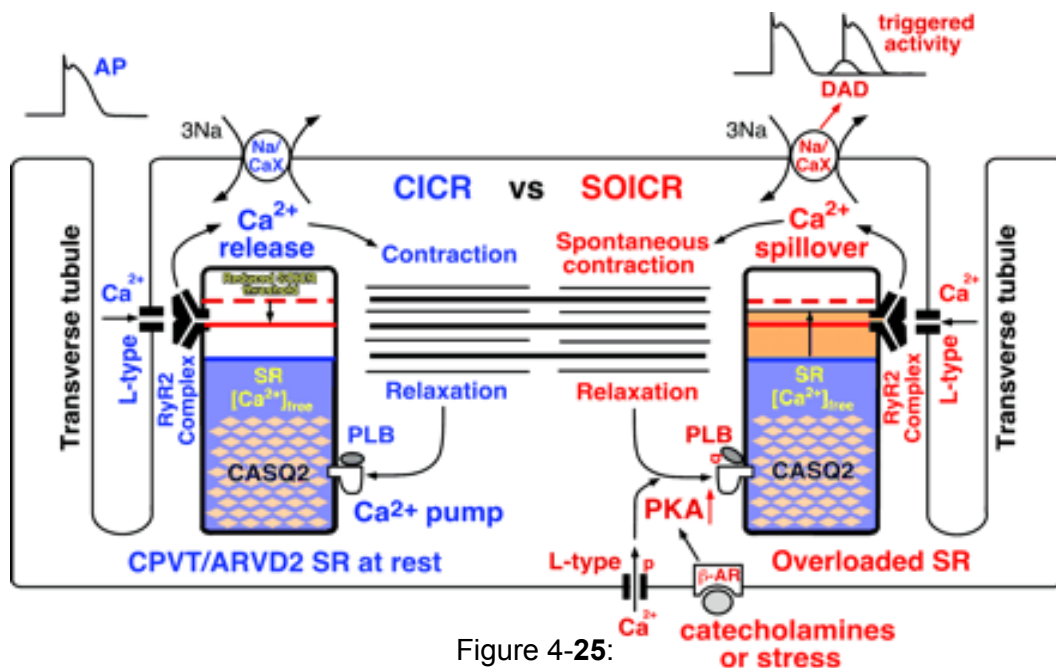


Figure 4-25:

A proposed model for RyR2-associated CPVT/ARVD2. The mechanisms of Ca^{2+} -induced Ca^{2+} release (CICR; left) and store overload-induced Ca^{2+} release (SOICR; right) are schematically shown. Some major proteins involved in cardiac Ca^{2+} cycling, including the L-type Ca^{2+} channel, the RyR2 channel complex, the Na/ Ca^{2+} exchanger, the SR Ca^{2+} pump, phospholamban (PLB), and calsequestrin (CASQ2) are indicated. The threshold for SOICR (depicted by a red bar), which is primarily determined by the RyR2 channel complex, is reduced in the CPVT/ARVD2 SR as compared with that in the normal SR (depicted by a red dash-line) because of RyR2 mutations. The SR free Ca^{2+} level, which is predominantly determined by CASQ2, is represented by the blue area. Under conditions of emotional and physical stresses or on infusion of catecholamines, β -adrenergic receptors are activated, leading to activation of PKA, which in turn phosphorylates the L-type Ca^{2+} channel and PLB. This PKA phosphorylation increases both Ca^{2+} influx and SR Ca^{2+} uptake, resulting in an abrupt increase in SR free Ca^{2+} (depicted by the yellow area). Because of its reduced threshold, SOICR will be more likely to occur from the CPVT/ARVD2 SR during SR Ca^{2+} loading. The resulting large SR Ca^{2+} spillover can lead to DAD and triggered arrhythmia[157].

5 Task

Calcium is a very important second messenger, which is essential for the communication in the cells and by this way it is involved in many processes in the body.

The major interest of my diploma thesis and my research will be focused on three different-permeant calcium channels (calcium influx pathways):

- 1) Calcium-release activated calcium (CRAC) channel – STIM1/Orai1
- 2) Transient receptor potential (TRP) ion channels (TRPC1, TRPV6)
- 3) Ryanodine receptor 2 (RyR2)

In chapter 1 I will investigate the effects of novel drugs on intracellular calcium levels in the cell as well as on native **CRAC channels**. Therefore the CRAC channel components STIM1 and Orai1 and the co-localization of these two proteins creates the unit of store-operated calcium entry. A low intracellular calcium level induces calcium depletion from the endoplasmic reticulum. On this account the CRAC channel is activated to replenish the intracellular calcium store. Upon the activation of the calcium sensor in the endoplasmic reticulum, STIM1, the pore of the CRAC channel ORAI1, located in the plasma membrane gets in contact with STIM1 via protein-protein interaction. By this interaction the intracellular calcium store will be refilled.

I will test the inhibition of native CRAC channels by the competitive CRAC channel blockers, GSK-5503A and GSK-7975A from the company Glaxo Smith Kline. Before testing the novel compounds directly on STIM1/Orai1 over-expressed in HEK293 cells, it is first necessary to test their effects on untransfected cells. For my experiments I will use the calcium imaging technique employing the fluorophore fura-2 as it is the only technique able to study intracellular calcium levels as well as the activation of native CRAC currents in HEK293 cells. I will investigate the intracellular calcium level before and after store-depletion of untransfected HEK293 cells in the absence/presence of the blockers. On this account I hope to exclude that these GSK-compounds cause supplementary endogenous effects in these cells. Additionally, in my fura-2 experiments I will ascertain that after maximum depletion of the ER-stores the native CRAC channels are fully inhibited by the GSK-blockers. These experiments will be supported by the patch-clamp technique. As soon as it is clear that the GSK compounds do not affect any processes in the cell, my colleagues will test the GSK-blockers regarding to their specificity on STIM/Orai channels electrophysiologically as well as by FRET measurements.

Transient receptor potential (TRP) ion channels (in special TRPC1, TRPV6). In chapter 2 the main focus lies on the investigation if TRPC1 channels, overexpressed in HEK293 cells can be activated by Carbachol (CCh) and Thapsigargin (TG). Since my colleagues

employing patch clamp, they were enable to monitor a TRPC1 current, I will investigate calcium entry by fura-2 of TRPC1 expressing HEK293 cells. These studies are necessary to continue investigations on the TRPC1 together with TRPV6. There I will compare the calcium entry of TRPV6, with that of TRPC1 channels overexpressed in HEK293 cells and also co-expressed with TRPV6.

On the other hand I will contribute in investigating the interaction mechanism of TRPC1 and TRPV6 via their ankyrin-like repeats. I will suppose with fura-2 microscopy that TRPC1 and especially co-expression of TRPC1/TRPV6 will have a significantly lower calcium influx than TRPV6 alone in overexpressed HEK293 cells.

These investigations will be supported by several techniques including molecular biology, confocal Förster Resonance Energy Transfer (FRET) microscopy and electrophysiological experiments, using the patch-clamp technique.

In the last chapter the main focus lies on the investigation of the **ryanodine receptor 2**. RyR2 is also a calcium channel located in the membrane of the sarcoplasmic reticulum. A high intracellular calcium level induces channel opening. It triggers an action potential. The action potential lets calcium flow to the heart muscle cell and by different mutations like RTN1A in the ryanodine receptor 2 “spontaneous SR calcium releases” can be treated. Spontaneous SR calcium releases will be measured by fura-2 and the calcium releases can be monitored by calcium oscillations. RyR2 mutations can increase the sensitivity to arrhythmia. These mutations will be linked to ventricular tachycardia and in the last resort to sudden death [157].

6 Material and Methods

6.1 Cell culture

6.1.1 Cell lines – Human embryonic kidney (HEK293) cells

6.1.2 Media and chemicals for HEK293

All cell culture techniques were executed in a laminar flow (Gelaire TC 48), solely autoclaved or sterilized solutions, reagents and materials were used. HEK293 cells were grown in 25 cm² tissue culture flasks in an incubator under humidified (95 %) atmosphere containing 5 % CO₂ at 37 °C. The cells for the experiments were transferred onto 12 mm coverslides in 35 mm Petri dishes with 3 coverslides per Petri dishes.

PBS (per liter)

NaCl	10.00 g
KCl	0.25 g
Na ₂ HPO ₄	1.44 g
KH ₂ PO ₄	0.25 g

Adjusted to pH 7.4 with NaOH, autoclaved at 120°C for 20 minutes, stored at room temperature.

Trypsin-EDTA (per liter)

NaCl	6.40 g
KCl	0.16 g
Na ₂ HPO ₄	0.92 g
KH ₂ PO ₄	0.16 g
Na-EDTA	0.16 g
Trypsin	0.50 g

Trypsin was filter sterilized and stored at -20°C.

- Dulbecco's Modified Eagle Medium (DMEM) with Sodium Pyruvate and L-Glutamine (PAA – The cell culture company, Pasching, Austria, Cat. No. E15-843)

Inorganic Salt	(mg/l)	Vitamins	(mg/l)
Calcium Chloride . 2H ₂ O	264,93	D-Calcium-Pantothenate	4,00
Ferric(III)-Nitrate . 9 H ₂ O	0,10	Choline Chloride	4,00
Potassium Chloride	400,00	Folic Acid	4,00
Magnesium Sulphate anhydrous	97,70	Myo-Inositol	7,20
Sodium Chloride	6400,00	Nicotinamide	4,00
Sodium Dihydrogen Phosphate . H ₂ O	141,31	Pyridoxal HCl	4,00
Sodium Hydrogen Carbonate	3700,00	Riboflavin	0,40
		Thiamine HCl	4,00

Amino Acids	(mg/l)	Other Components	(mg/l)
L-Arginine HCl	84,00	D-Glucose anhydrous	4500,00
L-Cystine	48,00	HEPES	5958,00
L-Glutamine	584,00	Phenol Red	15,00
Glycine	30,00	Sodium Pyruvate	110,00
L-Histidine HCl . H ₂ O	42,00		
L-Isoleucine	105,00		
L-Leucine	105,00		
L-Lysine HCl	146,00		
L-Methionine	30,00		
L-Phenylalanine	66,00		
L-Serine	42,00		
L-Threonine	95,00		
L-Tryptophan	16,00		
L-Tyrosine	72,00		
L-Valine	94,00		

- The following supplements were added to the media DMEM:
500 ml DMEM
10 % FCS (Fetal Calf Serum) (Introvigan SKU# 16000-044), stored at – 20°C
5 ml 100x Penicillin/Streptomycin (PAA – The cell culture company, Cat. No. P11-010), stored at ≤ -15°C

Penicillin	10.000 Units/ml
Streptomycin	10 mg/ml
Solvent	0.9 % NaCl

6.1.3 Cell cultivation

- A culture with 70 – 80 % confluence was chosen.
- DMEM including supplements, PBS and Trypsin-EDTA was heated up to 37 °C in a water bath.
- By means of a sterile pasteur pipette, the cell medium was removed from the cells growing in monolayer.
- The cells were washed with 8 ml PBS.

- 8 ml of Trypsin-EDTA solution were added in order to detach the cells from the bottom of the plate.
- The plate was gently swayed for 2 minutes until the cells were detached.
- 3 ml DMEM including the supplements were transferred into a 50 ml falcon tube.
- The cell suspension was transferred to the tube and gently mixed with the medium. The function of FCS in the medium is to stop the activity of Trypsin-EDTA.
- The cells were centrifuged at 1000 rpm for 5 minutes.
- The supernatant was taken off by a sterile pasteur pipette and the cells were resuspended in approximately 3 ml DMEM including supplements.
- The cell suspension was diluted again and approximately 250 µl of the suspension were put in a 75 cm² tissue culture flask equipped with 20 ml DMEM including supplements.
- After gently swaying the flask was put back in the incubator.

6.1.4 Transfection

- TransFectin Lipid Reagent (Bio-Rad#170-3352)
- DMEM high Glucose with L-Glutamine, with Sodium Pyruvate (PAA #E15-843)
- DMEM high Glucose with L-Glutamine, with Sodium Pyruvate (PAA #E15-843) + Supplements

At least 4 hours before transfection, the cells were transferred as described above, the cell suspension was diluted with medium (incl. supplements) and transferred into tissue culture dishes.

6.1.5 Bio-Rad Reagent (following manufacturers protocol)

- 2 Eppendorf tubes should be prepared for each transfection, one with 250 µl medium without supplements and DNA and the other one with 250 µl medium without supplements and 2 µl Bio-Rad reagent.
- After mixing the solutions, they are incubated for 20 minutes at room temperature for complex formation.
- The DNA-Bio-Rad mixture is dripped on the cells, the plates are shaken and put in the incubator for 4 hours.
- The medium need to be changed by taking of the old medium and adding 2 ml medium (incl. supplements).

- The cells are incubated over night.

6.2 Ca^{2+} Imaging with FURA-2

Calcium imaging is a research method and is useful for measuring the calcium status of a cell, tissue or medium. Calcium imaging techniques utilize calcium indicators, which change their spectral properties after binding calcium ions. For this research we use the most common calcium indicator Fura-2, chemical calcium indicators, which are small fluorescent molecules and have a high selectivity for calcium ions and can chelate them. Fura-2 loaded cells can be studied by using a fluorescent microscope, linked by a CCD camera and analyzed concerning to intensity which reflects the calcium status [158].

6.2.1 The Ca^{2+} indicator Fura-2: Structure and chemical characteristics

Roger Y. Tsien is very famous for developing different ratiometric fluorescent dyes. One developed dye by Tsien's group in 1985 mentioned in particular is fura-2, which binds the free intracellular calcium [159]. Fura-2 makes it able to see the movements of calcium in the cells. Fura-2 is found as sodium- or potassium salt, impermeable for the cell membrane [160]. Concerning to this fact the molecule is linked with an acetoxymethyl ester (AM). Fura-2-AM (the membrane-permeable derivative) passes after a passive diffusion the cell membrane. In the cell the acetoxymethyl groups are removed by cellular esterases, resulting first in an activation of the dye and second the dye stays in the cell. The fura-2 molecule has four carboxyl acid functional binding positions for calcium and build chelate complexes with the calcium ions [161, 162].

Fura-2 has similar properties, in particular the important fluorescent stilben-chromophore with the other calcium chelate-complex building molecules, EGTA and BAPTA [159].

A chemical characteristic for the fura-2 molecule is This molecule is attendant on an EGTA [163] (ethylene glycol-bis(2-aminoethylether)-*N,N,N',N'*-tetraacetic acid) homologue called BAPTA [164] (1,2-bis(o-aminophenoxy)ethane-*N,N,N',N'*-tetraacetic acid). The free carboxyl groups of this tetraacetic acid form chelate complexes together with calcium ions.

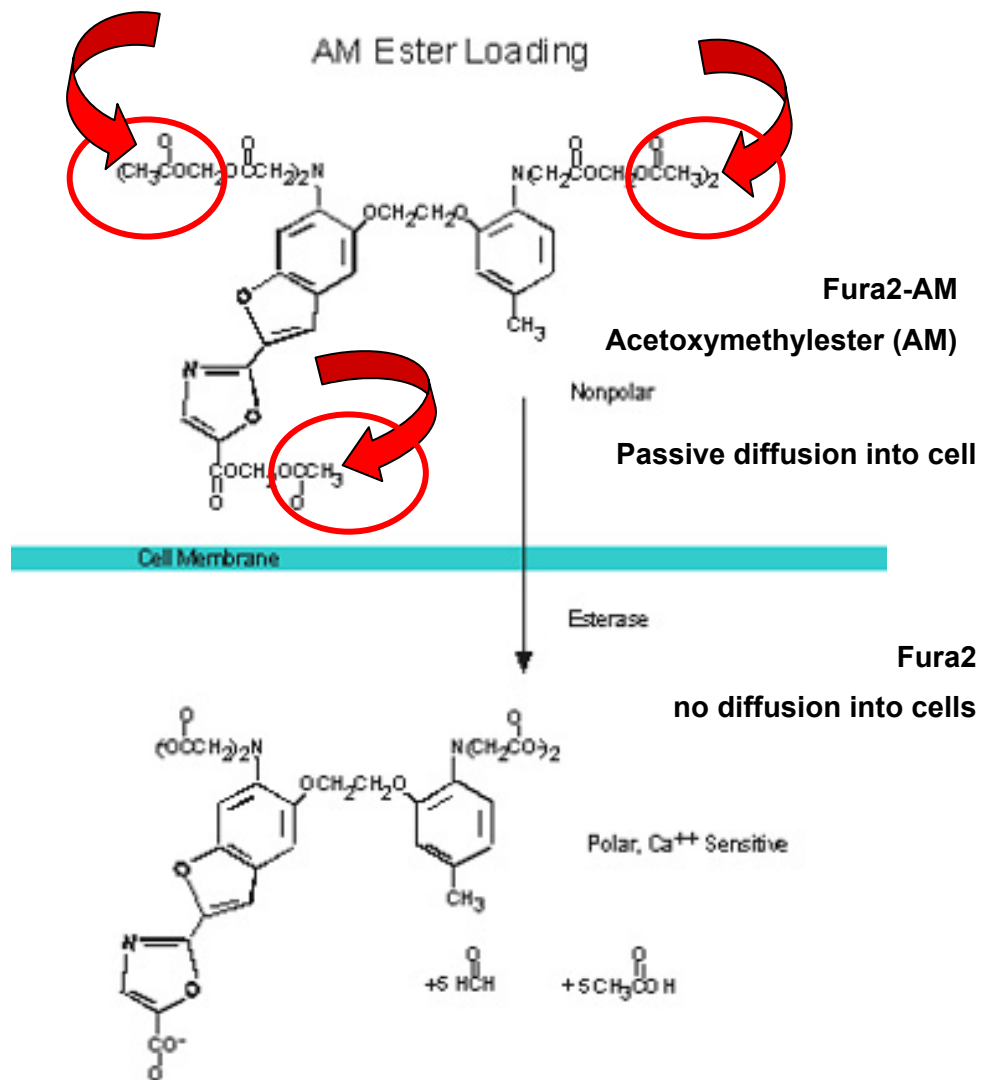


Figure 6-1:

Cellular Esterase activity on Fura-2 AM. Fura-2AM ester is a membrane permeable derivative of the ratiometric calcium indicator fura-2. Inside the cell, cellular esterases hydrolyze the molecule to Fura-2. Fura-2 can no longer cross the cell membrane and is trapped within the cell[165].

6.2.2 Fluorescent measurements with Fura-2

Fura-2 acetoxymethyl ester (AM) is a lipid-soluble derivative that is often used because of its ability to pass through cell membranes.

Fura-2AM (Fura-2-acetoxymethyl ester) is a highly sensitive ratiometric dye that works at a low wavelength (340 and 380nm). The effect is when calcium is not bound, Fura-2AM emits at 380nm. When calcium binds to the dye, it emits at 340nm. The camera on the setup switches between capturing images at 340 nm and 380 nm filters. It then combines the readouts of these filters to create a 340/380 ratio. The higher the 340/380 ratio, the more calcium there is within the cell.

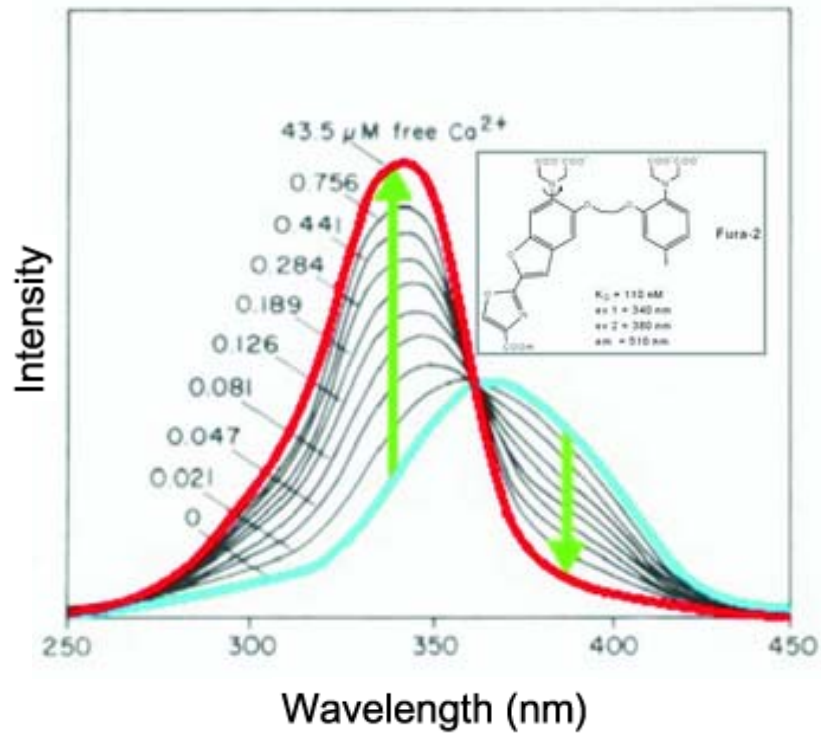


Figure 6-2:

Fluorescence intensity is plotted versus excitation wavelength for different Ca^{2+} concentrations[166].

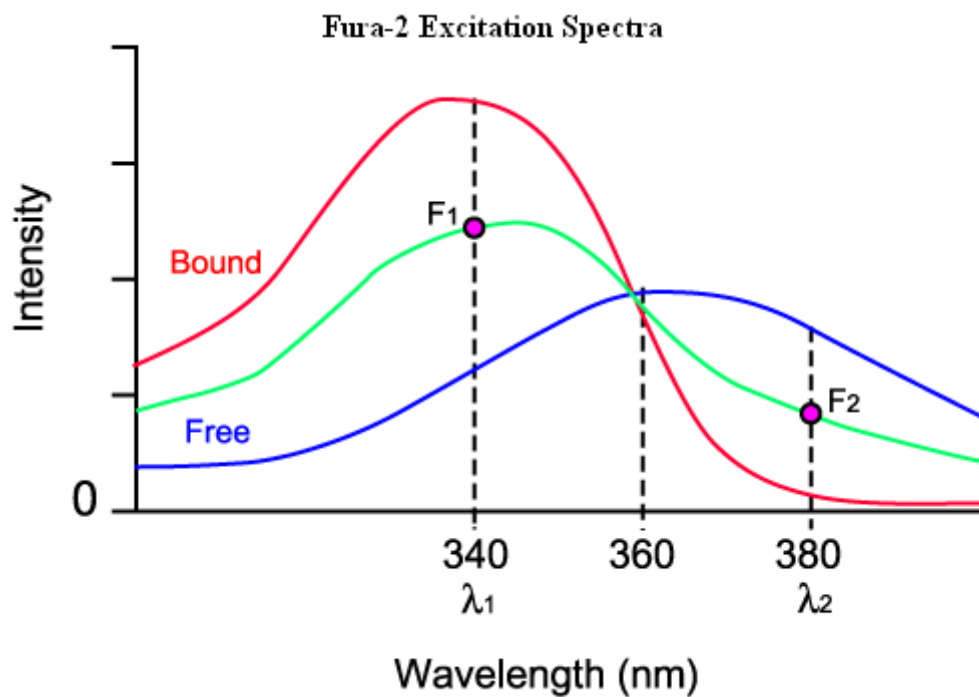


Figure 6-3:

Fura-2 Emission with (blue) and without free calciumions (red)[159]

6.2.3 The Ca^{2+} imaging setup

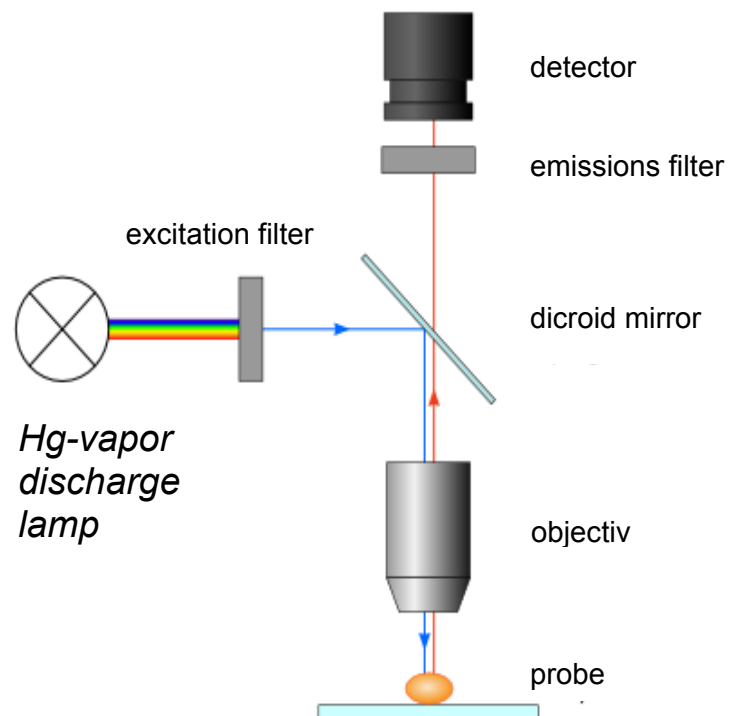
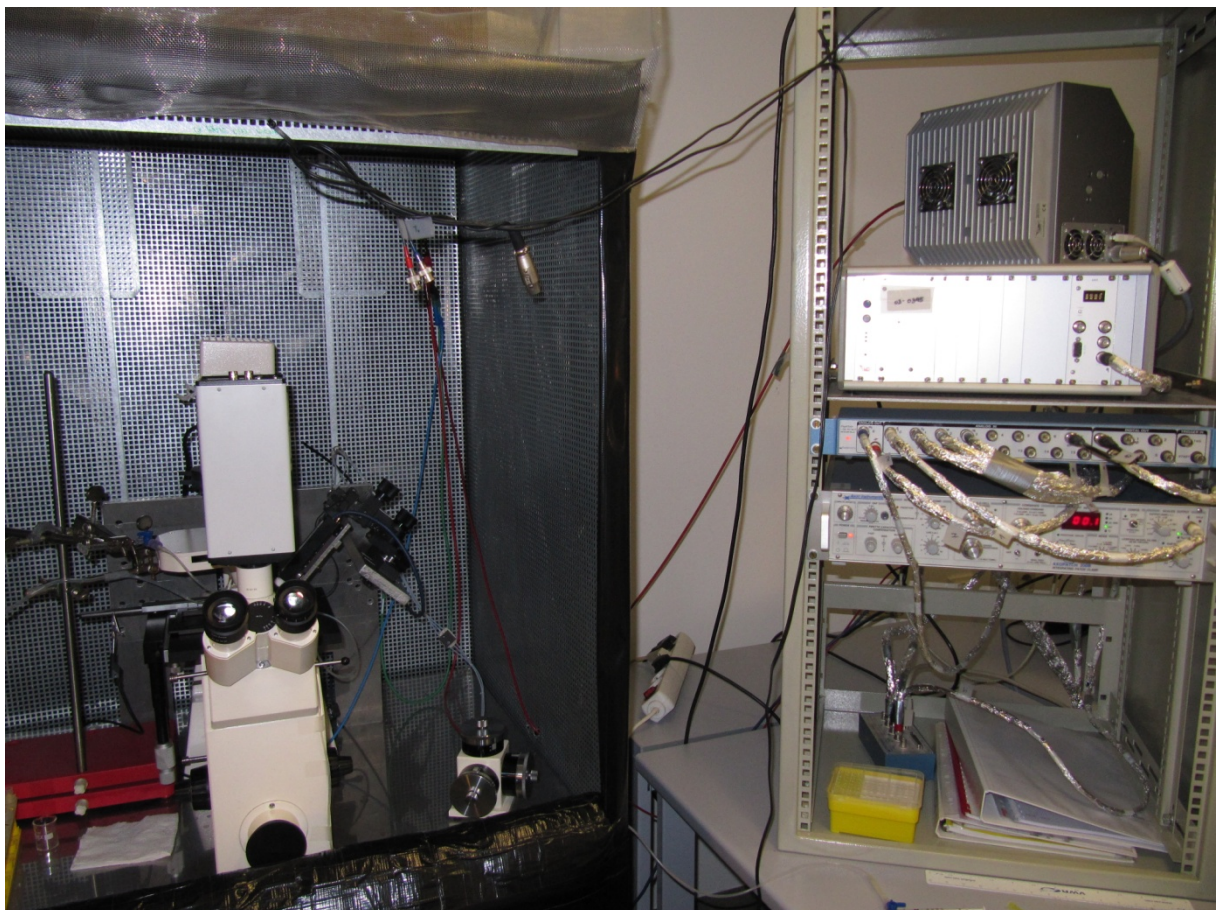


Figure 6-4:
The calcium imaging setup



6.3 Solutions and chemicals

The stated below solutions and chemicals are practiced for experimental approaches employing the calcium imaging using the fluorophore Fura-2AM.

6.3.1 Extracellular solution with 0, 1, 2 mM Ca^{2+}

NaCl	140.00 mM
CsCl	5.00 mM
MgCl ₂	1.00 mM
HEPES	10.00 mM
Glucose	10.00 mM
CaCl ₂	0, 1.00 or 2.00 mM

6.3.2 Fura-2AM

Fura-2AM (Sigma-Aldrich Handels GmbH, Vienna, Austria, Prod. No. F0888) was dissolved in anhydrous dimethylsulfoxide (DMSO, $\text{C}_2\text{H}_6\text{OS}$ – Merck Chemicals International, Darmstadt, Germany, ordering no.1029311000) to gain a stock solution of 1 mM. It was stored at -20°C and apart from light.

6.3.3 Hank's Balanced Salt Solution (HBSS)

HBSS (PAA – The Cell Culture Company, Pasching, Austria, Cat. No. H15-009) contains:

KCl	4.000 g/l
KH_2PO_4	0.060 g/l
NaCl	8.000 g/l
NaHCO_3	0.350 g/l
Na_2HPO_4	0.048 g/l
D-Glucose	1.000 g/l

7 Results

7.1 Calcium-release activated Calcium (CRAC) channel blockers, GSK-7975A

In this chapter I present my contribution to the following study: The action of selective CRAC channel blockers is affected by the Orai pore geometry[167]

The main way for calcium into the cell, more precisely into non excitable cells like T-cells and mastcells occurs through store-operated calcium channels, the so-calledSOCs. Calcium plays in T-lymphocytes and mastcells a pivotal role for immunological reactions and is involved in many essential processes in the human body. One main store-operated calcium channel represents the calcium release-activated calcium(CRAC) channel[168].

It has taken over two decades to unravel the mystery of the precise activation mechanism and structure of the CRAC transduction pathway. For a long time the transient receptor potential (TRP) channels have been supposed to form or to be part of the SOC/CRAC channels[66].

The anonymousness of the CRAC proteins has made it difficult to find selective inhibitors. So far only non-selective drugs inhibitory for calcium entry pathways into the cell or calcium channels have been found. Among them the following compounds/ ions have been used: divalent and trivalent cations such as La^{3+} and Gd^{3+} , diverse imidazoles, 2-APB (2-aminoethoxydiphenylborate), capsaicin[169], NPPB (5-nitro-2-(3-phenylpropylamino)-benzoic acid)[170-172] to designate a few examples. La^{3+} and Gd^{3+} are general blockers of calcium selective inflow pathways, encompassing voltage-dependent calcium, TRPV5/6 and also CRAC channels[9, 173].

In the years 2005 and shortly after 2006 the two components which are necessary and are parts of, to activate the CRAC channel machinery have been defined[15-19]. The two key players of the CRAC channel are the proteins STIM and Orai. So far the CRAC channel is also known under the designation STIM1/Orai1 complex.

These two molecular components represent specific targets for drug development.

STIM1 acts as a calcium sensor located in the endoplasmic reticulum[15, 16] and the second component, Orai1 forms the CRAC channel pore and an oligomerization of Orai1 builds the plasma membrane channel. Intriguingly a recent study based on crystallography revealed a hexameric structure for Orai channel [30]. As the molecular components of the CRAC signaling machinery are now discovered, they represent the molecular targets for selective drug discovery.

The ambition of this study “The action of selective CRAC channel blockers is affected by the Orai pore geometry[167]”, for full publication see the reviewed publication in chapter 11, was to analyse the effects of two selective CRAC channel blockers on currents derived from STIM/Orai heterologously expressed in HEK293 cells.

This study was performed in cooperation with Glaxo Smith Kline, UK, in order to determine the blocking effect, as well as specificity of two novel drugs on STIM1/Orai1 signaling cascade.

The following blockers were used to test.

GSK-5503A (2,6-difluoro-N-(1-(2-phenoxybenzyl)-1*H*-pyrazol-3-yl)benzamide)

is example 26 from the patent WO2010/122089

GSK-7975A (2,6-difluoro-N-(1-(4-hydroxy-2-(trifluoromethyl)benzyl)-1*H*-pyrazol-3-yl)benzamide)

is example 36 from the patent WO2010/122089

(kindly provided by GlaxoSmithKline, UK)

in comparison to Syntha-66 [174]

Syntha-66 (N-(2',5'-dimethoxy-[1,1'-biphenyl]-4-yl)-3-fluoroisonicotinamide)

is Example 66 from the patent WO2005/009954

The inhibitors were dissolved in DMSO to produce a 10 mM stock solution.

First of all, calcium imaging experiments had to be performed to examine the effect of the novel blockers on calcium stores in mock HEK293 cells. Thereby I focused especially on the effect on calcium store depletion as well as store-depletion calcium entry into the cell. The analysis of single cells employing Fura2- technique should demonstrate that the endogenous CRAC behaves equally for cells not treated in comparison to cells incubated with the novel blockers.

I employed the Ca^{2+} imaging technique using the fluorophore fura-2, because the intracellular change in calcium levels can only be measured with this technique. Another advantage of calcium imaging is that endogenous CRAC currents in HEK293 cells can only be measured with Fura-2, not by the patch-clamp technique.

BHQ (2,5-Di-*t*-butyl-1,4-benzohydroquinone) a synthetic phenolic antioxidant is a reversible blocker of the calcium ATPase of the sarco-endoplasmic reticulum (SERCA). The SERCA pump is involved in replenishing of the calcium stores [175, 176]. Other sarco-endoplasmic reticulum calcium ATPase pump inhibitors are thapsigargin and cyclopiazonic acid [176].

Carbachol (CCh) is a cholinomimetic drug that binds and activates the acetylcholine receptor subdivided into muscarinic (mAChR) and nicotinic receptor (nAChR) agonist. It is a

cholinergic agonist[177, 178]. Employing Fura-2, other studies have shown that treatment with 10 μ M carbachol (CCh) induces a rise in intracellular free calcium levels[179, 180]. TRPC homologs were tested referring to form store-operated channels or carbachol (CCh)-stimulated calcium entry pathways in HEK-293 cells[181].

In order to exclude that the GSK blockers effect calcium stores/ intracellular calcium levels I performed Fura-2 experiments on mock HEK293 cells treated with DMSO as control in comparison to the GSK-7975 blocker. Furthermore I stimulated the cells either with carbachol or BHQ and compared the cytosolic calcium levels in control cells and GSK-treated cells.

First I preincubated HEK293 cells with either DMSO (Dimethyl sulfoxide) or GSK-7975 in the presence of 0 mM Ca^{2+} solution.

After perfusion with 0 mM Ca^{2+} solution for 240 s, it follows stimulation with 100 μ M carbachol (CCh) in a standard solution 0 mM Ca^{2+} , also containing either DMSO or 10 μ M GSK-7975. Carbachol is necessary to stimulate potential Transient receptor potential channels (TRPs)/ or to stimulate store-depletion.

The calcium signal which was induced by carbachol was comparable for control cells compared to GSK-7975-treated cells. Hence, I conclude that this GSK-compound had neither an effect on calcium stores nor on endogenous TRPs.

In the second experiment I perfused BHQ (2,5-Di-*t*-butyl-1,4-benzohydroquinone) a reversible blocker of the SERCA pump instead of carbachol. First I also preincubated HEK293 cells with DMSO as control compared to 10 μ M GSK-7975 in the presence of 0 mM Ca^{2+} solution.

Then, I added 30 μ M BHQ in a 0 mM Ca^{2+} solution containing either DMSO or 10 μ M GSK-7975. BHQ led to the same outcome compared to the preceding experiments with CCh. The BHQ induced calcium signal was comparable for control and GSK-treated cells. Thus it had no effect on calcium stores by the blocker.

The previously described steps of the experiments were investigated during a 10-min application of a Ca^{2+} -free solution. Hence it can be achieved that calcium enters the cells through potentially open endogenous CRAC channels. In the next step tested if GSK blocker effect CRAC/Orai channels in the plasma membrane. Therefore I exchanged the 0 mM extracellular solution by 2 mM calcium solution after CCh/BHQ stimulation and GSK treatment.

The perfusion of the 2 mM Ca^{2+} solution for 2 min displayed in cells preincubated with GSK-7975 no increase in intracellular calcium levels in contrast to control cells.

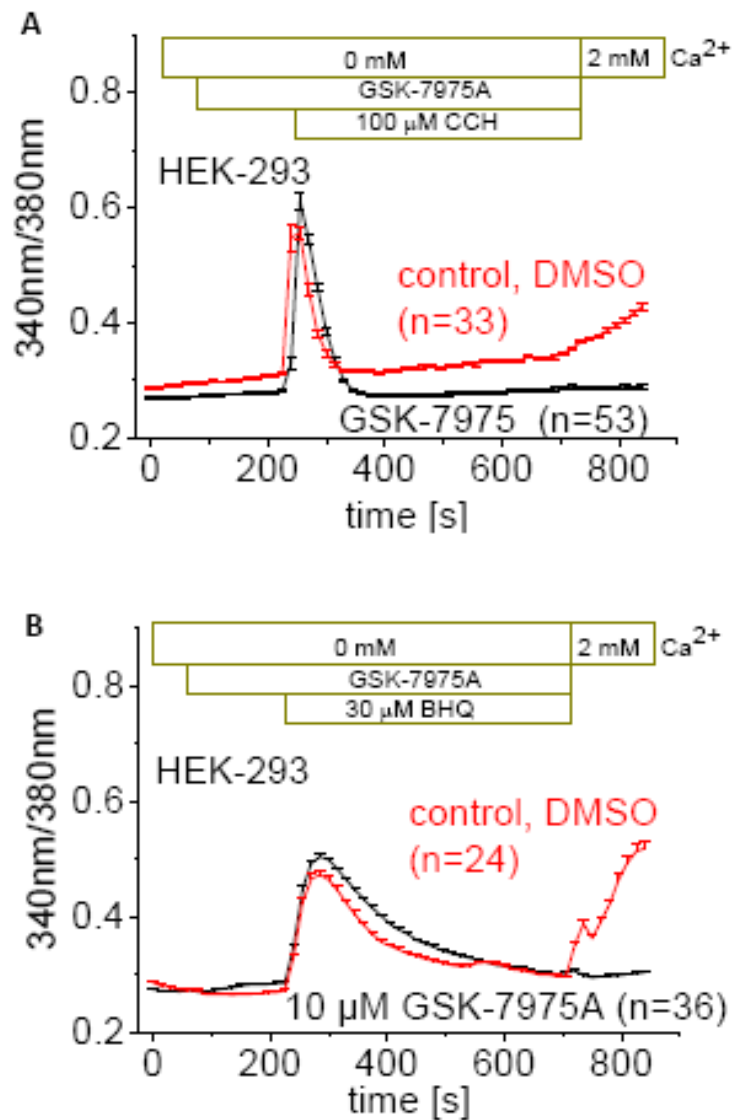


Figure 7-1:

Calcium Imaging, Fura-2 microscopy,Pre-incubation of HEK293 cells with 10 μ M GSK-7975A did not markedly alter the amount of Ca^{2+} released from ER stores via stimulation by either carbachol (CCH) or BHQ pointing to a minor effect of GSK-7975A on pathways affecting the ER Ca^{2+} content. The subsequent endogenous, store-operated Ca^{2+} entry was substantially inhibited by GSK-7975 compared to control[167].

After measurements with Fura-2 I determined that the blocker GSK-7975 has no effect on the intracellular calcium level in the HEK293 cells. Based on these results Romanins lab made investigations specific on the STIM1/Orai1 channel. On this account they co-expressed STIM1 with either Orai1 or Orai3 in HEK293 cells.

To begin with the well-known electrophysiological method, especially the whole-cell patch clamp technique for measuring the currents of STIM1/Orai1 expressed HEK293 cells. Next the Förster resonance energy transfer (FRET) technique, for doing measurements of interactions between the proteins.

The two GSK inhibitors (GSK-7975A and GSK-5503A) block both completely Orai1 currents at a concentration of 10 μ M, but in comparison with the conventional inhibitor La^{3+} in a slower time rate. To prove the effect of the two GSK compounds on STIM1-stimulated Orai currents (Orai1 or Orai3), my colleagues employed the patch-clamp technique in the whole-cell configuration to test the effect of GSK compounds on maximally activated Orai currents in comparison to the calcium channel blocker La^{3+} . For further detail they compared with the synthetic estrogen agonist diethylstilbestrol (DES) and 2-APB with the novel inhibitors. In summary, the conventional inhibitors blocked rapidly, while the two Orai1 current-blocking compounds GSK-7975A and GSK-5503A inhibited Orai1 currents fully with a 2.5-fold slower kinetic than the others, especially the conventional inhibitor La^{3+} .

To amplify the knowledge of the Orai family, they made also patch-clamp experiments on STIM1-activated Orai3 currents. They came to the same results, like for Orai1. Hence, conventional compounds like La^{3+} inhibited maximally activated currents faster than the two GSK-drugs. It seemed, however, that the GSK compounds block Orai3 currents a little faster than those of Orai1.

The blocking effect of GSK-7975 measured in patch clamp is in accordance with my Fura-2 experiments displaying a reduced calcium entry upon store-depletion and GSK-7975A treatment.

In wash-out studies of 4-5 min wash-out periods of the GSK compounds, the blocking of STIM1-activated Orai1/3 currents was irreversible. Hence, it is not anymore possible to recover the initial unblocked state.

As the two GSK compounds acted in a very comparable manner, my colleagues decided together with the company GlaxoSmithKline to focus only on one of the two blockers, which is in that case GSK-7975A.

The next experiments were made to answer the question: "Is the blocking effect on Orai1 and Orai3 channels due to interference in the coupling machinery of STIM1/Orai or direct pore blockage."

In order to identify if STIM1 oligomerization is influenced by GSK-7975A, Romanins lab pre-incubated CFP- and YFP-STIM1 expressing HEK293 cells with 10 μ M GSK-7975A for 5 min before store depletion. After emptying the calcium store with 2 μ M thapsigargin, FRET increased in a comparable manner for control and GSK-7975A treated cells. Thus, GSK-7975A has no influence on STIM1 oligomerization.

Summing up, it is very likely that the blocking effect of GSK-7975A on CRAC currents came from interference with gating or a pore blockage.

In an experiment to confirm that the modified pore geometry is the determining factor for the full inhibition by GSK-7975A, we tested different Orai1 pore mutants. In the experiment the low calcium selective Orai1 E106D pore mutant was not affected by perfusion of 10 μ M GSK-7975A. By elevating the concentration to 100 μ M, the inhibiting effect on STIM1-mediated Orai1 E106D currents was considerably reconstituted, but not fully. It becomes apparent that the geometry of the selectivity filter and accordingly the outer vestibule of the Orai1 pore are key points for the GSK-7975A barricading.

In extension endogenous CRAC channels in RBL cells were examined employing GSK-blockers. The current was also fully inhibited in RBL CRAC currents. Further they tested also a set of other calciumion channels:rat-TRPV6 and L-type calcium channels. By adding 10 μ M GSK-7975A the TRPV6 channel was fully inhibited, like with the classical La^{3+} blocker, but the L-type calcium channel was just lower blocked.

7.2 Canonical transient receptor potential (TRPC) 1 acts as a negative regulator for vanilloid TRPV6-mediated Ca^{2+} influx[182]

TRPC1 and TRPV6 in calcium Signaling

The transient receptor potential (TRP) proteins are found in many types of human tissues form cation permeable channels, are activated by a variety of different stimuli and have important physiological functions [183, 184].

These proteins are composed of 6 transmembrane domains and assemble to tetramer cation selective channels [116, 185, 186]. Besides the mostly connected homomeric channels, they can also heteromerize, especially identified within their homolog subfamilies. The unique TRP protein, TRPC1, is a member of the canonical transient receptor potential family and interacts with all members of the TRPC subfamily [187-190].

Concerning the present paper, it is worth mentioning to describe a second TRP channel family, the family of the **TRPV** transient receptor potential vanilloid channels. TRPV5 and TRPV6 form two highly calcium selective channels. The two proteins are found in transporting epithelia of the kidney and intestine [66] and are needed in the small intestine, kidney and bone for calcium entry [191].

Channel architecture of TRPs

The TRP family has a big diversity in channel formation possibilities whether in homo- or in heterocomplexes. By this way, particularly an N-terminal coiled-coil region is required for assembly of the homomeric TRPC1 and TRPM2, TRPM8, while TRPP2 needs C-terminal coiled-coils for forming tetramers. Rather, TRPC4 and TRPC5, TRPV4, TRPV5, and TRPV6 need the ankyrin-like repeats for homo- as well as heteromeric channel assembly and in addition to the ankyrin-like repeats the mentioned TRPCs need a C-terminal segment. Although, TRPC1 needs different protein sequences for forming homo- or heterocomplexes and an interaction between TRPC1 and TRPC3 is formed using their ankyrins.

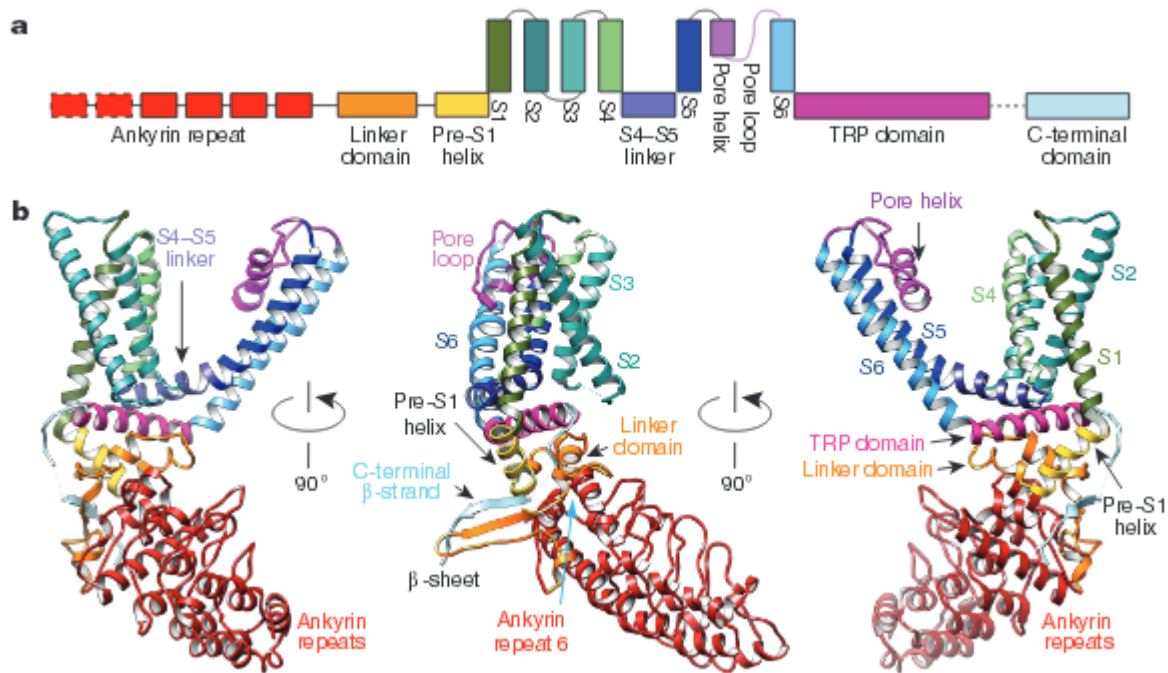
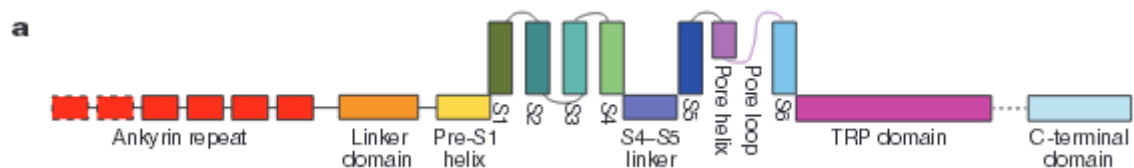


Figure 7-2 (a+b):
Structural domains and detailed subunit of the TRPV1 channel.
 in the ribbon diagram you see four of the six ankyrin repeats (coloured in red)[86]



Architecture of the TRPV1 channel. Adapted from[86]

Linear diagram shows beginning at the N-terminus six ankyrin repeats, followed by a linker. The linker tethers the ankyrin repeats together with the pre-S1 helix.

The TRPV1 channel contains in the N-terminal region six ankyrin repeats (Figure 7-2a, red colour). Below in the ribbon diagram showing three different views of a TRPV1 monomer including four of the six common ankyrin repeats (Figure 7-2 b, red colour). The characterization of the ankyrin repeats shows, that between each repeat the strongly packed linker domain including β -strand and α -helical elements are situated. In addition this linker domain is also placed at the pre-S1 helix and TRP domain. It is interesting to note, that the β -sheet structure of the linker separates the cytoplasmic N- to the C-terminal domains. In detail the antiparallel β -sheet from the linker domain and a β -strand from the C terminus are linking with two ankyrin repeats (Figure 7-2 b, second view) [86].

Relating to the ankyrin repeats, the focus of this study [182] was placed on a novel interaction between TRPC1 and the calcium selective TRPV6 channel. **The aim of this study “Canonical transient receptor potential (TRPC) 1 acts as a negative regulator for vanilloid TRPV6-mediated Ca^{2+} influx [182]” was to analyse the effects of a novel**

cross-family interaction of TRPC1 and TRPV6 via their ankyrin-like repeats on experiments derived from TRPC1/TRPV6 heterologous expressed in HEK293 cells. It should be established how the cellular/molecular consequences of a TRPC1/TRPV6 interaction function in vivo.

In consequence of the co-expression with TRPC1, TRPV6 is lower expressed in the plasma membrane and also the TRPV6 calcium currents are significantly suppressed. The significantly suppressed TRPV6 currents by TRPC1 could be linked to a reduced calcium influx. This special interaction could modulate cellular calcium homeostasis.

Comparison of the structures of TRPC1 with TRPV6 channels show that they contain ankyrin repeats in their N-terminus as potential interaction sides. This cytosolic segment triggers assembling of heteromeric interaction and build therefore a novel cross-interacting family.

This present study [182], for full publication see in chapter 11, was published 2012 in the Journal of biological chemistry and Romanins lab investigated a novel cross-family interaction of TRPC1 and TRPV6, a calcium selective member of the vanilloid TRP subfamily, via their ankyrin-like repeats.

TRPV6 manifested substantial co-localization and in vivo interaction with TRPC1 in HEK293 cells, on the contrary, no interaction of TRPV6 was observed with TRPC3, TRPC4, or TRPC5. The co-expression of TRPC1 and TRPV6 down-regulates TRPV6 expression in the plasma membrane, concomitant with a reduced TRPV6 calcium current. The downregulation of TRPV6 currents triggered by TRPC1 might be a novel mechanism controlling calcium homeostasis. Hence the novel TRPC1 and TRPV6 interaction increases the variety of regulatory proteins for calcium uptake.

In an alternative approach to patch-clamp experiments I observed a decreased calcium entry of TRPC1 and TRPV6 in expressing cells in comparison to TRPV6 calcium entry alone with Fura-2 microscopy.

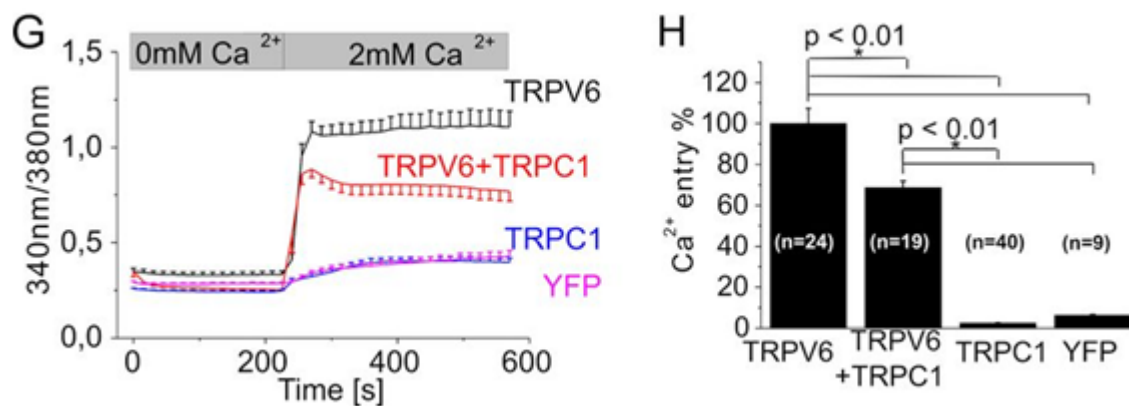


Figure 7-3(numbered in the paper Figure 1G, 1 H):

Calcium Imaging, Fura-2 microscopy, Co-expression of TRPC1 and TRPV6 significantly suppressed TRPV6 currents and Ca²⁺ entry. The Ca²⁺ entry was monitored in cells over-expressing TRPV6 and/or TRPC1 or YFP in the time course in a nominally Ca-free solution followed by addition of 2 mM Ca (=maximum Ca entry)[182].

TRPV6 currents are significantly suppressed by TRPC1 co-expression- Initially, I performed experiments with the calcium imaging technique employing Fura-2 to survey the calcium influx of HEK293 cells over-expressing TRPC1 and/or TRPV6 into the cell.

Figure 7-3(Figure 1G, bottom row, left) shows Fura-2-loaded cells first perfusion with 0 mM calcium solution for 240 s. The application of a calcium-free solution should imitate the biological cell environment to visualise resting cellular calcium conditions. Afterwards the 0 mM solution was exchanged by 2 mM calcium. Addition of 2 mM calcium solution for 6 min displays for TRPV6 expressing cells the highest calcium influx, due it's constitutive activation. TRPC1 over-expressing cells show similar low calcium influx into the cell as YFP – transfected control cells. In line, statistics on calcium entry revealed that TRPC1 over-expressing HEK293 cells compared with control cells are not significantly different. Hence the over-expression of TRPC1 has no influence of the intracellular calcium level Figure 7-3(Figure 1H). The co-expression of TRPV6 with TRPC1 reduces the influx of calcium into cells in comparison to TRPV6 expressing cells.

Quantification of the total amount of the calcium entry into the cells revealed that HEK293 cells co-expressed TRPC1 with TRPV6 lead to an about 30 % reduction of calcium entry in comparison to TRPV6 alone Figure 7-3(Fig. 1, G and H). These results are in line with recent findings of my colleagues employing the electrophysiological experiments.

Overall these experiments demonstrate that the calcium entry into the cell is significantly reduced in cells co-expressed with TRPV6 and TRPC1 compared to cells over-expressing TRPV6.

In a second approach, I investigated if TRPC1 over-expression results in activation of receptor or store-dependent activation.

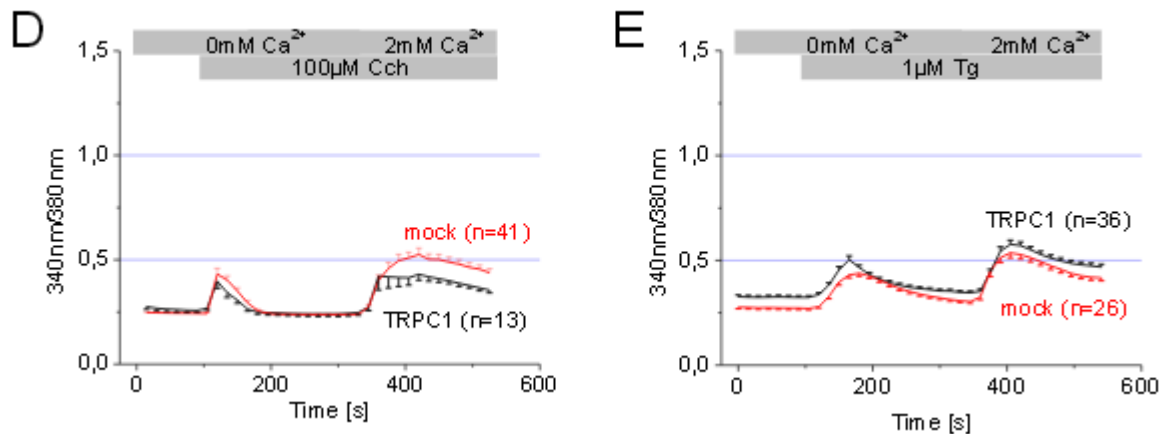


Figure 7-4(Supplementary Figure S1 D and E)

Intracellular $[Ca^{2+}]_i$ of Fura-2 loaded cells overexpressing TRPC1 are compared with a mock-transfection and monitored upon a stimulation with (D) carbachol (Cch, 100 μM) or (E) thapsigargin (TG, 1 μM) and subsequent addition of 2 mM calcium[182].

Carbachol and thapsigargin are able to stimulate store-depletion in two different pathways.

Carbachol (CCh), a non-selective muscarinic and nicotinic receptor agonist, binds and activates the acetylcholine receptor. The application of the physiological agonist carbachol (CCh) causes a rapid transient increase in intracellular free calcium $[Ca]_i$ [179, 180].

The sesquiterpene lactone thapsigargin is selective in blocking the calcium-ATPases of the sarco/endoplasmic reticulum (SERCA pumps)[83, 192, 193]. This blocking prevents a reuptake of calcium in the SR and therefore leads to passive store depletion.

In consequence of adding these two agents separately, in two different experiments, the emptied calcium stores of the endoplasmic reticulum lead in both cases to an increase in the concentration of cytosolic free calcium. The calcium store-depletion of HEK293 cells is a tool to investigate the role of intracellular calcium level on cellular signaling referring to the activation of CRAC channels [46, 194].

To evaluate the intracellular calcium level of human embryonic kidney cells upon these stimulations, we utilized Fura-2 microscopy for imaging of HEK293 cells that expressed TRPC1 in comparison with untransfected (mock) control cells. The calcium imaging experiments should show the behavior of native HEK293 cells to measure directly the intracellular calcium level before and after store depletion. Otherwise it should demonstrate the activity of TRPC1 channels, evident from the activation of calcium influx following stimulation of ER store depletion.

In further Fura-2 microscopy experiments, attached Figure 5-3 as supplementary Figure S1 D and E, HEK293 cells over-expressing TRPC1 compared with a mock control transfection (untransfected cells), stimulate by either carbachol (Cch; 100 μ M) or thapsigargin (TG; 1 μ M) and subsequent addition of 2 mM calcium are shown.

First perfusion with 0 mM calcium solution for 2 min, it follows stimulation of 100 μ M carbachol (Cch) in standard solution 0 mM calcium. Following ER store depletion by carbachol, the 0 mM extracellular solution was exchanged by 2 mM calcium solution. The perfusion of the 2 mM calcium solution for 2 min aimed to display calcium entry into the cell. We observed Figure 7-4(Figure 1D, left panel) the over-expressed TRPC1 HEK293 cells did not respond to the agent carbachol, as monitored in the time-course of calcium entry and is rather lower than the peak of the mock control cells. The uptake of calcium ions into the cells was significantly reduced compared with the mock-transfected cells.

The following experiments were made under equal conditions, over-expressed TRPC1 and mock control cells, and the fura-2-loaded HEK293 cells were treated with 1 μ M thapsigargin (TG) to deplete stores.

Store-depletion of TRPC1 and mock-transfected cells resulted in a similar calcium entry, suggesting that TRPC1 could not be stimulated by thapsigargin.

In summary, in calcium imaging experiments with fura-2-loaded overexpressed TRPC1 cells, the depletion of intracellular calcium stores showed neither by the addition of the physiological agonist carbachol (100 μ M; Figure 7-4, Figure S1 D) or thapsigargin (1 μ M; Figure 7-4, Figure S1 E) an elevated calcium influx compared with a mock control.

7.3 The reticulon protein RTN1A interacts with and modulates the ryanodine receptor 2 via its aminoterminal domain

This chapter focuses on my contributions to the following present study: Direct association of the reticulon protein RTN1A with the ryanodine receptor 2 in neurons[195]

Reticulon (RTN) genes code for a family of proteins which localize mainly in the endomembrane system found in all eukaryotic organism. The four known mammalian paralogues (RTN1, -2, -3, and -4/Nogo) have homologous carboxyl termini with two characteristic large hydrophobic regions [137].

Reticulons are ubiquitously expressed in vertebrates and for this reason researcher groups intended to investigate them on their diversity of the structure, localization and expression in tissues. The investigations ascertained that reticulons have multiple, diverse functions in the cells and play a role in the organisms, but they are hardly decoded. The results which have been gained so far leave many questions open.

The best characterized, member of the reticulon family is the RTN4-A/Nogo-A protein, which is thought to be an inhibitor for neurite outgrowth, restricting the regenerative capabilities of the mammalian CNS after injuries[137].

A more detailed view on the molecular structure of RTN proteins reveals a highly conserved domain of about 150 - 201 amino acids within the carboxy – terminal end of the molecule. This so called reticulon homology (RHD) comprises a hydrophilic loop that is flanked by two hydrophobic regions[138]. In contrast to these similarities, the amino-terminal regions of RTNs share only little sequence homology, which might account for the more distinct intrinsic properties of each of the respective isoforms. The following study supports the identification and characterization of putative target proteins that may act on this variable N-terminal region.

The ryanodine-sensitive calcium channels, also called ryanodine receptors, are intracellular calcium-release channels expressed in heart and brain and these channels have three isoforms (RyR₁₋₃) which have influence on the calcium signaling. Especially, the cardiac ryanodine receptor (RyR2) regulates the release of calcium from the sarcoplasmic reticulum, which initiates muscle contraction.

The common working mechanism of RyRs, known as calcium-induced calcium release (CICR), is a well described scenario where calcium influx through voltage- or ligand-gated calcium channels triggers the release of calcium from intracellular calcium pools. Among other things CICR has a functional role in the neurotransmitter release, influences synaptic-signal transduction pathways as well as gene expression.

My personal contribution to this present study “Direct association of the reticulon protein RTN1A with the ryanodine receptor 2 in neurons [195]”, was to analyse the influence of the direct binding partner RTN1A on HEK293 cells expressing RyR2.

This study was published 2013 in *Biochimica et Biophysica Acta (BBA) – Molecular Cell Research*, for full publication see the reviewed publication in chapter 11, in a collaboration with the Biocenter, Division of Neurobiochemistry, with the head Christine E. Bandtlow.

I participated in the investigations regarding calcium imaging experiments, Fura-2 microscopy to assert that the direct binding partner RTN1A has negative influence on the activity of RyR2, as well as to show HEK293 cells over-expressing RTN4-A/Nogo-A not influencing the RyR2 activity.

The following samples (constructs) were used to test.

mouse RyR2 cDNA

RTN1A full length, RTN1 523 = RTN1A (aa 1-523)

in comparison to RTN4-A/Nogo-A

(kindly provided by the Biocenter, Division of Neurobiochemistry)

In the present study we took a closer look specific on one member of the protein family, RTN1A. It is just situated in neurons (brain cells) and there it is expressed in abundance. After my experiments I want to answer the question how RTN1A as a direct binding partner influences RyR2 activity? RyR2 activity means the activation of the ryanodine receptors on the SR membrane. In detail, during the plateau phase of the action potential L-type voltage-dependent calcium channels (dihydropyridine receptors) are responsible for a small influx of calcium ions. This influx triggers a massive release of calcium from the SR via activation of the RyR2 channels, which in turn initiates muscle contraction[196].

To elucidate the communication between RTN1A and RyR2, we utilized the Fura-2 technique to reveal a direct impact on RyR2 activity via the N-terminus of RTN1A. A highly conserved 150-amino acid residue region of RyR2 was identified as the relevant domain for this functional interaction with RTN1A, which should either have an impact on RyR2-mediated calcium oscillations or RyR2-dependent calcium store depletion. RTN4A, a protein which does not act as a direct binding partner and therefore should not influence the RyR2 activity, was taken as a control. Fura-2 is very useful for measuring calcium signals in HEK293 cells for imaging of living human embryonic kidney 293 cells that expressed the proteins in fluorescent-labeled form. Transfected HEK293 cells were identified by their mcherry or EGFP

fluorescence and the evaluated proteins were either untagged RyR2 with mcherry or RyR2 with tagged m-cherry RTN1A or GFP-RTN4A.

Turning later specifically to the effects of the communication of the ryanodine receptor (RyR2) to the direct binding partner (RTN1A), previous it should make clear reference to the ryanodine receptor to identify the ryanodine function. With reference to the results of the RyR2 experiments it represents a basis for later comparisons between RyR2 alone, as control experiments and the two binding partners (RTN1A and RTN4A).

RyR2 –to provide a detailed characterization of the cardiac ryanodine receptor, we carefully analyzed RyR2 activity in principle at two sequential stages:

1. Visualizing of calcium oscillations as a result of applying a high extracellular calcium concentration. For the first we employed a Fura-2 based assay utilizing untagged RyR2 to monitor RyR2 oscillations following application of an elevated extracellular calcium concentration. The amount of the related release of calcium during oscillations was monitored over a time-period of 450 s.
2. RyR2 dependent store depletion upon stimulation with caffeine. The cardiac ryanodine receptor (RyR2) can be stimulated by Caffeine (1, 3, 7-trimethylxanthine), which is a widely used pharmacological agonist of the cardiac ryanodine receptor (RyR2) calcium release channel [197].

To overcome the limitation of an unlabeled RyR2 construct this drug was utilized as an indicator for RyR2 expression as its application results in a clear caffeine peak due to rapid and massive intracellular calcium store depletion. Hence, only cells with a peak at around 600 s were analyzed.

The upper left panel at Figure 7-5 (Figure 7C) shows Fura-2 ratio time-courses of single cells expressing RyR2 together with mcherry. HEK293 cells were sequentially perfused with buffer containing a 0 mM calcium, 1 mM calcium and 0 mM calcium with 10 mM caffeine solution (upper left panel). The lower right panel illustrates and summaries quantitative analysis as well as RyR2 dependent calcium oscillations.

To analyse the gained calcium-signals we decided to use a method where we compared the overall area under the respective curve by comparison of the total area under the curve (AUC). Furthermore, to estimate the overall expression rate of the RyR2, the number of cells that showed a clear caffeine peak, divided by the total amount of all measured HEK293 cells.

Due to this method, 87,1 % expressed cells actually the RyR2 gene Figure 7-5 (Figure 7C, right lower panel).

As shown in Figure 7-5 (Figure 7C, right upper panel) the RyR2-mediated calcium oscillations were monitored in HEK293 cells expressing RyR2 in the presence of RTN1A. A quantitative comparison of the two signals, as a result of the co-expression with mcherry-RTN1A revealed that, the amount of calcium releases via RyR2 oscillations was substantially reduced in comparison to control with m-cherry Figure 7-5 (Figure 7C, left and right upper panel, right lower panel). Additionally, the number of calcium oscillating HEK293 cells (87,1 %) was clearly reduced in RTN1A expressing cells (51,9 %) Figure 7-5 (Figure 7C, right lower panel).

In contrast, there was no indication of a significant difference of RyR2 activity between the untagged RyR2 and the co-expression of EGFP-RTN4A Figure 7-5 (Figure 7C, left lower panel). In line, the percentage of calcium oscillating HEK293 cells (74,6 %) was clearly above those with RTN1A co-expressed.

Interestingly, it seems that neither RTN1A nor RTN4A has an effect on the caffeine induced calcium release as the respective peaks were not significantly different (all statistics were performed by using a two-sample t-test).

Summing up, the evaluated results of the Fura-2 experiments targeted to the direct binding of RTN1A to RyR2 showing an influence on the RyR2-mediated calcium oscillations that means an effect in the regulation of intracellular calcium dynamics.

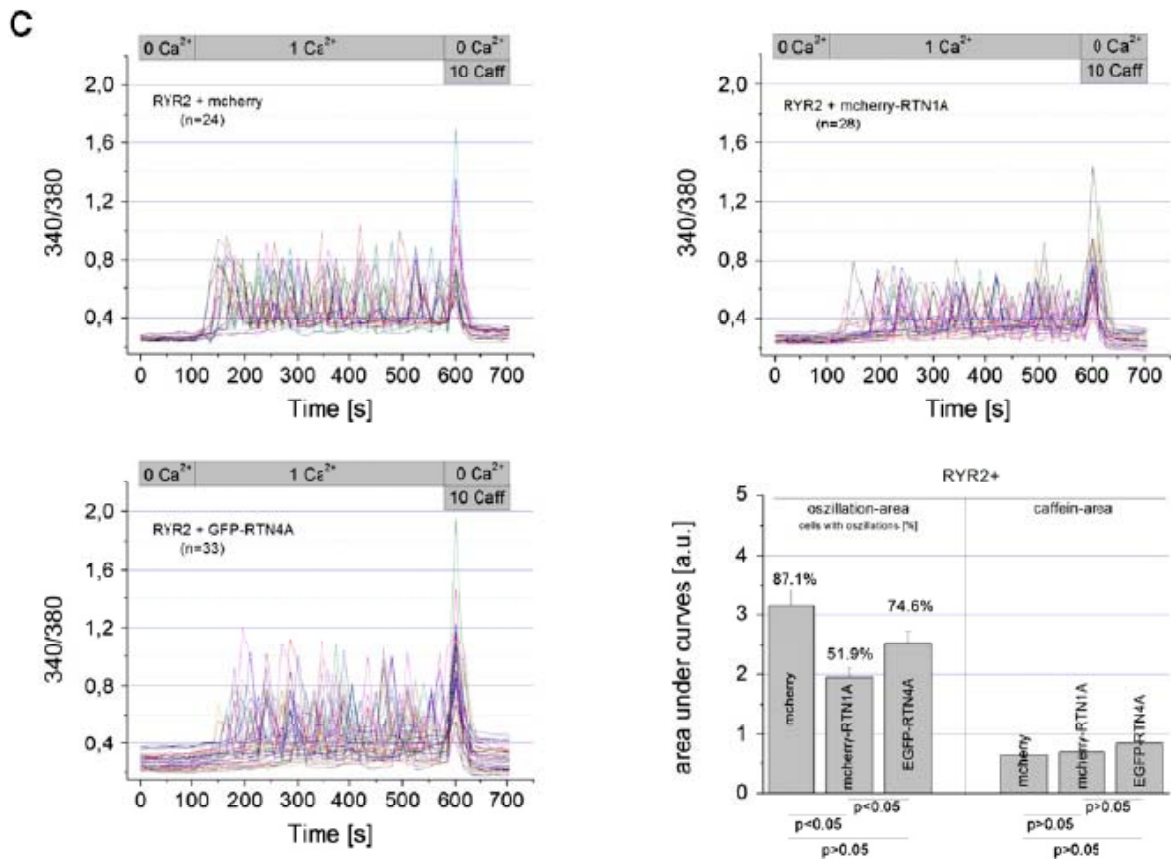


Figure 7-5 (Figure 7C)

Calcium Imaging, Fura-2 microscopy,

RyR2 evoked calcium oscillations in HEK293 cells. Upper and lower left panels represent Fura-2 ratio time-courses of single cells expressing RyR2 together with mcherry, mcherry-RTN1A or EGFP-RTN4A. Cells were continuously perfused with buffer containing 0 mM calcium (nominal free), 1 mM calcium and 0 mM calcium + 10 mM caffeine as indicated by the bars at the top. Lower right panel shows a quantitative analysis performed by integration of the respective single peak areas referred to area under curve for estimation of the total amount of the cytosolic calcium arising through RyR2 dependent calcium oscillations. The fraction of cells that showed both oscillations as well as a clear caffeine peak in comparison to those that lacked oscillations before a single caffeine peak are given in percentages in the graph. A two-sample t-test was carried out to test for significance as indicated by the p values at the bottom of the panel[195].

8 Discussion

8.1 Calcium-release activated Calcium (CRAC) channel blockers, GSK-7975A

The goal of the study was to test the GSK blockers, GSK-5503A and GSK-7975A regarding to their specificity on Orai1/Orai3 channels. GSK-7975A from GlaxoSmithKline was supposed to be a competitive calcium release activated calcium (CRAC) channel blocker.

In order to exclude that GSK-compounds influence other cellular effects, than the STIM1/Orai1 signalling cascade, I examined untransfected HEK293 cells pre-incubated with 10 μ M GSK-7975A by the calcium imaging technique employing Fura-2.

My study supports and extends especially the status and physiology of untransfected HEK293 cells to understand how HEK293 cells work and to measure directly the intracellular calcium level before and after store depletion. The intracellular level of GSK-7975A treated HEK293 cells compared with control cells behaves in the same manner. The blocker has no influence of the intracellular calcium level. The channel was fully inhibited by GSK-7975A compared to control cells with Dimethyl sulfoxide (DMSO).

The mode of depletion of the ER stores was conducted on the one hand by adding 100 μ M carbachol (CCh) to stimulate the TRPC-activity and on the other hand adding 30 μ M BHQ to examine the endogen basis by chemical blocking of the SERCA pumps. The CCh-induced TRPC effects stimulated in HEK cells, also the BHQ induced store depletion and blocking of the SERCA pumps behave in GSK-treated cells in a similar manner like the control cells.

Either CCh or BHQ induced increase of calcium concentration upon store-depletion was significantly different between DMSO and GSK-treated cells.

The intracellular calcium status remained unchanged in blocker-treated cells compared to control cells. Hence, after store depletion induced by CCh or BHQ the endogenous, store-operated calcium entry was definitely blocked in GSK-7975A treated cells compared to DMSO cells. The store-operated calcium influx after BHQ induced store-depletion was a significantly higher than in cells stimulated with CCH.

In conclusion my experiment showed that there is no effect on intracellular calcium stores. My study was very important, because calcium imaging is the only technique to monitor native CRAC channels in untransfected HEK293 cells. After my work, where I demonstrated with Fura-2AM fluorescence microscopy the behaviour of untransfected HEK293 cells, Romanins lab could exclude that GSK-blockers affect endogenous signalling cascades relevant after store-operated activation. Thus, they were able to test direct effects of GSK-blockers on STIM and Orai. By this way Romanins lab could support the inhibitory effect of

the GSK-7975A blocker on store-operated calcium entry into the cell. Hence, Fura-2 and patch clamp are perfectly in line.

Furthermore, the GSK-compound affected no TRPs and had no effect on calcium stores based on CCh and BHQ stimulation.

Summing up, my data show that store-operated calcium entry and also the endogenous CRAC channels were definitely blocked in the presence of GSK-7975A. The conclusions of my investigations were in accordance with the patch clamp experiments.

Taken together, in my fura-2 experiments you can see, after you reach a maximum depletion of the ER-stores with CCh or BHQ that pre-incubation of HEK293 cells with 10 μ M GSK-7975A fully inhibited native CRAC channels.

8.2 Canonical transient receptor potential (TRPC) 1 acts as a negative regulator for vanilloid TRPV6-mediated Ca²⁺ influx

TRPC1 and TRPV6 in calcium signaling

In the context of this thesis, I particularly investigated that TRPC1 and especially co-expression of TRPV6 with TRPC1 have a significantly lower calcium influx than TRPV6 overexpressed HEK cells. In addition, I measured also YFP-transfected control cells, to demonstrate the endogenous calcium homeostasis including store-depletion and calcium entry. My calcium imaging experiments supported the results of several techniques including molecular biology, confocal Förster Resonance Energy Transfer (FRET) microscopy and electrophysiological experiments, using the patch-clamp technique performed in the Romanin lab.

The Fura-2 microscopy allows to visualise both, an increased cytosolic calcium level due to store-depletion as well as subsequent store operated calcium entry. In order to evaluate the influence of expression of TRPC1 on HEK293 cells, statistical analysis of the calcium entry in HEK293 over-expressing TRPV6 and/or TRPC1 or YFP, compared the amount of calcium after adding a solution with an elevated concentration of calcium (2 mM).

The significance of TRPC1 mediated TRPV6 inhibition in this study is summarized in the results section in the bar chart Figure 5-2 (Figure 1H).

Fura-2-loaded cells are monitored co-expressing TRPV6 and TRPC1, TRPC1 and YFP-transfected cells as control sample. There is a significant drop of about 30 % of calcium influx at co-expressed TRPV6 and TRPC1 cells in comparison to TRPV6 alone. In TRPC1 expressing cells, only a very small calcium entry can be measured. TRPC1 and mock-transfected cells show a comparable calcium influx. Hence we could not observe a specific TRPC1 calcium entry.

TRPV6 shows the highest calcium influx into the cell without an additional stimulation of store-depletion, suggesting that TRPV6 is a constitutively active channel with high permeability for calcium ions.

The fact that TRPV6 calcium influx and/or current activity are considerably reduced in co-expression with TRPC1 could be explained by reduced localization of TRPV6 proteins in the plasma membrane, monitored by confocal microscopy. To compare the overall expression, we analysed TRPV6 with or without TRPC1 in Western blot experiments. It was demonstrated that the total expression level was not affected by TRPC1, while the plasma membrane located TRPV6 was largely reduced. Hence our results allow the conclusion, that

TRPC1 is able to reduce TRPV6 influx and/or current activity, because of the decreased expression in the plasma membrane.

Therefore TRPC1 has a modulatory function on TRPV6 channels, while we were unable to detect a homomeric TRPC1 channel activity.

In summary, my calcium imaging measurements are consistent with our electrophysiological approaches. Hence the results are continued with different research methods.

In further Fura-2 microscopy experiments, attached as supplementary figures (S1 D + E), I measured overexpressed TRPC1 HEK293 cells compared with a mock control transfection (untransfected cells), stimulated store-depletion of intracellular calcium pools by either carbachol (Cch; 100 μ M) or thapsigargin (TG; 1 μ M) and subsequent addition of 2 mM calcium.

The two different targeting points of the two agents are shortly described as follows.

Carbachol (Cch; 100 μ M) as a physiological agonist [179] and thapsigargin (TG; 1 μ M) appoint as an inhibitor of the calcium-ATPase pump in the endoplasmic reticulum [83, 192, 193] that is used to study store-operated calcium entry (SOCE) [46].

The result of my experiments was that the overexpressed TRPC1 HEK293 cells were **not** activated by the agent carbachol, as shown in the figure that the calcium peak is as high as the peak of the mocks or rather lower.

On the contrary, thapsigargin induces a significantly higher influx of calcium into the cytosol after depletion of intracellular calcium pools compared to mock-transfected cells. TRPC1 can also not be further activated by this agent.

These experiments are in contrast with other researcher groups, especially with the Muallem lab, a main statement is, which they have published in 2007 [198] that TRPC1 is stimulated by carbachol.

A major difference in the work of the Muallem lab to our results is the fact, that our TRPC1 construct has definitely no localization in the plasma membrane compared to a clear plasma-membrane localization in Muallem's group.

A possible reason for this distinct TRPC1 expression might be due to different cell culturing or different transfection methods (techniques) or to different, specific DNA quantities used.

Our results are in line with the Machaca lab. They expressed TRPC1 and TRPV6 in *Xenopus* oocytes and showed that these channels are permeable for divalent ions including calcium and especially magnesium [199]. The interaction between TRPC1 and TRPV6 subunits reduces TRPV6 currents, because endogenous TRPV6 maintains inactive. Further, co-expressed xTRPC1 and xTRPV6-cells showed a significantly decreased calcium influx. They also showed that over-expression of TRPC1 results in no specific current activation.

In contrast to our results they detected some plasma membrane localization of TRPV6 and TRPC1 by using fluorescent membrane markers [199].

Hence the heterocomplexes of TRPV6 with TRPC1 show a novel regulation activity and interact with further signaling cascades (pathways).

It is illustrated that TRPV6 assembles with TRPC1 to heteromeric channels that results in a suppressed TRPV6 function [199].

While in over-expression system homomeric TRP channels have been analysed, in endogenous tissues heteromeric TRP channel assembly is predominant.

Heteromeric TRP channels are best evidenced within the phospholipase C-coupled TRPC family and the subgroups TRPC1/4/5 interconnect with TRPC3/6/7. Amongst all TRPCs, the TRPC1 channel subtype is outstanding, because this protein is multifunctional and links together all other TRPC proteins. It has to be mentioned that the new formed heteromeric channels have a lower permeability for sodium and calcium ions compared with the equivalent homomeric form [189].

Both TRPC1 and TRPV6 have a broad tissue expression, suggesting that the novel hetero-complex can have multiple roles in calcium homeostasis.

Specifically TRPC1 and TRPV6 contribute to the calcium influx into prostate cells and in this context TRPV6 is associated with prostate cancer progress. Hence, further studies are required to investigate the function of TRPC1 and TRPV6 in prostate cancer cells.

The knowledge of the role of TRPC1 and TRPV6 in prostate cancer cells will provide a deeper insight in store-operated calcium channels (SOCs) in prostate cancer, as TRPC1 and TRPV6 are discussed to be part and have influence to SOC.

8.3 The reticulon protein RTN1A interacts with and modulates the ryanodine receptor 2 via its aminoterminal domain

The primary objective of the study was to demonstrate which impact has the reticulon RTN1A on the RyR2 physiological function. The main function of the RyR2 channel is that the cardiac excitation-contraction coupling relies on this key protein.

This common mechanism, called CICR is activated in heart muscle when an elevation in $[Ca^{2+}]_i$ mediated by L-type calcium channels (L-VGCCs) activates ryanodine receptors [200, 201]. Mutations in the RyR2 lead to an increased calcium level in the sarcoplasmic reticulum (SR). This calcium overload results in a so called “spontaneous SR calcium release” [147], which is mentioned as store-overload-induced calcium release (SOICR) [148].

The consequence is constant stress for the heart muscle. It has been shown that these RyR2 mutations which lead to an increased intracellular calcium level are linked to ventricular tachycardia and sudden death [157]. In this context more and more outcomes point out that ventricular tachycardia is linked with dysfunction of the calcium level in the sarcoplasmic reticulum [202, 203]. Hence, mutations in RyR2 have been linked to catecholaminergic polymorphic ventricular tachycardia (CPVT) and arrhythmogenic right ventricular cardiomyopathy type 2 (ARVD2).

It has been reported that CICR plays a role in a number of neuronal processes and has any influence in neural plasticity, including aging and memory, signal transduction pathways and cell development and differentiation [204].

By using the Fura-2AM fluorescence microscopy I make a substantial contribution about the functional impact of the direct binding between RyR2 and RTN1A. Christine Bandtlow's lab additionally has functional evidence. Christine Bandtlow's lab made experiments based on biochemical “binding-analyses”. They ascertain that the reticulon RTN1A is a direct binding partner of the RyR2. The results could not show, if the binding has an influence on the activity of RyR2. My measurements lead to the assumption, that the linkage has functional, negative effects on the calcium release of the sarcoplasmic reticulum.

RTN1A was supposed to be directly linked with the RyR2 channel by their N-terminal region. In order that the whole focus is not completely concentrated on the RTN1A-specific ER mediated effects, I examined a protein RTN4A/Nogo-A which does not interact with RyR2. RyR2, RTN1A or RTN4A/Nogo-A were co-expressed together with RyR2 in HEK293 cells and measured by the calcium imaging technique Fura-2.

The calcium imaging experiments were performed to monitor both the expression and functionality of unlabeled RyR2 as well as calcium oscillations as a result of the application of higher extracellular calcium concentration. For this reason transfected HEK293 cells were perfused with 0 mM calcium for RyR2 dependent calcium oscillations and on the response of single cardiac RyR2 channels to luminal or cytosolic calcium, followed by 10 mM caffeine to stimulate the spontaneous calcium release[205]. I could clearly measure that RyR2 was expressed in HEK293 cells as well show RyR2 dependent calcium oscillations.

To have a closer look on the working mechanism of the ryanodine receptor (RyR2), I wanted to compare RyR2 wildtype with the two binding partners (RyR2-RTN1A and RyR2-RTN4/Nogo-A).

If RyR2 is co-expressed with RTN1A in HEK cells, I could clearly measure reduced calcium oscillations, although the stimulation of the cardiac ryanodine receptor (RyR2) by caffeine, seen as clear caffeine peaks, were the same. The co-expression has no effect on the caffeine induced release.

Hence the RyR2 channel shows reduced calcium-induced calcium release (CICR) activity.

In contrast after stimulation of RTN4/Nogo-A I could clearly see the calcium oscillations behave in a similar manner like RyR2 wildtype. This leads to the assumption, that this protein, which does not act as a direct binding partner does not influence the RyR2 activity.

Reasons for the inhibitory effect of RTN1A on RyR2 function can be an over-expression of RTN1A in the ER. RyR2 and RTN1A are very close to each other in Purkinje cells or in mossy fibers in the hippocampus and additionally a low cytoplasmic calcium concentration under resting conditions are reasons for RTN1A binding to RyR2 channel[204]. Besides the neurotransmitter release the linkage of RTN1A and RyR2 have influence in an aging related dysbalance of calcium.

9 List of Abbreviations

AA	arachidonic acid
2-APB	2-Aminoethoxydiphenyl borate
ACh	Acetylcholine
AD	Alzheimer's disease
ARVD2	arrhythmogenic right ventricular cardiomyopathy type 2
ATP	adenosine triphosphate
BHQ	2,5-Di- <i>t</i> -butyl-1,4-benzohydroquinone
BP	bipolar disorder
Ca ²⁺	Calcium
CAD	CRAC channel activation domain
CAN	calcineurin
CC	coiled-coil (region)
CCh	Carbachol
CICR	calcium-induced calcium release
CMD	CRAC modulatory domain
CRAC	Calcium release activated Calcium (channel)
C-terminus	carboxy terminus
CPVT	catecholaminergic polymorphic ventricular tachycardia
DAD	delayed after depolarization
DAG	diacylglycerol
DMSO	dimethyl sulfoxide
EC-C	excitation-contraction coupling
EDTA	ethylenediaminetetraacetic acid
EGTA	ethyleneglycoltetraacetic acid
ER	endoplasmic reticulum
FRET	Förster resonance energy transfer/fluorescence resonance energy transferconfocal
GPCR	G protein-coupled receptor
HEK293	human embryonic kidney 293
hOrai	human Orai
ID _{STIM}	inactivation domain of STIM1
Ins (1,4,5)P ₃ or IP ₃	1,4,5-inositol trisphosphate
LGIC	ligand-gated ion channels
LTCC	L-type calcium channels
	L for Long-lasting also named as dihydropyridine

mAChR	muscarinic acetylcholine receptor
nAChR	nicotinic acetylcholine receptor
NFAT	nuclear factor of activated T-cells
N-terminus	amino terminus
OASF	Orai-activating small fragment
PI-pathways	phosphoinositide pathway
PIP ₂	phosphatidylinositol 4,5-bisphosphate
PLCβ	phospholipase Cβ
PM	plasma membrane
PMCA	plasma membrane calcium ATPases
RyR	ryanodine receptor
SAM	sterile alpha-motif
SCID	severe combined immunodeficiency
SERCA	sarcoendoplasmicreticular calcium ATPases
SHD	STIM1 homomerization domain
SOAR	STIM-Orai-activating region
SOCE	store operated calcium entry
SOICR	store-overload-induced calcium release
SR	sarcoplasmic reticulum
STIM1	stromal interacting molecule 1
TG	Thapsigargin
TKR	tyrosine kinase receptors
TM	transmembrane
TMD	transmembrane domain
TRPC	transient receptor potential canonical channel
TRPV	transient receptor vanilloid receptor
TTCC	T-type calcium channels
VDCC	voltage-dependent calcium channel
VR	ventricular tachycardia

10 References

1. Berridge, M.J., *Calcium signalling remodelling and disease*, in *Biochem Soc Trans*. 2012: England. p. 297-309.
2. image. *Calcium signaling machinery at a glance*. Available from: <http://yubinzhou.webs.com/>.
3. Berridge, M.J., *Inositol trisphosphate and calcium signalling*. *Nature*, 1993. **361**(6410): p. 315-25.
4. Wikipedia. *Calmodulin* <http://de.wikipedia.org/wiki/Calmodulin>. Wikipedia, the free encyclopedia.
5. Clapham, D.E., *Calcium signaling*. *Cell*, 2007. **131**(6): p. 1047-58.
6. Parekh, A.B. and J.W. Putney, Jr., *Store-operated calcium channels*. *Physiol Rev*, 2005. **85**(2): p. 757-810.
7. Putney, J.W., Jr., *A model for receptor-regulated calcium entry*. *Cell Calcium*, 1986. **7**(1): p. 1-12.
8. Hoth, M. and R. Penner, *Depletion of intracellular calcium stores activates a calcium current in mast cells*. *Nature*, 1992. **355**(6358): p. 353-6.
9. Hoth, M. and R. Penner, *Calcium release-activated calcium current in rat mast cells*. *J Physiol*, 1993. **465**: p. 359-86.
10. Feske, S., et al., *Gene regulation mediated by calcium signals in T lymphocytes*. *Nat Immunol*, 2001. **2**(4): p. 316-24.
11. Feske, S., et al., *A severe defect in CRAC Ca²⁺ channel activation and altered K⁺ channel gating in T cells from immunodeficient patients*. *J Exp Med*, 2005. **202**(5): p. 651-62.
12. Partiseti, M., et al., *The calcium current activated by T cell receptor and store depletion in human lymphocytes is absent in a primary immunodeficiency*. *J Biol Chem*, 1994. **269**(51): p. 32327-35.
13. Vig, M., et al., *Defective mast cell effector functions in mice lacking the CRACM1 pore subunit of store-operated calcium release-activated calcium channels*. *Nat Immunol*, 2008. **9**(1): p. 89-96.
14. Prakriya, M. and R.S. Lewis, *CRAC channels: activation, permeation, and the search for a molecular identity*. *Cell Calcium*, 2003. **33**(5-6): p. 311-21.
15. Liou, J., et al., *STIM is a Ca²⁺ sensor essential for Ca²⁺-store-depletion-triggered Ca²⁺ influx*. *Curr Biol*, 2005. **15**(13): p. 1235-41.
16. Roos, J., et al., *STIM1, an essential and conserved component of store-operated Ca²⁺ channel function*. *J Cell Biol*, 2005. **169**(3): p. 435-45.
17. Feske, S., et al., *A mutation in Orai1 causes immune deficiency by abrogating CRAC channel function*. *Nature*, 2006. **441**(7090): p. 179-85.
18. Vig, M., et al., *CRACM1 is a plasma membrane protein essential for store-operated Ca²⁺ entry*. *Science*, 2006. **312**(5777): p. 1220-3.
19. Zhang, S.L., et al., *Genome-wide RNAi screen of Ca(2+) influx identifies genes that regulate Ca(2+) release-activated Ca(2+) channel activity*. *Proc Natl Acad Sci U S A*, 2006. **103**(24): p. 9357-62.
20. Luik, R.M., et al., *Oligomerization of STIM1 couples ER calcium depletion to CRAC channel activation*. *Nature*, 2008. **454**(7203): p. 538-42.
21. Park, C.Y., et al., *STIM1 clusters and activates CRAC channels via direct binding of a cytosolic domain to Orai1*. *Cell*, 2009. **136**(5): p. 876-90.
22. Xu, P., et al., *Aggregation of STIM1 underneath the plasma membrane induces clustering of Orai1*. *Biochem Biophys Res Commun*, 2006. **350**(4): p. 969-76.
23. Muik, M., et al., *Dynamic coupling of the putative coiled-coil domain of ORAI1 with STIM1 mediates ORAI1 channel activation*. *J Biol Chem*, 2008. **283**(12): p. 8014-22.
24. Zheng, L., et al., *Biophysical characterization of the EF-hand and SAM domain containing Ca²⁺ sensory region of STIM1 and STIM2*. *Biochem Biophys Res Commun*, 2008. **369**(1): p. 240-6.
25. Parvez, S., et al., *STIM2 protein mediates distinct store-dependent and store-independent modes of CRAC channel activation*. *FASEB J*, 2008. **22**(3): p. 752-61.
26. Soboloff, J., et al., *STIM2 is an inhibitor of STIM1-mediated store-operated Ca²⁺ Entry*. *Curr Biol*, 2006. **16**(14): p. 1465-70.
27. Dziadek, M.A. and L.S. Johnstone, *Biochemical properties and cellular localisation of STIM proteins*. *Cell Calcium*, 2007. **42**(2): p. 123-32.
28. Brandman, O., et al., *STIM2 is a feedback regulator that stabilizes basal cytosolic and endoplasmic reticulum Ca²⁺ levels*. *Cell*, 2007. **131**(7): p. 1327-39.
29. Muik, M., et al., *Ca(2+) release-activated Ca(2+) (CRAC) current, structure, and function*. *Cell Mol Life Sci*, 2012. **69**(24): p. 4163-76.
30. Hou, X., et al., *Crystal structure of the calcium release-activated calcium channel Orai*. *Science*, 2012. **338**(6112): p. 1308-13.
31. Li, Z., et al., *Mapping the interacting domains of STIM1 and Orai1 in Ca²⁺ release-activated Ca²⁺ channel activation*. *J Biol Chem*, 2007. **282**(40): p. 29448-56.
32. Cahalan, M.D., et al., *Molecular basis of the CRAC channel*. *Cell Calcium*, 2007. **42**(2): p. 133-44.
33. Prakriya, M., et al., *Orai1 is an essential pore subunit of the CRAC channel*. *Nature*, 2006. **443**(7108): p. 230-3.
34. Gwack, Y., et al., *Biochemical and functional characterization of Orai proteins*. *J Biol Chem*, 2007. **282**(22): p. 16232-43.
35. Zhang, S.L., et al., *Store-dependent and -independent modes regulating Ca²⁺ release-activated Ca²⁺ channel activity of human Orai1 and Orai3*. *J Biol Chem*, 2008. **283**(25): p. 17662-71.
36. Mignen, O., J.L. Thompson, and T.J. Shuttleworth, *Orai1 subunit stoichiometry of the mammalian CRAC channel pore*. *J Physiol*, 2008. **586**(2): p. 419-25.

37. Yeromin, A.V., et al., *Molecular identification of the CRAC channel by altered ion selectivity in a mutant of Orai*. *Nature*, 2006. **443**(7108): p. 226-9.
38. Vig, M., et al., *CRACM1 multimers form the ion-selective pore of the CRAC channel*. *Curr Biol*, 2006. **16**(20): p. 2073-9.
39. Schindl, R., et al., *2-aminoethoxydiphenyl borate alters selectivity of Orai3 channels by increasing their pore size*. *J Biol Chem*, 2008. **283**(29): p. 20261-7.
40. Buckley, R.H., *The multiple causes of human SCID*. *J Clin Invest*, 2004. **114**(10): p. 1409-11.
41. Carroll, H.P., B.B. McNaul, and M. Gadina, *Immunodeficiency is a tough nut to CRAC: the importance of calcium flux in T cell activation*. *Mol Interv*, 2006. **6**(5): p. 253-6.
42. Gaspar, H.B. and A.J. Thrasher, *Gene therapy for severe combined immunodeficiencies*. *Expert Opin Biol Ther*, 2005. **5**(9): p. 1175-82.
43. Derler, I., et al., *Increased hydrophobicity at the N terminus/membrane interface impairs gating of the severe combined immunodeficiency-related ORAI1 mutant*. *J Biol Chem*, 2009. **284**(23): p. 15903-15.
44. Soboloff, J., et al., *Calcium signals mediated by STIM and Orai proteins--a new paradigm in inter-organelle communication*. *Biochim Biophys Acta*, 2006. **1763**(11): p. 1161-8.
45. Lewis, R.S. and M.D. Cahalan, *Mitogen-induced oscillations of cytosolic Ca²⁺ and transmembrane Ca²⁺ current in human leukemic T cells*. *Cell Regul*, 1989. **1**(1): p. 99-112.
46. Zweifach, A. and R.S. Lewis, *Mitogen-regulated Ca²⁺ current of T lymphocytes is activated by depletion of intracellular Ca²⁺ stores*. *Proc Natl Acad Sci U S A*, 1993. **90**(13): p. 6295-9.
47. Zhang, S.L., et al., *STIM1 is a Ca²⁺ sensor that activates CRAC channels and migrates from the Ca²⁺ store to the plasma membrane*. *Nature*, 2005. **437**(7060): p. 902-5.
48. Baba, Y., et al., *Coupling of STIM1 to store-operated Ca²⁺ entry through its constitutive and inducible movement in the endoplasmic reticulum*. *Proc Natl Acad Sci U S A*, 2006. **103**(45): p. 16704-9.
49. Liou, J., et al., *Live-cell imaging reveals sequential oligomerization and local plasma membrane targeting of stromal interaction molecule 1 after Ca²⁺ store depletion*. *Proc Natl Acad Sci U S A*, 2007. **104**(22): p. 9301-6.
50. Wu, M.M., et al., *Ca²⁺ store depletion causes STIM1 to accumulate in ER regions closely associated with the plasma membrane*. *J Cell Biol*, 2006. **174**(6): p. 803-13.
51. Frischauf, I., et al., *Molecular determinants of the coupling between STIM1 and Orai channels: differential activation of Orai1-3 channels by a STIM1 coiled-coil mutant*. *J Biol Chem*, 2009. **284**(32): p. 21696-706.
52. Muik, M., et al., *A Cytosolic Homomerization and a Modulatory Domain within STIM1 C Terminus Determine Coupling to ORAI1 Channels*. *J Biol Chem*, 2009. **284**(13): p. 8421-6.
53. Yuan, J.P., et al., *SOAR and the polybasic STIM1 domains gate and regulate Orai channels*. *Nat Cell Biol*, 2009. **11**(3): p. 337-43.
54. Kawasaki, T., I. Lange, and S. Feske, *A minimal regulatory domain in the C terminus of STIM1 binds to and activates ORAI1 CRAC channels*. *Biochem Biophys Res Commun*, 2009. **385**(1): p. 49-54.
55. Calloway, N., et al., *Molecular clustering of STIM1 with Orai1/CRACM1 at the plasma membrane depends dynamically on depletion of Ca²⁺ stores and on electrostatic interactions*. *Mol Biol Cell*, 2009. **20**(1): p. 389-99.
56. Hull, J.J., et al., *Bombyx mori homologs of STIM1 and Orai1 are essential components of the signal transduction cascade that regulates sex pheromone production*. *J Biol Chem*, 2009. **284**(45): p. 31200-13.
57. Calloway, N., D. Holowka, and B. Baird, *A basic sequence in STIM1 promotes Ca²⁺ influx by interacting with the C-terminal acidic coiled coil of Orai1*. *Biochemistry*, 2010. **49**(6): p. 1067-71.
58. Lis, A., et al., *A single lysine in the N-terminal region of store-operated channels is critical for STIM1-mediated gating*. *J Gen Physiol*, 2010. **136**(6): p. 673-86.
59. Hoover, P.J. and R.S. Lewis, *Stoichiometric requirements for trapping and gating of Ca²⁺ release-activated Ca²⁺ (CRAC) channels by stromal interaction molecule 1 (STIM1)*. *Proc Natl Acad Sci U S A*, 2011. **108**(32): p. 13299-304.
60. Hardie, R.C. and B. Minke, *The trp gene is essential for a light-activated Ca²⁺ channel in Drosophila photoreceptors*. *Neuron*, 1992. **8**(4): p. 643-51.
61. Cosens, D.J. and A. Manning, *Abnormal electroretinogram from a Drosophila mutant*. *Nature*, 1969. **224**(5216): p. 285-7.
62. Montell, C. and G.M. Rubin, *Molecular characterization of the Drosophila trp locus: a putative integral membrane protein required for phototransduction*. *Neuron*, 1989. **2**(4): p. 1313-23.
63. Montell, C., L. Birnbaumer, and V. Flockerzi, *The TRP channels, a remarkably functional family*. *Cell*, 2002. **108**(5): p. 595-8.
64. Montell, C., et al., *A unified nomenclature for the superfamily of TRP cation channels*. *Mol Cell*, 2002. **9**(2): p. 229-31.
65. Corey, D.P., *New TRP channels in hearing and mechanosensation*. *Neuron*, 2003. **39**(4): p. 585-8.
66. Clapham, D.E., *TRP channels as cellular sensors*. *Nature*, 2003. **426**(6966): p. 517-24.
67. Delmas, P., *Polycystins: from mechanosensation to gene regulation*. *Cell*, 2004. **118**(2): p. 145-8.
68. Moran, M.M., H. Xu, and D.E. Clapham, *TRP ion channels in the nervous system*. *Curr Opin Neurobiol*, 2004. **14**(3): p. 362-9.
69. Turner, H., et al., *Discrimination of intracellular calcium store subcompartments using TRPV1 (transient receptor potential channel, vanilloid subfamily member 1) release channel activity*. *Biochem J*, 2003. **371**(Pt 2): p. 341-50.

70. Zhang, L. and G.J. Barritt, *Evidence that TRPM8 is an androgen-dependent Ca²⁺ channel required for the survival of prostate cancer cells*. *Cancer Res*, 2004. **64**(22): p. 8365-73.
71. Pedersen, S.F., G. Owsianik, and B. Nilius, *TRP channels: an overview*. *Cell Calcium*, 2005. **38**(3-4): p. 233-52.
72. Hofmann, T., et al., *Transient receptor potential channels as molecular substrates of receptor-mediated cation entry*. *J Mol Med (Berl)*, 2000. **78**(1): p. 14-25.
73. Yuan, J.P., et al., *Homer binds TRPC family channels and is required for gating of TRPC1 by IP₃ receptors*. *Cell*, 2003. **114**(6): p. 777-89.
74. Zhu, X., et al., *trp, a novel mammalian gene family essential for agonist-activated capacitative Ca²⁺ entry*. *Cell*, 1996. **85**(5): p. 661-71.
75. Zitt, C., et al., *Cloning and functional expression of a human Ca²⁺-permeable cation channel activated by calcium store depletion*. *Neuron*, 1996. **16**(6): p. 1189-96.
76. Liu, X., B.B. Singh, and I.S. Ambudkar, *TRPC1 is required for functional store-operated Ca²⁺ channels. Role of acidic amino acid residues in the S5-S6 region*. *J Biol Chem*, 2003. **278**(13): p. 11337-43.
77. Xu, S.Z. and D.J. Beech, *TrpC1 is a membrane-spanning subunit of store-operated Ca(2+) channels in native vascular smooth muscle cells*. *Circ Res*, 2001. **88**(1): p. 84-7.
78. Brough, G.H., et al., *Contribution of endogenously expressed Trp1 to a Ca²⁺-selective, store-operated Ca²⁺ entry pathway*. *FASEB J*, 2001. **15**(10): p. 1727-38.
79. Antoniotti, S., et al., *Expression and functional role of bTRPC1 channels in native endothelial cells*. *FEBS Lett*, 2002. **510**(3): p. 189-95.
80. Mori, Y., et al., *Transient receptor potential 1 regulates capacitative Ca(2+) entry and Ca(2+) release from endoplasmic reticulum in B lymphocytes*. *J Exp Med*, 2002. **195**(6): p. 673-81.
81. Paria, B.C., et al., *Tumor necrosis factor-alpha-induced TRPC1 expression amplifies store-operated Ca²⁺ influx and endothelial permeability*. *Am J Physiol Lung Cell Mol Physiol*, 2004. **287**(6): p. L1303-13.
82. Hofmann, T., et al., *Subunit composition of mammalian transient receptor potential channels in living cells*. *Proc Natl Acad Sci U S A*, 2002. **99**(11): p. 7461-6.
83. Strubing, C., et al., *TRPC1 and TRPC5 form a novel cation channel in mammalian brain*. *Neuron*, 2001. **29**(3): p. 645-55.
84. Dietrich, A., et al., *Cation channels of the transient receptor potential superfamily: their role in physiological and pathophysiological processes of smooth muscle cells*. *Pharmacol Ther*, 2006. **112**(3): p. 744-60.
85. Ambudkar, I.S., et al., *Plasma membrane localization of TRPC channels: role of caveolar lipid rafts*. *Novartis Found Symp*, 2004. **258**: p. 63-70; discussion 70-4, 98-102, 263-6.
86. Liao, M., et al., *Structure of the TRPV1 ion channel determined by electron cryo-microscopy*. *Nature*, 2013. **504**(7478): p. 107-12.
87. Hofmann, T., et al., *Direct activation of human TRPC6 and TRPC3 channels by diacylglycerol*. *Nature*, 1999. **397**(6716): p. 259-63.
88. Wes, P.D., et al., *TRPC1, a human homolog of a Drosophila store-operated channel*. *Proc Natl Acad Sci U S A*, 1995. **92**(21): p. 9652-6.
89. Lucas, P., et al., *A diacylglycerol-gated cation channel in vomeronasal neuron dendrites is impaired in TRPC2 mutant mice: mechanism of pheromone transduction*. *Neuron*, 2003. **40**(3): p. 551-61.
90. Jungnickel, M.K., et al., *Trp2 regulates entry of Ca²⁺ into mouse sperm triggered by egg ZP3*. *Nat Cell Biol*, 2001. **3**(5): p. 499-502.
91. Freichel, M., et al., *Lack of an endothelial store-operated Ca²⁺ current impairs agonist-dependent vasorelaxation in TRP4-/- mice*. *Nat Cell Biol*, 2001. **3**(2): p. 121-7.
92. Tirupathi, C., et al., *Impairment of store-operated Ca²⁺ entry in TRPC4(-/-) mice interferes with increase in lung microvascular permeability*. *Circ Res*, 2002. **91**(1): p. 70-6.
93. Beech, D.J., K. Muraki, and R. Flemming, *Non-selective cationic channels of smooth muscle and the mammalian homologues of Drosophila TRP*. *J Physiol*, 2004. **559**(Pt 3): p. 685-706.
94. Walker, R.L., et al., *TRPC4 currents have properties similar to the pacemaker current in interstitial cells of Cajal*. *Am J Physiol Cell Physiol*, 2002. **283**(6): p. C1637-45.
95. Torihashi, S., et al., *Calcium oscillation linked to pacemaking of interstitial cells of Cajal: requirement of calcium influx and localization of TRP4 in caveolae*. *J Biol Chem*, 2002. **277**(21): p. 19191-7.
96. Lee-Kwon, W., et al., *Expression of TRPC4 channel protein that interacts with NHERF-2 in rat descending vasa recta*. *Am J Physiol Cell Physiol*, 2005. **288**(4): p. C942-9.
97. Philipp, S., et al., *TRP4 (CCE1) protein is part of native calcium release-activated Ca²⁺-like channels in adrenal cells*. *J Biol Chem*, 2000. **275**(31): p. 23965-72.
98. Firth, A.L., C.V. Remillard, and J.X. Yuan, *TRP channels in hypertension*. *Biochim Biophys Acta*, 2007. **1772**(8): p. 895-906.
99. Gunthorpe, M.J., et al., *The diversity in the vanilloid (TRPV) receptor family of ion channels*. *Trends Pharmacol Sci*, 2002. **23**(4): p. 183-91.
100. Benham, C.D., J.B. Davis, and A.D. Randall, *Vanilloid and TRP channels: a family of lipid-gated cation channels*. *Neuropharmacology*, 2002. **42**(7): p. 873-88.
101. Peng, J.B., E.M. Brown, and M.A. Hediger, *Epithelial Ca²⁺ entry channels: transcellular Ca²⁺ transport and beyond*. *J Physiol*, 2003. **551**(Pt 3): p. 729-40.
102. Brederson, J.D., P.R. Kym, and A. Szallasi, *Targeting TRP channels for pain relief*. *Eur J Pharmacol*, 2013. **716**(1-3): p. 61-76.
103. Julius, D., *TRP channels and pain*. *Annu Rev Cell Dev Biol*, 2013. **29**: p. 355-84.

104. Caterina, M.J., et al., *The capsaicin receptor: a heat-activated ion channel in the pain pathway*. Nature, 1997. **389**(6653): p. 816-24.
105. Jordt, S.E. and D. Julius, *Molecular basis for species-specific sensitivity to "hot" chili peppers*. Cell, 2002. **108**(3): p. 421-30.
106. Planells-Cases, R., et al., *Functional aspects and mechanisms of TRPV1 involvement in neurogenic inflammation that leads to thermal hyperalgesia*. Pflugers Arch, 2005. **451**(1): p. 151-9.
107. Van Der Stelt, M. and V. Di Marzo, *Endovanilloids. Putative endogenous ligands of transient receptor potential vanilloid 1 channels*. Eur J Biochem, 2004. **271**(10): p. 1827-34.
108. Puntambekar, P., et al., *Direct interaction of adenosine with the TRPV1 channel protein*. J Neurosci, 2004. **24**(14): p. 3663-71.
109. Wood, R.J., L. Tchack, and S. Taparia, *1,25-Dihydroxyvitamin D3 increases the expression of the CaT1 epithelial calcium channel in the Caco-2 human intestinal cell line*. BMC Physiol, 2001. **1**: p. 11.
110. Fixemer, T., et al., *Expression of the Ca²⁺-selective cation channel TRPV6 in human prostate cancer: a novel prognostic marker for tumor progression*. Oncogene, 2003. **22**(49): p. 7858-61.
111. R. Vennekens, J.G.H., J. Prenen, M. Stuiver, P.H. Willems, G. Droogmans, B. Nilius, R.J. Bindels, *Permeation and gating properties of the novel epithelial Ca²⁺ channel*. J Biol Chem, 2000. **275**: p. 3963-3969.
112. Nilius, B., et al., *Whole-cell and single channel monovalent cation currents through the novel rabbit epithelial Ca²⁺ channel ECaC*. J Physiol, 2000. **527 Pt 2**: p. 239-48.
113. Nilius, B., et al., *The single pore residue Asp542 determines Ca²⁺ permeation and Mg²⁺ block of the epithelial Ca²⁺ channel*. J Biol Chem, 2001. **276**(2): p. 1020-5.
114. Yue, L., et al., *CaT1 manifests the pore properties of the calcium-release-activated calcium channel*. Nature, 2001. **410**(6829): p. 705-9.
115. Schindl, R., et al., *Store depletion-activated CaT1 currents in rat basophilic leukemia mast cells are inhibited by 2-aminoethoxydiphenyl borate. Evidence for a regulatory component that controls activation of both CaT1 and CRAC (Ca²⁺) release-activated Ca²⁺ channel) channels*. J Biol Chem, 2002. **277**(30): p. 26950-8.
116. Hoenderop, J.G., et al., *Homo- and heterotetrameric architecture of the epithelial Ca²⁺ channels TRPV5 and TRPV6*. EMBO J, 2003. **22**(4): p. 776-85.
117. Roy, S.S. and G. Hajnoczky, *Calcium, mitochondria and apoptosis studied by fluorescence measurements*. Methods, 2008. **46**(3): p. 213-23.
118. Fatt, P. and B.L. Ginsborg, *The ionic requirements for the production of action potentials in crustacean muscle fibres*. J Physiol, 1958. **142**(3): p. 516-43.
119. Sherwood, L., *Human Physiology: From Cells to Systems*. Seventh ed. 2010: Yolanda Cassia.
120. Long, S.B., E.B. Campbell, and R. Mackinnon, *Voltage sensor of Kv1.2: structural basis of electromechanical coupling*. Science, 2005. **309**(5736): p. 903-8.
121. Page, W. *voltage-gated calcium channels_excitation-contraction coupling*. physprojekt-2011.wikispaces.com:[<http://physproject-2011.wikispaces.com/M.+MUSCLE+PHYSIOLOGY>].
122. picture. *voltage-gated calcium channels_excitation-contraction coupling*. physproject-2011.wikispaces.com:[<http://physproject-2011.wikispaces.com/M.+MUSCLE+PHYSIOLOGY>].
123. Ernst Mutschler, G.G., Heyo K. Kroemer, Peter Ruth, Monika Schäfer-Korting, *Mutschler Arzneimittelwirkungen: Lehrbuch der Pharmakologie und Toxikologie*. Vol. Auflage: 9. (1. April 2008). 2008. 1243.
124. Hajnoczky, G., E. Davies, and M. Madesh, *Calcium signaling and apoptosis*. Biochem Biophys Res Commun, 2003. **304**(3): p. 445-54.
125. Hilgemann, D.W., et al., *Molecular control of cardiac sodium homeostasis in health and disease*. J Cardiovasc Electrophysiol, 2006. **17 Suppl 1**: p. S47-S56.
126. Ogawa, Y., *Role of ryanodine receptors*. Crit Rev Biochem Mol Biol, 1994. **29**(4): p. 229-74.
127. picture. *Cellular Ca²⁺ regulation*. http://www.nature.com/nrm/journal/v4/n7/fig_tab/nrm1150_F1.html].
128. Page, W. *From global to local: a new understanding of cardiac electromechanical coupling*. http://tidsskriftet.no/article/2507376/en_GB].
129. Takeshima, H., et al., *Primary structure and expression from complementary DNA of skeletal muscle ryanodine receptor*. Nature, 1989. **339**(6224): p. 439-45.
130. Zorzato, F., et al., *Molecular cloning of cDNA encoding human and rabbit forms of the Ca²⁺ release channel (ryanodine receptor) of skeletal muscle sarcoplasmic reticulum*. J Biol Chem, 1990. **265**(4): p. 2244-56.
131. Otsu, K., et al., *Molecular cloning of cDNA encoding the Ca²⁺ release channel (ryanodine receptor) of rabbit cardiac muscle sarcoplasmic reticulum*. J Biol Chem, 1990. **265**(23): p. 13472-83.
132. Nakai, J., et al., *Primary structure and functional expression from cDNA of the cardiac ryanodine receptor/calcium release channel*. FEBS Lett, 1990. **271**(1-2): p. 169-77.
133. Coussin, F., et al., *Requirement of ryanodine receptor subtypes 1 and 2 for Ca²⁺-induced Ca²⁺ release in vascular myocytes*. J Biol Chem, 2000. **275**(13): p. 9596-603.
134. Giannini, G., et al., *The ryanodine receptor/calcium channel genes are widely and differentially expressed in murine brain and peripheral tissues*. J Cell Biol, 1995. **128**(5): p. 893-904.
135. picture. *Ryanodin Receptors*. <http://webdoc.sub.gwdg.de/diss/2000/krempler/einl.pdf>].
136. Priori, S.G. and C. Napolitano, *Cardiac and skeletal muscle disorders caused by mutations in the intracellular Ca²⁺ release channels*. J Clin Invest, 2005. **115**(8): p. 2033-8.

137. Oertle, T., et al., *A reticular rhapsody: phylogenic evolution and nomenclature of the RTN/Nogo gene family*. FASEB J, 2003. **17**(10): p. 1238-47.
138. Yang, Y.S. and S.M. Strittmatter, *The reticulons: a family of proteins with diverse functions*. Genome Biol, 2007. **8**(12): p. 234.
139. Oertle, T. and M.E. Schwab, *Nogo and its paRTNers*. Trends Cell Biol, 2003. **13**(4): p. 187-94.
140. picture. *action potential in a nerve cell*. <http://classroom.sdmesa.edu/eschmid/Chaper9-Zoo145.htm>].
141. picture. *the different phases and events of a typical action potential in a nerve cell*. <http://classroom.sdmesa.edu/eschmid/Chaper9-Zoo145.htm>].
142. picture. *action potential in a nerve cell vs cardiac myocyte*. <http://www.cvphysiology.com/Arrhythmias/A010.htm>].
143. picture. *actionpotential heart*. [www.studyblue.com:\[http://www.studyblue.com/notes/note/n/chapter-484950/deck/2790108\]](http://www.studyblue.com/notes/note/n/chapter-484950/deck/2790108).
144. Bers, D.M., *Cardiac excitation-contraction coupling*. Nature, 2002. **415**(6868): p. 198-205.
145. Kushnir, A., M.J. Betzenhauser, and A.R. Marks, *Ryanodine receptor studies using genetically engineered mice*. FEBS Lett, 2010. **584**(10): p. 1956-65.
146. picture. *muscle contraction*. http://faculty.weber.edu/nokazaki/Human_Physiology/Class%20notes/MUSCULAR-SYSTEM.htm].
147. Lakatta, E.G., *Functional implications of spontaneous sarcoplasmic reticulum Ca²⁺ release in the heart*. Cardiovasc Res, 1992. **26**(3): p. 193-214.
148. Jiang, D., et al., *RyR2 mutations linked to ventricular tachycardia and sudden death reduce the threshold for store-overload-induced Ca²⁺ release (SOICR)*. Proc Natl Acad Sci U S A, 2004. **101**(35): p. 13062-7.
149. Leenhardt, A., et al., *Catecholaminergic polymorphic ventricular tachycardia in children. A 7-year follow-up of 21 patients*. Circulation, 1995. **91**(5): p. 1512-9.
150. Laitinen, P.J., et al., *Genes, exercise and sudden death: molecular basis of familial catecholaminergic polymorphic ventricular tachycardia*. Ann Med, 2004. **36 Suppl 1**: p. 81-6.
151. Priori, S.G., et al., *Clinical and molecular characterization of patients with catecholaminergic polymorphic ventricular tachycardia*. Circulation, 2002. **106**(1): p. 69-74.
152. Laitinen, P.J., et al., *Mutations of the cardiac ryanodine receptor (RyR2) gene in familial polymorphic ventricular tachycardia*. Circulation, 2001. **103**(4): p. 485-90.
153. Tiso, N., et al., *Identification of mutations in the cardiac ryanodine receptor gene in families affected with arrhythmogenic right ventricular cardiomyopathy type 2 (ARVD2)*. Hum Mol Genet, 2001. **10**(3): p. 189-94.
154. Lahat, H., et al., *A missense mutation in a highly conserved region of CASQ2 is associated with autosomal recessive catecholamine-induced polymorphic ventricular tachycardia in Bedouin families from Israel*. Am J Hum Genet, 2001. **69**(6): p. 1378-84.
155. Postma, A.V., et al., *Absence of calsequestrin 2 causes severe forms of catecholaminergic polymorphic ventricular tachycardia*. Circ Res, 2002. **91**(8): p. e21-6.
156. picture. *irregular heart beats*. <http://www.nature.com/nm/journal/v17/n8/full/nm.2441.html>].
157. Jiang, D., et al., *Enhanced store overload-induced Ca²⁺ release and channel sensitivity to luminal Ca²⁺ activation are common defects of RyR2 mutations linked to ventricular tachycardia and sudden death*. Circ Res, 2005. **97**(11): p. 1173-81.
158. Wikipedia. *Calcium Imaging* http://en.wikipedia.org/wiki/Calcium_imaging. Wikipedia, the free encyclopedia 24 September 2012.
159. Grynkiewicz, G., M. Poenie, and R.Y. Tsien, *A new generation of Ca²⁺ indicators with greatly improved fluorescence properties*. J Biol Chem, 1985. **260**(6): p. 3440-50.
160. Wikipedia. *Fura-2AM_deutsch* <http://de.wikipedia.org/wiki/Fura-2AM>. Wikipedia, the free encyclopedia.
161. Wikipedia. *Fura-2* <http://en.wikipedia.org/wiki/Fura-2>. Wikipedia, the free encyclopedia.
162. Wikipedia. *Fura-2AM* http://en.wikipedia.org/wiki/Fura-2-acetoxymethyl_ester. Wikipedia, the free encyclopedia.
163. Wikipedia. *EGTA (chemical)* [http://en.wikipedia.org/wiki/EGTA_\(chemical\)](http://en.wikipedia.org/wiki/EGTA_(chemical)). Wikipedia, the free encyclopedia.
164. Wikipedia. *BAPTA* <http://en.wikipedia.org/wiki/BAPTA>. Wikipedia, the free encyclopedia.
165. picture. *Fura-2AM_Fura-2* http://mktg.biotech.com/tektalk/2006/0206/featuredapp_0206.htm.
166. picture. *fluoreszenzmaxima of fura-2* (340/380). <http://www.tphys.jku.at/macke/prtrg/pr345/wmss03ig.shtml>].
167. Derler, I., et al., *The action of selective CRAC channel blockers is affected by the Orai pore geometry*. Cell Calcium, 2012.
168. Berridge, M.J., M.D. Bootman, and H.L. Roderick, *Calcium signalling: dynamics, homeostasis and remodelling*. Nat Rev Mol Cell Biol, 2003. **4**(7): p. 517-29.
169. Fischer, B.S., et al., *Capsaicin inhibits Jurkat T-cell activation by blocking calcium entry current I(CRAC)*. J Pharmacol Exp Ther, 2001. **299**(1): p. 238-46.
170. Gericke, M., et al., *Inhibition of capacitative Ca²⁺ entry by a Cl⁻ channel blocker in human endothelial cells*. Eur J Pharmacol, 1994. **269**(3): p. 381-4.
171. Li, J.H., et al., *Properties of Ca(2+) release-activated Ca(2+) channel block by 5-nitro-2-(3-phenylpropylamino)-benzoic acid in Jurkat cells*. Eur J Pharmacol, 2000. **394**(2-3): p. 171-9.
172. Reinsprecht, M., et al., *Blockade of capacitive Ca²⁺ influx by Cl⁻ channel blockers inhibits secretion from rat mucosal-type mast cells*. Mol Pharmacol, 1995. **47**(5): p. 1014-20.

173. Ross, P.E. and M.D. Cahalan, *Ca²⁺ influx pathways mediated by swelling or stores depletion in mouse thymocytes*. J Gen Physiol, 1995. **106**(3): p. 415-44.
174. Beech, D.J., *Orai1 calcium channels in the vasculature*. Pflugers Arch, 2012. **463**(5): p. 635-47.
175. Kostyuk, P. and A. Verkhratsky, *Calcium stores in neurons and glia*. Neuroscience, 1994. **63**(2): p. 381-404.
176. Scamps, F., et al., *Sarco-endoplasmic ATPase blocker 2,5-Di(tert-butyl)-1, 4-benzohydroquinone inhibits N-, P-, and Q- but not T-, L-, or R-type calcium currents in central and peripheral neurons*. Mol Pharmacol, 2000. **58**(1): p. 18-26.
177. Ogden, D.C. and D. Colquhoun, *Ion channel block by acetylcholine, carbachol and suberyldicholine at the frog neuromuscular junction*. Proc R Soc Lond B Biol Sci, 1985. **225**(1240): p. 329-55.
178. Wikipedia. *Carbachol*, <http://en.wikipedia.org/wiki/Carbachol>. Wikipedia, the free encyclopedia
179. Mayerhofer, A., et al., *Carbachol increases intracellular free calcium concentrations in human granulosa-lutein cells*. J Endocrinol, 1992. **135**(1): p. 153-9.
180. Edelman, J.L., et al., *Differential effects of carbachol on calcium entry and release in CHO cells expressing the m3 muscarinic receptor*. Cell Calcium, 1994. **16**(3): p. 181-93.
181. Zagranichnaya, T.K., X. Wu, and M.L. Villereal, *Endogenous TRPC1, TRPC3, and TRPC7 proteins combine to form native store-operated channels in HEK-293 cells*. J Biol Chem, 2005. **280**(33): p. 29559-69.
182. Schindl, R., et al., *Canonical transient receptor potential (TRPC) 1 acts as a negative regulator for vanilloid TRPV6-mediated Ca²⁺ influx*. J Biol Chem, 2012. **287**(42): p. 35612-20.
183. Venkatachalam, K. and C. Montell, *TRP channels*. Annu Rev Biochem, 2007. **76**: p. 387-417.
184. Wu, L.J., T.B. Sweet, and D.E. Clapham, *International Union of Basic and Clinical Pharmacology. LXXVI. Current progress in the mammalian TRP ion channel family*. Pharmacol Rev, 2010. **62**(3): p. 381-404.
185. Kedei, N., et al., *Analysis of the native quaternary structure of vanilloid receptor 1*. J Biol Chem, 2001. **276**(30): p. 28613-9.
186. Cheng, W., C. Sun, and J. Zheng, *Heteromerization of TRP channel subunits: extending functional diversity*. Protein Cell, 2010. **1**(9): p. 802-10.
187. Jardin, I., et al., *Orai1 mediates the interaction between STIM1 and hTRPC1 and regulates the mode of activation of hTRPC1-forming Ca²⁺ channels*. J Biol Chem, 2008. **283**(37): p. 25296-304.
188. Liu, X., et al., *Molecular analysis of a store-operated and 2-acetyl-sn-glycerol-sensitive non-selective cation channel. Heteromeric assembly of TRPC1-TRPC3*. J Biol Chem, 2005. **280**(22): p. 21600-6.
189. Strubing, C., et al., *Formation of novel TRPC channels by complex subunit interactions in embryonic brain*. J Biol Chem, 2003. **278**(40): p. 39014-9.
190. Storch, U., et al., *Transient receptor potential channel 1 (TRPC1) reduces calcium permeability in heteromeric channel complexes*. J Biol Chem, 2012. **287**(5): p. 3530-40.
191. Nijenhuis, T., et al., *Localization and regulation of the epithelial Ca²⁺ channel TRPV6 in the kidney*. J Am Soc Nephrol, 2003. **14**(11): p. 2731-40.
192. Thastrup, O., *Role of Ca²⁺-ATPases in regulation of cellular Ca²⁺ signalling, as studied with the selective microsomal Ca²⁺-ATPase inhibitor, thapsigargin*. Agents Actions, 1990. **29**(1-2): p. 8-15.
193. DeHaven, W.I., et al., *TRPC channels function independently of STIM1 and Orai1*. J Physiol, 2009. **587**(Pt 10): p. 2275-98.
194. Taylor, C.W. and L.M. Broad, *Pharmacological analysis of intracellular Ca²⁺ signalling: problems and pitfalls*. Trends Pharmacol Sci, 1998. **19**(9): p. 370-5.
195. Kaya, L., et al., *Direct association of the reticulon protein RTN1A with the ryanodine receptor 2 in neurons*. Biochim Biophys Acta, 2013.
196. Fabiato, A. and F. Fabiato, *Calcium-induced release of calcium from the sarcoplasmic reticulum of skinned cells from adult human, dog, cat, rabbit, rat, and frog hearts and from fetal and new-born rat ventricles*. Ann N Y Acad Sci, 1978. **307**: p. 491-522.
197. Porta, M., et al., *Single ryanodine receptor channel basis of caffeine's action on Ca²⁺ sparks*. Biophys J, 2011. **100**(4): p. 931-8.
198. Yuan, J.P., et al., *STIM1 heteromultimerizes TRPC channels to determine their function as store-operated channels*. Nat Cell Biol, 2007. **9**(6): p. 636-45.
199. Courjaret, R., et al., *The Xenopus TRPV6 homolog encodes a Mg²⁺ -permeant channel that is inhibited by interaction with TRPC1*. J Cell Physiol, 2013. **228**(12): p. 2386-98.
200. Cannell, M.B., H. Cheng, and W.J. Lederer, *The control of calcium release in heart muscle*. Science, 1995. **268**(5213): p. 1045-9.
201. Lopez-Lopez, J.R., et al., *Local calcium transients triggered by single L-type calcium channel currents in cardiac cells*. Science, 1995. **268**(5213): p. 1042-5.
202. Janse, M.J., *Electrophysiological changes in heart failure and their relationship to arrhythmogenesis*. Cardiovasc Res, 2004. **61**(2): p. 208-17.
203. Pogwizd, S.M. and D.M. Bers, *Cellular basis of triggered arrhythmias in heart failure*. Trends Cardiovasc Med, 2004. **14**(2): p. 61-6.
204. Usachev, Y.M. and S.A. Thayer, *All-or-none Ca²⁺ release from intracellular stores triggered by Ca²⁺ influx through voltage-gated Ca²⁺ channels in rat sensory neurons*. J Neurosci, 1997. **17**(19): p. 7404-14.

205. Furuichi, T., et al., *Multiple types of ryanodine receptor/Ca²⁺ release channels are differentially expressed in rabbit brain*. J Neurosci, 1994. **14**(8): p. 4794-805.

11 Peer reviewed publications



The action of selective CRAC channel blockers is affected by the Orai pore geometry

Isabella Derler^a, Rainer Schindl^a, Reinhard Fritsch^a, Peter Heftberger^a, Maria Christine Riedl^a, Malcolm Begg^b, David House^b, Christoph Romanin^{a,*}

^a Institute of Biophysics, University of Linz, 4040 Linz, Austria

^b Respiratory Therapy Area Unit, GlaxoSmithKline, Stevenage SG1 2NY, UK

ARTICLE INFO

Article history:

Received 3 September 2012

Received in revised form 2 November 2012

Accepted 3 November 2012

Available online 5 December 2012

Keywords:

Calcium-release activated calcium (CRAC) channel

GSK-7975A

I_{CRAC}

Orai1

Orai3

Stromal interaction molecule 1 (STIM1)

ABSTRACT

As the molecular composition of calcium-release activated calcium (CRAC) channels has been unknown for two decades, elucidation of selective inhibitors has been considerably hampered. By the identification of the two key components of CRAC channels, STIM1 and Orai1 have emerged as promising targets for CRAC blockers. The aim of this study was to thoroughly characterize the effects of two selective CRAC channel blockers on currents derived from STIM1/Orai heterologously expressed in HEK293 cells. The novel compounds GSK-7975A and GSK-5503A were tested for effects on STIM1 mediated Orai1 or Orai3 currents by whole-cell patch-clamp recordings and for the effects on STIM1 oligomerisation or STIM1/Orai coupling by FRET microscopy. To investigate their site of action, inhibitory effects of these molecules were explored using Orai pore mutants. The GSK blockers inhibited Orai1 and Orai3 currents with an IC_{50} of approximately $4 \mu M$ and exhibited a substantially slower rate of onset than the typical pore blocker La^{3+} , together with almost no current recovery upon wash-out over 4 min. For the less Ca^{2+} -selective Orai1 E106D pore mutant, I_{CRAC} inhibition was significantly reduced. FRET experiments indicated that neither STIM1–STIM1 oligomerization nor STIM1–Orai1 coupling was affected by these compounds.

These CRAC channel blockers are acting downstream of STIM1 oligomerization and STIM1/Orai1 interaction, potentially via an allosteric effect on the selectivity filter of Orai. The elucidation of these CRAC current blockers represents a significant step toward the identification of CRAC channel-selective drug compounds.

© 2012 Elsevier Ltd. All rights reserved.

1. Introduction

Store-operated channels (SOCs) represent a widespread route for Ca^{2+} entry into non-excitable cells [1] among which Ca^{2+} release-activated Ca^{2+} (CRAC) channels are the most highly characterized. Besides their involvement in a variety of processes such as muscle contraction, gene expression, proliferation, cell growth, and cell death [1], CRAC channels are vital for immunological reactions of T-cells and mast cells. CRAC channels therefore provide a promising means of modulating the immune system and represent attractive targets for asthma and allergic disorders.

The long-standing mystery of the molecular composition of CRAC channels has hampered the identification of specific inhibitors. Nevertheless a variety of compounds that strongly inhibit CRAC currents has been identified including divalent and trivalent cations such as La^{3+} and Gd^{3+} , diverse imidazoles,

2-APB (2-aminoethoxydiphenylborate), capsaicin [2], NPPB (5-nitro-2-(3-phenylpropylamino)-benzoic acid) [3–5], BTP2 (a bistrifluoromethyl-pyrazole derivative) [6–8], DES (diethylstilbestrol) [9], BEL (bromenol lactone) [10], bile acids [11] and ML-9 (1-(5-chloronaphthalene-1-sulfonyl)homopiperazine) [12]. La^{3+} and Gd^{3+} represent general inhibitors of Ca^{2+} -selective influx pathways comprising voltage-dependent Ca^{2+} , TRPV5/6 and also CRAC channels [13,14]. Although 2-APB is widely used as CRAC channels blocker, its pharmacology is complex; at low concentrations of 2-APB (1–5 μM) CRAC currents are enhanced, whereas at concentrations higher than 10 μM they are completely blocked [15]. Furthermore 2-APB alters the kinetics of fast Ca^{2+} -dependent inactivation of I_{CRAC} , increasing its rate at low concentrations and completely blocking inactivation above 10 μM [15]. The immunosuppressive agent BTP2 potently blocks interleukin-2 (IL-2) production in lymphocytes [6], at least in part through the inhibition of CRAC channels. [7,8].

While these compounds have proven useful tools for exploring CRAC channel biology, their activity against other ion channels and signaling processes such as the transient receptor potential (TRP) channels limits their utility [7,8,15–34]. Identification of

* Corresponding author. Tel.: +43 73224687604; fax: +43 73224687609.

E-mail address: christoph.romanin@jku.at (C. Romanin).

more selective CRAC channel blockers therefore represents a major step toward their utilization as therapeutics.

In 2006 a genome wide screen using RNA interference led to the identification of the stromal interaction molecule STIM1 and Orai1 as the limiting components of the CRAC pathway in human T-cells [35–37]. STIM1 functions as a calcium sensor located in the endoplasmic reticulum and Orai1 represents the CRAC channel pore. Together these proteins represent promising targets for the identification of novel and selective blockers targeting specific steps within the signaling cascade.

The widely used CRAC blocker 2-APB exhibits a similar bimodal effect on over-expressed STIM1 and Orai1 channels as compared with endogenous CRAC channels [28,38]. While low concentrations of 2-APB enhance Orai1 currents (5 μ M) [39–41], higher concentrations (>40 μ M) inhibit them [39–41]. Higher concentrations of 2-APB reversed cluster formation of STIM1, although this process was attenuated when Orai1 was co-expressed [42–44]. Therefore 2-APB-dependent inhibition of STIM1 and Orai1 mediated currents are expected to result at least in part from a reduction of STIM1 punctae formation. Moreover 2-APB represents a potent tool to distinguish between over-expressed Orai1, Orai2 and Orai3 channels. In contrast to the robust block of Orai1 by high 2-APB concentrations (50 μ M), Orai2 is less sensitive, while Orai3 is robustly stimulated by 2-APB [38,40,42,43,45,46]. 2-APB stimulated Orai3 channels develop independently of STIM1 and exhibit altered ion selectivity [42,43,45,46] with an increase in pore diameter [45].

In this study we present selective CRAC blockers which inhibit STIM1 mediated Orai1 and Orai3 currents with significantly slower kinetics than the conventional blockers La^{3+} , Gd^{3+} and 2-APB. We observed no interference of these drugs with STIM1/STIM1 oligomerization or STIM1/Orai1 interaction. Furthermore, they do not inhibit Orai pore mutants at concentrations that fully block the wild-type Orai channels suggesting a target site close or allosterically linked to the selectivity filter. The detailed characterization of these molecules strongly supports their use as agents for the wider investigation of CRAC channel biology.

2. Materials and methods

2.1. Cell culture

Experiments were performed on HEK293 cells cultured as described previously [28]. HEK293 cells are grown in an incubator (*Forma Scientific*) under a humidified (95%) atmosphere containing 8% CO_2 and a temperature of 37 °C. RBL-2H3 cells were obtained from ATCC and cultured in RPMI 1640 supplemented with 10% FBS, 1% penicillin–streptomycin and 1% L-glutamine (all Gibco, UK) at 37 °C in a 5% CO_2 humidified incubator.

2.2. Molecular cloning and mutagenesis

Human Orai1 (Orai1; accession number NM.032790) was kindly provided by A. Rao's Lab, Harvard Medical School, USA. C-terminally tagged pECFP-N1 and pEYFP-N1/Orai1 constructs were cloned using the XhoI and BamHI sites of the templated vectors. N-terminally tagged Orai1 constructs were cloned *via* Sall and SmaI restriction sites of pECFP-C1 and pEYFP-C1 expression vectors (Clontech). Human STIM1 (STIM1; accession number NM.003156) N-terminally ECFP- and EYFP-tagged was kindly provided by T. Meyer's Lab, Stanford University, USA. C-terminally EYFP-tagged STIM1 was purchased from GeneCopoeia™ (Catalog No.: EX-S0521-M02). The integrity of all resulting clones was confirmed by sequence analysis. The rat (r)TRPV6 construct (accession # AF160798, kindly provided by M. Hediger, University of Berne, Switzerland) was used. The coding region of rTRPV6 was cleaved

from pTracer-CMV2 (Invitrogen, USA) and transferred to the plasmid of pEYFP-C1 (Clontech, Germany). For subcloning of rTRPV6 the coding region was cleaved with the restriction enzymes NaeI and XbaI and the purified fragment was ligated with SmaI and XbaI digested pEYFP-C1. This resulted in N-terminally tagged EYFP-constructs. *pcDNA3-77* encoding for voltage-gated L-type Ca^{2+} channel $\alpha_{1C,77}$ subunit has been described previously [47]. *pcDNA3- β_{2a}* and *pcDNA3- α_2 - δ* encoding subunits of the L-type ion channel are kindly provided by Franz Hofmann (Institute of Pharmacology, Munich).

2.3. Transfection

Transfection of HEK cells [28] was performed using TransFectin (Biorad, Germany) with the corresponding plasmids. Measurements were carried out 24 h following transfection.

2.4. CRAC channel blockers

The CRAC channel blockers used in this study were obtained from GlaxoSmithKline, UK. Synta-66 (*N*-(2',5'-dimethoxy-[1,1'-biphenyl]-4-yl)-3-fluoroisonicotinamide) is Example 66 from the patent WO2005/009954. GSK-5503A (2,6-difluoro-*N*-(1-(2-phenoxybenzyl)-1*H*-pyrazol-3-yl)benzamide) and GSK-7975A (2,6-difluoro-*N*-(1-(4-hydroxy-2-(trifluoromethyl)benzyl)-1*H*-pyrazol-3-yl)benzamide) are Examples 26 and 36, respectively, from the GSK patent WO2010/122089. The inhibitors were dissolved in DMSO to produce a 10 mM stock solution.

2.5. Electrophysiology

Electrophysiological recordings comparing characteristics of 2–3 constructs were carried out in paired comparison on the same day. Expression patterns and levels of the various constructs were carefully monitored by confocal fluorescence microscopy and were not significantly changed by the introduced mutations. Electrophysiological experiments were performed at 20–24 °C, using the patch-clamp technique in the whole-cell recording configuration. For STIM1/Orai current measurements voltage ramps were usually applied every 5 s from a holding potential of 0 mV, covering a range of –90 to +90 mV over 1 s. The internal pipette solution for passive store-depletion contained (in mM) 3.5 MgCl_2 , 145 cesium methane sulfonate, 8 NaCl, 10 HEPES, 20 EGTA, pH 7.2. Extracellular solution consisted of (in mM) 145 NaCl, 5 CsCl, 1 MgCl_2 , 10 HEPES, 10 glucose, 10 CaCl_2 , pH 7.4. Na^+ divalent free (DVF) solution included 150 NaCl, 10 HEPES, 10 glucose and 10 EDTA. CRAC currents shown were leak-corrected either by subtraction of the initial trace or that following application of 10 μ M La^{3+} at the end of the experiment.

2.6. Confocal Förster resonance energy transfer (FRET) fluorescence microscopy

Confocal FRET microscopy was performed as described previously [48]. In brief, a QLC100 Real-Time Confocal System (VisiTech Int., UK) was used for recording fluorescence images connected to two Photometrics CoolSNAPHQ monochrome cameras (Roper Scientific, USA) and a dual port adapter (dichroic: 505lp; cyan emission filter: 485/30; yellow emission filter: 535/50; Chroma Technology Corp., USA). This system was attached to an Axiovert 200M microscope (Zeiss, Germany) in conjunction with an argon ion multi-wavelength (457, 488, 514 nm) laser (Spectra Physics, USA). The wavelengths were selected by an Acousto Optical Tuneable Filter (VisiTech Int., UK). MetaMorph 5.0 software (Universal Imaging Corp.) was used to acquire images and to control the confocal system. Illumination times of about 900–1500 ms were typically used for CFP, FRET and YFP images that were consecutively recorded

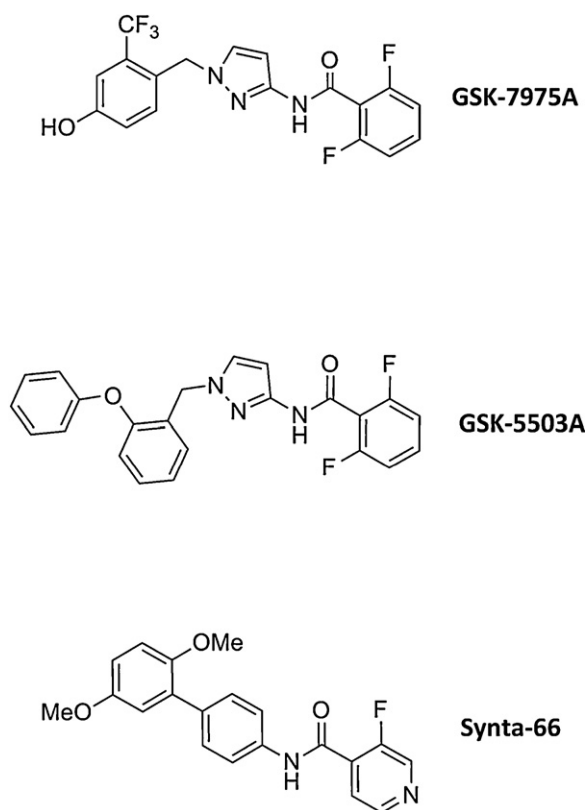


Fig. 1. Structures of GSK-CRAC channel inhibitors in comparison to Synta-66.

with a minimum delay. Prior to the calculation the images had to be corrected due to cross-talk as well as cross-excitation. For this, the appropriate crosstalk calibration factors were determined for each of the constructs on the day the FRET experiments were performed. The corrected FRET image (N_{FRET}) was calculated on a pixel to pixel basis after background subtraction and threshold determination using custom-made software [49] integrated in MatLab 7.0.4 according to the published method [50]. The local ratio between CFP and YFP might vary due to different localisations of diverse protein constructs, which could lead to the calculation of false FRET values [51]. Accordingly, the analysis was limited to pixels with a CFP:YFP molar ratio between 1:10 and 10:1 to yield reliable results [51].

Statistics: Mean \pm S.E.M. values were shown throughout the manuscript. Significance analysis was performed with the two-tailed Mann–Whitney test.

2.7. Calcium influx assay

24 h prior to experimentation cells were harvested, adjusted to a density of 0.2×10^6 cells/ml and $100 \mu\text{l}$ loaded into each well of a 96-well clear, flat bottomed, black sided plate (Costar, UK). The assay buffer contained (in mM) NaCl (145), KCl (2.5), HEPES (10), glucose (10), MgCl_2 (1.2), CaCl_2 (2.0), and probenecid (2.5) (all Sigma, UK). The loading buffer was assay buffer supplemented with $2 \mu\text{M}$ Fluo-4 AM (dissolved in 50:50 DMSO/pluronic acid, Invitrogen, UK).

Media was aspirated and replaced with loading buffer before being incubated at room temperature in the dark for 60 min. Loading buffer was aspirated and replaced with assay buffer. Loaded cells were incubated with GSK-7975A for 30 min at room temperature in the dark before being stimulated with $1 \mu\text{M}$ thapsigargin and returned to the dark for a further 5 min. The plate was read

on a Tecan Sapphire fluorescence plate reader. Samples were read at excitation 488 nm and emission 520 nm with each data point being expressed as fold over basal using an unstimulated vehicle control.

3. Results

Fig. 1 depicts the chemical structure of the two GSK compounds (GSK-7975A and GSK-5503A) studied along with a previously described CRAC channel blocker Synta-66 [52].

3.1. Both GSK compounds fully block Orai1 currents at $10 \mu\text{M}$ concentrations

To evaluate the overall effect of the GSK compounds on STIM1-stimulated Orai currents, we employed the patch-clamp technique to investigate their effects on maximally activated STIM1-dependent Orai1/Orai3 currents in comparison with the conventional Ca^{2+} channel blocker La^{3+} . HEK293 cells co-expressing STIM1 with either Orai1 or Orai3 were clamped in the whole-cell configuration employing 20 mM EGTA in the pipette solution for passive store-depletion. Following whole-cell formation, currents were measured in response to repetitive voltage-ramps from -90 mV to $+90 \text{ mV}$ applied from a holding potential of 0 mV , and the time-course of current inhibition during drug administration was determined at -74 mV (Fig. 2A and B) from each ramp (Fig. 2C and D). Time-axis in Fig. 2A and B were shifted to superimpose time-points of drug administration. Under our conditions the well-known complete inhibition of Orai1 currents by $10 \mu\text{M}$ La^{3+} occurred with a $t_{1/2}$ of $\sim 25 \text{ s}$ (Fig. 2A and E). Application of the two novel compounds GSK-7975A and GSK-5503A at $10 \mu\text{M}$ concentrations also resulted in complete Orai1 current inhibition, but at a substantially slower rate with a $t_{1/2}$ in the range $75\text{--}100 \text{ s}$ (Fig. 2A and E). Similarly, $10 \mu\text{M}$ of the Synta-66 compound reduced Orai1 currents with a $t_{1/2}$ of 75 s (Fig. 2B and E).

For comparison, we extended our pharmacological investigations to compounds already known to inhibit CRAC currents [53] including the synthetic estrogen agonist diethylstilbestrol (DES) and 2-aminoethoxydiphenylborate (2-APB). In agreement with the effective block of CRAC/SOC currents in RBL cells by DES at concentrations of $30 \mu\text{M}$, STIM1-activated Orai1 currents exhibited full and rapid blockade within $\sim 50 \text{ s}$ (Fig. 2B). The CRAC channel blocker 2-APB displayed its unique dual effect on STIM1/Orai1 currents characterized by a transient stimulation followed by a complete inhibition of STIM1/Orai1 currents. Both DES and 2-APB rapidly inhibited STIM1/Orai1 currents with $t_{1/2}$ of $\sim 25 \text{ s}$ comparable with La^{3+} . In summary, the two Orai1 current-blocking compounds GSK-7975A and GSK-5503A fully inhibited Orai1 currents at $10 \mu\text{M}$ with 2.5-fold slower kinetics than La^{3+} .

3.2. Both GSK compounds effectively inhibit Orai1 and Orai3 currents

To evaluate specificity among the Orai protein family we further examined the effect of GSK-7975A and GSK-5503A on STIM1-activated Orai3 currents. Time-axis in Fig. 3A and B were shifted to superimpose time-points of drug administration. The two GSK compounds fully inhibited Orai3 currents at $10 \mu\text{M}$ (Fig. 3A, C, and D) with a comparable $t_{1/2}$ of 75 s (Fig. 3E), indicating no obvious selectivity between Orai1 and Orai3. Similarly, Synta-66 (Fig. 3B and E) inhibited Orai3 currents at a similar rate to the GSK compounds. By contrast, $10 \mu\text{M}$ La^{3+} blocked Orai3 currents more rapidly with a $t_{1/2}$ of $\sim 20 \text{ s}$ (Fig. 3B and E) analogous to Orai1 current inhibition. The GSK compounds appeared to inhibit Orai3 currents slightly faster than those of Orai1. Overall these GSK compounds

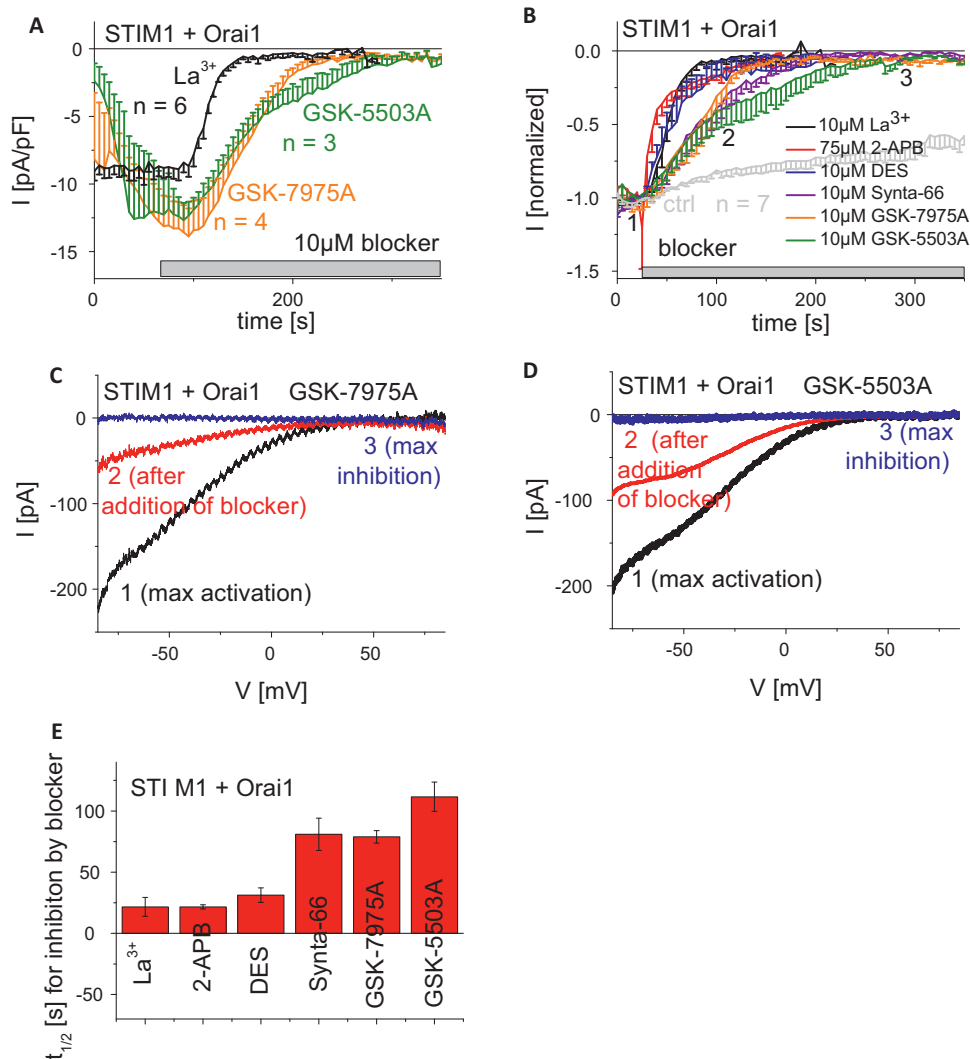


Fig. 2. Inhibitory profiles of known and GSK-CRAC channel blockers on STIM1/Orai1 currents. (A) Time-course of whole cell inward currents at -74 mV maximally activated upon passive store-depletion of HEK293 cells co-expressing CFP-STIM1 with YFP-Orai1 upon perfusion of $10 \mu\text{M}$ La^{3+} , $10 \mu\text{M}$ GSK-5503A and $10 \mu\text{M}$ GSK-7975A. Time-axes in (A and B) were shifted to superimpose time-points of drug administration. (B) Time-course of normalized whole cell inward currents at -74 mV, maximally activated upon passive store-depletion of HEK293 cells co-expressing CFP-STIM1 with YFP-Orai1 upon perfusion of $10 \mu\text{M}$ La^{3+} , $10 \mu\text{M}$ GSK-5503A and $10 \mu\text{M}$ GSK-7975A in comparison to $75 \mu\text{M}$ 2-APB, $10 \mu\text{M}$ DES and $10 \mu\text{M}$ Synta-66 ($t=0$ s was shifted to a time-point where currents had already reached their maximum). (C and D) Corresponding I/V relationships to (A, B: 1, 2, 3) of STIM1/Orai1 currents after maximal activation (1), after \sim half maximal block (2) as well as complete block (3) by $10 \mu\text{M}$ GSK-7975A (C) or $10 \mu\text{M}$ GSK-5503A (D). (E) Block diagram representing half-maximal inhibition time $t_{1/2}$ of $10 \mu\text{M}$ La^{3+} , $75 \mu\text{M}$ 2-APB, $10 \mu\text{M}$ DES, $10 \mu\text{M}$ Synta-66, $10 \mu\text{M}$ GSK-5503A and $10 \mu\text{M}$ GSK-7975A.

were equally effective at blocking Orai1 and Orai3, and inhibition occurred at a substantially slower rate than La^{3+} .

3.3. Inhibition of Orai currents by GSK compounds is not readily reversible

In a subsequent study we investigated recovery of Orai1/3 currents following maximal inhibition by GSK compounds. Wash-out of drugs was performed by re-perfusion of the 10 mM Ca^{2+} containing extracellular solution onto STIM1/Orai expressing HEK293 cells that exhibited fully blocked Orai1/Orai3 currents. Neither Orai1 (Fig. 4A–D) nor Orai3 (Fig. 4E–H) currents showed substantial recovery from block by GSK-7975A (Fig. 4A, C, E, and G) or GSK-5503A (Fig. 4B, D, F, and H) over a 4–5 min wash-out period. Hence, the blockade of STIM1-activated Orai1/3 currents by these compounds is not readily reversible within the time frame of this experiment.

3.4. Inhibition of Orai1/3 currents by GSK-7975A occurs with a half maximal concentration of approximately $4 \mu\text{M}$

As both GSK compounds demonstrated similar behavior toward Orai current inhibition, we focused on a more detailed characterization of GSK-7975A. Concentration–response curves for the inhibitory action of GSK-7975A on Orai1 and Orai3 currents were generated. Single concentrations (0.1 , 0.3 , 1 , 3 , $10 \mu\text{M}$) were applied to maximally activated Orai currents in individual cells, which was required due to the slow rate of reaching steady-state inhibition (Fig. 5). The IC_{50} values of GSK-7975A were estimated as $4.1 \mu\text{M}$ and $3.8 \mu\text{M}$ for Orai1 (Fig. 5E) and Orai3 (Fig. 5F), respectively. The Hill coefficient for the inhibition of both Orai currents by GSK-7975A was calculated to be ~ 1 , suggesting a 1:1 molar interaction of GSK-7975A with the Orai channels. The similar IC_{50} of $\sim 4 \mu\text{M}$ for both Orai1 and Orai3 currents suggested conserved binding sites for GSK-7975A in both channels.

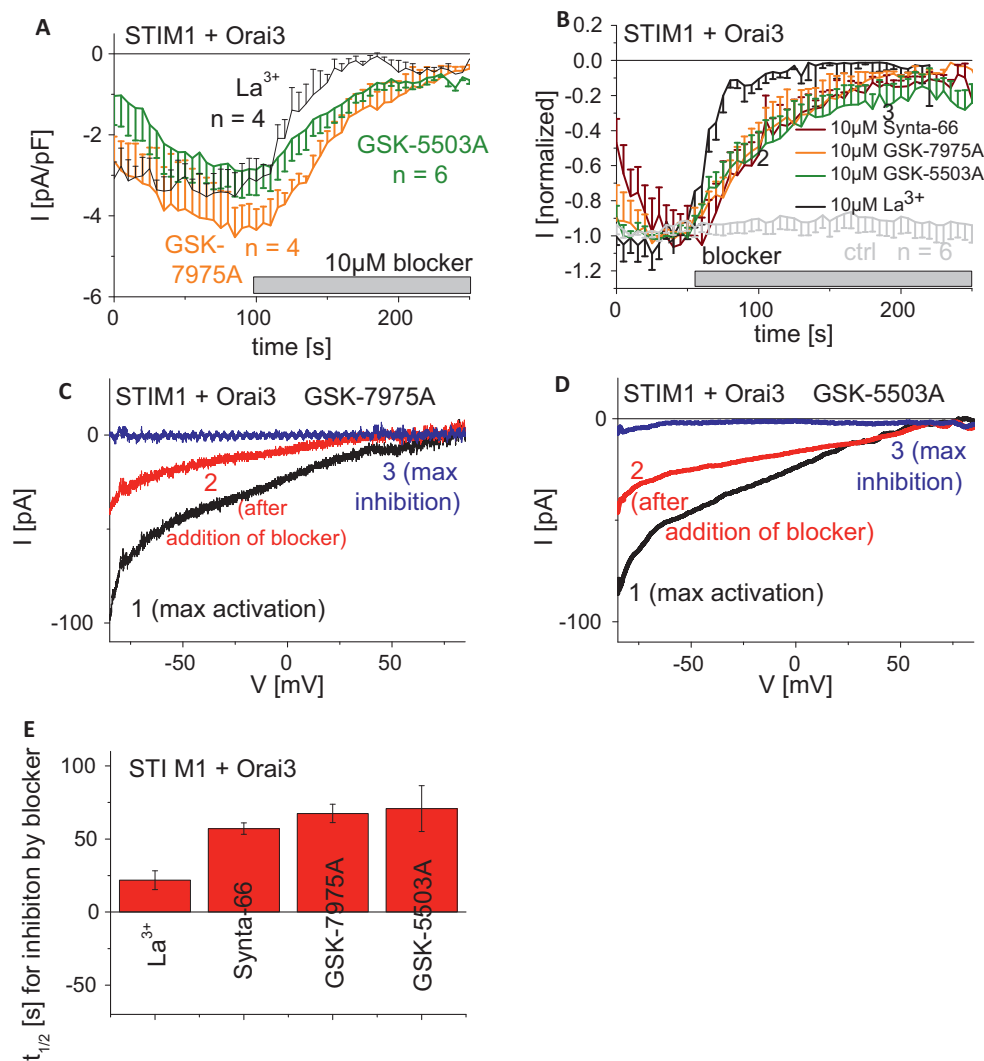


Fig. 3. Inhibitory profiles of known and GSK-CRAC channel blockers on STIM1/Orai3 currents. (A) Time-course of whole cell inward currents at -74 mV maximally activated upon passive store-depletion of HEK293 cells co-expressing CFP-STIM1 with YFP-Orai3 upon perfusion of $10 \mu\text{M}$ La^{3+} , $10 \mu\text{M}$ GSK-5503A and $10 \mu\text{M}$ GSK-7975A. Time-axes in (A and B) were shifted to superimpose time-points of drug administration. (B) Time-course of normalized whole cell inward currents at -74 mV maximally activated upon passive store-depletion of HEK293 cells co-expressing CFP-STIM1 with YFP-Orai3 upon perfusion of $10 \mu\text{M}$ La^{3+} , $10 \mu\text{M}$ GSK-5503A and $10 \mu\text{M}$ GSK-7975A in comparison to $10 \mu\text{M}$ Synta-66 ($t=0$ s was shifted to a time-point where currents had already reached their maximum). (C and D) Corresponding I/V relationships to (A, B: 1, 2, 3) of STIM1/Orai3 currents after maximal activation (1), after \sim half maximal block (2) as well as complete block (3) by $10 \mu\text{M}$ GSK-7975 (C) or $10 \mu\text{M}$ GSK-5503A (D). (E) Block diagram representing half-maximal inhibition time $t_{1/2}$ of $10 \mu\text{M}$ La^{3+} , $10 \mu\text{M}$ Synta-66, $10 \mu\text{M}$ GSK-5503A and $10 \mu\text{M}$ GSK-7975A.

3.5. GSK-7975A affects neither STIM1 oligomerization nor STIM1/Orai1 interaction

The inhibitory effect upon Orai1 and Orai3 channels might evolve from a compound-induced impairment of the STIM1/Orai coupling processes or more classically from pore blockade. The former mechanism was approached by FRET measurements (Fig. 6) monitoring STIM1/STIM1 or STIM1/Orai1 interaction. We [54] and others [55] have recently reported that CFP- and YFP-labeled STIM1 proteins display an increase in FRET upon store-depletion reflecting store-operated oligomerization as a prerequisite for subsequent STIM1/Orai1 coupling. To approach the potential impairment of STIM1 oligomerization by GSK-7975A, we applied $10 \mu\text{M}$ GSK-7975A to CFP- and YFP-STIM1 expressing cells 5 min before store-depletion. Following the addition of $2 \mu\text{M}$ thapsigargin, FRET significantly increased and was unaffected by the presence of GSK-7975A (Fig. 6A). STIM1 oligomerization was therefore not affected by GSK-7975A.

A potential effect on STIM1/Orai1 interaction was next investigated in HEK cells co-expressing STIM1-CFP and Orai1-YFP. Upon

store-depletion these two proteins displayed a robust increase in FRET indicating their direct interaction. Application of $10 \mu\text{M}$ GSK-7975A did not significantly alter the FRET plateau representing STIM1/Orai1 interaction after store-depletion by thapsigargin (Fig. 6B). Hence GSK-7975A is unlikely to interfere with the interaction of STIM1 and Orai1. Taken together, these results imply that the inhibitory effect of GSK-7975A on CRAC currents does not result from interference with the overall processes that trigger the interaction of STIM1/Orai but rather involves a potential impairment of gating or pore blockade.

3.6. 2-APB stimulated Orai3 currents are less susceptible to GSK-7975A

Orai3, in contrast to STIM1-activated Orai1, exhibits robust current stimulation by $75 \mu\text{M}$ 2-APB [56–58]. These 2-APB evoked Orai3 currents are independent of STIM1, exhibit less Ca^{2+} -selectivity and display a double rectifying current-voltage relationship that reflects the altered permeation properties linked to an increased pore size [57]. In a first approach we applied $10 \mu\text{M}$

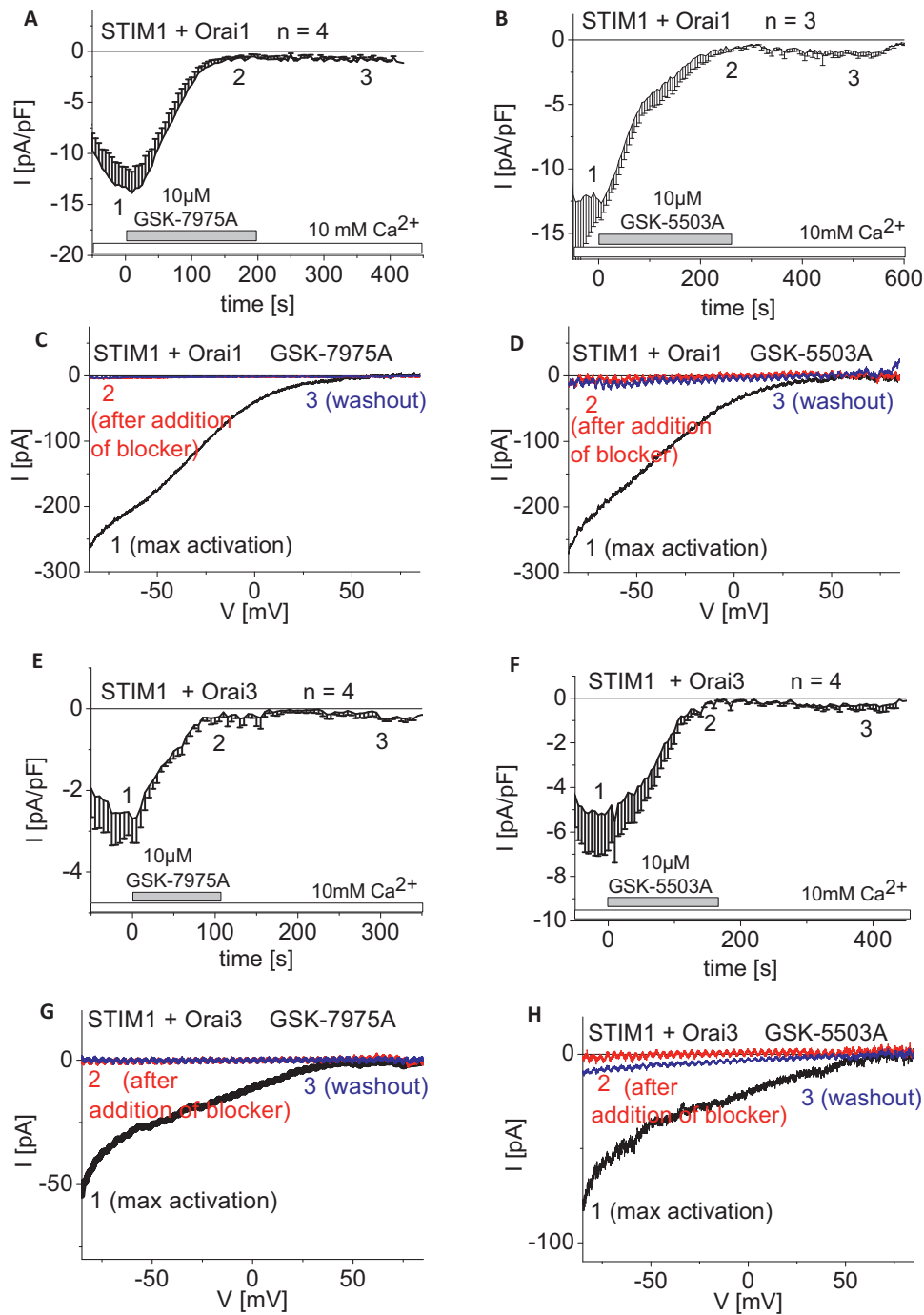


Fig. 4. Wash-out of GSK-CRAC channel blockers following inhibition of STIM1/Orai1 and STIM1/Orai3 currents. Time-course of whole cell inward currents at -74 mV maximally activated upon passive store-depletion of HEK293 cells co-expressing CFP-STIM1 with YFP-Orai1 (A and B) or YFP-Orai3 (E and F). Upon full blockade of STIM1/Orai currents by $10 \mu\text{M}$ GSK-7975A (A and E) or $10 \mu\text{M}$ GSK-5503A (B and F) 10 mM Ca^{2+} solution was perfused for wash-out ($t=0$ s was shifted to a time-point where currents had already reached their maximum). Corresponding I/V relationships to (A, B, E, F: 1, 2, 3) of STIM1/Orai1 (C and D) and STIM1/Orai3 (G and H) currents upon maximal store-operated activation (1), upon complete inhibition (2) of $10 \mu\text{M}$ GSK-7975A (C and G) or $10 \mu\text{M}$ GSK-5503A (D and H) and after washout (3) of the respective blocker.

GSK-7975A to maximally 2-APB stimulated Orai3 currents (Fig. 7A and D). Strikingly, $10 \mu\text{M}$ GSK-7975A was totally ineffective in inhibiting these Orai3 currents in contrast to those activated via STIM1. Upon application of increased concentrations of GSK-7975A to maximally 2-APB activated Orai3 currents we observed 50% inhibition by $50 \mu\text{M}$ GSK-7975A (Fig. 7B and D) and full inhibition by $100 \mu\text{M}$ GSK-7975A (Fig. 7C and D). Thus, the 2-APB elicited Orai3 currents were approximately 10-fold less sensitive to inhibition by GSK-7975A, which might result from the distinct mode

of activation and/or the altered pore geometry as evident from the lower Ca^{2+} -selectivity.

3.7. The Orai1 E106D pore mutant also lacks inhibition by $10 \mu\text{M}$ GSK-7975A

In an attempt to identify whether the altered pore geometry is linked to the less efficient inhibition of GSK-7975A, we utilized several Orai1 pore mutants which are still fully dependent on STIM1

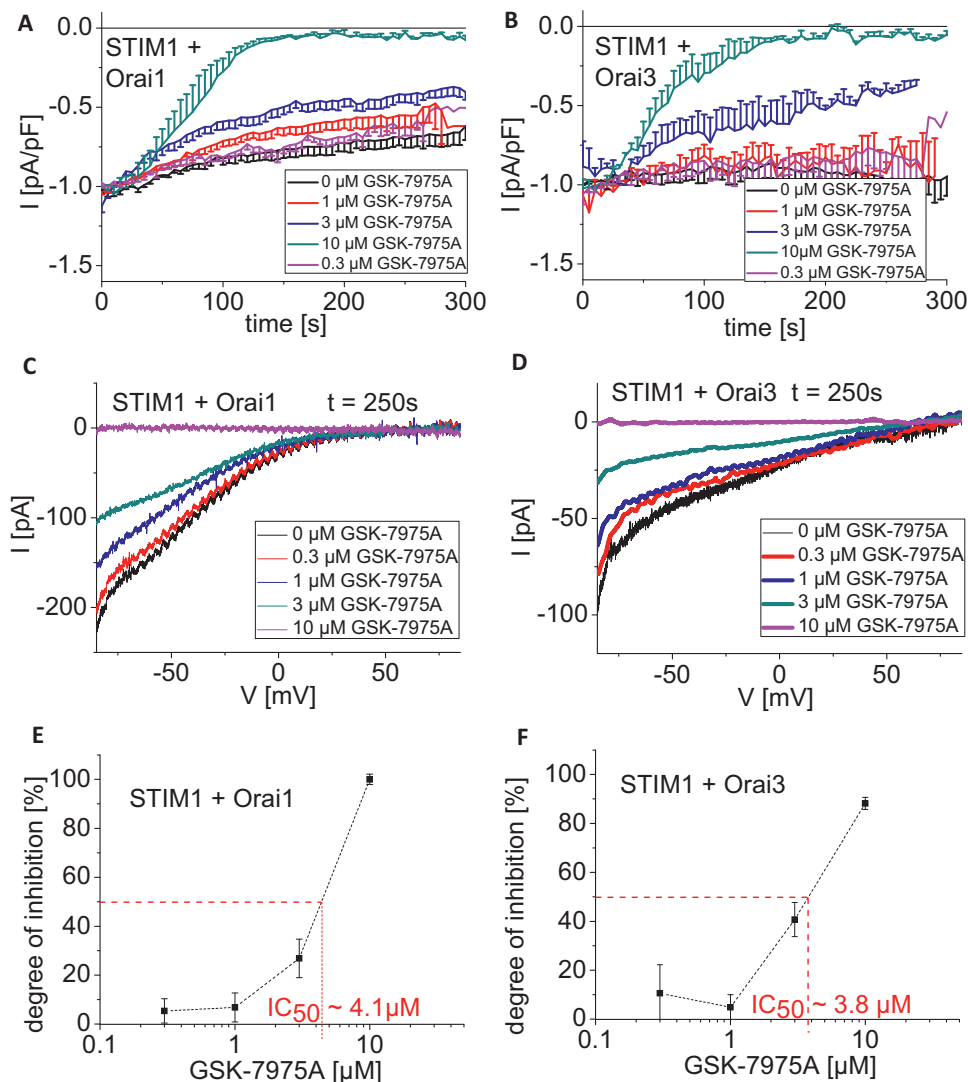


Fig. 5. Dose-response relationships of the CRAC channel blocker GSK-7975A on STIM1/Orai1 and STIM1/Orai3 currents. (A and B) Time-course of whole cell inward currents at -74 mV maximally activated upon passive store-depletion of HEK293 cells co-expressing CFP-STIM1 with YFP-Orai1 (A) or YFP-Orai3 (B) upon perfusion of 0.3μ M, 1μ M, 3μ M, 10μ M GSK-7975A ($t=0$ s was shifted to a time-point where currents had already reached their maximum). (C and D) Corresponding I/V relationships to (A and B) of STIM1/Orai1 (C) and STIM1/Orai3 (D) currents upon maximal inhibition by $0, 0.3, 1, 3, 10 \mu$ M GSK-7975A. (E and F) Concentration-response relationship depicting the inhibitory effect of GSK-7975A on CFP-STIM1-mediated YFP-Orai1 (E) and YFP-Orai3 (F) currents.

for activation. The Orai1 E106D pore mutant displayed less Ca^{2+} -selectivity together with a left-shifted reversal potential and an enhanced pore diameter [59–61]. STIM1-activated maximum Orai1 E106D currents exhibited no inhibition by application of 10μ M GSK-7975A similar to observations on 2-APB stimulated Orai3 currents (Fig. 8A and C). Nevertheless, increasing concentrations of GSK-7975A to 100μ M substantially but not fully restored the inhibitory effect on STIM1-mediated Orai1 E106D currents (Fig. 8B and D). For comparison, we examined Orai1 D110/112/114A with mutations in the outer vestibule of the pore that lead to a moderate left-shift of the reversal potential to ~ 40 mV and an increased pore diameter to about 4.4 \AA [61]. Following STIM1-dependent maximum store-operated activation of this pore mutant, application of 10μ M GSK-7975A resulted in a substantial inhibition almost comparable to that of wild-type Orai1 (Fig. 8E and G), but distinctly different to the Orai1 E106D form. This observation suggested that the conformation of the selectivity filter rather than the outer vestibule of the Orai1 pore represented a molecular determinant for GSK-7975A blockade. Simple removal of Ca^{2+} ions from the

extracellular solution as evaluated by a divalent free solution with sodium ions as main charge carriers led to the typical increases in inward currents, which were still fully blocked by 10μ M GSK-7975A (Fig. 8F and H). This further suggested that the presence of Ca^{2+} ions within the permeation pathway is not required for the inhibitory action of 10μ M GSK-7975A.

3.8. Endogenous CRAC channels of RBL mast cells are inhibited by GSK-7975A

For comparison with expressed Orai1 channels, we examined the inhibitory profile of GSK-7975A on rat basophilic leukemia (RBL-2H3) cells that are widely studied for their endogenous CRAC channels. 10μ M GSK-7975A fully blocked RBL CRAC currents at a slightly slower rate than 10μ M La^{3+} (Fig. 9A). A concentration-response curve obtained for the inhibition of thapsigargin-induced Ca^{2+} entry following a 30 min pre-incubation with increasing GSK-7975A concentrations yielded an IC_{50} of $0.8 \pm 0.1 \mu$ M (Fig. 9B, $n=6$). This value compares with

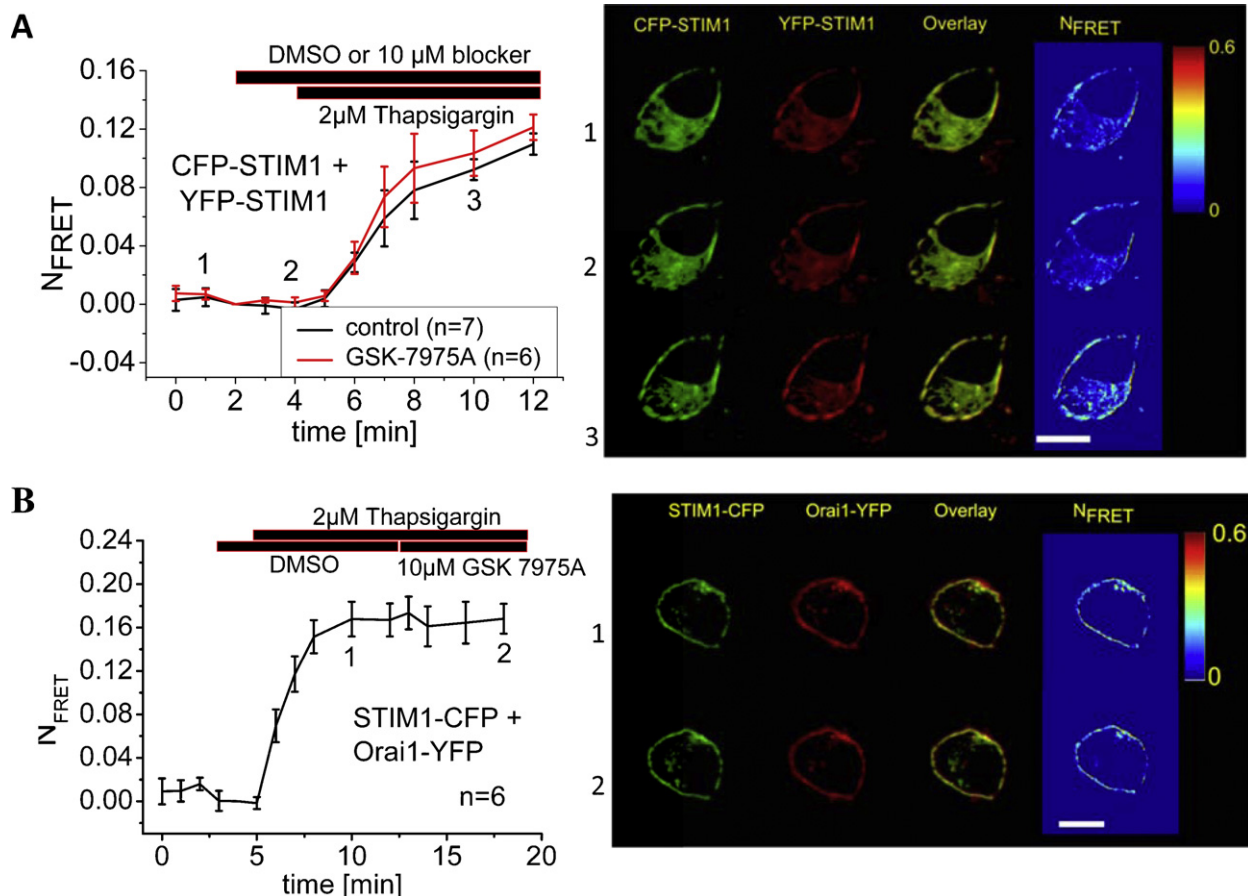


Fig. 6. GSK-7975A impaired neither STIM1 oligomerization nor STIM1/Orai1 coupling. (A) Left: time course of relative FRET between CFP-STIM1 and YFP-STIM1 with or without perfusion of GSK-7975A. Right: localization, overlay and calculated FRET life cell image series of YFP-STIM1 and CFP-STIM1 (1) in the absence and (2) presence of GSK-7975A and (3) following store-depletion in the presence of GSK-7975A. (B) Left: time course of relative FRET between STIM1-CFP and Orai1-YFP upon store-depletion and after application of GSK-7975A. Right: localization, overlay and calculated FRET life cell image series of STIM1-CFP and Orai1-YFP (1) after store-depletion and (2) after perfusion of GSK-7975A.

the $\sim 4 \mu$ M estimated from the electrophysiological experiments on Orai1/STIM1-derived currents from HEK cells.

3.9. Inhibitory profile of GSK-7975A on other ion channels

To explore selectivity against other ion channels, GSK-7975A was profiled against a variety of recombinantly expressed ion channel proteins including several members of the TRP channel family. [Supplemental Table 1](#) lists the potential antagonistic (IC_{50}) or agonistic (EC_{50}) activity of GSK-7975A at concentrations up to 10 μ M on sixteen ion channels revealing only a slight inhibitory effect on L-type ($CaV1.2$) Ca^{2+} channels.

Given the IC_{50} of $\sim 8 \mu$ M for L-type Ca^{2+} channels we went on to investigate by electrophysiology the inhibition of both L-type and TRPV6 channels, the most Ca^{2+} -selective channels and compared the effects of GSK-7975A to the typical Ca^{2+} channel blocker La^{3+} . While La^{3+} fully blocked both Ca^{2+} channels, 10 μ M GSK-7975A completely inhibited rat-TRPV6 channels at a similar rate as La^{3+} (Fig. 10A), but only exhibited moderate inhibition of L-type Ca^{2+} channels (Fig. 10B, [Suppl. Table 1](#)).

TRPV6 and L-type calcium channels have almost no primary sequence homology so in some ways it is surprising that GSK-7975A inhibits both of these channels. This might be explained by architectural similarities in the selectivity filters of these channels, with both L-type channels and TRPV6 containing a similar ring of negative charges [62]. While the selectivity filters appear structurally similar, it should be noted that the pore diameter at its

narrowest point is slightly larger for L-type channels ($\sim 6.2 \text{ \AA}$) than TRPV6 ($\sim 5.4 \text{ \AA}$) [62]. By contrast, the selectivity filter of Orai1 channels has been determined to be much smaller at just 3.6 \AA [61].

4. Discussion

CRAC channels are important in the physiology and pathophysiology of particular immune cell types and underlie several disease states including a severe combined immunodeficiency syndrome [63]. Their molecular components STIM1 and Orai1 have emerged as potential targets for drug discovery [64,65]. To date, compounds described in the literature as CRAC channel inhibitors have been found to lack selectivity by blocking other signaling pathways and/or have poorly characterized sites of action on CRAC channels [64,66].

Here we characterized for the first time CRAC channel inhibitors which exert their action downstream of the STIM1–Orai coupling machinery, since they leave STIM1 oligomerization and STIM1–Orai1 interaction unaffected. CRAC currents derived from HEK cells expressing STIM1/Orai1 were inhibited with an IC_{50} of $\sim 4 \mu$ M and a Hill coefficient of ~ 1 . A similar inhibitory profile has been reported for Synta-66 [67,68] on RBL mast cells exhibiting an IC_{50} of $\sim 1\text{--}3 \mu$ M and a Hill coefficient of 1.1. The detailed mechanism of the Synta-66 compound is unknown, though it has been found in smooth muscle cells that it does not interfere with STIM1 clustering [69] consistent with our findings for GSK-7975A. The action of GSK-7975A is apparently determined

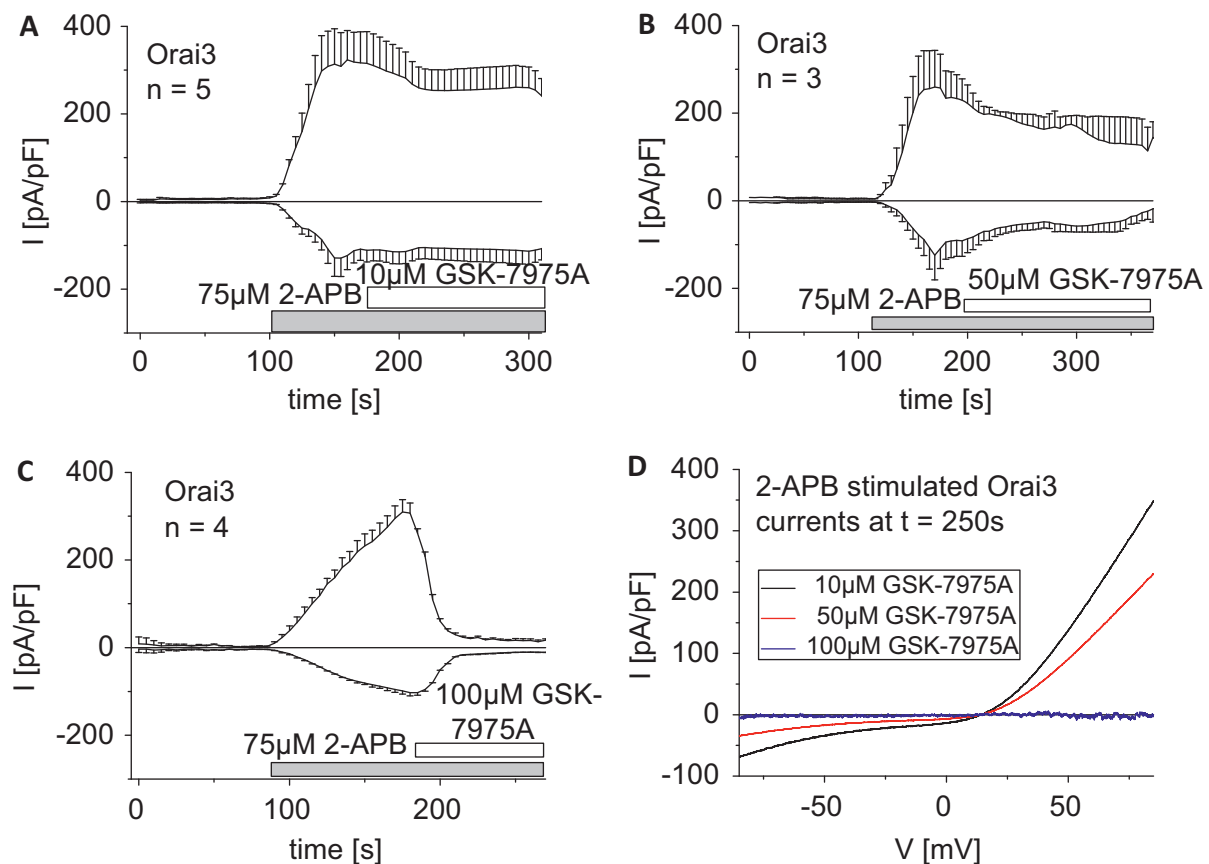


Fig. 7. The less Ca^{2+} -selective Orai3 current elicited by 2-APB is substantially less susceptible to GSK-7975A inhibition. (A–C) Time-courses of 2-APB-stimulated Orai3 currents, which were treated after maximal activation with 10 μM (A), 50 μM (B) and 75 μM (C) GSK-7975A. (D) I/V -relationship of 2-APB-stimulated Orai3 currents upon addition of 10 μM , 50 μM or 100 μM GSK-7975A.

by the geometry of the selectivity filter of the Orai pore, since the Orai1 E106D pore mutant required at least 10-fold higher concentrations for inhibition compared to wild-type Orai1. This apparent loss in affinity might be caused by the altered pore geometry, reflected in the lower Ca^{2+} selectivity, and increased pore diameter of 5.3 Å compared to 3.8 Å for the wild-type form. Alternatively, GSK-7975A might act as a gating modifier strengthening Ca^{2+} -induced inactivation [61] to promote channel closure. As Ca^{2+} -induced fast inactivation is almost eliminated in the Orai1 E106D mutant [61], this could conceivably have interfered with the action of GSK-7975A. However, application of 3 μM GSK-7975A, a submaximal inhibitory concentration for Orai1 block, did not significantly increase inactivation (Suppl. Fig. 1) rendering an altered Ca^{2+} -induced fast inactivation as the mechanism of inhibition by GSK-7975A less likely. As the onset of action was much slower than that of the widely used Ca^{2+} channel blocker La^{3+} , the GSK compounds may have restricted access to their site of action. The inhibitory fast action of La^{3+} on Orai currents has been attributed to an interaction with the negatively charged residues within the first extracellular loop, but not with the E106 at the selectivity filter [70,71]. Neutralization of the negatively charged residues in the first extracellular loop of Orai1 did not affect overall characteristics of inhibition by the CRAC blocker GSK-7975A rendering this site an unlikely target, consistent with its slow action compared to La^{3+} . Thus it is tempting to speculate that these GSK compounds interfere with the permeation through the Orai1 pore by binding to a site that is close or allosterically linked to the selectivity filter compatible with the shift in affinity observed when increasing the pore size via mutation (Orai1 E106D) or 2-APB (Orai3). While it may be the case that access to the binding site occurs via the

narrow channel pore, we cannot exclude the possibility that these compounds reach their site of action by diffusion through the cellular membrane given their moderate lipophilicity (clogP 3.4 for GSK-7975A) and high artificial membrane permeability (360 nm/s for GSK-7975A). Intracellular application of 10 μM GSK-7975A led only to a slight inhibition of CRAC currents probably due to the compound leaking out of the cell (data not shown). Further identification of the binding site using fluorescently labeled compounds has so far proven unsuccessful due to loss of affinity of the labeled compounds.

The GSK CRAC channel blockers did not differentiate between Orai1 and Orai3 channels consistent with the conserved pore geometry and selectivity filter among the Orai isoforms. Hence, the GSK blockers characterized in this study interfere with the permeation through the Orai pore by slow access to a site which is affected by alterations in the selectivity filter.

The native CRAC current of RBL mast cells was also inhibited by 10 μM GSK-7975A consistent with a recent report on its action in human lung mast cells where it significantly reduced Ca^{2+} influx and release of inflammatory mediators at a concentration of 3 μM [72]. Furthermore, endogenous, store-operated Ca^{2+} entry of HEK293 cells was substantially inhibited by pre-incubation with 10 μM GSK-7975A. However, the amount of Ca^{2+} released from ER stores via stimulation by either carbachol (CCH) or BHQ was not markedly altered pointing to a minor effect of GSK-7975A on pathways affecting the ER Ca^{2+} content (Suppl. Fig. 2).

Extension of the characterization of GSK-7975A to other ion channels revealed a high degree of selectivity (Supplemental Table 1). Only two ion channels were affected by GSK-7975A, and while

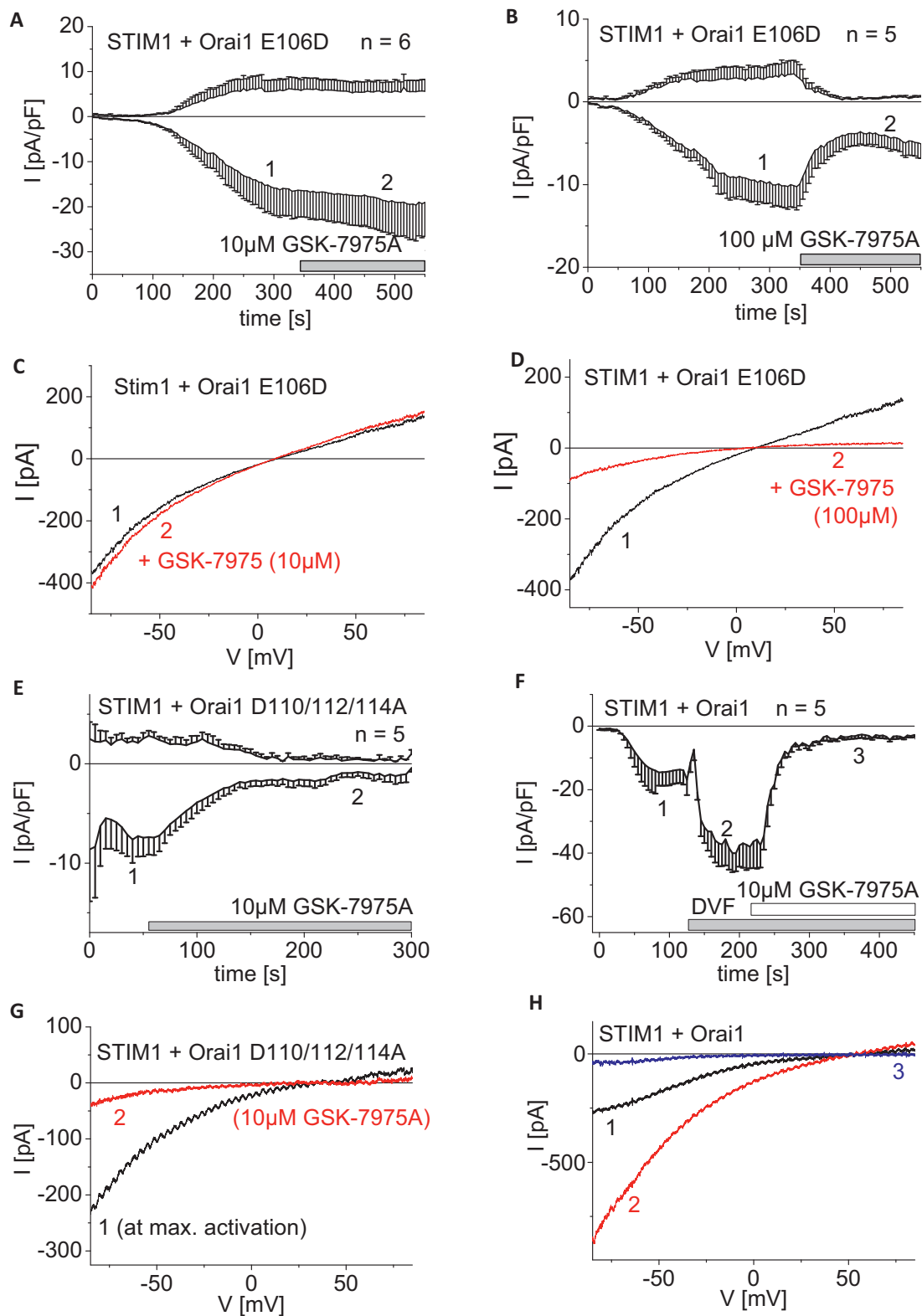


Fig. 8. Inhibitory profile of GSK-7975A on less Ca^{2+} -selective or monovalent Orai1 currents. (A and B) Time course of whole cell inward currents at -74 mV maximally activated upon passive store-depletion of HEK293 cells co-expressing CFP-STIM1 with YFP-Orai1 E106D upon perfusion of 10 μ M (A) and 100 μ M (B) GSK-7975A. (C and D) Corresponding I/V relationships to (A, B: 1, 2) of STIM1/Orai1 E106D currents after maximal store-operated activation (1) and upon addition (2) of 10 μ M (C) or 100 μ M (D) GSK-7975A. (E) Time course of whole cell inward currents at -74 mV maximally activated upon passive store-depletion of HEK293 cells co-expressing CFP-STIM1 with YFP-Orai1 D110/112/114A upon perfusion of 10 μ M GSK-7975A ($t=0$ s was shifted to a time-point where currents had already reached their maximum). (F) Time course of whole cell inward currents at -74 mV maximally activated upon passive store-depletion of HEK293 cells co-expressing CFP-STIM1 with YFP-Orai1 in 10 mM Ca^{2+} solution. Afterwards 10 mM Ca^{2+} solution was exchanged by a DVF solution and blocked by 10 μ M GSK-7975A. (G) Corresponding I/V relationships to (E: 1, 2) of STIM1/Orai1 D110/112/114A currents after maximal store-operated activation (1) and upon addition (2) of 10 μ M GSK-7975A. (H) Corresponding I/V relationships to (F: 1, 2, 3) of maximal activated STIM1/Orai1 current in 10 mM Ca^{2+} containing solution (1), DVF solution (2) and upon addition (3) of 10 μ M GSK-7975A in DVF solution.

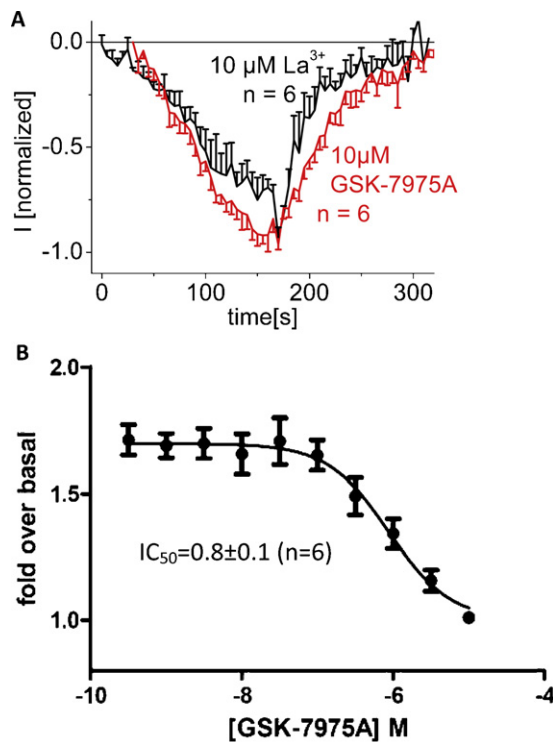


Fig. 9. Inhibitory profile of GSK-7975A on endogenous CRAC currents and Ca²⁺ entry of RBL cells. (A) Time course of whole cell inward currents at -74 mV maximally activated upon passive store-depletion of RBL-2H3 cells upon perfusion of $10\text{ }\mu\text{M}$ GSK-7975A in comparison to $10\text{ }\mu\text{M}$ La³⁺. (B) Concentration-dependent inhibition of thapsigargin-evoked Ca²⁺ influx from Fura-4 loaded RBL cells expressed as fold over unstimulated cells.

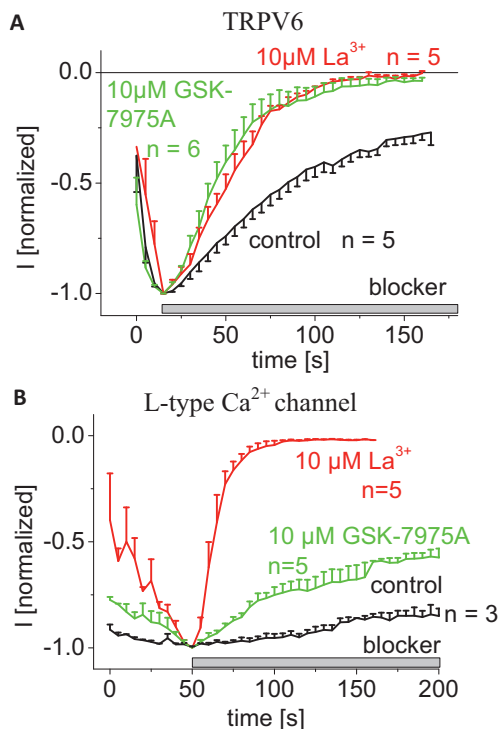


Fig. 10. Inhibitory profile of GSK-7975A on other Ca²⁺-selective channels. (A) Time course of whole cell inward currents at -74 mV of TRPV6 expressing HEK293 cells upon perfusion of $10\text{ }\mu\text{M}$ GSK-7975A in comparison to $10\text{ }\mu\text{M}$ La³⁺. (B) Time course of whole cell inward currents at -74 mV of L-type Ca²⁺-channel expressing HEK293 cells upon perfusion of $10\text{ }\mu\text{M}$ GSK-7975A in comparison to $10\text{ }\mu\text{M}$ La³⁺.

inhibition of L-type Ca²⁺ channels occurred only to a weak extent, TRPV6 channels displayed complete block at a rate similar to the inhibition obtained with La³⁺. Hence, it might be supposed that TRPV6 and Orai proteins share some structural similarities in their target site for the GSK blocker, although the pore diameter [73] of TRPV6 is much larger (5.4 Å) and is of similar size to that of the Orai1 E106D mutant [61].

In summary, the two GSK CRAC channel blockers described herein target Orai channels and will function as lead compounds to facilitate the discovery of highly selective inhibitors. Furthermore these compounds will help validate the role of CRAC channels in asthma and allergic diseases.

Conflict of interest

The authors declared that there is no conflict of interest.

Acknowledgements

Isabella Derler (T466) is a Hertha-Firnberg scholarship holder. This work was in part supported by GlaxoSmithKline and by the Austrian Science Foundation (FWF): project P22747 to R.S. and project P22565 to C.R.

Appendix A. Supplementary data

Supplementary data associated with this article can be found, in the online version, at <http://dx.doi.org/10.1016/j.ceca.2012.11.005>.

References

- [1] M.J. Berridge, M.D. Bootman, H.L. Roderick, Calcium signalling: dynamics, homeostasis and remodelling, *Nature Reviews Molecular Cell Biology* 4 (7) (2003) 517–529.
- [2] B.S. Fischer, D. Qin, K. Kim, T.V. McDonald, Capsaicin inhibits Jurkat T-cell activation by blocking calcium entry current I(CRAC), *Journal of Pharmacology and Experimental Therapeutics* 299 (1) (2001) 238–246.
- [3] M. Gericke, M. Oike, G. Droogmans, B. Nilius, Inhibition of capacitative Ca²⁺ entry by a Cl[−] channel blocker in human endothelial cells, *European Journal of Pharmacology* 269 (3) (1994) 381–384.
- [4] J.H. Li, K.T. Spence, P.G. Dargis, E.P. Christian, Properties of Ca(2+) release-activated Ca(2+) channel block by 5-nitro-2-(3-phenylpropylamino)-benzoic acid in Jurkat cells, *European Journal of Pharmacology* 394 (2–3) (2000) 171–179.
- [5] M. Reinsprecht, M.H. Rohn, R.J. Spadinger, I. Pecht, H. Schindler, C. Romanin, Blockade of capacitive Ca²⁺ influx by Cl[−] channel blockers inhibits secretion from rat mucosal-type mast cells, *Molecular Pharmacology* 47 (5) (1995) 1014–1020.
- [6] J. Ishikawa, K. Ohga, T. Yoshino, R. Takezawa, A. Ichikawa, H. Kubota, et al., A pyrazole derivative, YM-58483, potentially inhibits store-operated sustained Ca²⁺ influx and IL-2 production in T lymphocytes, *Journal of Immunology* 170 (9) (2003) 4441–4449.
- [7] R. Takezawa, H. Cheng, A. Beck, J. Ishikawa, P. Launay, H. Kubota, et al., A pyrazole derivative potentially inhibits lymphocyte Ca²⁺ influx and cytokine production by facilitating transient receptor potential melastatin 4 channel activity, *Molecular Pharmacology* 69 (4) (2006) 1413–1420.
- [8] C. Zitt, B. Strauss, E.C. Schwarz, N. Spaeth, G. Rast, A. Hatzelmann, et al., Potent inhibition of Ca²⁺ release-activated Ca²⁺ channels and T-lymphocyte activation by the pyrazole derivative BTP2, *Journal of Biological Chemistry* 279 (13) (2004) 12427–12437.
- [9] S.I. Zakharov, T. Smani, Y. Dobrydenova, F. Monje, C. Fichandler, P.F. Blackmore, et al., Diethylstilbestrol is a potent inhibitor of store-operated channels and capacitative Ca(2+) influx, *Molecular Pharmacology* 66 (3) (2004) 702–707.
- [10] M.V. Winstead, J. Balsinde, E.A. Dennis, Calcium-independent phospholipase A(2): structure and function, *Biochimica et Biophysica Acta* 1488 (1–2) (2000) 28–39.
- [11] E.C. Aromataris, J. Castro, G.Y. Rychkov, G.J. Barritt, Store-operated Ca(2+) channels and stromal interaction molecule 1 (STIM1) are targets for the actions of bile acids on liver cells, *Biochimica et Biophysica Acta* 1783 (5) (2008) 874–885.
- [12] Q.K. Tran, H. Watanabe, H.Y. Le, L. Pan, M. Seto, K. Takeuchi, et al., Myosin light chain kinase regulates capacitative Ca(2+) entry in human monocytes/macrophages, *Arteriosclerosis, Thrombosis, and Vascular Biology* 21 (4) (2001) 509–515.
- [13] M. Hoth, R. Penner, Calcium release-activated calcium current in rat mast cells, *Journal of Physiology* 465 (1993) 359–386.

- [14] P.E. Ross, M.D. Cahalan, Ca^{2+} influx pathways mediated by swelling or stores depletion in mouse thymocytes, *Journal of General Physiology* 106 (3) (1995) 415–444.
- [15] M. Prakriya, R.S. Lewis, Potentiation and inhibition of Ca^{2+} release-activated Ca^{2+} channels by 2-aminoethoxydiphenyl borate (2-APB) occurs independently of IP(3) receptors, *Journal of Physiology* 536 (Pt 1) (2001) 3–19.
- [16] K.G. Chandy, H. Wulff, C. Beeton, M. Pennington, G.A. Gutman, M.D. Cahalan, K^{+} channels as targets for specific immunomodulation, *Trends in Pharmacological Sciences* 25 (5) (2004) 280–289.
- [17] M.K. Chung, H. Lee, A. Mizuno, M. Suzuki, M.J. Caterina, 2-Aminoethoxydiphenyl borate activates and sensitizes the heat-gated ion channel TRPV3, *Journal of Neuroscience* 24 (22) (2004) 5177–5182.
- [18] J. Cui, J.S. Bian, A. Kagan, T.V. McDonald, CaT1 contributes to the stores-operated calcium current in Jurkat T-lymphocytes, *Journal of Biological Chemistry* 277 (49) (2002) 47175–47183.
- [19] P. Delmas, Assembly and gating of TRPC channels in signalling microdomains, *Novartis Foundation Symposium* 258 (2004) 75–89, discussion 89–102, 283–266.
- [20] J.M. Diver, S.O. Sage, J.A. Rosado, The inositol trisphosphate receptor antagonist 2-aminoethoxydiphenylborate (2-APB) blocks Ca^{2+} entry channels in human platelets: cautions for its use in studying Ca^{2+} influx, *Cell Calcium* 30 (5) (2001) 323–329.
- [21] L.P. He, T. Hewavitharana, J. Soboloff, M.A. Spassova, D.L. Gill, A functional link between store-operated and TRPC channels revealed by the 3,5-bis(trifluoromethyl)pyrazole derivative, BTP2, *Journal of Biological Chemistry* 280 (12) (2005) 10997–11006.
- [22] M.C. Hermosura, M.K. Monteilh-Zoller, A.M. Scharenberg, R. Penner, A. Fleig, Dissociation of the store-operated calcium current I(CRAC) and the Mg-nucleotide-regulated metal ion current MagNum, *Journal of Physiology* 539 (Pt 2) (2002) 445–458.
- [23] A. Hinman, H.H. Chuang, D.M. Bautista, D. Julius, TRP channel activation by reversible covalent modification, *Proceedings of the National Academy of Sciences of the United States of America* 103 (51) (2006) 19564–19568.
- [24] D. Kim, E.J. Cavanaugh, Requirement of a soluble intracellular factor for activation of transient receptor potential A1 by pungent chemicals: role of inorganic polyphosphates, *Journal of Neuroscience* 27 (24) (2007) 6500–6509.
- [25] J.P. Lievreumont, G.S. Bird, J.W. Putney Jr., Mechanism of inhibition of TRPC cation channels by 2-aminoethoxydiphenylborane, *Molecular Pharmacology* 68 (3) (2005) 758–762.
- [26] L. Missiaen, K. Van Acker, K. Van Baelen, L. Raeymaekers, F. Wuytack, J.B. Parys, et al., Calcium release from the Golgi apparatus and the endoplasmic reticulum in HeLa cells stably expressing targeted aequorin to these compartments, *Cell Calcium* 36 (6) (2004) 479–487.
- [27] B. Nilius, J. Prenen, R. Vennekens, J.G. Hoenderop, R.J. Bindels, G. Droogmans, Pharmacological modulation of monovalent cation currents through the epithelial Ca^{2+} channel ECaC1 , *British Journal of Pharmacology* 134 (3) (2001) 453–462.
- [28] R. Schindl, H. Kahr, I. Graz, K. Groschner, C. Romanin, Store depletion-activated CaT1 currents in rat basophilic leukemia mast cells are inhibited by 2-aminoethoxydiphenyl borate. Evidence for a regulatory component that controls activation of both CaT1 and CRAC (Ca^{2+} release-activated Ca^{2+} channel) channels, *Journal of Biological Chemistry* 277 (30) (2002) 26950–26958.
- [29] M. Trebak, G.S. Bird, R.R. McKay, J.W. Putney Jr., Comparison of human TRPC3 channels in receptor-activated and store-operated modes. Differential sensitivity to channel blockers suggests fundamental differences in channel composition, *Journal of Biological Chemistry* 277 (24) (2002) 21617–21623.
- [30] H. Turner, A. Fleig, A. Stokes, J.P. Kinet, R. Penner, Discrimination of intracellular calcium store subcompartments using TRPV1 (transient receptor potential channel, vanilloid subfamily member 1) release channel activity, *Biochemical Journal* 371 (Pt 2) (2003) 341–350.
- [31] T. Voets, J. Prenen, A. Fleig, R. Vennekens, H. Watanabe, J.G. Hoenderop, et al., CaT1 and the calcium release-activated calcium channel manifest distinct pore properties, *Journal of Biological Chemistry* 276 (51) (2001) 47767–47770.
- [32] Y. Wang, M. Deshpande, R. Payne, 2-Aminoethoxydiphenyl borate inhibits phototransduction and blocks voltage-gated potassium channels in *Limulus* ventral photoreceptors, *Cell Calcium* 32 (4) (2002) 209–216.
- [33] S.Z. Xu, F. Zeng, G. Boulay, C. Grimm, C. Harteneck, D.J. Beech, Block of TRPC5 channels by 2-aminoethoxydiphenyl borate: a differential, extracellular and voltage-dependent effect, *British Journal of Pharmacology* 145 (4) (2005) 405–414.
- [34] T. Yoshino, J. Ishikawa, K. Ohga, T. Morokata, R. Takezawa, H. Morio, et al., YM-58483, a selective CRAC channel inhibitor, prevents antigen-induced airway eosinophilia and late phase asthmatic responses via Th2 cytokine inhibition in animal models, *European Journal of Pharmacology* 560 (2–3) (2007) 225–233.
- [35] J. Liou, M.L. Kim, W.D. Heo, J.T. Jones, J.W. Myers, J.E. Ferrell Jr., et al., STIM is a Ca^{2+} sensor essential for Ca^{2+} -store-depletion-triggered Ca^{2+} influx, *Current Biology* 15 (13) (2005) 1235–1241.
- [36] C. Peinelt, M. Vig, D.L. Koomoa, A. Beck, M.J. Nadler, M. Koblan-Huberson, et al., Amplification of CRAC current by STIM1 and CRACM1 (Orai1), *Nature Cell Biology* 8 (7) (2006) 771–773.
- [37] J. Soboloff, M.A. Spassova, X.D. Tang, T. Hewavitharana, W. Xu, D.L. Gill, Orai1 and STIM reconstitute store-operated calcium channel function, *Journal of Biological Chemistry* 281 (30) (2006) 20661–20665.
- [38] A. Lis, C. Peinelt, A. Beck, S. Parvez, M. Monteilh-Zoller, A. Fleig, et al., CRACM1, CRACM2, and CRACM3 are store-operated Ca^{2+} channels with distinct functional properties, *Current Biology* 17 (9) (2007) 794–800.
- [39] S. Feske, Y. Gwack, M. Prakriya, S. Srikanth, S.H. Puppel, B. Tanasa, et al., A mutation in Orai1 causes immune deficiency by abrogating CRAC channel function, *Nature* 441 (7090) (2006) 179–185.
- [40] J.C. Mercer, W.I. Dehaven, J.T. Smyth, B. Wedel, R.R. Boyles, G.S. Bird, et al., Large store-operated calcium selective currents due to co-expression of Orai1 or Orai2 with the intracellular calcium sensor Stim1, *Journal of Biological Chemistry* 281 (34) (2006) 24979–24990.
- [41] M.A. Spassova, J. Soboloff, L.P. He, W. Xu, M.A. Dziadek, D.L. Gill, STIM1 has a plasma membrane role in the activation of store-operated Ca^{2+} channels, *Proceedings of the National Academy of Sciences of the United States of America* 103 (11) (2006) 4040–4045.
- [42] W.I. Dehaven, J.T. Smyth, R.R. Boyles, G.S. Bird, J.W. Putney Jr., Complex actions of 2-aminoethoxydiphenyl borate (2-APB) on store-operated calcium entry, *Journal of Biological Chemistry* 283 (28) (2008) 19265–19273.
- [43] C. Peinelt, A. Lis, A. Beck, A. Fleig, R. Penner, 2-APB directly facilitates and indirectly inhibits STIM1-dependent gating of CRAC channels, *Journal of Physiology* 586 (13) (2008) 3061–3073.
- [44] N.A. Tamarina, A. Kuznetsov, L.H. Philipson, Reversible translocation of EYFP-tagged STIM1 is coupled to calcium influx in insulin secreting beta-cells, *Cell Calcium* 44 (6) (2008) 533–544.
- [45] R. Schindl, J. Bergsmann, I. Frischauf, I. Derler, M. Fahrner, M. Muik, et al., 2-Aminoethoxydiphenyl borate alters selectivity of Orai3 channels by increasing their pore size, *Journal of Biological Chemistry* 283 (29) (2008) 20261–20267.
- [46] S.L. Zhang, J.A. Kozak, W. Jiang, A.V. Yeromin, J. Chen, Y. Yu, et al., Store-dependent and -independent modes regulating CRAC channel activity of human Orai1 and Orai3, *Journal of Biological Chemistry* 283 (25) (2008) 17662–17674.
- [47] C. Romanin, R. Gamsjaeger, H. Kahr, D. Schaufeller, O. Carlson, D.R. Abernethy, et al., Ca^{2+} sensors of L-type Ca^{2+} channel, *FEBS Letters* 487 (2) (2000) 301–306.
- [48] A. Singh, D. Hamedinger, J.C. Hoda, M. Gebhart, A. Koschak, C. Romanin, et al., C-terminal modulator controls Ca^{2+} -dependent gating of $\text{CaV}1.4$ L-type Ca^{2+} channels, *Nature Neuroscience* 9 (9) (2006) 1108–1116.
- [49] I. Derler, M. Hofbauer, H. Kahr, R. Fritsch, M. Muik, K. Kepplinger, et al., Dynamic but not constitutive association of calmodulin with rat TRPV6 channels enables fine tuning of Ca^{2+} -dependent inactivation, *Journal of Physiology* 577 (Pt 1) (2006) 31–44.
- [50] Z. Xia, Y. Liu, Reliable and global measurement of fluorescence resonance energy transfer using fluorescence microscopes, *Biophysical Journal* 81 (4) (2001) 2395–2402.
- [51] C. Berney, G. Danuser, FRET or no FRET: a quantitative comparison, *Biophysical Journal* 84 (6) (2003) 3992–4010.
- [52] D.J. Beech, Orai1 calcium channels in the vasculature, *Pflügers Archiv: European Journal of Physiology* 463 (5) (2012) 635–647.
- [53] Z.K. Sweeney, A. Minatti, D.C. Button, S. Patrick, Small-molecule inhibitors of store-operated calcium entry, *ChemMedChem* 4 (5) (2009) 706–718.
- [54] M. Muik, I. Frischauf, I. Derler, M. Fahrner, J. Bergsmann, P. Eder, et al., Dynamic coupling of the putative coiled-coil domain of Orai1 with STIM1 mediates Orai1 channel activation, *Journal of Biological Chemistry* 283 (12) (2008) 8014–8022.
- [55] L. Navarro-Borelly, A. Somasundaram, M. Yamashita, D. Ren, R.J. Miller, M. Prakriya, STIM1–Orai1 interactions and Orai1 conformational changes revealed by live-cell FRET microscopy, *Journal of Physiology* 586 (Pt 22) (2008) 5383–5401.
- [56] W.I. DeHaven, J.T. Smyth, R.R. Boyles, G.S. Bird, J.W. Putney Jr., Complex actions of 2-aminoethoxydiphenyl borate on store-operated calcium entry, *Journal of Biological Chemistry* 283 (28) (2008) 19265–19273.
- [57] R. Schindl, J. Bergsmann, I. Frischauf, I. Derler, M. Fahrner, M. Muik, et al., 2-Aminoethoxydiphenyl borate alters selectivity of Orai3 channels by increasing their pore size, *Journal of Biological Chemistry* 283 (29) (2008) 20261–20267.
- [58] S.L. Zhang, J.A. Kozak, W. Jiang, A.V. Yeromin, J. Chen, Y. Yu, et al., Store-dependent and -independent modes regulating Ca^{2+} release-activated Ca^{2+} channel activity of human Orai1 and Orai3, *Journal of Biological Chemistry* 283 (25) (2008) 17662–17671.
- [59] M. Prakriya, S. Feske, Y. Gwack, S. Srikanth, A. Rao, P.G. Hogan, Orai1 is an essential pore subunit of the CRAC channel, *Nature* 443 (7108) (2006) 230–233.
- [60] M. Vig, A. Beck, J.M. Billingsley, A. Lis, S. Parvez, C. Peinelt, et al., CRACM1 multimers form the ion-selective pore of the CRAC channel, *Current Biology* 16 (20) (2006) 2073–2079.
- [61] M. Yamashita, L. Navarro-Borelly, B.A. McNally, M. Prakriya, Orai1 mutations alter ion permeation and Ca^{2+} -dependent fast inactivation of CRAC channels: evidence for coupling of permeation and gating, *Journal of General Physiology* 130 (5) (2007) 525–540.
- [62] G. Owsianik, K. Talavera, T. Voets, B. Nilius, Permeation and selectivity of trp channels, *Annual Review of Physiology* 68 (2006) 685–717.
- [63] S. Feske, CRAC channelopathies, *Pflügers Archiv: European Journal of Physiology* 462 (2) (2010) 417–435.

- [64] I. Derler, F.R. Schindl, R. Romanin C, CRAC channels: inhibitors and potential applications, *Expert Opinion in Drug Discovery* 3 (2008) 787–800.
- [65] I. Derler, R. Fritsch, R. Schindl, C. Romanin, CRAC inhibitors: identification and potential, *Expert Opinion on Drug Discovery* 3 (7) (2008) 787–800.
- [66] J.W. Putney, Pharmacology of store-operated calcium channels, *Molecular Interventions* 10 (4) (2010) 209–218.
- [67] A. Di Sabatino, L. Rovedatti, R. Kaur, J.P. Spencer, J.T. Brown, V.D. Morisset, et al., Targeting gut T cell Ca^{2+} release-activated Ca^{2+} channels inhibits T cell cytokine production and T-box transcription factor T-bet in inflammatory bowel disease, *Journal of Immunology* 183 (5) (2009) 3454–3462.
- [68] S.W. Ng, J. di Capite, K. Singaravelu, A.B. Parekh, Sustained activation of the tyrosine kinase Syk by antigen in mast cells requires local Ca^{2+} influx through Ca^{2+} release-activated Ca^{2+} channels, *Journal of Biological Chemistry* 283 (46) (2008) 31348–31355.
- [69] J. Li, L. McKeown, O. Ojelabi, M. Stacey, R. Foster, D. O'Regan, et al., Nanomolar potency and selectivity of a Ca^{2+} release-activated Ca^{2+} channel inhibitor against store-operated Ca^{2+} entry and migration of vascular smooth muscle cells, *British Journal of Pharmacology* 164 (2) (2011) 382–393.
- [70] B.A. McNally, M. Yamashita, A. Engh, M. Prakriya, Structural determinants of ion permeation in CRAC channels, *Proceedings of the National Academy of Sciences of the United States of America* 106 (52) (2009) 22516–22521.
- [71] A.V. Yeromin, S.L. Zhang, W. Jiang, Y. Yu, O. Safrina, M.D. Cahalan, Molecular identification of the CRAC channel by altered ion selectivity in a mutant of Orai, *Nature* 443 (7108) (2006) 226–229.
- [72] I. Ashmole, S.M. Duffy, M.L. Leyland, V.S. Morrison, M. Begg, P. Bradding, CRACM/Orai ion channel expression and function in human lung mast cells, *Journal of Allergy and Clinical Immunology* 129 (6) (2012) 1628–1635.
- [73] G. Owsianik, D. D'Hoedt, T. Voets, B. Nilius, Structure–function relationship of the TRP channel superfamily, *Reviews of Physiology Biochemistry and Pharmacology* 156 (2006) 61–90.

Signal Transduction:
Canonical Transient Receptor Potential (TRPC) 1 Acts as a Negative Regulator for Vanilloid TRPV6-mediated Ca^{2+} Influx



Rainer Schindl, Reinhard Fritsch, Isaac Jardin,
Irene Frischauf, Heike Kahr, Martin Muik,
Maria Christine Riedl, Klaus Groschner and
Christoph Romanin

J. Biol. Chem. 2012, 287:35612-35620.

doi: 10.1074/jbc.M112.400952 originally published online August 29, 2012

Access the most updated version of this article at doi: [10.1074/jbc.M112.400952](https://doi.org/10.1074/jbc.M112.400952)

Find articles, minireviews, Reflections and Classics on similar topics on the [JBC Affinity Sites](#).

Alerts:

- [When this article is cited](#)
- [When a correction for this article is posted](#)

[Click here](#) to choose from all of JBC's e-mail alerts

Supplemental material:

<http://www.jbc.org/content/suppl/2012/08/29/M112.400952.DC1.html>

This article cites 52 references, 29 of which can be accessed free at
<http://www.jbc.org/content/287/42/35612.full.html#ref-list-1>

Canonical Transient Receptor Potential (TRPC) 1 Acts as a Negative Regulator for Vanilloid TRPV6-mediated Ca^{2+} Influx^{*[5]}

Received for publication, July 13, 2012, and in revised form, August 24, 2012. Published, JBC Papers in Press, August 29, 2012, DOI 10.1074/jbc.M112.400952

Rainer Schindl^{†1}, Reinhard Fritsch[‡], Isaac Jardin^{§2}, Irene Frischau^{†3}, Heike Kahr[¶], Martin Muik[‡], Maria Christine Riedl[‡], Klaus Groschner^{||}, and Christoph Romanin^{†4}

From the [†]Institute for Biophysics, University of Linz, A-4020 Linz, Austria, the ^{||}Institute of Pharmacology and Toxicology, University of Graz, A-8010 Graz, Austria, the [§]Department of Physiology, University of Extremadura, 10003 Cáceres, Spain, and the [¶]School of Engineering/Environmental/Sciences, University of Applied Sciences Upper Austria, A-4600 Wels, Austria

Background: Heteromerization of TRP family members can affect their physiological and biophysical properties.

Results: TRPV6 and TRPC1 associate via their ankyrin-like repeat domains. Co-expression of TRPV6 and TRPC1 reduced TRPV6 expression in the plasma membrane, and hence reduces TRPV6 influx currents.

Conclusion: TRPC1 acts as negative regulator on TRPV6 mediated Ca^{2+} signaling.

Significance: We show here a novel regulation in TRPV6 activity by formation of heterocomplexes with TRPC1.

TRP proteins mostly assemble to homomeric channels but can also heteromerize, preferentially within their subfamilies. The TRPC1 protein is the most versatile member and forms various TRPC channel combinations but also unique channels with the distantly related TRPP2 and TRPV4. We show here a novel cross-family interaction between TRPC1 and TRPV6, a Ca^{2+} selective member of the vanilloid TRP subfamily. TRPV6 exhibited substantial co-localization and *in vivo* interaction with TRPC1 in HEK293 cells, however, no interaction was observed with TRPC3, TRPC4, or TRPC5. Ca^{2+} and Na^{+} currents of TRPV6-overexpressing HEK293 cells are significantly reduced by co-expression of TRPC1, correlating with a dramatically suppressed plasma membrane targeting of TRPV6. In line with their intracellular retention, remaining currents of TRPC1 and TRPV6 co-expression resemble in current-voltage relationship that of TRPV6. Studying the N-terminal ankyrin like repeat domain, structurally similar in the two proteins, we have found that these cytosolic segments were sufficient to mediate a direct heteromeric interaction. Moreover, the inhibitory role of TRPC1 on TRPV6 influx was also maintained by expression of only its N-terminal ankyrin-like repeat domain. Our experiments provide evidence for a functional interaction of TRPC1 with TRPV6 that negatively regulates Ca^{2+} influx in HEK293 cells.

The transient receptor potential (TRP)⁵ proteins display a broad tissue expression with a large diversity of cation selectivity, modes of activation and physiological functions (1, 2). All TRP proteins consist of 6 transmembrane domains and assemble into tetramers (3–6). While heterologous expression of TRP proteins predominantly leads to homomeric oligomerization, knock-down strategies have revealed that most native TRPs are aggregated to heteromeric channels that are embedded in larger signaling complexes (7, 8).

Heteromeric TRP channels are well demonstrated within the phospholipase C-coupled TRPC family. TRPCs multimerize within TRPC1/4/5 and TRPC3/6/7 subgroups (9, 10). Only TRPC1 can form heteromers with all other TRPC proteins (11–14) exhibiting a reduced Ca^{2+} permeability compared with the respective homomeric TRPC channel subtype. A novel receptor-dependent ion channel is formed by a heteromer of TRPC1 with the distinctly related polycystic TRPP2 (15–17).

Within the vanilloid TRP channels, TRPV5/6 proteins are not only co-expressed in similar tissues but they can also form heteromeric channels (3, 18). Various heteromeric combinations have been reported within TRPV1 to TRPV4 (20) while Hellwig *et al.* only observed interaction between TRPV1 and TRPV2 (18). Melastatin, mucolipin, and polycystic TRP include heteromeric channels within their subfamily (5).

Heteromerization between members of TRPC and TRPV subfamilies plays an important role in the regulation of cation influx in a number of tissues. TRPV4 interacts with TRPC1-forming complexes that modulate Ca^{2+} influx in endothelial cells (21). TRPC1 and TRPC6 channels associate with TRPV4 to mediate mechanical hyperalgesia and primary afferent nociceptor sensitization (22). TRPC1 and TRPV6 contributed to Ca^{2+} entry in prostate cells, where TRPV6 expression is shown to be closely related with prostate cancer (23).

* This work was supported by the Austrian Science Foundation (to F. W. F.): Project P22747 (to R. S.), Project P21925 (to K. G.), and Project P18169 as well as P22565 (to C. R.).

Author's Choice—Final version full access.

[5] This article contains supplemental Fig. S1.

¹ To whom correspondence may be addressed: Institute of Biophysics, Johannes Kepler University Linz Gruberstrasse, 40-4020 Linz (Austria). Tel.: +4373224687606; E-mail: rainer.schindl@jku.at.

² Supported by MCI fellowship (Ref. BES-2008-002875).

³ Recipient of a Hertha-Firnberg scholarship (T442).

⁴ To whom correspondence may be addressed: Institute of Biophysics, Johannes Kepler University Linz Gruberstrasse, 40-4020 Linz (Austria). E-mail: christoph.romanin@jku.at.

⁵ The abbreviations used are: TRP, transient receptor potential; FRET, Förster resonance energy transfer; TRPC, canonical TRP; TRPV6, vanilloid TRP 6; SOCE, store-operated calcium entry; DVF, divalent-free.

Because of its huge variety, the formation of these homo- and heterocomplexes in the TRP family may involve different protein motifs. Homomeric TRPC1 assembly is dependent on an N-terminal coiled-coil region (24), while TRPM2, TRPM8, and TRPP2 use C-terminal coiled-coils for tetramerization (25–30). Instead, TRPC4 and TRPC5 (31), TRPV4 (32), TRPV5, and TRPV6 (33–35) require the ankyrin-like repeats for homo- as well as heteromeric channel assembly. In addition to the ankyrin like repeats, TRPC channels require a C-terminal segment as well (36). Interestingly, TRPC1 seems to use different domains for homo- and heteromerization, and oligomerizes with TRPC3 via their ankyrins (12).

In the present study, we report a novel interaction of TRPC1 and TRPV6 via their ankyrin-like repeats, which down-regulates both TRPV6 expression in the plasma membrane and TRPV6 Ca^{2+} current. The observed down-regulation of TRPV6 currents by TRPC1 may increase the cellular diversity to fine-tune Ca^{2+} homeostasis.

EXPERIMENTAL PROCEDURES

Cell Culture and Molecular Cloning—Human embryonic kidney 293 (HEK293) cells were cultured in DMEM supplemented with L-glutamine (2 mM), streptomycin (100 $\mu\text{g}/\text{ml}$), penicillin (100 units/ml), and 10% fetal calf serum at 37 °C in a humidity-controlled incubator with 7% CO_2 . HEK293 cells were transfected with 4 μl of Transfectin (Bio-Rad) and 1 μg of DNA of CFP/YFP-TRPC1 (GenBankTM accession number: NM_003304.4), TRPC3 (U47050), TRPC4 (NM_016984.1), TRPC5 (NM_009428), TRPV6 (AF160798) or fragments. Internal restriction sites were used to generate TRPC1 fragments, TRPV6 constructs have been previously described (37).

Förster Resonance Energy Transfer (FRET) Microscopy—Transfected HEK293 cells grown on cover slips for 1–2 days were transferred to a standard bath solution, including (in mM): 140 NaCl, 5 KCl, 1 MgCl_2 , 2 CaCl_2 , 10 glucose, 10 Hepes, pH 7.4 (NaOH).

A QLC100 Real-Time Confocal System (Visitron Systems GmbH, Germany) was used for recording fluorescence images connected to a dual port adapter (dichroic: 505lp; emission 1: 485/30; emission 2: 535/50; Chroma Technology Corp.) and two Photometrics CoolSNAPHQ monochrome cameras (Roper Scientific). This system was attached to an Axiovert 200 M microscope (Zeiss, Germany) and used in conjunction with an argon ion multi-wavelength (454–514 nm) laser (Spectra Physics). The wavelengths were selected by an Acousto Optical Tuneable Filter (VisiTech Int.). MetaMorph 5.0 software (Universal Imaging Corp.) was used to acquire images and to control the confocal system. Illumination times for CFP/FRET and YFP images that were recorded with a minimum delay consecutively of 900 ms. The images were analyzed for FRET using a self-written MatLab 7 programs (37) where the algorithm proposed by Xia (52) was implemented. In short, the recorded FRET image (ex: 457 nm, em 535/50) was corrected for crosstalk from the other imaging channels. The appropriate crosstalk calibration factors were determined for all the constructs used in separate experiments on the days the experiments were done.

Electrophysiology—Electrophysiological experiments were performed at 20–24 °C, using the patch-clamp technique (38)

in the whole-cell recording configuration one or 2 days after transfection. Voltage ramps were usually applied every 5 s from a holding potential of +70 mV, covering a range of –90 to 90 mV over 200 ms. In all recordings that were performed in divalent-free (DVF) solutions, a 100 ms ramp (–90 mV to +90 mV) was applied every 2 s from a holding potential of 0 mV. Pipette solution was used to decrease cytosolic Ca^{2+} levels containing (in mM) 145 Cs methane sulfonate, 8 NaCl, 5 MgCl_2 , 10 HEPES, 10 EGTA, pH 7.2. For carbachol and thapsigargin-stimulated HEK293 cells overexpressing TRPC1 or TRPC1/TRPC5, pipette solution was adjusted to 100 nM cytosolic Ca^{2+} by addition of 4.3 CaCl_2 . Extracellular solution for Ca^{2+} currents consisted of 145 NaCl (or 145 TEA-Cl), 5 CsCl, 1 MgCl_2 , 10 HEPES, 10 glucose, 10 CaCl_2 , pH 7.4. DVF solution contained 165 NaCl, 5 CsCl, 10 HEPES, 10 glucose, 10 EDTA, pH 7.4/CsOH. A liquid junction correction of +12 mV resulted from a Cl^- -based bath solution and a sulfonate-based pipette solution.

Biotinylation of Cell Surface Membrane Proteins—HEK293 cells were transfected with YFP-TRPV6 or with GFP-TRPV6 and TRPC1. After 24–72 h, cell surface proteins were biotinylated for 30 min at 4 °C using sulfo-NHS-LC-LC-biotin or sulfo-NHS-SS-biotin (0.5 mg/ml; Pierce) as described previously (39). Briefly, cells were incubated 1 h at 4 °C with the biotinylation agent. After incubation, 100 mM Tris was added to stop the reaction. Cells were washed twice with PBS to remove excess biotinylation agent and lysed with lysis buffer, pH 8.0, containing 100 mM NaCl, 20 mM Tris, 2 mM EDTA, 10% glycerol, 0.5% Nonidet P40, and supplemented by 20 $\mu\text{l}/\text{ml}$ protease inhibitor mixture (Roche Applied Science). Lysed samples were centrifuged at $14,000 \times g$ for 15 min. Finally, biotinylated proteins in the supernatant were precipitated using High Capacity Streptavidin Agarose Resin (Pierce) overnight at 4 °C on a rocking platform. The samples were resolved by 10% SDS-PAGE, and protein detection was done as described in Ref. 39. Anti- β -actin (A5441; Sigma) was used to normalize protein expression.

Immunoprecipitation and Immunoblots—Immunoprecipitation and Western blotting were performed as described previously (40). Briefly, 500- μl aliquots of HEK293 suspension (2×10^5 cell/ml) were lysed with an equal volume of lysis buffer, pH 8.0, containing 200 mM NaCl, 40 mM Tris, 4 mM EDTA, 20% glycerol, 1% Nonidet P40, and supplemented by 20 $\mu\text{l}/\text{ml}$ protease inhibitor mixture (Roche Applied Science). Aliquots of HEK293 lysates (1 ml) were immunoprecipitated by incubation with 2 μg of either anti-GFP (Sigma-Aldrich) or anti-TRPC1 antibody (Alomone) and 25 μl of protein A-agarose overnight at 4 °C on a rocking platform. The immunoprecipitates were resolved by 10% SDS-PAGE and separated proteins were electrophoretically transferred onto nitrocellulose membranes for subsequent probing. Blots were incubated 1 h with 10% (w/v) BSA in tris-buffered saline with 0.1% Tween 20 (TBST) to block residual protein binding sites. Immunodetection of hTRPV6 and hTRPC1 was achieved using the anti-GFP antibody diluted 1:1000 in TBST or the anti-hTRPC1 antibody diluted 1:250 in TBST overnight, respectively. The primary antibody was removed, and blots were washed six times for 5 min each with TBST. To detect the primary antibody, blots were incubated for 1 h with horseradish peroxidase-conjugated rabbit anti-mouse IgG antibody or horseradish peroxidase-conjugated goat anti-

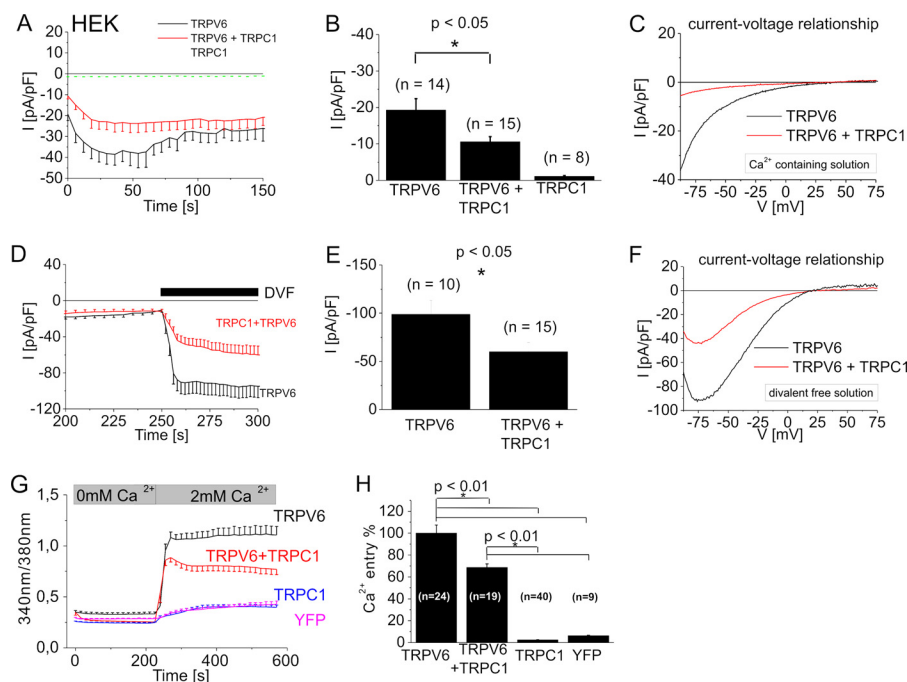


FIGURE 1. Co-expression of TRPC1 and TRPV6 significantly suppressed TRPV6 currents and Ca^{2+} entry. Time course of whole-cell voltage ramps (A) and statistics on initial currents (B) for CFP-TRPC1 and/or YFP-TRPV6 overexpressing HEK293 cells were recorded at -86 mV during voltage ramps with a 10 mM Ca^{2+} bath-solution. Representative current-voltage relationship (C) is shown for either TRPV6 or co-expression of TRPC1 and TRPV6. In a DVF solution, co-expression of TRPC1 and TRPV6 in comparison to TRPV6 alone is depicted in the time course (D), statistical analysis for current maxima (E) and current-voltage relationship (F). Intracellular $[\text{Ca}^{2+}]$, of Fura-2-loaded cells (G) was monitored in the time course in a nominally Ca^{2+} -free solution followed by addition of 2 mM Ca^{2+} . Ca^{2+} entry in cells overexpressing TRPV6 and/or TRPC1 or YFP is shown in the time course (G) or maximum Ca^{2+} entry (H).

rabbit IgG antibody diluted 1:10,000 in TBST and then exposed to enhanced chemiluminescence reagents for 5 min. Blots were then exposed to photographic films. The density of bands on the film was measured using scanning densitometry. Data were normalized to the amount of protein recovered by the antibody used for the immunoprecipitation.

To determine the amount of TRPC1 that is expressed both in the plasma membrane and in the cytosolic fraction, we performed a double immunoprecipitation using the anti hTRPC1 antibody, directed toward the sequence 557–571 of human hTRPC1, which is located in the pore-forming region between the fifth transmembrane domain and region VII of hTRPC1 (41). Cells with overexpressed, untagged TRPC1 were stimulated with 100 μM CCH for 60 s before mixing with paraformaldehyde (1.5% in PBS). Fixed cells were washed and incubated with 2 μg of anti-TRPC1 (557–571) antibody, which binds an extracellular motif within TRPC1 (11, 42, 43), for 2 h, washed, and lysed. Immunoprecipitation was performed for 2 further hours in the presence of agarose beads and in the absence of anti-TRPC1 antibody. The beads were precipitated by centrifugation, washed, and suspended in loading buffer. The supernatant, containing the TRPC1 cytosolic fraction, was immunoprecipitated overnight with 2 μg of TRPC1 and agarose beads. Both fractions were resolved in a SDS-GEL, and the Western blot was performed using the anti-TRPC1 antibody.

Fura-2 Microscopy—HEK293 cells were grown on coverslips for 2 days and loaded with Fura-2/AM (1 μM) for 30 min at 20°C in Dulbecco's modified Eagle's medium, washed for three times and dyes were allowed to deesterify for 15 min at 20°C . Coverslips were transferred to an extracellular solution (see "FRET microscopy") without Ca^{2+} and mounted at an inverted

Axiovert 100 TV microscope (Zeiss, Germany). Excitation of Fura-2 was performed at 340 nm and 380 nm, and Ca^{2+} measurements are shown as 340/380 ratios of both YFP and untransfected HEK293 cells.

Statistical Analysis—Data are expressed as means \pm S.E., and statistical analysis using Student's *t* test with Origin software (OriginLab, Northampton, MA). Differences are considered significant when *p* values are <0.05 .

RESULTS

TRPV6 Currents Are Significantly Suppressed by TRPC1 Co-expression—The TRPC1 protein is the most versatile heteromerization partner of the TRP channels, hence we examined for its impact on the Ca^{2+} -selective TRPV6 channel. We performed whole-cell patch-clamp experiments using a 10 mM Ca^{2+} containing extracellular solution to address the current characteristics of homo- and potentially heteromeric channels. Recordings of yellow fluorescent protein (YFP)-tagged TRPV6 expressing HEK293 cells yielded constitutively active inward currents. Their time courses were monitored at -86 mV by applying repetitive voltage ramps (Fig. 1A). TRPV6 currents transiently increased by using a holding potential of $+70$ mV, followed by a Ca^{2+} /calmodulin-dependent inactivation (33, 37). We analyzed break-in currents immediately after obtaining whole cell configuration for statistical comparison, to avoid Ca^{2+} -dependent modulation (Fig. 1B). Larger maximum TRPV6 currents resulted in a more dominant inactivation (data not shown). In contrast, heterologously expressed TRPC1 tagged with cyan fluorescent protein (CFP) did not generate significant current activity (Fig. 1A). Co-expression of TRPC1 and TRPV6 led to a similar inwardly rectifying current-voltage

relationship with a reversal potential of $> +30$ mV as observed with TRPV6 alone (Fig. 1C), yet with significantly down-regulated initial currents (Fig. 1B). For all experiments, cells with a similar TRPV6 expression (based on fluorescence) were chosen. When extracellular Ca^{2+} solution was exchanged by a divalent-free solution, TRPV6 currents were enhanced, reversed at $+16 \pm 5$ mV ($n = 10$) and exhibited a typical negative slope at negative potentials in the current voltage relationship (44, 45). A similar current-voltage relationship remained also for the co-expression of TRPC1 and TRPV6 channels with a reversal potential of $+17 \pm 2$ mV ($n = 14$), although again with significantly reduced inward-currents (Fig. 1, D–F). These experiments demonstrate that two typical TRPV6 current-voltage characteristics are fully retained, when TRPV6 was expressed alone or together with TRPC1. TRPC proteins typically yield less selective Ca^{2+} currents and TRPC1 decreases Ca^{2+} selectivity in heteromeric TRPC channels, in comparison to a respective homomeric TRPC channel (2, 14). Hence a heteromeric TRPCV6/TRPC1 channel might lead to an altered TRPV6 IV relationship, which was clearly not the case.

Additionally we utilized Fura-2 microscopy to investigate Ca^{2+} entry of HEK293 cells overexpressing TRPC1 and/or TRPV6. Fura-2-loaded HEK293 cells were initially bathed in a Ca^{2+} free solution. Addition of 2 mM Ca^{2+} resulted in a robust Ca^{2+} entry (Fig. 1G) for TRPV6 expressing cells, whereas TRPC1 overexpression led only to a very small Ca^{2+} entry, that was in a similar range as YFP-transfected cells (Fig. 1G). Co-expression of TRPC1 and TRPV6 again resulted in an about 30% reduction of Ca^{2+} entry in comparison to TRPV6 alone (Fig. 1, G and H), consistent with our electrophysiological approach.

Cytosolic TRPC1 Is Relocated to the Plasma Membrane in TRPC1/TRPC5 Heteromers—In our standard conditions, we observed no TRPC1 activity; hence we aimed to stimulate whole-cell currents of TRPC1-overexpressing cells by receptor stimulation or an alternative store depletion. Yet no clear activation was observed upon an application of the physiological agonist carbachol (100 μM ; supplemental Fig. S1A), or thapsigargin (TG; 1 μM ; supplemental Fig. S1C), an inhibitor of the Ca^{2+} -ATPase pump in the endoplasmic reticulum that is widely used to study store-operated calcium entry (SOCE) in line with previous results (9, 46). In Fura-2 microscopy experiments, overexpressed TRPC1 failed to exhibit an enhanced Ca^{2+} entry in comparison to a mock control by either carbachol (100 μM , supplemental Fig. S1D) or thapsigargin (1 μM , supplemental Fig. S1E). Instead, carbachol-activated TRPC5-expressing HEK293 cells yielded an inward-rectifying current-voltage relationship (supplemental Fig. S1, A and B). A co-expression of TRPC1 and TRPC5 yielded carbachol-sensitive currents with a reduced inward as well as enhanced outward current suggesting a heteromeric TRPC1/C5 channel (supplemental Fig. S1, A and B) (9, 14). As TRPC1 has been shown to mediate carbachol-dependent currents (47), we analyzed whether under our conditions overexpressed TRPC1 might be retained intracellularly in HEK293 cells as previously reported (8, 48). Confocal microscopy revealed a cytosolic localization of overexpressed TRPC1 (supplemental Fig. S1F and Fig. 2D). In contrast co-expressed TRPC1 and TRPC5 exhibited co-localization (supple-

mental Fig. S1G), with a partial but clear plasma membrane staining of both TRPC proteins.

Reduced Plasma Membrane Localization of TRPV6 Protein by Co-expression with TRPC1—A possible interpretation of suppressed TRPV6 Ca^{2+} entry/current is that co-expression of TRPC1 reduces the plasma membrane localization of TRPV6. Therefore, we quantitatively compared plasma membrane levels of TRPV6 in cells co-expressing TRPV6 and TRPC1 with those exclusively expressing TRPV6 using surface biotinylation. When TRPV6 is expressed alone in HEK293, the channel is partially located in the plasma membrane in resting cells. When YFP-TRPV6 and an untagged TRPC1 were coexpressed, the amount of TRPV6 in the plasma membrane was reduced, compared with those cells that expressed the TRPV6 protein alone (control TRPV6: 23522 ± 1916 versus control TRPV6 & TRPC1: 4245 ± 411 ; $n = 5$; Fig. 2A, top panel). To exclude that the reduced expression of TRPV6 in the plasma membrane was due to diminished overall expression of TRPV6 in the cell, we analyzed the total amount of TRPV6 in HEK293 cells either overexpressing TRPV6 alone or together with TRPC1 by Western blot. The obtained data demonstrate that co-expression of TRPC1 together with TRPV6 did not alter the total expression of TRPV6 in HEK293 cells (control TRPV6: 32537 ± 1916 versus control TRPV6 & TRPC1: 31245 ± 411 ; $n = 5$; Fig. 2B, top panel). Western blotting of the same membranes with the anti β -actin antibody was used for normalization (Fig. 2, A and B; bottom panel). To determine the amount of TRPC1 that is expressed both in the plasma membrane and in the cytosolic fraction, untagged TRPC1 overexpressed cells were stimulated with 100 μM CCH for 60 s, fixed and the TRPC1 fractions were isolated performing a double immunoprecipitation as described under “Experimental Procedures.” Under our conditions we did not detect overexpressed TRPC1 in the plasma membrane fraction either in resting or carbachol (CCH)-stimulated HEK293 cells (Fig. 2C). By contrast, the cytosolic fraction showed a clear expression of TRPC1 (Fig. 2C). Alternatively we monitored the cellular localization of overexpressed TRPC1 in comparison to TRPV6-expressing cells and their co-expression by confocal microscopy. While TRPC1 remained intracellularly, better visible in an amplified region near the plasma membrane (Fig. 2D), TRPV6 exhibited a clustered localization with partial plasma membrane localization (Fig. 2D). Upon co-expression of TRPC1 and TRPV6 both proteins exhibited a substantial co-localization, while the plasma membrane expression of TRPV6 was clearly reduced (Fig. 2E). Together, these results suggest that TRPC1 is able to suppress TRPV6 dependent currents/entry because of a reduction of TRPV6 plasma membrane expression.

In Vivo Interaction of TRPC1 and TRPV6—It has been described that some members of the TRPC and TRPV families interact and their association may mediate Ca^{2+} influx in endothelial cells (21). We have used confocal Förster Resonance Energy Transfer (FRET) to examine a possible interaction of various TRPC proteins with TRPV6 in a living HEK293 cell. Co-expression of N-terminally tagged CFP-TRPC1 (Fig. 3A, image 2) or YFP-TRPV6 (Fig. 3A, image 3), respectively, revealed substantial intracellular co-localization (Fig. 3A, image 4), similar as TRPC1 overexpression alone (Fig. 3A, image 1). A

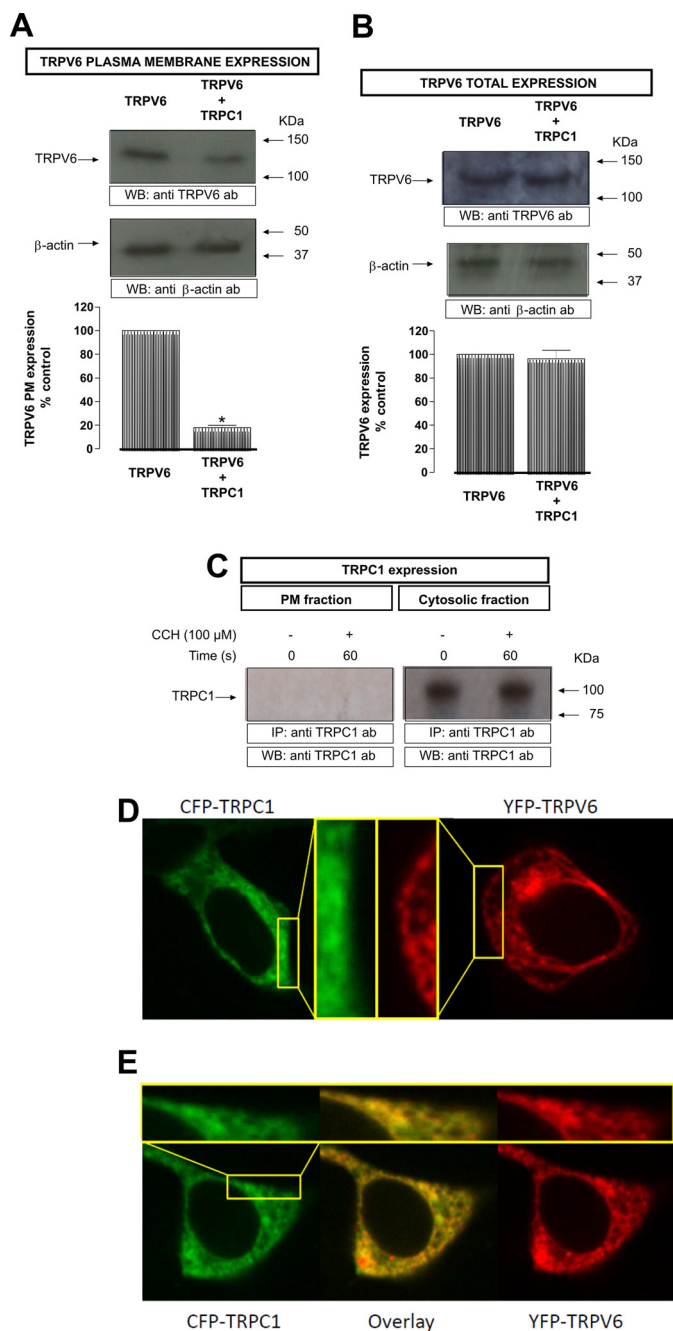


FIGURE 2. TRPV6 expression in HEK293 cells: A, HEK293 cells, co-expressing either YFP-TRPV6 and/or TRPC1 were incubated for 1 h at 4 °C with the biotinylation agent. After incubation, 100 mM Tris was added to stop the reaction. Lysed samples were precipitated using streptavidin beads overnight at 4 °C on a rocking platform. B, HEK293 cells, co-expressing either TRPV6 or TRPV6 and TRPC1 were lysed. In both cases, the samples were resolved by 10% SDS-PAGE and Western blotting using anti-GFP antibody (top). Membranes were re-probed with anti-β-actin antibody (bottom). Positions of molecular weight markers are shown on the right. These results are representative of five independent experiments. Values are mean ± S.E. *, $p < 0.05$ versus resting cells. C, HEK293 cells, co-expressing either TRPC1 were stimulated with 100 μM CCH, fixed and the two TRPC1 fractions were isolated by immunoprecipitation. The samples were resolved by 10% SDS-PAGE and Western blotting using anti-TRPC1 antibody. Positions of molecular weight markers are shown on the right. These results are representative of six independent experiments. Values are mean ± S.E. *, $p < 0.05$ versus resting cells. D, localization of a representative CFP-TRPC1 (left) as well as YFP-TRPV6 (right) transfected HEK293 cell. E, localization and overlay of a representative CFP-TRPC1 and YFP-TRPV6 co-expression. The insets in D and E show a higher magnification of a plasma membrane near region.

mean nFRET value of 0.07 suggests a direct coupling of these TRP proteins (Fig. 3, A, image 5 and F). Furthermore, we studied the association between TRPV6 and the other members of the TRPC family, to reveal a potential selectivity. In contrast to the predominant intracellular localization of YFP-TRPV6, expression of CFP-TRPC3 mainly targeted to the plasma membrane. Upon their co-expression the plasma membrane staining of TRPC3 was clearly distinct from TRPV6 localization, with minor FRET (Fig. 3B). CFP-TRPC4 (Fig. 3C) and CFP-TRPC5 (Fig. 3D) exhibited a punctate localization in the plasma membrane and vesicular intracellular structures. Both proteins showed partial co-localization with YFP-TRPV6 with small nFRET values (< 0.02 ; Fig. 3F). In comparison to the TRPC1/TRPV6 interaction, average FRET of the homomeric assembly of either CFP-/YFP-TRPC1 (Fig. 3E) or previously described CFP-/YFP-TRPV6 (35) are 2-fold increased (Fig. 3F). Clearly the TRPC1 isoform exhibited the most pronounced co-localization and highest FRET with TRPV6, in comparison to the other examined TRPC proteins.

Furthermore, to corroborate FRET results we have studied TRPV6-TRPC1 interaction by co-immunoprecipitation. Immunoprecipitation and subsequent SDS-PAGE and Western blotting were conducted using resting HEK293 cells, in the presence of extracellular Ca^{2+} . After immunoprecipitation with anti-TRPC1 antibody, Western blotting revealed the presence of TRPV6. Blotting of the same membranes with the antibody used for immunoprecipitation confirmed similar TRPC1 protein content in all lanes (Fig. 3G, bottom panel). These data suggest that TRPC1 and TRPV6 proteins are able to assemble within protein complexes and interact with each other when co-expressed in HEK293 cells.

N-terminal Ankyrin-like Repeat Segments of TRPC1 and TRPV6 Interacted Directly—Key domains for functional TRPV6 channel assembly are the six ankyrin-like repeats in the TRPV6 N-terminal strand (33, 35). As TRPC1 also includes three N-terminal ankyrin-like repeats, we focused on these domains as potential interaction sites. Confocal FRET microscopy was used to monitor interaction of CFP- N_{198} -TRPV6, a fragment with four ankyrins that has been previously shown to mediate self-oligomerization (35), with various N-terminal fragments of TRPC1. Co-expression of CFP- N_{198} -TRPV6 (Fig. 4A, 1st image) with YFP- N_{193} -TRPC1 (Fig. 4A, 2nd image) that includes all three ankyrin-like repeats, resulted in cytosolic co-localization (Fig. 4A, 3rd image) and robust FRET (Fig. 4A, 4th image). Average FRET values (Fig. 4D) were even stronger than those of the full-length TRPC1-TRPV6 complex (Fig. 3F). A dramatically reduced FRET value was calculated for N_{115} -TRPC1 (Fig. 4, B and D) that included only the first two ankyrin-like repeats or N_{49} -TRPC1 (Fig. 4, C and D), lacking all ankyrins, when co-expressed with N_{198} -TRPV6. These experiments demonstrate an intrinsic ability of the ankyrin-like repeat domains of TRPC1 and TRPV6 to heteromize *in vivo*.

N-terminal Fragments of TRPC1 that Contain Ankyrin-like Repeats Suppressed TRPV6 Currents—Next, we determined if the ankyrin-mediated interaction is sufficient to down-regulate TRPV6 currents. Co-expression of N_{193} -TRPC1 and TRPV6 indeed significantly reduced TRPV6 currents (Fig. 5A), as

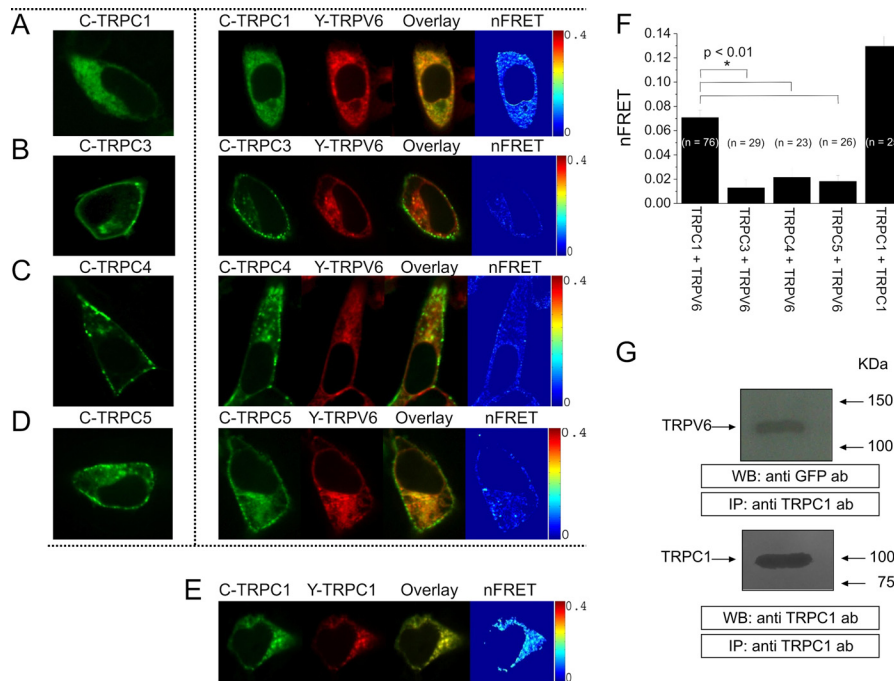


FIGURE 3. Co-localization and interaction of TRPC1 and TRPV6: Localization of a representative CFP-TRPC1-expressing cell (A, E, image 1) as well as for a co-expression of CFP-TRPC1 (A, image 2) with YFP-TRPV6 (A, image 3), their overlay (A, image 4) and calculated FRET values (A, image 5) are presented. Similar image series are shown for co-expression of CFP-TRPC3 (B), CFP-TRPC4 (C), or CFP-TRPC5 (D) with YFP-TRPV6 as well as CFP-/YFP-TRPC1 (E). The FRET values depicted in F were calculated from the averages of whole cell areas determined from the respective number of cells showing significantly increased FRET values and co-localization of cells co-expressing either CFP-TRPC1 and YFP-TRPV6 (FRET = 0.07 ± 0.01) and CFP-/YFP-TRPC1 (FRET = 0.13 ± 0.01) in contrast to CFP-TRPC3 and YFP-TRPV6 (FRET = 0.01 ± 0.01), CFP-TRPC4 and YFP-TRPV6 (FRET = 0.02 ± 0.01) or CFP-TRPC5 and YFP-TRPV6 (FRET = 0.02 ± 0.01). G, HEK293 cells, co-expressing YFP-TRPV6 and TRPC1 were lysed and immunoprecipitated (IP) with anti-TRPC1 antibody followed by Western blotting using anti-GFP antibody (top). Membranes were reprobed with the immunoprecipitating antibody (bottom). Positions of molecular mass markers are shown on the right. These results are representative of four independent experiments. Values are mean \pm S.E. of four independent experiments. *, $p < 0.05$ versus resting cells.

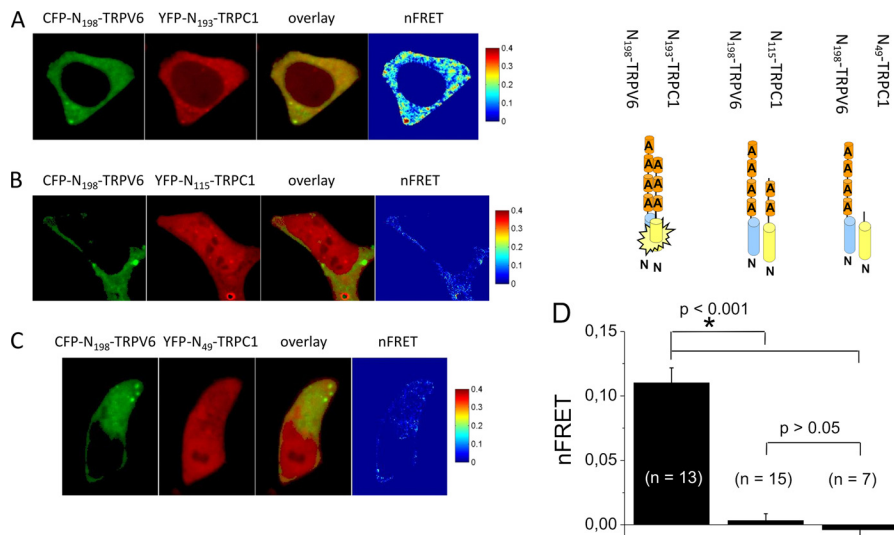


FIGURE 4. In vivo interaction of the ankyrin-like repeat domains of TRPC1 and TRPV6: Localization of CFP-N₁₉₈-TRPV6 (A, image 1) and YFP-N₁₉₃-TRPC1 (A, image 2), overlay (A, image 3), and calculated FRET values (A, image 4) are presented for a representative HEK293 cell. Similar image series are shown for co-expression of CFP-N₁₉₈-TRPV6 with YFP-N₁₁₅-TRPC1 (B) or YFP-N₄₉-TRPC1 (C). Average FRET values depicted in D showed significantly increased FRET values and good co-localization of cells co-expressing CFP-N₁₉₈-TRPV6 and YFP-N₁₉₃-TRPC1 (FRET = 0.11 ± 0.01) in contrast to CFP-N₁₉₈-TRPV6 and YFP-N₁₁₅-TRPC1 (FRET = 0.00 ± 0.01) or CFP-N₁₉₈-TRPV6 and YFP-N₄₉-TRPC1 (FRET = 0.00 ± 0.01).

shown in the time courses and statistical analysis on inward currents immediately after whole cell break-in. In contrast, currents of cells co-expressing TRPV6 with Δ N₁₉₃-TRPC1, a TRPC1 mutant lacking the ankyrin-like repeat domain, (Fig. 5B) were not significantly different to those recorded from TRPV6-expressing HEK293 cells. Additionally, N₁₁₅-TRPC1 (2

ankyrin-like repeats; Fig. 5C) or N₄₉-TRPC1 (no ankyrin-like repeats; Fig. 5D) failed to significantly reduce TRPV6 currents, in comparison to control TRPV6. None of the TRPC1 fragments affected the inward rectifying current-voltage relationship of TRPV6 (Fig. 5E). These experiments suggest that the ankyrin-like repeats mediate an important role in the interac-

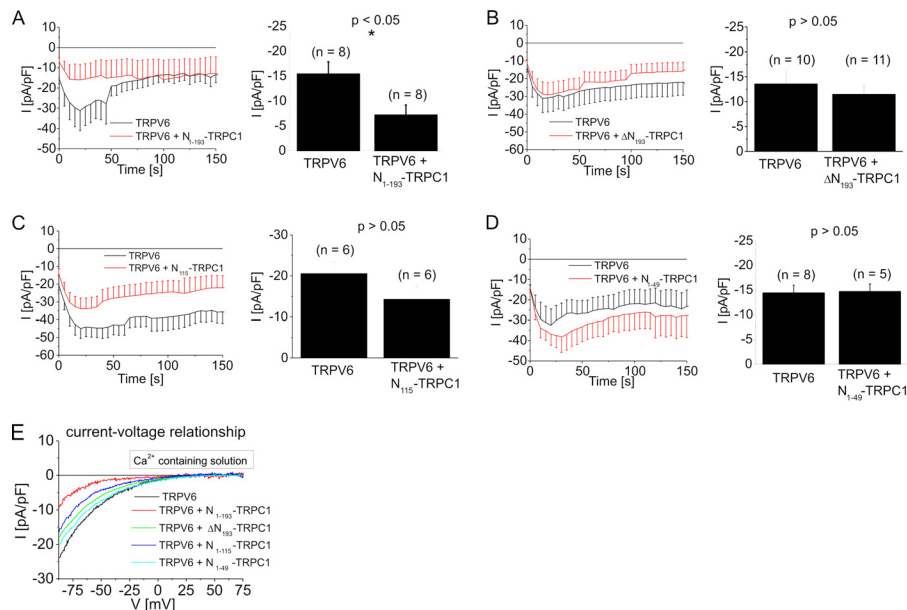


FIGURE 5. Dominant negative effect of a TRPC1 fragment including the whole ankyrin domain on TRPV6: Time course and statistics on initial inward currents showed that co-expression of N₁₉₃-TRPC1 fragment and TRPV6 (A) yielded significantly down-regulated currents in comparison to TRPV6-expressing cells. In contrast neither ΔN₁₉₃-TRPC1 (B), TRPC1 lacking all N-terminal ankyrin-like repeats, nor N₁₁₅-TRPC1 (C) or N₄₉-TRPC1 (D) were able to suppress co-expressed TRPV6 currents in HEK293 cells. Representative current-voltage relationships (E) are shown for experiments shown in A–D.

tion of TRPC1 and TRPV6, thereby reducing the amount of plasma membrane-targeted TRPV6.

DISCUSSION

In the present study we identified a specific interaction between TRPC1 and TRPV6 by confocal FRET microscopy and co-immunoprecipitation in HEK293 cells. Heterologous co-expression of TRPC1 and TRPV6 resulted in a strongly diminished plasma membrane expression of TRPV6 corresponding with significantly down-regulated TRPV6-mediated Ca^{2+} entry/currents. The current-voltage relationship of the remaining TRPC1/TRPV6 currents was identical to that of TRPV6 suggesting that this interaction retains TRPV6 in intracellular compartments.

In the small intestine, kidney and bone TRPV6 channel is required for Ca^{2+} influx (49). To tightly control the cytosolic Ca^{2+} levels, TRPV6 expression is adjusted by caliotropic hormones, pH and Ca^{2+} -dependent mechanism (50). In addition, various channel-associated proteins, including S100A10, calmodulin, 80K-H, or Rab11a (50) can regulate TRPV6 activity. Hence, the here discovered TRPC1 and TRPV6 interaction increases the variety of regulatory proteins for Ca^{2+} uptake.

Our biotinylation experiments and confocal images suggested an intracellular retention of TRPV6 by TRPC1 co-expression. Moreover confocal FRET microscopy revealed that an interaction of TRPC1 and TRPV6 already occurred in intracellular compartments. TRPC1 *per se* remained in intracellular compartments in HEK293 cells in line with Ref. 8, 48, hence interaction with TRPV6 interferes with the plasma membrane targeting of the latter. The remaining currents of TRPC1 and TRPV6-co-expressing cells resembled those of TRPV6, suggesting that this current is formed by a fraction of remaining homomeric TRPV6 channels.

Our experiments did not favor a heteromeric channel of TRPC1 and TRPV6 resulting in a decreased channel activity.

TRPC1 proteins can clearly contribute to a functional pore in homomeric (47) and heteromeric (9, 13, 14) TRPC channels. However, heteromeric TRPC channels, including TRPC1 with any other TRPC isoform yielded unique permeation properties that could be distinguished from their respective homomeric TRPC channels. Co-expression of TRPC1 and TRPV6 retained the current-voltage profile in a Ca^{2+} and Na^{+} divalent free solution. Hence it is more likely that in a co-expression of TRPC1 and TRPV6, only a remaining TRPV6 channel fraction is targeted to the plasma membrane.

In contrast to TRPC1, co-localization of TRPC3, TRPC4 or TRPC5 with TRPV6 in living HEK293 cells was weak, failed to affect the partial plasma membrane targeting of TRPV6 and yielded very small FRET values. The interaction of TRPC1 and TRPV6 was intrinsically mediated by their N-terminal ankyrin-like repeats. Cytosolic TRPC1/V6 ankyrin segments were sufficient to associate *in vivo* as monitored by confocal FRET microscopy. Consistently, electrophysiological measurements revealed that the ankyrin-like repeats of TRPC1 significantly down-regulated TRPV6 currents, while a TRPC1 mutant lacking these repeats failed to exert a dominant negative effect on TRPV6.

The N-terminal ankyrin-like repeat domain is present in the seven members of canonical TRPCs, the six vanilloid TRPV and TRPA1. Indeed mutations, splice variants or deletion of single ankyrin-like repeats in TRPC5, TRPV5 and TRPV6 disrupted their ability to multimerize (31–34). However, analytical size exclusion chromatography as well as crystallization yielded a monomeric TRPV6 ankyrin-like repeat in solution (19). These *in vitro* studies in comparison to our and other *in vivo* experiments can be reconciled if endogenous factors may facilitate the ankyrin-like repeat assembly.

An important function of TRPV6 is the Ca^{2+} uptake in the small intestine, kidney, and bone (51). Yet a physiological role

and the localization of TRPC1 in these tissues are hampered as long as TRPV6 currents are not functionally identified in native cell systems. Further studies are needed to analyze the physiological consequence of this intrinsic TRPC1-TRPV6 interaction in the small intestine, kidney, and bone.

Acknowledgment—We thank S. Buchegger for excellent technical assistance.

REFERENCES

- Venkatachalam, K., and Montell, C. (2007) TRP channels. *Annu. Rev. Biochem.* **76**, 387–417
- Wu, L. J., Sweet, T. B., and Clapham, D. E. (2010) International Union of Basic and Clinical Pharmacology. LXXVI. Current progress in the mammalian TRP ion channel family. *Pharmacol. Rev.* **62**, 381–404
- Hoenderop, J. G., Voets, T., Hoefs, S., Weidema, F., Prenen, J., Nilius, B., and Bindels, R. J. (2003) Homo- and heterotetrameric architecture of the epithelial Ca^{2+} channels TRPV5 and TRPV6. *EMBO J.* **22**, 776–785
- Kedei, N., Szabo, T., Lile, J. D., Treanor, J. J., Olah, Z., Iadarola, M. J., and Blumberg, P. M. (2001) Analysis of the native quaternary structure of vanilloid receptor 1. *J. Biol. Chem.* **276**, 28613–28619
- Cheng, W., Sun, C., and Zheng, J. (2010) Heteromerization of TRP channel subunits: extending functional diversity. *Protein Cell* **1**, 802–810
- Schindl, R., and Romanin, C. (2007) Assembly domains in TRP channels. *Biochem. Soc. Trans.* **35**, 84–85
- Freichel, M., Vennekens, R., Olausson, J., Stolz, S., Philipp, S. E., Weissgerber, P., and Flockerzi, V. (2005) Functional role of TRPC proteins in native systems: implications from knockout and knock-down studies. *J. Physiol.* **567**, 59–66
- Beech, D. J., Xu, S. Z., McHugh, D., and Flemming, R. (2003) TRPC1 store-operated cationic channel subunit. *Cell Calcium* **33**, 433–440
- Strübing, C., Krapivinsky, G., Krapivinsky, L., and Clapham, D. E. (2001) TRPC1 and TRPC5 form a novel cation channel in mammalian brain. *Neuron* **29**, 645–655
- Hofmann, T., Schaefer, M., Schultz, G., and Gudermann, T. (2002) Subunit composition of mammalian transient receptor potential channels in living cells. *Proc. Natl. Acad. Sci. U.S.A.* **99**, 7461–7466
- Jardin, I., Lopez, J. J., Salido, G. M., and Rosado, J. A. (2008) Orai1 mediates the interaction between STIM1 and hTRPC1 and regulates the mode of activation of hTRPC1-forming Ca^{2+} channels. *J. Biol. Chem.* **283**, 25296–25304
- Liu, X., Bandyopadhyay, B. C., Singh, B. B., Groschner, K., and Ambudkar, I. S. (2005) Molecular analysis of a store-operated and 2-acetyl-sn-glycerol-sensitive non-selective cation channel. Heteromeric assembly of TRPC1-TRPC3. *J. Biol. Chem.* **280**, 21600–21606
- Strübing, C., Krapivinsky, G., Krapivinsky, L., and Clapham, D. E. (2003) Formation of novel TRPC channels by complex subunit interactions in embryonic brain. *J. Biol. Chem.* **278**, 39014–39019
- Storch, U., Forst, A. L., Philipp, M., Gudermann, T., and Mederos y Schnitzler, M. (2012) Transient receptor potential channel 1 (TRPC1) reduces calcium permeability in heteromeric channel complexes. *J. Biol. Chem.* **287**, 3530–3540
- Tsiokas, L., Arnould, T., Zhu, C., Kim, E., Walz, G., and Sukhatme, V. P. (1999) Specific association of the gene product of PKD2 with the TRPC1 channel. *Proc. Natl. Acad. Sci. U.S.A.* **96**, 3934–3939
- Bai, C. X., Giamarchi, A., Rodat-Despoix, L., Padilla, F., Downs, T., Tsiokas, L., and Delmas, P. (2008) Formation of a new receptor-operated channel by heteromeric assembly of TRPP2 and TRPC1 subunits. *EMBO Rep.* **9**, 472–479
- Kobori, T., Smith, G. D., Sandford, R., and Edwardson, J. M. (2009) The transient receptor potential channels TRPP2 and TRPC1 form a heterotetramer with a 2:2 stoichiometry and an alternating subunit arrangement. *J. Biol. Chem.* **284**, 35507–35513
- Hellwig, N., Albrecht, N., Harteneck, C., Schultz, G., and Schaefer, M. (2005) Homo- and heteromeric assembly of TRPV channel subunits. *J. Cell Sci.* **118**, 917–928
- Phelps, C. B., Huang, R. J., Lishko, P. V., Wang, R. R., and Gaudet, R. (2008) Structural analyses of the ankyrin repeat domain of TRPV6 and related TRPV ion channels. *Biochemistry* **47**, 2476–2484
- Cheng, W., Yang, F., Takanishi, C. L., and Zheng, J. (2007) Thermosensitive TRPV channel subunits coassemble into heteromeric channels with intermediate conductance and gating properties. *J. Gen. Physiol.* **129**, 191–207
- Ma, X., Qiu, S., Luo, J., Ma, Y., Ngai, C. Y., Shen, B., Wong, C. O., Huang, Y., and Yao, X. (2010) Functional role of vanilloid transient receptor potential 4-canonical transient receptor potential 1 complex in flow-induced Ca^{2+} influx. *Arterioscler. Thromb. Vasc. Biol.* **30**, 851–858
- Alessandri-Haber, N., Dina, O. A., Chen, X., and Levine, J. D. (2009) TRPC1 and TRPC6 channels cooperate with TRPV4 to mediate mechanical hyperalgesia and nociceptor sensitization. *J. Neurosci.* **29**, 6217–6228
- Vanden Abeele, F., Shuba, Y., Roudbaraki, M., Lemonnier, L., Vanoverberghe, K., Mariot, P., Skryma, R., and Prevarskaya, N. (2003) Store-operated Ca^{2+} channels in prostate cancer epithelial cells: function, regulation, and role in carcinogenesis. *Cell Calcium* **33**, 357–373
- Engelke, M., Friedrich, O., Budde, P., Schäfer, C., Niemann, U., Zitt, C., Jüngling, E., Rocks, O., Lückhoff, A., and Frey, J. (2002) Structural domains required for channel function of the mouse transient receptor potential protein homologue TRP1 β . *FEBS Lett.* **523**, 193–199
- Mei, Z. Z., Xia, R., Beech, D. J., and Jiang, L. H. (2006) Intracellular coiled-coil domain engaged in subunit interaction and assembly of melastatin-related transient receptor potential channel 2. *J. Biol. Chem.* **281**, 38748–38756
- Mei, Z. Z., and Jiang, L. H. (2009) Requirement for the N-terminal coiled-coil domain for expression and function, but not subunit interaction, of the ADPR-activated TRPM2 channel. *J. Membr. Biol.* **230**, 93–99
- Tsuruda, P. R., Julius, D., and Minor, D. L., Jr. (2006) Coiled coils direct assembly of a cold-activated TRP channel. *Neuron* **51**, 201–212
- Hanaoka, K., Qian, F., Boletta, A., Bhunia, A. K., Piontek, K., Tsiokas, L., Sukhatme, V. P., Guggino, W. B., and Germino, G. G. (2000) Co-assembly of polycystin-1 and -2 produces unique cation-permeable currents. *Nature* **408**, 990–994
- Yu, F., Sun, L., and Machaca, K. (2009) Orai1 internalization and STIM1 clustering inhibition modulate SOCE inactivation during meiosis. *Proc. Natl. Acad. Sci. U.S.A.* **106**, 17401–17406
- Giamarchi, A., Feng, S., Rodat-Despoix, L., Xu, Y., Bubenshchikova, E., Newby, L. J., Hao, J., Gaudioso, C., Crest, M., Lupas, A. N., Honoré, E., Williamson, M. P., Obara, T., Ong, A. C., and Delmas, P. (2010) A polycystin-2 (TRPP2) dimerization domain essential for the function of heteromeric polycystin complexes. *EMBO J.* **29**, 1176–1191
- Schindl, R., Frischauf, I., Kahr, H., Fritsch, R., Krenn, M., Derndl, A., Vales, E., Muik, M., Derler, I., Groschner, K., and Romanin, C. (2008) The first ankyrin-like repeat is the minimum indispensable key structure for functional assembly of homo- and heteromeric TRPC4/TRPC5 channels. *Cell Calcium* **43**, 260–269
- Arniges, M., Fernández-Fernández, J. M., Albrecht, N., Schaefer, M., and Valverde, M. A. (2006) Human TRPV4 channel splice variants revealed a key role of ankyrin domains in multimerization and trafficking. *J. Biol. Chem.* **281**, 1580–1586
- Erlr, I., Hirnet, D., Wissenbach, U., Flockerzi, V., and Niemeyer, B. A. (2004) Ca^{2+} -selective transient receptor potential V channel architecture and function require a specific ankyrin repeat. *J. Biol. Chem.* **279**, 34456–34463
- Chang, Q., Gyftogianni, E., van de Graaf, S. F., Hoefs, S., Weidema, F. A., Bindels, R. J., and Hoenderop, J. G. (2004) Molecular determinants in TRPV5 channel assembly. *J. Biol. Chem.* **279**, 54304–54311
- Kahr, H., Schindl, R., Fritsch, R., Heinze, B., Hofbauer, M., Hack, M. E., Mörtelmaier, M. A., Groschner, K., Peng, J. B., Takanaga, H., Hediger, M. A., and Romanin, C. (2004) CaT1 knock-down strategies fail to affect CRAC channels in mucosal-type mast cells. *J. Physiol.* **557**, 121–132
- Lepage, P. K., and Boulay, G. (2007) Molecular determinants of TRP channel assembly. *Biochem. Soc. Trans.* **35**, 81–83
- Derler, I., Hofbauer, M., Kahr, H., Fritsch, R., Muik, M., Kepplinger, K., Hack, M. E., Moritz, S., Schindl, R., Groschner, K., and Romanin, C. (2006)

- Dynamic but not constitutive association of calmodulin with rat TRPV6 channels enables fine tuning of Ca^{2+} -dependent inactivation. *J. Physiol.* **577**, 31–44
38. Hamill, O. P., Marty, A., Neher, E., Sakmann, B., and Sigworth, F. J. (1981) Improved patch-clamp techniques for high-resolution current recording from cells and cell-free membrane patches. *Pflügers Arch.* **391**, 85–100
 39. de Groot, T., van der Hagen, E. A., Verkaart, S., te Boekhorst, V. A., Bindels, R. J., and Hoenderop, J. G. (2011) Role of the transient receptor potential vanilloid 5 (TRPV5) protein N terminus in channel activity, tetramerization, and trafficking. *J. Biol. Chem.* **286**, 32132–32139
 40. Jardin, I., Gómez, L. J., Salido, G. M., and Rosado, J. A. (2009) Dynamic interaction of hTRPC6 with the Orai1-STIM1 complex or hTRPC3 mediates its role in capacitative or non-capacitative $\text{Ca}(2+)$ entry pathways. *Biochem. J.* **420**, 267–276
 41. Wes, P. D., Chevesich, J., Jeromin, A., Rosenberg, C., Stetten, G., and Montell, C. (1995) TRPC1, a human homolog of a *Drosophila* store-operated channel. *Proc. Natl. Acad. Sci. U.S.A.* **92**, 9652–9656
 42. Rosado, J. A., Brownlow, S. L., and Sage, S. O. (2002) Endogenously expressed Trp1 is involved in store-mediated Ca^{2+} entry by conformational coupling in human platelets. *J. Biol. Chem.* **277**, 42157–42163
 43. Jardín, I., Redondo, P. C., Salido, G. M., and Rosado, J. A. (2008) Phosphatidylinositol 4,5-bisphosphate enhances store-operated calcium entry through hTRPC6 channel in human platelets. *Biochim. Biophys. Acta* **1783**, 84–97
 44. Voets, T., Prenen, J., Fleig, A., Vennekens, R., Watanabe, H., Hoenderop, J. G., Bindels, R. J., Droogmans, G., Penner, R., and Nilius, B. (2001) CaT1 and the calcium release-activated calcium channel manifest distinct pore properties. *J. Biol. Chem.* **276**, 47767–47770
 45. Schindl, R., Kahr, H., Graz, I., Groschner, K., and Romanin, C. (2002) Store depletion-activated CaT1 currents in rat basophilic leukemia mast cells are inhibited by 2-aminoethoxydiphenyl borate. Evidence for a regulatory component that controls activation of both CaT1 and CRAC ($\text{Ca}(2+)$ release-activated $\text{Ca}(2+)$ channel) channels. *J. Biol. Chem.* **277**, 26950–26958
 46. DeHaven, W. I., Jones, B. F., Petranka, J. G., Smyth, J. T., Tomita, T., Bird, G. S., and Putney, J. W., Jr. (2009) TRPC channels function independently of STIM1 and Orai1. *J. Physiol.* **587**, 2275–2298
 47. Huang, G. N., Zeng, W., Kim, J. Y., Yuan, J. P., Han, L., Muallem, S., and Worley, P. F. (2006) STIM1 carboxyl-terminus activates native SOC, I(crac) and TRPC1 channels. *Nat. Cell Biol.* **8**, 1003–1010
 48. Alfonso, S., Benito, O., Alicia, S., Angélica, Z., Patricia, G., Diana, K., Vaca, L., and Luis, V. (2008) Regulation of the cellular localization and function of human transient receptor potential channel 1 by other members of the TRPC family. *Cell Calcium* **43**, 375–387
 49. Nijenhuis, T., Hoenderop, J. G., van der Kemp, A. W., and Bindels, R. J. (2003) Localization and regulation of the epithelial Ca^{2+} channel TRPV6 in the kidney. *J. Am. Soc. Nephrol.* **14**, 2731–2740
 50. Schoeber, J. P., van de Graaf, S. F., Lee, K. P., Wittgen, H. G., Hoenderop, J. G., and Bindels, R. J. (2009) Conditional fast expression and function of multimeric TRPV5 channels using Shield-1. *Am. J. Physiol. Renal Physiol.* **296**, F204–F211
 51. Bianco, S. D., Peng, J. B., Takanaga, H., Suzuki, Y., Crescenzi, A., Kos, C. H., Zhuang, L., Freeman, M. R., Gouveia, C. H., Wu, J., Luo, H., Mauro, T., Brown, E. M., and Hediger, M. A. (2007) Marked disturbance of calcium homeostasis in mice with targeted disruption of the *Trpv6* calcium channel gene. *J. Bone Miner. Res.* **22**, 274–285
 52. Xia, Z., and Liu, Y. (2001) Reliable and global measurement of fluorescence resonance energy transfer using fluorescence microscopes. *Biophys. J.* **81**, 2395–2402



Direct association of the reticulon protein RTN1A with the ryanodine receptor 2 in neurons



Levent Kaya^a, Barbara Meissner^a, Maria Christine Riedl^b, Martin Muik^b, Christoph Schwarzer^c, Francesco Ferraguti^c, Bettina Sarg^d, Herbert Lindner^d, Rüdiger Schweigreiter^a, Hans-Günther Knaus^e, Christoph Romanin^b, Christine E. Bandtlow^{a,*}

^a Division of Neurobiochemistry, Biocenter, Innsbruck Medical University, Innsbruck, Austria

^b Institute of Biophysics, University of Linz, 4040 Linz, Austria

^c Institute of Pharmacology, Innsbruck Medical University, Innsbruck, Austria

^d Division of Clinical Biochemistry, Innsbruck Medical University, Innsbruck, Austria

^e Department for Medical Genetics, Molecular and Clinical Pharmacology, Innsbruck Medical University, Innsbruck, Austria

ARTICLE INFO

Article history:

Received 15 November 2012

Received in revised form 11 February 2013

Accepted 14 February 2013

Available online 27 February 2013

Keywords:

Reticulon

Brain

Protein–protein interaction

Calcium homeostasis

ABSTRACT

RTN1A is a reticulon protein with predominant localization in the endoplasmic reticulum (ER). It was previously shown that RTN1A is expressed in neurons of the mammalian central nervous system but functional information remains sparse. To elucidate the neuronal function of RTN1A, we chose to focus our investigation on identifying possible novel binding partners specifically interacting with the unique N-terminus of RTN1A. Using a nonbiased approach involving GST pull-downs and MS analysis, we identified the intracellular calcium release channel ryanodine receptor 2 (RyR2) as a direct binding partner of RTN1A. The RyR2 binding site was localized to a highly conserved 150-amino acid residue region. RTN1A displays high preference for RyR2 binding *in vitro* and *in vivo* and both proteins colocalize in hippocampal neurons and Purkinje cells. Moreover, we demonstrate the precise subcellular localization of RTN1A in Purkinje cells and show that RTN1A inhibits RyR channels in [³H]ryanodine binding studies on brain synaptosomes. In a functional assay, RTN1A significantly reduced RyR2-mediated Ca²⁺ oscillations. Thus, RTN1A and RyR2 might act as functional partners in the regulation of cytosolic Ca²⁺ dynamics in neurons.

© 2013 Elsevier B.V. All rights reserved.

1. Introduction

Reticulons (RTNs) are a highly conserved eukaryotic protein family residing in the endomembrane system. In mammals 4 reticulon genes are known (RTN1–RTN4), which encode various protein isoforms [1,2]. Reticulons share little sequence homology except for the reticulon homology domain (RHD), a C-terminally located domain of ~200 amino acids composed of two short hairpin domains separated by a highly conserved loop-region. While their physiological relevance is still poorly understood, recent findings suggest that reticulons partition into tubules of the ER *via* their RHD and act as membrane curvature proteins responsible for shaping ER-tubules and ER-sheet edges. Moreover, by interacting with other hairpin loop-containing proteins, such as REEP1, atlastin-1 and M1 spastin, RTNs appear to participate in a network of ER morphogens [3].

Abbreviations: RTN, reticulon protein; ER, endoplasmic reticulum; RyR, ryanodine receptor; RHD, reticulon homology domain; CICR, calcium induced calcium release; IPTG, isopropyl-β-D-thiogalactopyranoside; PB, phosphate buffer; DAB, 3,3'-diaminobenzidine tetrahydrochloride dihydrate; CA, cornu ammonis

* Corresponding author at: Innsbruck Medical University, Biocenter, Division of Neurobiochemistry, Innrain 80/82, A-6020 Innsbruck, Austria. Tel.: +43 512 900370280.

E-mail address: christine.bandtlow@i-med.ac.at (C.E. Bandtlow).

In the mammalian nervous system the role of RTNs remains unclear, though a variety of functions have been postulated for specific RTNs, including vesicular and membrane trafficking [4], neuroendocrine secretion [5], hereditary spastic paraplegia [6], inhibition of enzymatic activity [7], apoptosis [8,9], and regulation of axonal growth and plasticity [10]. RTN1A, the longest isoform of the *rtn1* gene, was the first RTN protein described to be widely expressed in the developing and mature brain [11,12]. As opposed to the well studied Nogo/RTN4 proteins, RTN1A in the adult brain is located exclusively in the neurons but not in the glial cells [11]. RTN1C was shown to interact with Spastin [13], Sec61 [14] and AP-2 [15] suggesting that it might be involved in regulating intracellular vesicle transport, although a firm conclusive answer is missing. While these interactions are mediated *via* the C-terminal RHD, common to all RTNs, little is known about the variable N-terminal regions, specific for each RTN isoform. Assuming that the N-terminal domains are specialized for distinct functions by associating with different target proteins, we have set out to search for binding proteins that specifically bind to the N-terminal domain of neuronal RTN1A. Using a GST pull-down and co-immunoprecipitation strategy, we demonstrate for the first time that in rodent brain RTN1A forms a stable association with the ryanodine receptor RyR2, but not the closely related family member RyR1 and that this interaction was found to modify RyR2 channel function, as judged

from ryanodine binding experiments and single cell calcium imaging analysis. Our observations suggest that RyR2 channels may form stable interactions with RTN1A, leading to a reduction of RyR2-mediated Ca^{2+} oscillations.

RyR2 is a member of the intracellular ryanodine receptor Ca^{2+} -release channels (RyRs) localized in the ER. Three RyR isoforms have been purified in mammals (RyR1, RyR2 and RyR3) that coordinate many calcium signaling events such as muscle contraction and neurotransmission. RyR1 is predominant in the skeletal muscle and in the cerebellar Purkinje neurons. RyR2 is mainly expressed in the cardiac muscles and is the predominant subtype in the brain, while the brain specific RyR3 is weakly expressed throughout the brain [16]. RyRs contribute to the regulation of the cytosolic calcium dynamics, by release of calcium from intracellular Ca^{2+} stores as a consequence of Ca^{2+} influx through voltage- or ligand-gated Ca^{2+} channels, the so-called Ca^{2+} -induced Ca^{2+} release (CICR) [17]. CICR from the intracellular calcium stores that amplifies further the Ca^{2+} signal is thought to be involved in more profound and lasting changes in neurons, regulating neurotransmitter release, synaptic plasticity, gene expression, and signal transduction to the nucleus [18]. Recent evidence supports a role of RyR2-mediated control of calcium homeostasis in stress-induced defects in cognitive function and postsynaptic plasticity in hippocampal neurons [19]. Moreover, leaky neuronal RyR2 channels are also implicated in neurodegeneration, including Alzheimer's disease and aging.

2. Materials and methods

2.1. Plasmid constructs

pcDNA3.1-RyR2 containing full length mouse cardiac RyR2 cDNA, GenBank™ accession no. NP_076357.2 was kindly provided by Wayne Chen (University of Calgary, Calgary; [20]), and a pCI-neo vector (Promega) with a full length rabbit skeletal RyR1 insert (GenBank accession no. X15209) was kindly provided by P. D. Allen (Brigham and Women's Hospital, Boston; [21]). GST-RTN1₅₂₃ (aa 1–523; 5'-CTGGG ATCCATGGCCGCA CCGCCGGATCTGCAAG-3' forward and 5'-CAGCCCG GTCAATGATGATGATGATGAT GACCACGCTGAGTATCGGGTCAGGTTCC ACAG-3' reverse and GST-HHD (aa 376–523; 5'-AATGGATCCCCAGTG GGCCAGGCGGCCGAC-3' forward) and 5'-CAGCCCGGGTC AATGATGAT GATGATGATGACACCGCTGAGTATCGGGTCAGGTTCCACAG-3' reverse) were generated by PCR amplification using rat full length RTN1A as a template [2], and cloned into pGEX-6P (Amersham Pharmacia). GST-LNT1 (aa 1–375, 5'-CTGGGATCCATGG CCGCACC GCCGATCTGCA AG-3' forward and 5'-TCAATGATGATGATGATGATGACTGGCCTTGA CTCTCGGTG-3' reverse) was generated by PCR amplification using GST-RTN1₅₂₃ as a template and cloned into pGEX-6P. GST-NiR was described previously [22]. mCherry-RTN1₅₂₃ (5'-ACGAAGCTTCGCC ACCATGGTGTGCGCCGACCGCCGGATCTG CAAG-3' forward and 5'-TGCGGATCCGCGCTGAGTATCGGGTCAGGTTCCACAG-3' reverse) was generated via PCR amplification using rat RTN1A-eGFP as template and cloned into mCherryN (Clontech). Restriction sites used for sub-cloning are underlined. All constructs were verified by sequencing analysis (MWG, Ebersberg, Germany).

2.2. Expression and purification of recombinant GST fusion proteins

Recombinant protein expression of transformed *E. coli* (BL21(DE3)) cells was induced with 1 mM IPTG (isopropyl-β-D-thiogalactopyranoside) for 4 h at 20 °C. Cells were then harvested by centrifugation and 1 g of bacterial pellet was resuspended in 4 mL of lysis buffer (50 mM sodium phosphate buffer, pH 7.4, 150 mM NaCl, 0.1% Triton X-100, 0.05% Tween-20) supplemented with Lysozyme (1 mg/mL), Protease Inhibitor Cocktail (Roche) and DNase (0.1 mg/mL). The lysate was sonicated 5 times for 15 s each (on ice) and was then cleared by centrifugation at 15,000 ×g for 15 min at 4 °C. For dual purification, the precleared supernatant was first run over a GSTrap Affinity Column

(GE Healthcare) attached to a chromatography apparatus (ÅKTA prime, GE Healthcare). Bound proteins were eluted with 50 mM reduced glutathione in TBS, pH 8.0 containing 0.1 mM β-mercaptoethanol. GST-purified eluate was collected, and subjected on a HisTrap Affinity Column (GE Healthcare). Bound protein was eluted with wash buffer (50 mM sodium phosphate buffer at pH 7.4, 0.1% Triton X-100, 0.05% Tween-20, 150 mM NaCl) containing imidazole at a final concentration of 500 mM. Samples of the eluted tagged purified recombinant proteins were analyzed by SDS-PAGE and Silver Staining [23,24] and immobilized to Glutathione Sepharose Beads (GE Healthcare) for 2 h at 4 °C.

2.3. GST pull-down assays

For *in vitro* GST pull-down assays, whole adult mouse brains (BL6, 10 weeks) were homogenized by 50 strokes of a dounce homogenizer in ice-cold lysis buffer (50 mM HEPES pH 7.4, 25 mM NaCl, 10 mM EDTA, 1% Triton X-100) and complete protease and phosphatase inhibitor cocktail (Roche; 1:10; w/v). The homogenate was centrifuged for 30 min at 20,000 ×g, 4 °C and supernatant was passed through a 0.45 μm filter (BD Biosciences). 40 mg of total brain extract (10 mg/mL) was precleared by incubation for 2 h at 4 °C with 0.20 mL of glutathione agarose followed by centrifugation (500 ×g for 2 min) and assayed for protein content. 2.5 mg of the recovered brain extract (2.5 mg/mL) was incubated overnight at 4 °C with indicated concentrations of recombinant GST-fusion proteins immobilized to Glutathione Sepharose Beads (GE Healthcare). GST or Glutathione agarose (0.2 mL) served as controls. Agarose beads were washed five times in lysis buffer at 4 °C and resuspended in Laemmli sample buffer. Samples were separated by 12.5% SDS-PAGE, and analyzed by silver staining or immunoblotting using standard procedures.

2.4. MS analysis

For MS analysis, silver stained protein bands were cut out and subjected to in-gel digestion as published previously [25]. Protein digests were analyzed using an UltiMate 3000 nano-HPLC system (Dionex, Germering, Germany) coupled to an LTQ Orbitrap XL mass spectrometer (ThermoScientific, Bremen, Germany) equipped with a nanospray ionization source. A homemade fritless fused silica microcapillary column (75 μm i.d. × 280 μm o.d.) packed with 10 cm of 3 μm reverse-phase C₁₈ material (Reprosil) was used. The gradient (solvent A: 0.1% formic acid; solvent B: 0.1% formic acid in 85% acetonitrile) started at 4% B. The concentration of solvent B was increased linearly from 4% to 50% during 50 min and from 50% to 100% during 5 min. A flowrate of 250 nL/min was applied. Protein identification was performed using the Mascot search engine and the NCBI nr database (mus) accepting variable modifications, carbamidomethyl (C), oxidation (M). Specific cleavage sites for trypsin (KR) were selected with two missed cleavage sites allowed. Peptide tolerance was ± 10 ppm and MS/MS tolerance was ± 1 Da. Peptides with a Mascot score below 30 were skipped. Only best matches were considered.

2.5. Co-immunoprecipitation and immunoblotting

Total brain extract was prepared from adult Sprague–Dawley cerebella in a manner similar to the GST pull-down experiments. 1 mg of cleared lysate (4 mg/mL) was then incubated for 1 h at 4 °C with 5 μg of either mouse anti-RyR2 (Clone c3-33, Pierce), mouse anti-RTN1A (MON162; MuBio, Netherlands), mouse anti-RTN4A (clone 11C7; 22), rabbit anti-RTN1A [2], rabbit anti-RTN4 [22] or rabbit IgG (Sigma). 25 μL of Protein G Dynabeads (Invitrogen) were then added for 1 h and rotated at 4 °C. Beads were washed five times in lysis buffer at 4 °C and were removed from the supernatant using Dynal Magnetic Particle concentrators (Invitrogen). Beads were boiled in Laemmli sample buffer and samples were loaded on 6% SDS-PAGE gels and blotted onto PVDF membranes (GE Healthcare). After staining with Ponceau S

(Sigma-Aldrich) to visualize proteins, membranes were blocked in 5% Skim-Milk (Merck) in TBS-Tween 20 (TBS-T; 10 mM Tris-base, 150 mM NaCl, and 0.2% Tween 20, pH 8.0) for 2 h at RT. Wherever feasible, the PVDF membranes were probed with antibodies different from those used for immunoprecipitation to maximize the specificity of the immunoreactive product obtained. For RTN1A in particular, we used either of two antibodies highly specific for RTN1A: a rabbit antibody specific for the cytoplasmic domain of RTN1A (1:100,000; [2]) and a monoclonal one raised against amino acids 338–422 of RTN1A (MON162; 1:1000; MuBio, Netherlands). RyR2 was identified with a mouse antibody recognizing all RyR isoforms (1:1000; Pierce), RyR1 with rabbit anti-RyR1 (1:1000; Alomone Labs, Israel), IP3R1 with rabbit anti-IP3R1 (1:4000; Alomone Labs, Israel) and RTN4A with either rabbit or mouse anti-RTN4A [22]. Primary antibody incubation was performed at RT for 2 h followed by several washing steps in TBST-T. Antibody binding to proteins was detected using secondary antibody conjugated to horseradish peroxidase (1:20,000; Thermo Scientific) and visualized by enzyme-linked chemiluminescence using ECL Detection Kit (Amersham), and a Typhoon Scanner Device (Amersham Biosciences).

2.6. HEK293 cell culture and transfection

HEK293 cells were maintained in Dulbecco's modified Eagle's Medium-High Glucose as previously described and transfected with 2–10 µg mouse RyR2 or rabbit RyR1 cDNAs with or without 0.2–1 µg rat RTN1A-myc, RTN4A-myc, RTN1₅₂₃-mCherry or mCherry cDNAs using Ca²⁺ phosphate precipitation [26]. Cells were either lysed 40 h post-transfection and processed for immunoprecipitation as described above or fixed in 4% paraformaldehyde for 15 min, permeabilized in 0.1% Triton-X100 in PBS for 20 min and immunostained using mouse monoclonal antibodies against RyR2 (1:1000; Clone c3-33, Pierce), or RyR1 (1:500; Alomone Labs, Israel), followed by subsequent detection using secondary antibodies conjugated to Alexa488 (1:1000; Invitrogen). Single cells transfected with untagged RyR1 or RyR2 were double stained with rabbit anti-calreticulin (1:500; Abcam) and mouse pan-RyR antibody (1:1000; Pierce). Images were captured using a Leica SP5 microscope and a Leica PL APO 63×/1.4 oil-immersion lens. Quantification of colocalization depicted is an average of 10 independent cells per group. Colocalization and quantification were performed using Pearson's coefficient of colocalization of red and green fluorescent signals captured of the same microscopy field, using the LAS AF software (Leica, Mannheim, Germany).

2.7. Ca²⁺-imaging

Transfection of HEK cells [27] was performed using TransFectin (Biorad, Germany) with the corresponding plasmids, i.e. 2 µg RyR2, 0.2 µg mcherry or 0.3 µg of either mcherry-RTN1A or EGFP-RTN4A. Measurements were carried out 24 to 48 h following transfection. Employing Fura-2 microscopy, transfected HEK293 cells grown on coverslips for 1–2 days were loaded with Fura-2/AM (1 µM) for 30 min at room temperature in an extracellular, nominally Ca²⁺ free solution (0 mM Ca²⁺; 140 NaCl, 5 KCl, 1 MgCl₂, 10 glucose, 10 Hepes, pH 7.4 (NaOH)) and mounted at an inverted Axiovert 100 TV microscope (Zeiss, Germany). Excitation of Fura-2 was performed at 340 nm and 380 nm, and Ca²⁺ measurements are shown as 340/380 ratios of transfected HEK293 cells which were corrected for EGFP crossexcitation in the case of EGFP-RTN4A. To evoke Ca²⁺ oscillations according to [28] the nominally Ca²⁺ free solution was exchanged by a 1 mM Ca²⁺ extracellular solution (140 NaCl, 5 KCl, 1 MgCl₂, 1 CaCl₂, 10 glucose, 10 Hepes, pH 7.4 (NaOH)). The amount of Ca²⁺ released during oscillations over a 450 s time-period was estimated by the cumulative area of the oscillations peaks. Transfected HEK293 cells were identified by their mcherry or EGFP fluorescence and a response to 10 mM caffeine in nominally Ca²⁺-free solution which was taken as an indicator for RyR2 expression.

2.8. Animals, tissue preparation and immunohistochemistry for light and electron microscopy

Adult male Sprague Dawley rats (300–400 g; Dept. Laboratory Animals and Genetics, Medical University Vienna, Vienna, Austria) were used for light and electron microscopy experiments. All experimental protocols were approved by the Austrian Animal Experimentation Ethics Board in compliance with both the European Convention for the Protection of Vertebrate Animals used for Experimental and Other Scientific Purposes (ETS no. 123) and the European Communities Council Directive of 24 November 1986 (86/609/EEC). Every effort was made to minimize the number and suffering of the animals used. Animals were deeply anesthetized by intraperitoneal injection of thiopental (100 mg/kg, i.p.) and perfused transcardially with phosphate buffered saline (PBS; 25 mM, 0.9% NaCl, pH 7.4) followed for 15 min by ice-cold fixative made of 4% w/v paraformaldehyde, for light microscopy experiments, or with the addition of 15% v/v of a saturated solution of picric acid and 0.05% glutaraldehyde immediately before the perfusion for pre-embedding electron microscopy. Brains were then immediately removed from the skull, washed in 0.1 M phosphate buffer (PB) and sliced coronally in 40 or 70 µm thick sections on a vibratome (Leica Microsystems VT1000S, Vienna, Austria). Sections were stored in 0.1 M PB containing 0.05% sodium azide at 6 °C.

Adjacent free floating 40 µm sections were permeabilized in 0.4% Triton X-100 (TBS-T) for 30 min, blocked with 10% normal goat serum in TBS-T, and incubated for 65 h at 4 °C with polyclonal rabbit antibodies directed against RTN1A (1:2000; 2) or RyR 2 (1:2000; [16]). After three consecutive washes in TBS-T, the sections were incubated with HRP-coupled secondary antibody (P0448 goat anti-rabbit 1:500; DAKO, Glostrup, Denmark) in 10% blocking serum/TBS-T for 2.5 h. Immunoreactions were visualized using 3,3'-diaminobenzidine tetrahydrochloride dihydrate (DAB, Sigma-Aldrich, Vienna, Austria). Sections were mounted on glass slides in 60% ethanol and allowed to dry overnight. After dehydration in ethanol and clearing in butyl acetate, they were coverslipped using Eukitt mounting medium. Controls included omission of the primary serum or its substitution by nonimmune rabbit serum, and no specific staining was visible on such preparations. In some experiments, RTN1A antibody solution has been pre-incubated with excess of recombinant RTN1A or RACK protein (10 µg/mL) at 4 °C overnight. Staining was absent in sections pretreated with such a solution (Suppl. Fig. 1). Analysis was performed under a Zeiss AxioPhot microscope equipped with Plan-Neofluar and Plan-Apo objective lenses (Zeiss, Vienna, Austria). Images were acquired with an AxioCam HR (Zeiss) controlled by the Openlab software (version 5.5.0; Improvision, Coventry, UK). For immunohistochemistry, sections for pre-embedding electron microscopy were incubated with the mouse monoclonal RTN1A MON162 antibody (diluted 1:250) and the antigen-antibody complex was visualized either by HRP or by nanogold-silver-enhanced reaction. Sections processed for the HRP reaction were incubated with biotinylated anti-mouse secondary antibodies (diluted 1:100; Vector Laboratories) and then in ABC complex (diluted 1:100; Vector Laboratories) made up in TB overnight at 6 °C. Visualization was carried out with DAB (0.5 mg/mL) using 0.003% H₂O₂ for 3–6 min. For the nanogold-silver-enhanced reaction, sections were incubated with Fab fragment secondary antibodies coupled to nanogold (1.4 nm, Nanoprobes Inc., Stony Brook, NY) and then extensively washed in milliQ water before silver enhancement of the gold particles with the HQ kit (Nanoprobes Inc.) for ~8–10 min. After both reactions, sections were subsequently washed with 0.1 M PB and treated with 2% OsO₄ in 0.1 M PB for 40 min at RT and contrasted with 1% uranyl-acetate in 50% ethanol for 30 min at RT. Sections were dehydrated and transferred into epoxy resin (Durcupan ACM, Sigma-Aldrich, Gillingham, UK) overnight at RT. The following day, the sections were transferred onto greased slides, coverslipped, and incubated for 3 days at 60 °C. Blocks of the cerebellar cortex were cut under a stereomicroscope and re-embedded in epoxy resin. Ultrathin sections (70 nm) were cut using a diamond knife (Diatome, Biel, Switzerland) on an ultramicrotome (Ultracut,

Vienna, Leica), collected on copper slot grids coated with pioloform and analyzed at 80 kV in a Philips CM120 electron microscope (Eindhoven, the Netherlands).

2.9. [^3H]Ryanodine Binding Assay

Preparation of purified rat forebrain synaptosomal membrane vesicles was described previously [29]. Equilibrium [^3H]ryanodine binding was essentially performed as described [30,31]. Briefly, 200 μg vesicles (12.5 $\mu\text{g}/\text{mL}$) were incubated at 0.5 M or 1 M KCl, 25 mM Pipes, pH 7.4 and varying free calcium concentrations, with 10 nM [^3H]ryanodine (American Radiolabeled Chemicals Inc., St. Louis, MO) for 2 h at 37 °C in the presence or absence of 0.1 μM GST-RTN₅₂₃ or 0.1 μM GST as control. Nonspecific binding was determined by measuring [^3H]ryanodine binding in the presence of 10 μM unlabeled ryanodine (Ascent Laboratories, UK). Bound [^3H]ryanodine was separated from free ligand by vacuum filtering through glass fiber filters (Whatman GF/C). Filters were washed 3 times with 5 mL each of ice-cold 10% binding buffer (0.1 M KCl, 2.5 mM Pipes, pH 7.4). Radioactivity was quantified by liquid scintillation counting. Specific binding was calculated as the difference between total and nonspecific binding measured in parallel assays. All binding assays were done in triplicates. Results shown are means \pm S.E.M. for $n = 3$ –4 independent experiments. Statistical significance was evaluated using Student's *t*-test. [Free Ca^{2+} concentrations were calculated using MaxChelator software. (<http://www.stanford.edu/~cpatton/maxc.html>)].

3. Results

3.1. Identification of RyR2 as a binding partner of RTN1A

To better understand the function of neuronal RTN1A, we searched for protein-binding partners using pull-down experiments from mouse brain extracts with a GST-His-tagged fusion protein comprising aa 1–523 of rat RTN1A (GST-RTN₁₅₂₃) (Fig. 1A). Specifically bound proteins were resolved by SDS-PAGE and visualized by Silver staining. One prominent band at high molecular weight was consistently pulled down with varying amounts of the GST-RTN₁₅₂₃ (Fig. 1A, arrow). This band was not seen in control lanes using GST, glutathione beads or GST-NiR, a recombinant fusion protein comprising aa 1–172 of rat reticulon protein NogoA/RTN-4A (Fig. 1A). We excised this band and subjected it to MS analysis, which identified 25 different peptides that belong to the cardiac RyR2, an ER-associated calcium-release channel, expressed in heart and brain (Suppl. Fig. 2; [32]). The association of GST-RTN₁₅₂₃ and RyR2 was confirmed by Western blotting with an antibody specific for RyR2 (Fig. 1B). Two immunoreactive bands larger than 500 kDa, consistent with the size of RyR2, were detected. The higher molecular mass band corresponds most likely to intact RyR2, while the lower band presumably represents a proteolytic degradation fragment of RyR2. The intensity of the RyR2 bands increased proportionally with increasing amounts of GST-RTN₁₅₂₃. Taken together, these results demonstrate that *in vitro* the RTN1A/RyR2 interaction was robust and concentration-dependent as GST-RTN₁₅₂₃ was increased.

3.2. RTN1A associates with RyR2 *in vitro* and *in vivo*

To verify that RTN1A and RyR2 interact in a cellular system, we performed both *in vitro* and *in vivo* co-immunoprecipitation experiments. Full length myc-tagged RTN1A and untagged RyR2 were cotransfected into HEK293 cells, which lack endogenous expression of RTN1A or RyR2. As expected, RyR2 was readily co-immunoprecipitated with RTN1A (Fig. 2A), but not in the control experiments, when RyR2 was co-expressed with RTN4A-myc or if non-immune rabbit IgG was used as the precipitating antibody (Fig. 2A). Expression levels of RTN1A, RTN4A, and RyR2 were comparable between transfections as indicated by immunoblotting a fraction of the immunoprecipitation inputs

(Fig. 2A). This shows that full length RTN1A can associate with RyR2 after heterologous expression in HEK293 cells.

Next we addressed if RyR2 and RTN1A interact under endogenous conditions in brain tissue. Because both RTN1A and RyR2 are expressed in the cerebellum [33,11] we employed reverse co-immunoprecipitation experiments using anti-RTN1A antibodies to precipitate RTN1A from rat cerebellar homogenate. Again, RyR2 was found to co-precipitate robustly with two different RTN1A antibodies. In contrast, RyR2 was not immunoprecipitated with non-immune IgG or two different anti-RTN4A antibodies, indicating the specificity of the co-immunoprecipitation (Fig. 2B,C). When RyR2 was immunoprecipitated using RyR2 specific antibodies, only RTN1A but not RTN4A was robustly precipitated with RyR2, again supporting a specific association of RTN1A and RyR2 (Fig. 2C). Moreover, RTN1A's *in vivo* interaction with RyR2 was isoform specific as it interacts with RyR2, but not with RyR1 (Fig. 2D) or InsP3R1, another ER-associated calcium release channel abundantly expressed in the cerebellum (Supp. Fig. 3; [33,34]). Our immunoblots also indicate that RTN1A associates with RTN4A, as rabbit anti-RTN1A antibodies co-precipitated RTN4A (Fig. 2B, lane 2). Similarly, RTN1A was weakly detected in immunoprecipitates with monoclonal anti-RTN4A antibodies (Fig. 2C, lane 4). This is in line with previous reports, showing that RTNs can form hetero-oligomers *via* their RHD domains [35,36].

Together, the results from these co-immunoprecipitation experiments suggest that RTN1A associates specifically with the RyR2 channel in the brain and possibly forms complexes composed of additional reticulon isoforms.

3.3. RyR2-dependent redistribution of RTN1₅₂₃ in HEK293 cells

As an independent verification of the data, we expressed mCherry-RTN₁₅₂₃, alone or in the presence of the RyR2 receptor in HEK293 cells, and examined the subcellular distribution of the RTN₁₅₂₃ construct. Expression of mCherry-RTN₁₅₂₃ lacking the RHD displayed a diffuse distribution in the cytoplasm (Fig. 3A, a), confirming that the RHD of reticulons plays a role in targeting and stabilization of the proteins in the ER membrane [37,38]. In comparison, immunocytochemical stainings of cells single-transfected with untagged RyR2 or RyR1 revealed a well defined and typical staining pattern of ER targeted proteins with a highly organized web-like distribution throughout the cell (Fig. 3A,b–c).

Double immunofluorescence staining confirmed that both RyR isoform proteins are localized to the ER as evidenced by the strong colocalization of their staining with calreticulin, an endogenous ER marker (Fig. 3B). Interestingly, co-expression of mCherry-RTN₁₅₂₃ with RyR2 resulted in a partial redistribution of RTN₁₅₂₃ from cytosolic to ER location, overlapping with RyR2 in the perinuclear region as well as tubular network (Fig. 3A, d–f). Notably, the redistribution of RTN₁₅₂₃ was specifically dependent on its interaction with RyR2, as RTN₁₅₂₃ maintained a diffuse localization in the cytosol when it was co-expressed with RyR1 (Fig. 3A, g–i), that was unable to bind RTN1A (Fig. 2D). As a result, the rate of colocalization as quantified by using the Pearson's correlation coefficient was much higher between RTN₁₅₂₃ and RyR2 (Pearson's coefficient = 0.76 ± 0.10) than between RTN₁₅₂₃ and RyR1 (Pearson's coefficient = 0.28 ± 0.09 ; $p = 0.003$) (Fig. 3C). Thus, the colocalization between RTN₁₅₂₃ and RyR2 supports a highly specific direct interaction of both proteins.

3.4. RyR2 binds to a conserved domain in the N-terminal region of RTN1A

To define more specifically the RyR2 binding region within RTN1A, we generated two non-overlapping sub-fragments of RTN₁₅₂₃ (long N-terminal fragment, LNT, aa 1–375; high homology domain, HHD, aa 376–523; Fig. 4A) and performed GST pull-down assays on mouse brain lysates. As shown in Fig. 4B, RyR2 specifically interacted with GST-RTN₁₅₂₃ and GST-HHD, but not with GST-LNT or the negative controls (Fig. 4B, upper panel). These data indicate that the HHD domain, aa

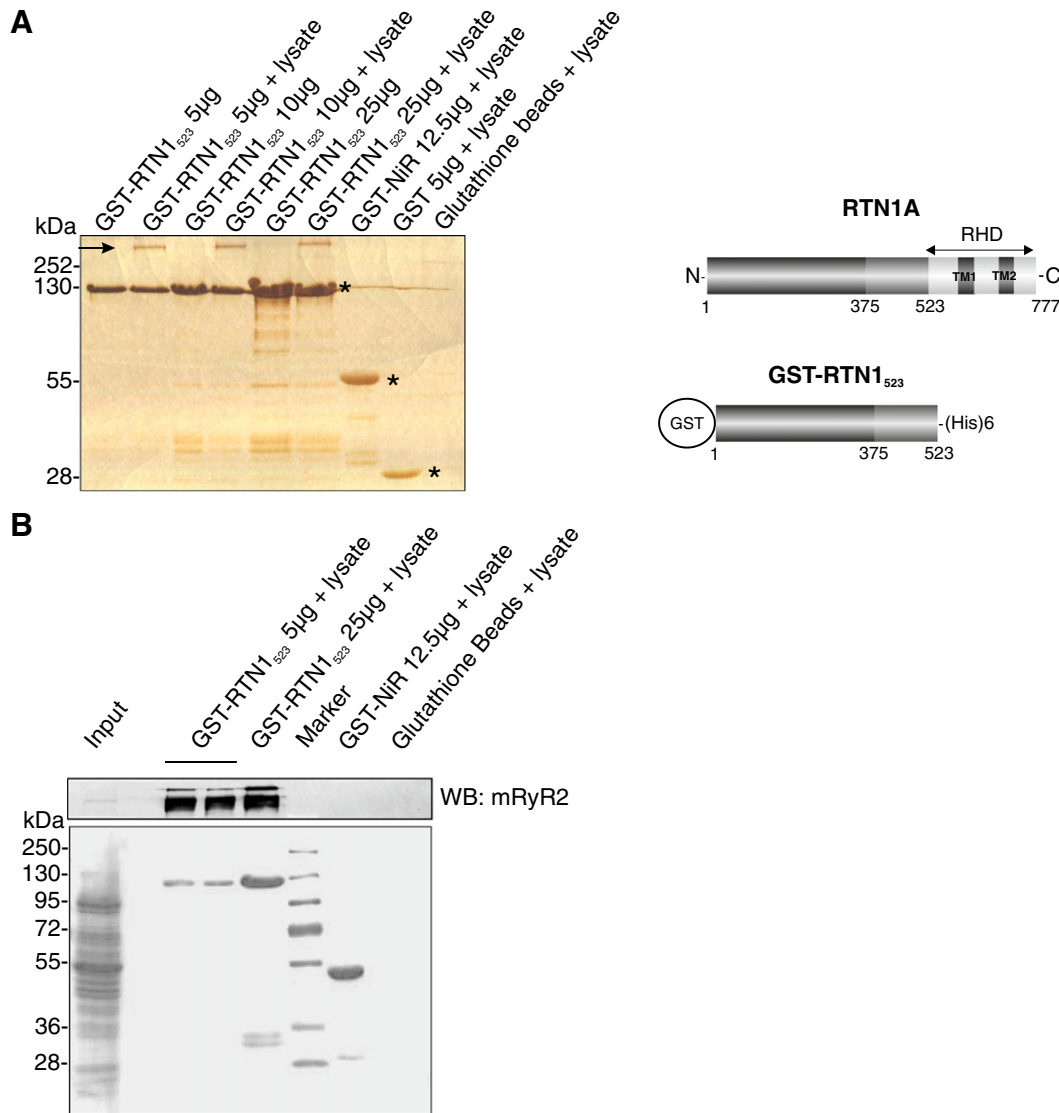


Fig. 1. Identification of RyR2 as a binding partner of RTN1A. (A) Schematic representation of full length RTN1A and the GST-RTN1₅₂₃ construct (right). RHD: reticulon homology domain; TM1 and TM2: transmembrane domain 1 and 2. GST pull-downs were performed with GST-RTN1₅₂₃ using detergent-solubilized mouse brain proteins. GST or empty glutathione beads served as negative controls, whereas GST-NiR was tested to control for GST-RTN1₅₂₃ binding specificity. Arrow denotes protein band that was consistently pulled down with GST-RTN1₅₂₃ and from which RyR2 was identified by mass spectrometry. Note that this band is absent in the different control samples. Asterisks indicate the GST fusion proteins and their relative amounts used in the GST pull-down. The silver stained gel shown is representative of three independent experiments. (B) *Upper panel*, Western Blot of samples from (A) probed with RyR2 antibody. Note the double-band that is identified as RyR2. The higher molecular mass band corresponds to intact RyR2, while the lower band presumably represents a proteolytic degradation fragment of RyR2. The intensity of the RyR2 bands increase with increasing amounts of GST-RTN1₅₂₃. *Lower panel*, shows Ponceau S staining of the pull-downs to assess the relative amounts of each GST fusion protein. Input lane shows one-twentieth of the amount used for pull-down. WB, Western blot. The Western blot shown is representative of three independent experiments.

376–523 of RTN1A, contains the binding site(s) for RyR2 *in vitro*. Interestingly, this region was found to display significant sequence homology from human to *Xenopus*, (thus we termed this region high homology domain, HHD), suggesting that this domain was highly conserved over evolution.

3.5. RTN1A displays an overlapping expression pattern with RyR2 in brain

RTN1A and RyR2 have been both reported to be expressed in brain [11,12,39–41]. Because our GST fusion protein affinity pull-down and co-immunoprecipitation experiments from total brain or cerebellar extracts provide biochemical evidence for the association of RTN1A and RyR2 in a complex, we predicted that their expression patterns would overlap. To address this hypothesis, we examined the distribution of RyR2 and RTN1A in different regions and cell types of the brain using

immunohistochemical analysis on adult rat brain sections. Indeed, RTN1A and RyR2 were found to be codistributed in many brain regions, although their staining pattern was not identical. The highest immunoreactivity of both RTN1A and RyR2 was in the hippocampus and cerebellar Purkinje neurons (Fig. 5). In line with a previous study, RyR2 displayed intense immunoreactivity in the molecular layer of the dentate gyrus as well as in mossy fibers and stratum lucidum, a region of high synaptic plasticity where mossy fibers synapse with CA3 pyramidal cell apical dendrites (Fig. 5B; [40]). A similar staining pattern was found for RTN1A (Fig. 5A), revealing strong expression in mossy fibers and stratum lucidum. In the adult rat cerebellum, two independent anti-RTN1A antibodies revealed a strong immunoreactivity in Purkinje cell somata, axons and dendrites whereas cerebellar interneurons, Bergman glia and granule cells remained unlabeled (Fig. 5C, D). Consistent with previous reports, immunofluorescent RyR2 specific staining was predominantly found in granule cells, and more moderately in Purkinje cell somata and

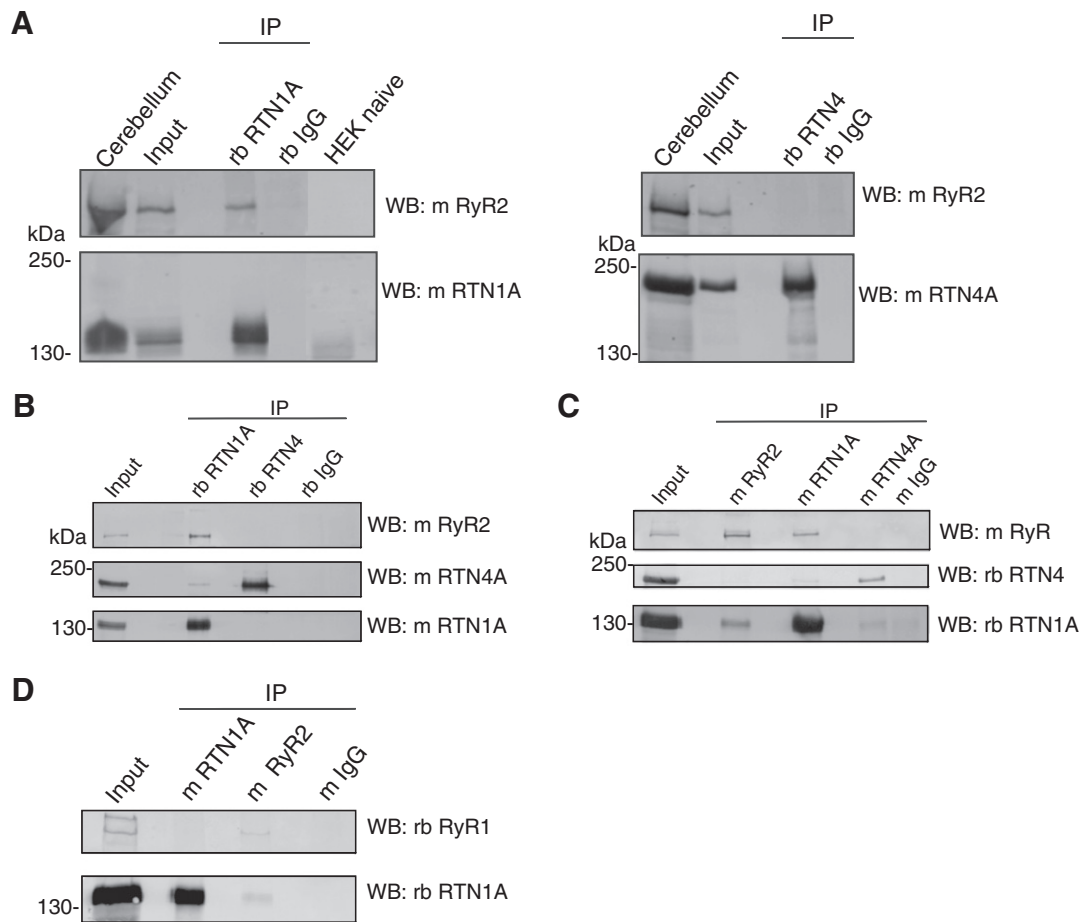


Fig. 2. RTN1A associates preferentially with RyR2 channel *in vivo*. (A) *Left panels*, detergent-solubilized protein from HEK293 cells transiently transfected with untagged RyR2 plus RTN1A-myc was immunoprecipitated (IP) with rabbit polyclonal anti-RTN1A antibodies or control rabbit IgG. Immunoprecipitated proteins were detected on immunoblots with monoclonal anti-RyR2 or anti-RTN1A antibodies. Note that native HEK293 cells do not express endogenous levels of RTN1A or RyR2. *Right panels*, detergent-solubilized protein from HEK293 cells transiently transfected with untagged RyR2 plus RTN4A-myc was immunoprecipitated with rabbit polyclonal anti-RTN4A antibodies or control rabbit IgG. Immunoprecipitated proteins were detected on immunoblots with monoclonal anti-RyR2 or anti-RTN4A antibodies. Input lane shows one-eighth of the amount used for immunoprecipitation. WB, Western blot. (B) Detergent-solubilized protein from rat cerebellum was used for co-immunoprecipitations with rabbit anti-RTN1A, rabbit anti-RTN1A, or control rabbit IgG. Immunoprecipitated proteins were resolved by SDS-PAGE blotted on PVDF membranes and probed with monoclonal antibodies as indicated at the right. Input lane shows one-tenth of the amount used for immunoprecipitation. WB, Western blot. (C) Detergent-solubilized protein from rat cerebellum was used for co-immunoprecipitations with mouse anti-RyR2, mouse anti-RTN1A, mouse anti-RTN1A, or control mouse IgG. Immunoprecipitated proteins were resolved by SDS-PAGE, blotted on PVDF membranes and probed with antibodies as indicated at the right. Input lane shows one-tenth of the amount used for immunoprecipitation. WB, Western blot. (D) Detergent-solubilized protein from rat cerebellum was immunoprecipitated with mouse anti-RTN1A, mouse anti-RyR2, or control mouse IgG. Immunoprecipitated proteins were resolved by SDS-PAGE, blotted on PVDF membranes and probed with antibodies as indicated at the right. Note that RyR1 co-immunoprecipitates with mouse anti-RyR2, but not with mouse anti-RTN1A antibodies. Input lane shows one-fifth of the amount used for immunoprecipitation. WB, Western blot.

dendrites (Fig. 5E; [40]). Unfortunately, our attempts to reveal double immunofluorescent staining for RTN1A and RyR2 showed somewhat variable results due to inconsistency with the monoclonal RyR2 antibody.

3.6. Subcellular localization of RTN1A by immuno EM

Next, to resolve the precise subcellular distribution of RTN1A in Purkinje cells, we carried out pre-embedding immunoelectron microscopy visualizing the antigen-antibody complex either by means of the HRP-DAB reaction, because of the higher sensitivity, or by silver-enhanced nanogold reaction, which allows a more confined localization of the complex. In the molecular layer, the electron opaque peroxidase end product was observed in Purkinje cell dendrites and dendritic spines in apparent association with cisternal organelles and membranes of the smooth endoplasmic reticulum (Fig. 6A–B). On the other hand, other organelles such as mitochondria, lysosomes and multivesicular bodies, as well as the plasma membrane were unlabeled (Fig. 6A–B). Likewise, in parallel fiber axons and boutons, in axon terminals forming symmetric synapses and in glial processes we could not detect any

RTN1A-IR. The silver-enhanced immunogold reaction confirmed that in the somatodendritic domain of Purkinje cells RTN1A-IR was exclusively intracellular. Immunometal particles decorated cisterns and vesicles of the smooth ER in Purkinje cell dendrites (Fig. 6C) and spines (Fig. 6D).

3.7. GST-RTN1₅₂₃ causes a decrease in [³H]ryanodine-binding

To assess the functional impact of RTN1A interaction on the RyR2 Ca²⁺-release channel, we performed equilibrium [³H]ryanodine-binding assays on rat brain synaptosomes. Because ryanodine binds only to the open conformation of RyR this assay is considered a reliable measure of the open/closed state of RyR channels [42]. We determined the calcium dependence of [³H]ryanodine binding to the population of RyR channels present in synaptosomes from rat brain in the presence or absence of RTN1A (purified GST-RTN1₅₂₃ at 0.1 μM). In line with previous studies for brain RyRs [43–48] our determinations showed that [³H]ryanodine binding was similar to background levels in the virtual absence of [Ca²⁺], reflecting the closed state of RyR channels, but was increased at higher [Ca²⁺], with a characteristic “bell-shaped” [Ca²⁺] dependence

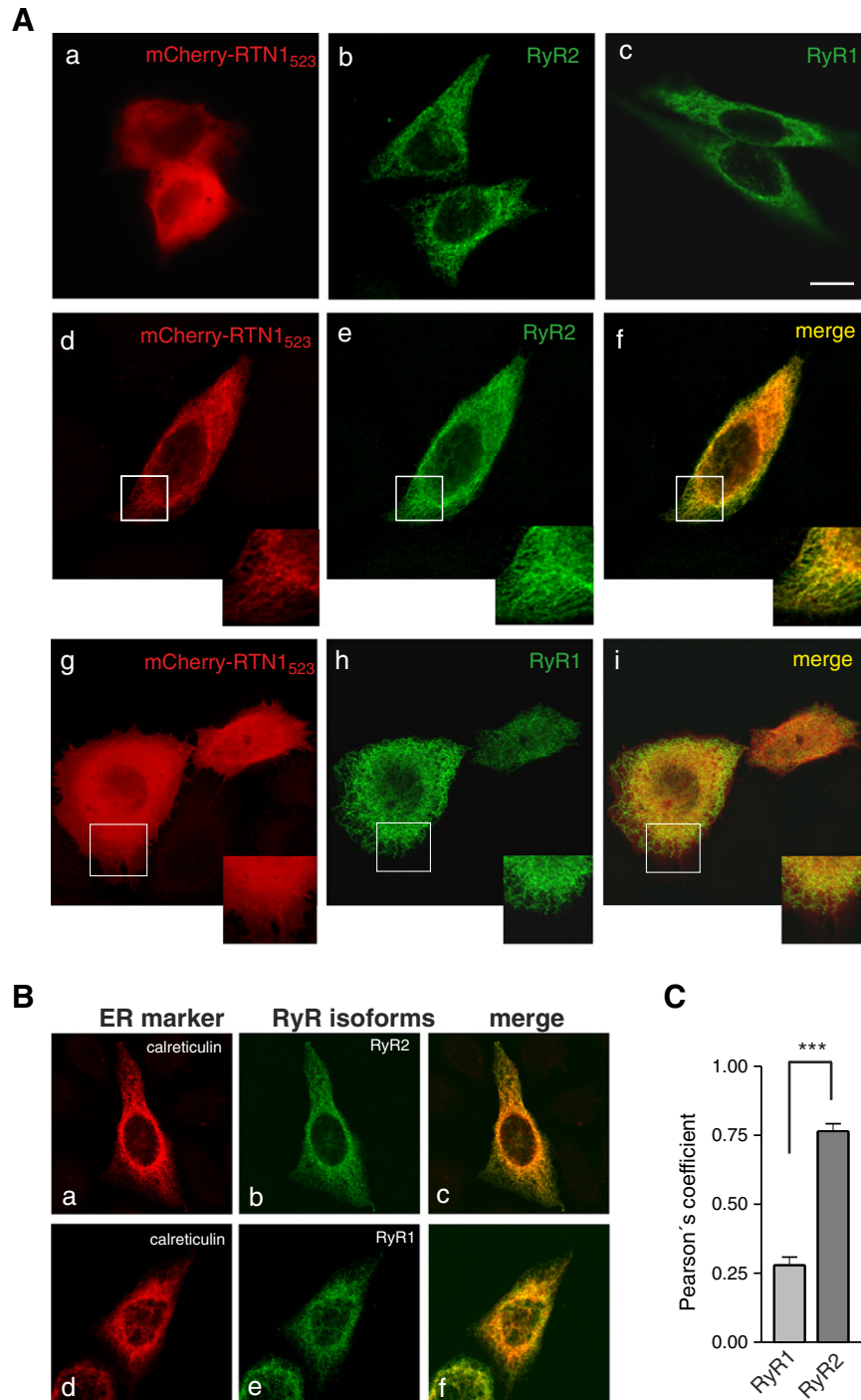


Fig. 3. Immunocytochemical distribution of mCherry-RTN1₅₂₃ and RyRs in HEK293 cells. (A) HEK293 cells were transiently transfected with mCherry-RTN1₅₂₃ in the absence (a) or presence of untagged RyR2 (d–f) or RyR1 (g–i). Single-transfections of untagged RyR2 (b) and RyR1 (c) were carried out as a comparison. Cells were immunostained with anti-RyR2 (b,d–f) or anti-RyR1 (c,g–i) antibodies and visualized by confocal microscopy. Note that single-transfected mCherry-RTN1₅₂₃ is uniformly distributed in the cytosol (a), but altered to a more reticular staining pattern when co-expressed with RyR2 (d–f). mCherry-RTN1₅₂₃ remained uniformly distributed in cells cotransfected with RyR1 (g–i). Cells shown represent at least 20 representative cells per condition. (B) Immunofluorescence confocal microscopy analysis of RyR ER localization in HEK293 cells. HEK293 cells were single-transfected with untagged RyR1 cDNA or RyR2 cDNA, immunostained with the indicated antibodies and imaged using immunofluorescence microscopy to demonstrate RyR and calreticulin (ER-specific marker) colocalization. Cells were immunostained for RyR isoforms (green) and Calreticulin (red), respectively. Space bar: 10 μ m. (C) Extent of colocalization between mCherry-RTN1₅₂₃ and RyR isoforms was quantified using Pearson correlation coefficient and determined through correlation analysis with Leica SP5 software from 10 different cells per group. (***) $p = 0.003$ by Student's t -test).

(Fig. 7A). Maximal activation of [³H]ryanodine binding occurred between 1 and 10 μ M Ca^{2+} , which is in agreement with previous studies [42–46]. Addition of 0.1 μ M recombinant GST-RTN1₅₂₃ specifically reduced [³H]ryanodine binding to synaptosomes at all calcium concentrations (Fig. 7A) without a major change in the profile of Ca^{2+} dependence. The presence of GST-RTN1₅₂₃ did not change the minimal [Ca^{2+}] for

RyR activation (>10 nM Ca^{2+}), and maximal activity of RyRs was reached at the same [Ca^{2+}] as in the absence of GST-RTN1₅₂₃. To compare the results obtained with different vesicle preparations, binding was normalized against the value determined in the absence of recombinant proteins. As shown in Fig. 7B, at 0.3 μ M [Ca^{2+}], GST-RTN1₅₂₃ specifically inhibited [³H]ryanodine binding to synaptosomes by

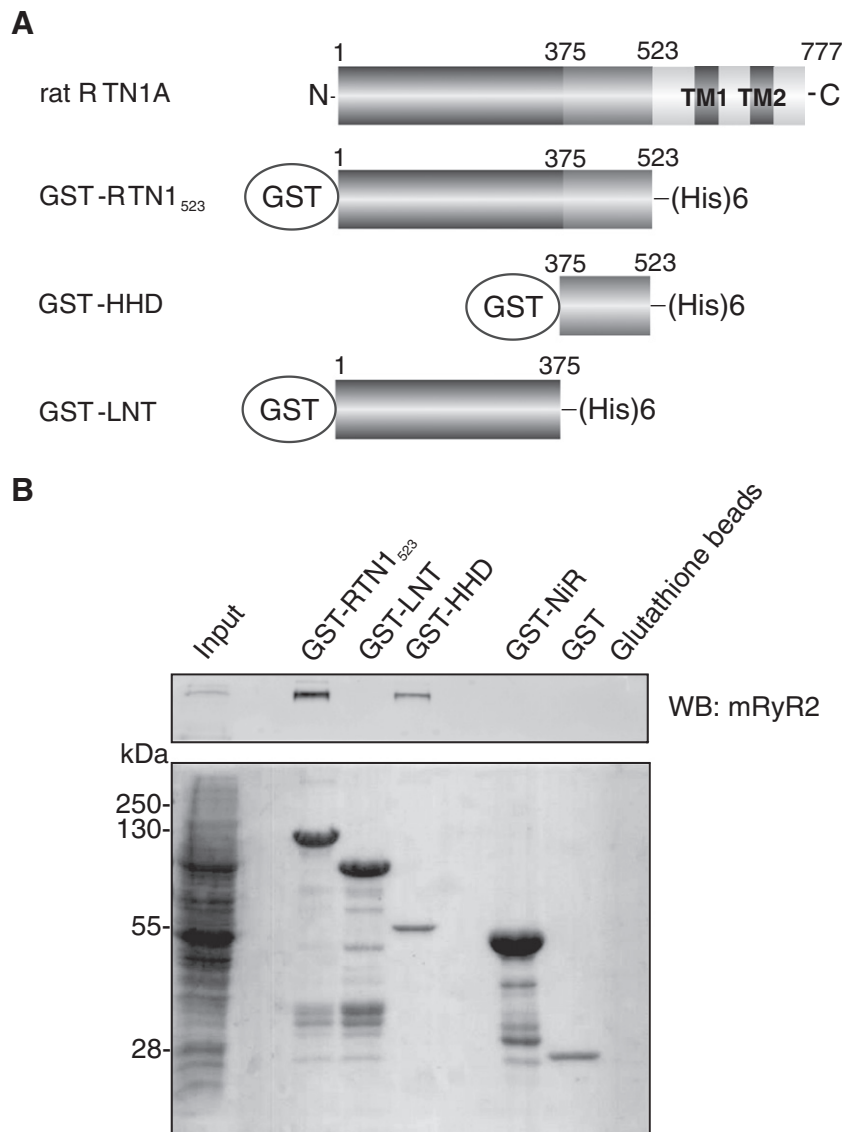


Fig. 4. Identification of the RyR2 binding domain. (A) Schematic representation of rat RTN1A protein and RTN1A fragments used to construct GST fusion proteins for the pull-down experiments. HHD: high homology domain; LNT: long N-terminal fragment. (B) GST-RTN1 fragments were used as baits in pull-down experiments using detergent-solubilized mouse brain proteins. GST, GST-NiR or empty glutathione beads served as negative controls. Binding of RyR2 was subsequently detected by immunoblot (upper panel). Ponceau S staining of the pull-downs shows the relative amounts of each GST fusion protein (lower panel). Input lane shows one-tenth of the amount used for immunoprecipitation. WB, Western blot. Results are representative of three independent experiments.

$31.5 \pm 4.3\%$ compared to control conditions ($n = 3$; $p = 0.011$). This effect is entirely attributable to recombinant GST-RTN1₅₂₃ since $0.1 \mu\text{M}$ GST had no significant effect ($1.4 \pm 5.3\%$) in three parallel experiments. This downward shift in the [^3H]-ryanodine binding produced by RTN1₅₂₃, indicated a decreased Ca^{2+} -induced activation of RyR compared with control and is indicative of a decrease in RyR channel activity, since ryanodine binding increases as RyR activity increases.

3.8. RTN1A reduces RyR2-mediated Ca^{2+} oscillations

Ca^{2+} oscillations mediated by RyR2-expressing HEK293 cells at increased extracellular calcium concentrations were taken as a sensitive measure to detect an effect of RTN1A on RyR2 activity. As shown in Fig. 7C, Ca^{2+} transients were monitored in individual HEK293 cells expressing RyR2 in the absence or presence of RTN1A. To elicit maximal amount of RyR2-mediated Ca^{2+} oscillations, cells were perfused with 1 mM [Ca^{2+}]. By a quantitative analysis based on the overall area

under the oscillations peaks during 450 s, the amount of Ca^{2+} -released via RyR2 was significantly reduced when mcherry-RTN1A was co-expressed in comparison to control with mcherry (Fig. 7C, left and right upper panel, right lower panel). Furthermore, the number of Ca^{2+} oscillating HEK293 cells (87.1%) was clearly reduced in the presence of RTN1A (51.9%) (Fig. 7C; right lower panel). In order to evaluate non RTN1A-specific ER-mediated effects on RyR2, we utilized RTN4A as an ER-resident control protein that did not interact with RyR2 based on our co-immunoprecipitation studies. Although co-expression of RTN4A with RyR2 slightly decreased the amount of Ca^{2+} released via RyR2, this effect was not significant (Fig. 7C; left lower panel). Additionally, the percent of HEK293 cells that developed RyR2-mediated Ca^{2+} oscillations (74.6%) was clearly above those with RTN1A co-expressed. The magnitude of Ca^{2+} released during 10 mM caffeine exposure was not substantially altered when RyR2 was co-expressed with either RTN1A or RTN4A (Fig. 7C; right lower panel). Together, these results suggest that a functional role for the association of RTN1A with RyR2 in neurons

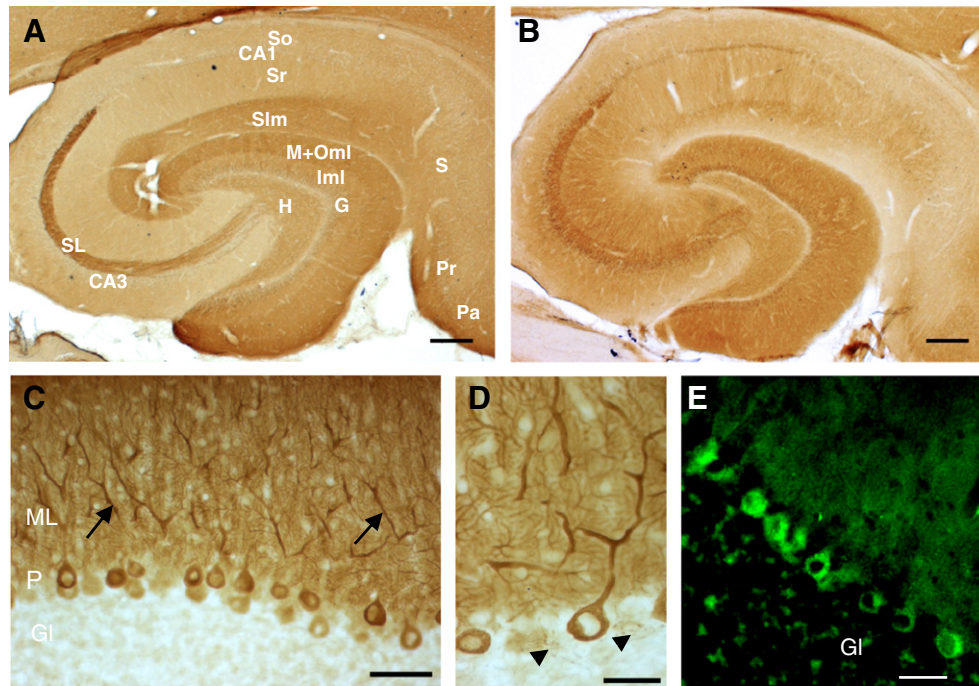


Fig. 5. Immunohistochemical distribution pattern of RTN1A and RyR2 in rat hippocampus and cerebellum. Representative staining patterns for RTN1A (A,C,D) and RyR2 (B,E) on sections of rat hippocampus (A,B) and cerebellar cortex (C,D,E). In the hippocampus, immunoreactivity for both proteins is found in granule cells (G), mossy fiber axons, and in stratum lucidum (SL). In the cerebellum, RTN1A-immunoreactivity was confined to Purkinje cell bodies (P), their dendrites in ML (C; arrow) and axons (D; arrowheads). (E) Confocal immunofluorescent image showing RyR2 staining in Purkinje cells. Unlike RTN1A, RyR2 was also found in granule cell layer (GI). Scale bars: A and B, 500 μ m; H, hilus; G, Granule cell layer; So, stratum oriens; Sr, stratum radiatum; SIm, stratum lacunosum molecular; Iml, inner molecular layer; M + Oml, Middle & outer molecular layer; CA1-3, Cornu ammonis; SL, stratum lucidum; S, Subiculum; Pr, Presubiculum; Pa, Parasubiculum.

is in the regulation of intracellular calcium dynamics of pre- and post-synaptic calcium stores.

4. Discussion

Despite the abundant expression of RTN1A in the adult brain, our understanding of its functional role still remains elusive. In this study, using a combination of co-immunoprecipitation, colocalization, GST pull-down assays and MS analysis we identify the intracellular calcium release channel RyR2 as a RTN1A binding partner in neurons. Moreover, we show that soluble RTN1₅₂₃ reduces Ca²⁺-induced activation of RyR on brain synaptosomes and that RTN1A markedly decreases the occurrence of RyR2-mediated Ca²⁺ oscillations at elevated extracellular Ca²⁺ concentrations.

4.1. Interaction of RTN1A and RyR2

In our study we provide evidence for a direct interaction of RTN1A and RyR2. Several approaches were used to confirm this finding. First, different RTN1A antibodies immunoprecipitated RyR2 after heterologous expression in HEK293 cells and from detergent-solubilized brain extract. This interaction was not seen with precipitating RTN4A/NogoA antibodies. Second, cytosolic mCherry-RTN1₅₂₃ relocalized when co-expressed with RyR2 but not with RyR1 in HEK293 cells. Third, GST-RTN1₅₂₃ affinity beads were shown to pull-down RyR2 but not RyR1 from detergent-solubilized brain extract. Thus, it seems that both proteins form a functional complex in neurons, although we cannot completely exclude the possibility that the two proteins may indirectly interact by virtue of each binding to an intermediary protein.

Previous studies in non-neuronal cells have suggested that all reticulons including RTN1A partition into the outer leaflet of the ER membrane bilayer via their RHD, placing the N-terminal and C-terminal

domains in the cytoplasm [37,38,49,50]. Since we used the N-terminal domain of RTN1A (aa 1–523) for interaction analysis we propose that in intact cells RTN1A–RyR2 interaction occurs from the cytosolic surface from the ER membrane via cytosolic domains. More specifically, the principal region of RTN1A responsible for binding RyR2 was mapped to HHD, the portion of the protein spanning amino acid residues 376 and 523 (Fig. 4). No binding was detected within the N-terminal half of the protein between residues 1 and 375. Strikingly, this RyR2 binding region of RTN1A is highly conserved among all RTN1A and RTN1B isoforms that have so far been characterized from different species including African clawed frog (*Xenopus laevis*), chicken (*Gallus gallus*), Carolina anole (*Anolis carolinensis*), gray short-tailed opossum (*Monodelphis domestica*), platypus (*Ornithorhynchus anatinus*), house mouse (*Mus musculus*), Norwegian rat, (*Rattus norvegicus*), Cattle (*Bos taurus*), and man (*Homo sapiens*), suggesting a central role for the HHD region in the function of these two proteins. An unexpected finding from this study is the preferential interaction of RTN1A to RyR2 relative to RyR1. The similarities in protein structure and subcellular localization between both RyRs led us to investigate whether RyR1, like RyR2, is capable of binding to RTN1A. Although our present biochemical analysis did not detect a RyR1 association with RTN1A (Figs. 2D and 3), we cannot exclude that both proteins may associate weakly/transiently, or alternatively, that only minor amounts of these proteins interact in specific neurons. Nevertheless, this selectivity could reflect preferential binding of RTN1A to RyR2 in the absence of RyR1 such as in hippocampal mossy fibers (see below). Interestingly, in muscle cells, the two FK506-binding proteins (FKBPs), FKBP12 and FKBP12.6, also known as immunophilins, also exhibit selectivity binding to certain RyR subtypes. While FKBP12 can potentially regulate all three RyR subtypes, with a selectivity of RyR1 > RyR3 > RyR2 [51,52], FKBP12.6 associates preferentially with RyR2 [53] and regulates RyR2 mediated Ca²⁺ release by stabilizing the channel in its closed state [54]. Future studies will need

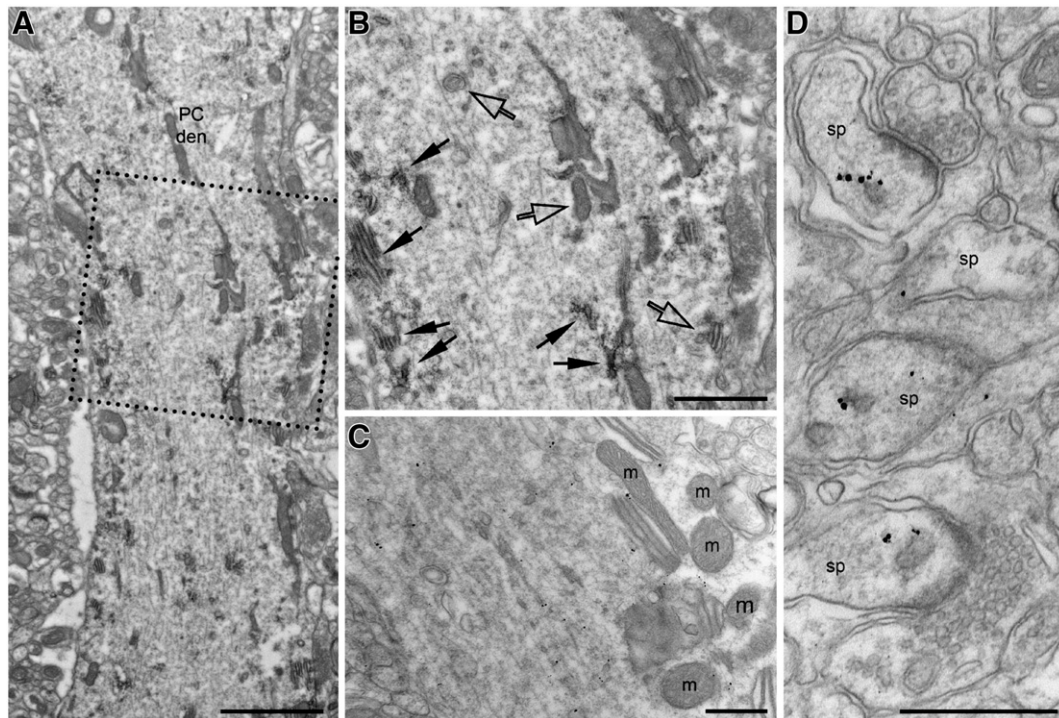


Fig. 6. Subcellular distribution of RTN1A in Purkinje cells. (A) Electron micrograph of a Purkinje cell dendrite immunolabeled for RTN1A (MON162 antibody) using the HRP-DAB technique. (B) Higher magnification of the area boxed in A. The electron opaque peroxidase end product can be seen around cisternal organelles and vesicles of the smooth endoplasmic reticulum (indicated by filled arrows), but not the plasma membrane of the Purkinje cell. Empty arrows indicate unlabeled organelles. (C) Electron micrograph of a Purkinje cell dendrite immunolabeled for RTN1A (MON162 antibody) using the silver-enhanced nanogold technique. Immunometal particles can be seen decorating the membrane of the smooth endoplasmic reticulum within Purkinje cell spines (sp). Scale bars: A, 2 μ m; B, 1 μ m; C–D, 500 nm.

to explore the potential for RyR subtype-specific interactions with other RTN isoforms.

4.2. Expression and subcellular localization of RTN1A in neurons

Thus far, little information is available for detailed subcellular localization of different RTN isoforms. Here, we explored the cellular and subcellular distribution of RTN1A in detail. Immunohistochemical studies revealed an intense labeling of RTN1A in mossy fibers of the hippocampus as well as in axons, dendrites and spines of Purkinje cells. Immunoelectron microscopy clearly showed that RTN1A was highly enriched in dendrites and spines, and mostly distributed around the smooth ER. Although RTNs are generally thought to be predominantly located in the endomembrane system, RTN4A, -B, -C and RTN2B were reported to reside also on the cell surface of neurons and non-neuronal cells [55,56,36,4]. In contrast, in our immunoelectron microscopy study we did not observe plasma membrane associated RTN1A-IR in Purkinje cells (Fig. 6). This finding is in perfect agreement with previous cell surface biotinylation assays on cultured neurons, which failed to detect cell surface-exposed RTN1A [4]. Moreover, in contrast to the RHD of RTN2, -3 and -4 proteins, RHD of RTN1 lacks binding to the axonal Nogo-66 receptor, NgR1 [57] thought to be responsible for axonal growth inhibition. Hence, it seems likely that RTN1A exerts primarily an intracellular function related to its localization within the ER of pre- and postsynaptic sites. Although RTN1A shows a similar distribution in the brain as the RyR2 channel, it also exhibits a distinct expression pattern compared to RyR2 when examined in detail locally. For example, both proteins are highly expressed in cerebellum; however, RTN1A is more abundant in Purkinje cells whereas RyR2-IR is strong in granule cells, which are clearly devoid of RTN1A-IR, implying that RTN1A/RyR2 association may play distinct roles in subregions of the cerebellum.

4.3. Physiological function of RTN1A–RyR2 association

At present, the physiological significance of the RTN1A–RyR2 association remains to be defined. However, it is tempting to speculate that RTN1A might exert a regulatory effect on RyR2 channel function. Initial evidence for a modulatory role of RTN1A is provided by our ryanodine binding assays, showing that soluble RTN1₅₂₃ inhibits the calcium-dependent activation of [³H]ryanodine binding in forebrain synaptosomes by 32% (Fig. 7A,B). Because RyR2 was shown to be the most abundant isoform of total RyR content in mammalian brain cortex [58,41], we assume that this decrease in [³H]ryanodine binding is largely attributable to RTN1₅₂₃ association to RyR2. Consistent with this view, we have shown that RTN1A reduces the frequency of RyR2-mediated Ca²⁺ oscillations in HEK293 cells expressing RyR2. Although this effect appeared to be specific for RTN1A, we cannot fully exclude that overexpression of RTN1A in the ER additionally contributed to its specific inhibitory action on RyR2 function. Hence, the apparent close physical proximity of the RyR2 and RTN1A in Purkinje cells or in mossy fibers in the hippocampus (Fig. 5) may enable RTN1A to bind to the RyR2 channel with high avidity even when cytoplasmic Ca²⁺ concentration is low under resting conditions. Accordingly, RyR2 channels that are bound to RTN1A may have a lower open probability, resulting in a decreased sensitivity to RyR2-mediated CICR. Emerging evidence indicates that CICR appears to play a vital role in neuronal functions including those that regulate synaptic efficacy, aging and memory. CICR has been demonstrated in neurons where intracellular Ca²⁺ release from RyRs is found to be linked to Ca²⁺ influx through voltage-dependent channels [59]. In cerebellar Purkinje cells, for example, Ca²⁺ influx via activation of both ionotropic and metabotropic glutamate receptors is shown to be essential for subsequent RyR-mediated Ca²⁺ release [60]. In addition, RyR mediated Ca²⁺ release from intracellular stores is reported to

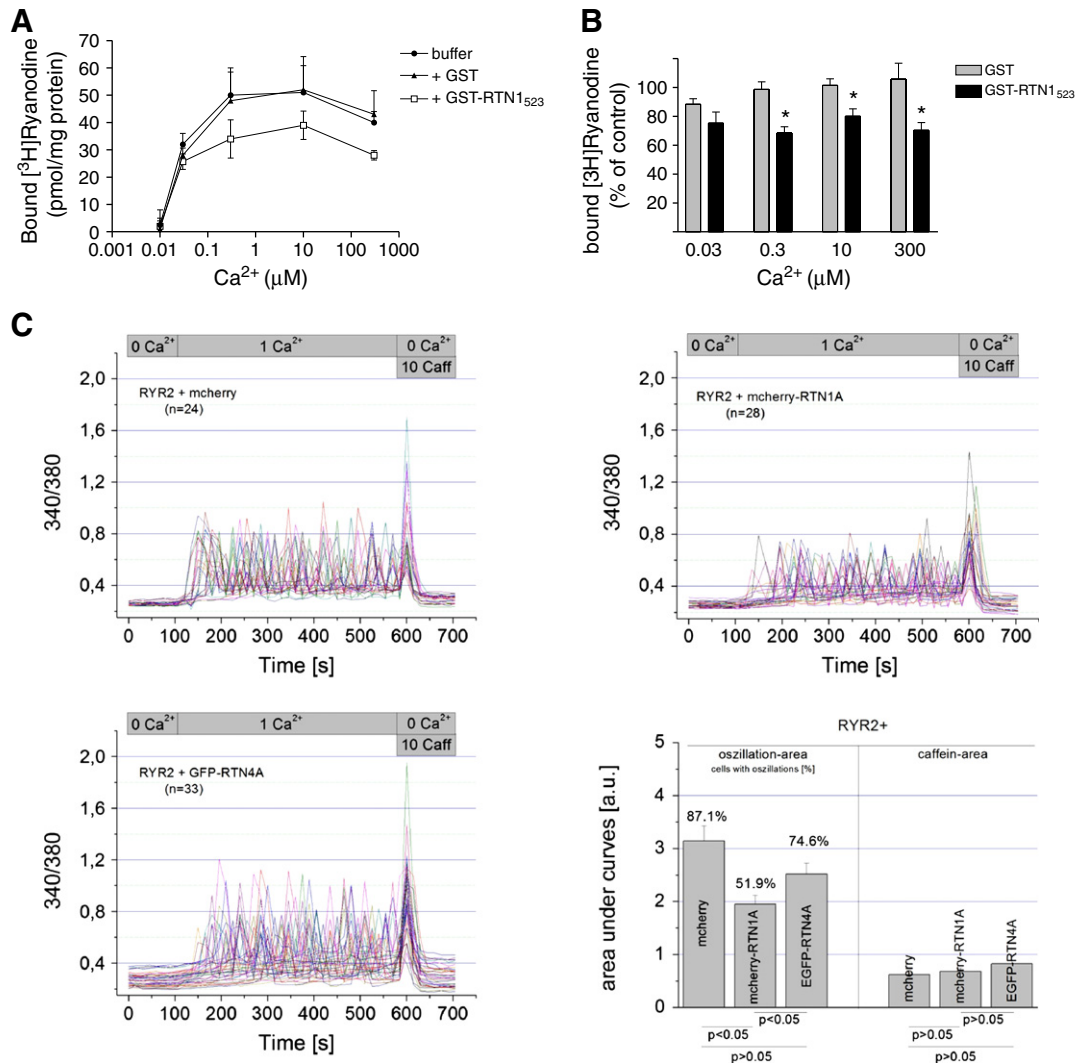


Fig. 7. GST-RTN₁₅₂₃ inhibits specific [³H]ryanodine binding to rat brain synaptosomes. (A) Equilibrium [³H]ryanodine binding to rat forebrain synaptosomal membrane preparations was carried out in binding buffer containing 10 nM [³H]ryanodine at the indicated free calcium concentrations in control conditions (closed circles) and in the presence of 0.1 μM GST (closed triangles) or 0.1 μM GST-RTN₁₅₂₃ (open squares). [Ca²⁺] was maintained, in the range 0.01 μM–1 mM, by a combination of EGTA and CaCl₂. Free Ca²⁺ concentrations were calculated as described in material and methods. Data points shown are the mean ± S.E.M., from three separate experiments performed in triplicates. (B) [³H]ryanodine binding in the presence of 0.1 μM GST or GST-RTN₁₅₂₃ is presented as percent of control. No specific [³H]ryanodine binding was observed at 0.01 μM Ca²⁺ in the presence of GST or GST-RTN₁₅₂₃. Difference in [³H]ryanodine binding was plotted as percent decrease in specific binding. Data points shown are the mean ± S.E.M., from three separate experiments (**p* = 0.011 by Student's *t*-test). (C) RyR2 evoked Ca²⁺ oscillations in HEK293. Upper and lower left panels represent Fura-2 ratio time-courses of single cells expressing RyR2 together with mcherry, mcherry-RTN1A or EGFP-RTN4A. Cells were continuously perfused with buffer containing 0 mM Ca²⁺ (nominal free), 1 mM Ca²⁺ and 0 mM Ca²⁺ + 10 mM caffeine as indicated by the bars at the top. Lower right panel shows a quantitative analysis performed by integration of the respective single peak areas referred to area under curve for estimation of the total amount of the cytosolic [Ca²⁺] arising through RyR2 dependent Ca²⁺ oscillations. The fraction of cells that showed both oscillations as well as a clear caffeine peak in comparison to those that lacked oscillations before a single caffeine peak are given in percentages in the graph. A two-sample *t*-test was carried out to test for significance as indicated by the *p* values at the bottom of the panel.

be required for induction of long-term potentiation in the hippocampus [61,62] and long-term depression in both the hippocampus and cerebellum [63–66]. Notably, in the hippocampus, activity dependent presynaptic CICR at the mossy fiber synapse is mediated by RyR2 [40], thereby facilitating robust presynaptic forms of plasticity at the mossy fiber-CA3 synapse. Hippocampal expression of RyR2 increases after spatial memory learning [63] and is involved in BDNF-induced hippocampal synaptic plasticity and spatial memory formation [67].

The RTN1A and RyR2 association might not only be involved in neurotransmitter release but also in aging-related Ca²⁺ dysregulation. Similar as in the muscle (see above), neuronal FKBP12.6 inhibits cytosolic Ca²⁺ rises by inhibiting directly L-VGCCs and RyR2. Interestingly, experimental silencing or downregulation of FKBP12.6, led to hippocampal Ca²⁺

dysregulation resulting in dampened neuronal excitability and function, typical signs of aging or pathological neurons [68]. Thus, in analogy, it is possible to envision that, in neurons, RTN1A may function together with RyR2 and FKBP molecules in a multimeric Ca²⁺ regulating complex, in which RTN1A and FKBP12.6 tonically inhibit RyR2 by direct interaction.

In conclusion, we identified RyR2 as a novel binding partner of RTN1A and show that RTN1A exerts a regulatory, inhibitory effect on the RyR2 activity. These results suggest that a functional coupling of RTN1A and RyR2 may play a vital role in controlling regulation of neurotransmitter release and long-term potentiation induction by modulation of intracellular Ca²⁺ release.

Supplementary data to this article can be found online at <http://dx.doi.org/10.1016/j.bbamcr.2013.02.012>.

Acknowledgements

We thank P.D. Allen and Wayne Chen for generously providing rabbit RyR1 and mouse RyR2 cDNA constructs, and Vincenzo Sorrentino for the polyclonal anti-RyR2 antibody. We are very grateful to Sabrina Riepler, Antje Kurz and Gabi Schmid for excellent technical assistance, Gerald Obermair for advice on statistical analysis, Martin Offerdinger for help on colocalization studies and the SPIN consortium for critical discussions. This work was supported by the Austrian Research Foundation (FWF W1206) and an IFTZ-grant to CEB. LK was supported by the Graduate program ‘Signal processing in neurons’ (SPIN).

References

- [1] Y.S. Yang, S.M. Strittmatter, The reticulons: a family of proteins with diverse functions, *Genome Biol.* 8 (2007) 234.
- [2] T. Oertle, M.E. Schwab, Nogo and its partners, *Trends Cell Biol.* 13 (4) (2003) 187–194.
- [3] S.H. Park, C. Blackstone, Further assembly required: construction and dynamics of the endoplasmic reticulum network, *EMBO Rep.* 11 (7) (2010) 515–521.
- [4] Y. Liu, S. Vidensky, A.M. Ruggiero, S. Maier, H.H. Sitte, J.D. Rothstein, Reticulon RTN2B regulates trafficking and function of neuronal glutamate transporter EAAC1, *J. Biol. Chem.* 283 (10) (2008) 6561–6571.
- [5] P. Steiner, K. Kulangara, J.C.F. Sarria, L. Glauser, R. Regazzi, H. Hirling, Reticulon 1-C/neuroendocrine-specific protein-C interacts with SNARE proteins, *J. Neurochem.* 89 (3) (2004) 569–580.
- [6] G. Montenegro, A.P. Rebelo, J. Connell, R. Allison, C. Babalini, M.D. Aloia, P. Montieri, R. Schüle, H. Ishiura, J. Price, A. Strickland, M.A. Gonzalez, L. Baumbach-Reardon, T. Deconinck, J. Huang, G. Bernardi, J.M. Vance, M.T. Rogers, S. Tsuji, P. De Jonghe, M.A. Pericak-Vance, L. Schöls, A. Orlicchio, E. Reid, S. Züchner, Mutations in the ER-shaping protein reticulon 2 cause the axon-degenerative disorder hereditary spastic paraplegia type 12, *J. Clin. Invest.* 122 (2012) 538–544.
- [7] W. He, Y. Lu, I. Qahwash, X.-Y. Hu, A. Chang, R. Yan, Reticulon family members modulate BACE1 activity and amyloid-beta peptide generation, *Nat. Med.* 10 (9) (2004) 959–965.
- [8] S. Tagami, Y. Eguchi, M. Kinoshita, M. Takeda, Y. Tsujimoto, A novel protein, RTN-XS, interacts with both Bcl-XL and Bcl-2 on endoplasmic reticulum and reduces their anti-apoptotic activity, *Oncogene* 19 (50) (2000) 5736–5746.
- [9] F. Di Sano, B. Fazi, G. Citro, P.E. Lovat, G. Cesareni, M. Piacentini, Glucosylceramide synthase and its functional interaction with RTN-1C regulate chemotherapeutic-induced apoptosis in neuroepithelioma cells, *Cancer Res.* 63 (14) (2003) 3860–3865.
- [10] M.E. Schwab, Functions of Nogo proteins and their receptors in the nervous system, *Nat. Rev. Neurosci.* 11 (12) (2010) 799–811.
- [11] H.J. van de Velde, A.J. Roebroek, F.W. van Leeuwen, W.J. Van de Ven, Molecular analysis of expression in rat brain of NSP-A, a novel neuroendocrine-specific protein of the endoplasmic reticulum, *Brain Res. Mol. Brain Res.* 23 (1–2) (1994) 81–92.
- [12] H.J. van de Velde, A.J. Roebroek, N.H. Senden, F.C. Ramaekers, W.J. Van de Ven, NSP-encoded reticulons, neuroendocrine proteins of a novel gene family associated with membranes of the endoplasmic reticulum, *J. Cell Sci.* 107 (1994) 2403–2416.
- [13] A.U. Mannan, J. Boehm, S.M. Sauter, A. Rauber, P.C. Byrne, J. Neesen, W. Engel, Spastin, the most commonly mutated protein in hereditary spastic paraplegia interacts with Reticulon 1 an endoplasmic reticulum protein, *Neurogenetics* 7 (2) (2006) 93–103.
- [14] X. Zhao, J. Jäntti, Functional characterization of the trans-membrane domain interactions of the Sec61 protein translocation complex beta-subunit, *BMC Cell Biol.* 10 (2009) 76.
- [15] J. Iwahashi, N. Hamada, Human reticulon 1-A and 1-B interact with a medium chain of the AP-2 adaptor complex, *Cell. Mol. Biol.* 49 (6) (2003) 467–471.
- [16] G. Giannini, A. Conti, S. Mammarella, M. Scrobogna, V. Sorrentino, The ryanodine receptor/calcium channel genes are widely and differentially expressed in murine brain and peripheral tissues, *J. Cell Biol.* 128 (5) (1995) 893–904.
- [17] K. Tully, S.N. Treisman, Distinct intracellular calcium profiles following influx through N- versus L-type calcium channels: role of Ca²⁺-induced Ca²⁺ release, *J. Neurophysiol.* 92 (2004) 135–143.
- [18] V. Sorrentino, R. Rizzuto, Molecular genetics of Ca(2+) stores and intracellular Ca(2+) signalling, *Trends Pharmacol. Sci.* 22 (9) (2001) 459–464.
- [19] X. Liu, M.J. Betzenhauser, S. Reiken, A.C. Meli, W. Xie, B.X. Chen, O. Arancio, A.R. Marks, Role of leaky neuronal ryanodine receptors in stress-induced cognitive dysfunction, *Cell* 150 (5) (2012) 1055–1067.
- [20] M. Zhao, P. Li, X. Li, L. Zhang, R.J. Winkfein, S.R. Chen, Molecular identification of the ryanodine receptor pore-forming segment, *J. Biol. Chem.* 274 (37) (1999) 25971–25974.
- [21] J. Nakai, T. Ogura, F. Protasi, C. Franzini-Armstrong, P.D. Allen, K.G. Beam, Functional nonequivalence of the cardiac and skeletal ryanodine receptors, *Proc. Natl. Acad. Sci. U. S. A.* 94 (3) (1997) 1019–1022.
- [22] T. Oertle, M.E. van der Haar, C.E. Bandtlow, A. Robeva, P. Burfeind, A. Buss, A.B. Huber, M. Simonen, L. Schnell, C. Brösamle, K. Kaupmann, R. Vallon, M.E. Schwab, Nogo-A inhibits neurite outgrowth and cell spreading with three discrete regions, *J. Neurosci.* 23 (13) (2003) 5393–5406.
- [23] H. Blum, H. Beier, H.J. Gross, Improved silver staining of plant proteins, RNA and DNA in polyacrylamide gels, *Electrophoresis* 8 (2) (1987) 93–99.
- [24] A. Shevchenko, M. Wilm, O. Vorm, M. Mann, Mass spectrometric sequencing of proteins silver-stained polyacrylamide gels, *Anal. Chem.* 68 (5) (1996) 850–858.
- [25] R. Arnitz, B. Sarg, H.W. Ott, A. Neher, H. Lindner, M. Nagl, Protein sites of attack of N-chlorotaurine in *Escherichia coli*, *Proteomics* 6 (2006) 865–869.
- [26] C. Chen, H. Okayama, High-efficiency transformation of mammalian cells by plasmid DNA, *Mol. Cell. Biol.* 7 (8) (1987) 2745–2752.
- [27] R. Schindl, H. Kahr, I. Graz, K. Groschner, C. Romanin, Store depletion-activated CaT1 currents in rat basophilic leukemia mast cells are inhibited by 2-aminoethoxydiphenyl borate. Evidence for a regulatory component that controls activation of both CaT1 and CRAC (Ca(2+) release-activated Ca(2+) channel) channels, *J. Biol. Chem.* 277 (2002) 26950–26958.
- [28] D. Jiang, R. Wang, B. Xiao, H. Kong, D.J. Hunt, P. Choi, L. Zhang, S.R. Chen, Enhanced store overload-induced Ca²⁺ release and channel sensitivity to luminal Ca²⁺ activation are common defects of RyR2 mutations linked to ventricular tachycardia and sudden death, *Circ. Res.* 97 (2005) 1173–1181.
- [29] C.A. Sailer, H. Hu, W.A. Kaufmann, M. Trieb, C. Schwarzer, J.F. Storm, H.-G. Knaus, Regional differences in distribution and functional expression of small-conductance Ca²⁺-activated K⁺ channels in rat brain, *J. Neurosci.* 22 (22) (2002) 9698–9707.
- [30] D.J. West, E.C. Smith, A.J. Williams, A novel and rapid approach to isolating functional ryanodine receptors, *Biochem. Biophys. Res. Commun.* 294 (2) (2002) 402–407.
- [31] S. Zissimopoulos, D.J. West, A.J. Williams, F.A. Lai, Ryanodine receptor interaction with the SNARE-associated protein snapin, *J. Cell Sci.* 119 (2006) 2386–2397.
- [32] F.A. Lai, M. Dent, C. Wickenden, L. Xu, G. Kumari, M. Misra, H.B. Lee, M. Sar, G. Meissner, Expression of a cardiac Ca²⁺-release channel isoform in mammalian brain, *Biochem. J.* 288 (1992) 553–564.
- [33] Y. Ouyang, T.J. Deerinck, P.D. Walton, J.A. Airey, J.L. Sutko, M.H. Ellisman, Distribution of ryanodine receptors in the chicken central nervous system, *Brain Res.* 620 (2) (1993) 269–280.
- [34] M.A. Dent, G. Raisman, F.A. Lai, Expression of type 1 inositol 1,4,5-trisphosphate receptor during axogenesis and synaptic contact in the central and peripheral nervous system of developing rat, *Development* 122 (1996) 1029–1039.
- [35] T. Nakagawa, H. Okano, T. Furuichi, J. Aruga, K. Mikoshiba, The subtypes of the mouse inositol 1,4,5-trisphosphate receptor are expressed in a tissue-specific and developmentally specific manner, *Proc. Natl. Acad. Sci. U. S. A.* 88 (1991) 6244–6248.
- [36] D.A. Dodd, B. Niederoest, S. Bloechlinger, L. Dupuis, J.P. Loeffler, M.E. Schwab, Nogo-A, -B, and -C are found on the cell surface and interact together in many different cell types, *J. Biol. Chem.* 280 (13) (2005) 12494–12502.
- [37] Y. Shibata, C. Voss, J.M. Rist, J. Hu, T.A. Rapoport, W.A. Prinz, G.K. Voeltz, The reticulon and DP1/Yop1p proteins form immobile oligomers in the tubular endoplasmic reticulum, *J. Biol. Chem.* 283 (27) (2008) 18892–18904.
- [38] N. Zurek, L. Sparks, G. Voeltz, Reticulon short hairpin transmembrane domains are used to shape ER tubules, *Traffic* 3 (2011) 28–41.
- [39] P.S. McPherson, K.P. Campbell, Characterization of the major brain form of the ryanodine receptor/Ca²⁺ release channel, *J. Biol. Chem.* 268 (26) (1993) 19785–19790.
- [40] H. Shimizu, M. Fukaya, M. Yamasaki, M. Watanabe, T. Manabe, H. Kamiya, Use-dependent amplification of presynaptic Ca²⁺ signaling by axonal ryanodine receptors at the hippocampal mossy fiber synapse, *Proc. Natl. Acad. Sci. U. S. A.* 105 (33) (2008) 11998–12003.
- [41] R. Bull, J.P. Finkelstein, J. Gálvez, G. Sánchez, P. Donoso, M.I. Behrens, C. Hidalgo, Ischemia enhances activation by Ca²⁺ and redox modification of ryanodine receptor channels from rat brain cortex, *J. Neurosci.* 28 (38) (2008) 9463–9472.
- [42] F. Lai, M. Misra, L. Xu, A. Smith, G. Meissner, The ryanodine receptor Ca²⁺-release channel complex of skeletal muscle sarcoplasmic reticulum: evidence for a cooperatively coupled, negatively charged homotetramer, *J. Biol. Chem.* 264 (28) (1989) 16776–16785.
- [43] R.A. Padua, W.H. Wan, J.I. Nagy, J.D. Geiger, [3H]ryanodine binding sites in rat brain demonstrated by membrane binding and autoradiography, *Brain Res.* 542 (1) (1991) 135–140.
- [44] R.A. Padua, J.I. Nagy, J.D. Geiger, Subcellular localization of ryanodine receptors in rat brain, *Eur. J. Pharmacol.* 298 (2) (1996) 185–189.
- [45] I. Zimanyi, I.N. Pessah, Pharmacological characterization of the specific binding of [3H]ryanodine to rat brain microsomal membranes, *Brain Res.* 561 (2) (1991) 181–191.
- [46] T. Murayama, Y. Ogawa, Similar Ca²⁺ dependences of [3H]ryanodine binding to α - and β -ryanodine receptors purified from bullfrog skeletal muscle in an isotonic medium, *FEBS Lett.* 380 (3) (1996) 267–271.
- [47] R. Bull, J.P. Finkelstein, A. Hummer, M.I. Behrens, C. Hidalgo, Effects of ATP, Mg²⁺, and redox agents on the Ca²⁺ dependence of RyR channels from rat brain cortex, *Am. J. Physiol. Cell Physiol.* 293 (1) (2007) 162–171.
- [48] D.M. Balshaw, N. Yamaguchi, G. Meissner, Modulation of intracellular calcium-release channels by calmodulin, *J. Membr. Biol.* 185 (1) (2002) 1–8.
- [49] G.K. Voeltz, W. Prinz, Y. Shibata, J.M. Rist, T.A. Rapoport, A class of membrane proteins shaping the tubular endoplasmic reticulum, *Cell* 124 (3) (2006) 573–586.
- [50] I. Sparkes, N. Tolley, I. Aller, J. Svozil, A. Osterrieder, S. Botchway, C. Mueller, et al., Five Arabidopsis reticulon isoforms share endoplasmic reticulum location, topology, and membrane-shaping properties, *Plant Cell* 22 (4) (2010) 1333–1343.
- [51] M.G. Chelu, C.I. Danila, C.P. Gilman, S.L. Hamilton, Regulation of ryanodine receptors by FK506 binding proteins, *Trends Cardiovasc. Med.* 14 (6) (2004) 227–234.
- [52] T. Jayaraman, A.M. Brillantes, A.P. Timerman, S. Fleischer, H. Erdjument-Bromage, P. Tempst, A.R. Marks, FK506 binding protein associated with the calcium release channel (ryanodine receptor), *J. Biol. Chem.* 267 (14) (1992) 9474–9477.

- [53] A.P. Timerman, H. Onoue, H.B. Xin, S. Barg, J. Copello, G. Wiederrecht, S. Fleischer, Selective binding of FKBP12.6 by the cardiac ryanodine receptor, *J. Biol. Chem.* 271 (34) (1996) 20385–20391.
- [54] X.H.T. Wehrens, S.E. Lehnart, S.R. Reiken, S.-X. Deng, J.A. Vest, D. Cervantes, J. Coromilas, D.W. Landry, A.R. Marks, Protection from cardiac arrhythmia through ryanodine receptor-stabilizing protein calstabin 2, *Science* 304 (2004) 292–296.
- [55] T. GrandPré, F. Nakamura, T. Vartanian, S.M. Strittmatter, Identification of the Nogo inhibitor of axon regeneration as a Reticulon protein, *Nature* 403 (2000) 439–444.
- [56] X. Wang, S.J. Chun, H. Treloar, T. Vartanian, C.A. Greer, S.M. Strittmatter, Localization of Nogo-A and Nogo-66 receptor proteins at sites of axon-myelin and synaptic contact, *J. Neurosci.* 22 (13) (2002) 5505–5515.
- [57] J. Laurén, F. Hu, J. Chin, J. Liao, M.S. Airaksinen, S.M. Strittmatter, Characterization of myelin ligand complexes with neuronal Nogo-66 receptor family members, *J. Biol. Chem.* 282 (8) (2007) 5715–5725.
- [58] T. Furuichi, D. Furutama, Y. Hakamata, J. Nakai, H. Takeshima, K. Mikoshiba, Multiple types of ryanodine receptor/Ca²⁺ release channels are differentially expressed in rabbit brain, *J. Neurosci.* 14 (8) (1994) 4794–4805.
- [59] Y.M. Usachev, S.A. Thayer, All-or-none Ca²⁺ release from intracellular stores triggered by Ca²⁺ influx through voltage-gated Ca²⁺ channels in rat sensory neurons, *J. Neurosci.* 17 (19) (1997) 7404–7414.
- [60] D.L. Gruol, J.G. Netzeband, K.L. Parsons, Ca²⁺ signaling pathways linked to glutamate receptor activation in the somatic and dendritic regions of cultured cerebellar purkinje neurons, *J. Neurophysiol.* 76 (5) (1996) 3325–3340.
- [61] E.D. Martín, W. Buño, Caffeine-mediated presynaptic long-term potentiation in hippocampal CA1 pyramidal neurons, *J. Neurophysiol.* 89 (6) (2003) 3029–3038.
- [62] S. Sajikumar, Q. Li, W.C. Abraham, Z.C. Xiao, Priming of short-term potentiation and synaptic tagging/capture mechanisms by ryanodine receptor activation in rat hippocampal CA1, *Learn. Mem.* 16 (3) (2009) 178–186.
- [63] W. Zhao, N. Meiri, H. Xu, S. Cavallaro, A. Quattrone, L. Zhang, D.L. Alkon, Spatial learning induced changes in expression of the ryanodine type II receptor in the rat hippocampus, *FASEB J.* 14 (2) (2000) 290–300.
- [64] K. Kobayashi, T. Manabe, T. Takahashi, Calcium-dependent mechanisms involved in presynaptic long-term depression at the hippocampal mossy fibre-CA3 synapse, *Eur. J. Neurosci.* 11 (1999) 1633–1638.
- [65] Y. Wang, M.J. Rowan, R. Anwyl, Ryanodine produces a low frequency stimulation-induced NMDA receptor-independent long-term potentiation in the rat dentate gyrus *in vitro*, *J. Physiol.* 495 (1996) 755–767.
- [66] M. Reyes, P.K. Stanton, Induction of hippocampal long-term depression requires release of Ca²⁺ from separate presynaptic and postsynaptic intracellular stores, *J. Neurosci.* 16 (19) (1996) 5951–5960.
- [67] T. Adasme, P. Haeger, A.C. Paula-Lima, I. Espinoza, M.M. Casas-Alarcón, M.A. Carrasco, C. Hidalgo, Involvement of ryanodine receptors in neurotrophin-induced hippocampal synaptic plasticity and spatial memory formation, *Proc. Natl. Acad. Sci. U. S. A.* 108 (7) (2011) 3029–3034.
- [68] J.C. Gant, K.C. Chen, C.M. Norris, I. Kadish, O. Thibault, E.M. Blalock, N.M. Porter, P.W. Landfield, Disrupting function of FK506-binding protein 1b/12.6 induces the Ca²⁺-dysregulation aging phenotype in hippocampal neurons, *J. Neurosci.* 31 (5) (2011) 1693–1703.

12 Curriculum vitae

Maria Christine Riedl
Lorcher Straße 15
4470 Enns
Austria
Mobile: +43-664-393 42 02
E-mail: christine@riedl.at



Personal Information

Date of birth:	26/05/1984
Place of birth:	4020 Linz, Austria
Nationality:	Austrian
Family status:	unmarried
Parents:	Regina and Dipl.-Ing. Ludwig Riedl
Siblings:	1 brother (Oliver Riedl)

Education

06/2012-02/2014	Diploma student at the Institute of Biophysics, Johannes-Kepler University Linz, Gruberstraße 40, 4020 Linz, Austria Group of Univ.- Prof. Dr. Christoph Romanin
03/2004-2014	Student at the University of Vienna, Faculty of Life Science, Althanstraße 14, A-1090 Vienna, Austria Field of Study: Pharmaceutical Sciences
09/1998 - 06/2003	Secondary school: Höhere Bundeslehranstalt für wirtschaftliche Berufe (HLW), 4400 Steyr, Austria Focus of education: Health management Key course element: nutrition science
09/1994 – 07/1998	Grammar school: Hauptschule II, 4470 Enns, Austria economic center of gravity
09/1990 – 07/1994	Elementary school: Volksschule, 4482 Ennsdorf, Austria